ANALYTICAL AND EXPERIMENTAL

STUDIES ON MICROWAVE ASSISTED CVD

DIAMOND COATINGS ON Si_3N_4 AND

CEMENTED WC TOOLS AND GROWTH OF

POLYCRYSTALLINE DIAMOND ON

SEVERAL TRANSITION METALS
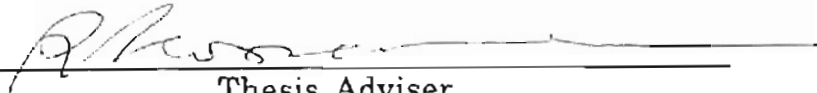

By

MALLIKA KAMARAJUGADDA

Bachelor of Science
Osmania University
Hyderabad, India
1988

Master of Science
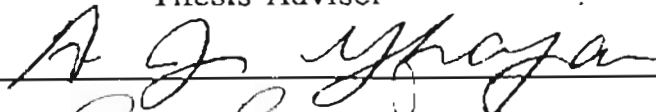Osmania University
Hyderabad, India
1990

Submitted to the Faculty of the
Graduate College of the
Oklahoma State University
in partial fulfillment of
the requirements for
the Degree of
DOCTOR OF PHILOSOPHY
MAY, 1998

ANALYTICAL AND EXPERIMENTAL
STUDIES ON MICROWAVE ASSISTED CVD
DIAMOND COATINGS ON Si_3N_4 AND
CEMENTED WC TOOLS AND GROWTH OF
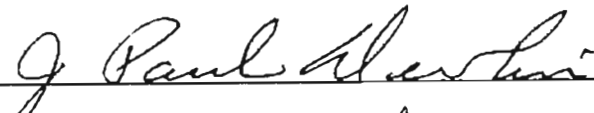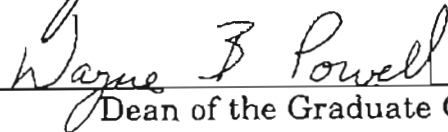POLYCRYSTALLINE DIAMOND ON
SEVERAL TRANSITION METALS

Thesis Approved:

_____
Thesis Adviser

_____

_____

_____

_____
Dean of the Graduate College

ii

ACKNOWLEDGEMENTS

TABLE OF CONTENTS

LIST OF TABLES

LIST OF FIGURES

CHAPTER 1

INTRODUCTION

Among the plethora of scientific inventions during the 20th century, synthesis of diamond is perhaps one of the most challenging technological inventions with significant economic impact. Besides being the hardest material (knoop hardness ~ 8000 kg/mm^2) known to man, it has many unique properties such as low friction and wear, optical transparency, high chemical resistance, and high thermal conductivity (2-5 times that of copper). As a result, diamond films/coatings can be used for a wide range of applications including cutting, grinding, polishing, optical, laser, IR, UV and electronic applications (Field 1979).

Diamond from ages has fascinated man and there is a evidence of much earlier attempts to synthesize this most exquisite gem (Tennant, 1797). However, it remained for a group of innovative scientists from General Electric to synthesize diamond using a high pressure and high temperature (HP-HT) technique (Bundy et al., 1955). Practical applications of synthetic diamond, however, have been limited to those cases where diamond's extreme hardness is a prerequisite due to the high cost of this HP-HT technique (Angus et al., 1988). Besides being expensive, these techniques can only produce bulk crystals or powders, which further limits the applications of the HP-HT synthetic diamond. The advent of novel methods of low pressure diamond synthesis under conditions far from thermodynamic equilibrium in the early 1970's has focused a new light on

1

synthetic diamond technology (Angus et al., 1993). These methods are capable of yielding well-crystallized diamond at much lower cost and in various shapes including thin films, coatings or even free standing thin sheets or ribbons (Lux et al., 1996).

The realization of deposition of diamond films on various kinds of substrates has great impact on the thin-film and coating technologies essential for improving surface quality in many industrial applications. The quality of the film and/or coating can, to some extent, determine the performance, and even the life time of a device. Within the last decade, a number of low pressure diamond synthesis techniques have been developed. These techniques can be grouped into two major categories: thermally activated Chemical Vapor Deposition (CVD) and plasma activated CVD (Anthony, 1991).

Similarities among various CVD processes include process parameters such as gas pressure (~ 10 mbar - 1 bar), % of hydrogen in the mixture ($CH_4 + H_2$) (~95 -99 %) and the resulting film morphology. However, there are other parameters which are technique specific. For example, the conditions for, and the modes of gas activation are different for cold plasma CVD and thermal plasma CVD, and in turn both are considerably different from combustion flame deposition. These process parameters lead to the differences in the energy partitioning in the deposition process, thermal and chemical species distribution, deposition efficiency, deposition rate, and film uniformity. Thus a detailed comparison between various processes would be formidable. Even within a specific plasma based deposition method, the size of the reactor, the exact geometry and materials used in a particular plasma reactor are important,

and thus comparisons of parameters from one deposition system to another are difficult. So, any parametric study conducted with a given CVD system is mainly to investigate the trends. Thus, the optimum conditions would be system specific and in general cannot be applied to scaled up systems.

Despite the fact that significant research efforts have focused on the low pressure diamond synthesis since the late 1980's, this technique is still far from meeting the general needs of large scale industrial applications. Many problems still need to be solved. A sound understanding of the nature of the CVD process, a better control of the diamond deposition to reduce or eliminate structural imperfections in the films to improve the quality of diamond films, and an increase of growth rates and deposition areas are some important areas requiring further investigation.

In order to improve the wear resistance of the diamond coated tools, diamond films have to adhere well to the substrates. Cemented tungsten carbide cutting tools are the work horse of the metal cutting industry because of their high wear resistance and fracture toughness properties. However, these tools wear rapidly while machining abrasive high Al-Si alloys and glass-epoxy composites. Polycrystalline diamond (PCD) tools on a WC-Co substrate is generally used for this purpose. Unfortunately, they are rather expensive. Diamond films deposited using CVD techniques can be relatively inexpensive, and could be deposited on tools of any geometry. This is because of the low cost of the equipment used for coating and high cost of grinding and shaping of polycrystalline diamond tools. Hence numerous research efforts have been directed towards developing CVD diamond coatings on cemented carbides. However, problems exist on the adhesion of diamond films on cemented carbides (Hintermann, 1997). One

of the major reasons attributed for the poor adhesion is the presence of the cobalt binder (Saijo et al., 1991; Haubner et al., 1989). Pretreatment of substrates and use of interlayers to reduce the thermal mismatch are two techniques adopted by various researchers to address this problem (Quinto, 1996). Efforts have also been directed at developing diamond coatings on Si_3N_4 based ceramics (Mason, 1990; Soderberg et al., 1991; Itoh et al., 1996, 1997; Peng et al., 1995). Some approaches have been reported for improved adhesion strength of diamond coatings (Oles et al., 1996; Nesladek et al., 1995; Shen, 1996; Singh et al., 1996; Drory 1997).

However, limited quantitative data are provided correlating various substrate materials, substrate conditions and deposition parameters to the quality and adhesion of diamond coatings. These issues provided the incentive for the proposed investigation to systematically and quantitatively evaluate the effect of some of process variables and substrate materials on the quality and adhesion strength of diamond films.

One of the objectives of this research is to evaluate the effects of various process variables, substrate pretreatments, and residual stresses on the quality and adhesion of diamond films on selected substrate materials. Indentation adhesion testing, a qualitative method of measuring coating adherence was used to evaluate the adhesion strength of the diamond coatings. Microstructural and interfacial characterizations of the samples were done to identify the beneficial characteristics in terms of diamond film quality and adherence. Chemical structural and phase identification were obtained using X-ray diffraction (XRD). Optical and scanning electron microscopy were used for surface morphology analysis. In-depth characterization of the diamond coatings was done by using μ-

Raman spectroscopy to determine the phase purity, relative amounts of diamond and non-diamond carbon phases qualitatively as well as quantitatively. μ-Raman spectroscopy was also used to estimate the residual stresses. This research has emphasized the influences of these parameters on the quality of diamond films, which, in turn, is believed to govern the adhesion of diamond coatings. An attempt was also made towards understanding the growth mechanism of diamond on various transition substrate materials.

Three different issues namely, diamond coatings on Si_3N_4, diamond coatings on cemented WC with different cobalt content and diamond growth studies on transition metals have been addressed during this research and are presented in this dissertation. Chapter 2 presents relevant background including the literature review of the development of the low pressure synthesis of polycrystalline diamond coatings. More detailed literature surveys are provided in the introductions of the pertinent chapters. Chapter 3 gives the problem statement. Chapters 4 and 5 describe the experimental setup and the characterization techniques employed in this investigation. Diamond coatings on silicon nitride substrates is presented in Chapter 6. Chapter 7 discusses diamond coatings on cemented tungsten carbides. CVD diamond growth studies on transition metals as substrate materials is presented in Chapter 8. General conclusions of this research are given in Chapter 9. Chapter 10 outlines the future work. Appendix A gives the properties of diamond and Appendix B gives the specifications of the various instruments used.

CHAPTER 2

LITERATURE REVIEW

2.1   Introduction

Over the last four decades, a variety of techniques have evolved for the synthesis of diamond, including high-pressure, high temperature (HP-HT) processes, chemical vapor deposition (CVD), and physical vapor deposition (PVD) processes. The "premodern" era of diamond CVD technology, started in 1949 and was connected with the names of Eversole, Deryagin and Angus. Thorough review of these investigations, including the history of vapor deposited diamond were written by Devries (1987), Angus et al.,(1988, 1989). The first detailed descriptions of diamond forming processes were given in several papers by the Japanese research group at the National Institute for Research in Inorganic Materials (Matsumoto et al, 1982, 1983,1985a, 1985b; Kamo et al., 1983). These papers mark the beginning of an intense world-wide effort to develop diamond forming CVD processes and to open new fields of application for CVD diamond films, thus creating a new diamond technology. Since then, considerable number of papers have appeared dealing with various aspects of the low pressure diamond synthesis and its wide applications. Excellent reviews of various methods of diamond synthesis, growth mechanisms, properties and applications have been written by Angus et al., (1993a, 1993b), Spear (1989), Anthony (1991), Ashfold et al., (1994), Liu et al.,(1995), Bachmann et al.,(1991), Klages (1993), Wei et al., (1995), Lux and Haubner (1991, 1996), Heggie et al.,(1996), Hintermann (1996). In addition, several books dealing

with aspects of CVD diamond technology have been published (NATO series, 1990; Electrochemical society series, 1994; MRS Symposium Proceedings 1995; New Diamond Science and Technology Proceedings, 1991).

The discussion of the literature on the low pressure diamond synthesis will proceed as follows. In the first section some of the important historical events that led to the synthesis of diamond are presented. This will be followed by a discussion of various CVD techniques used for diamond synthesis. Some of the important process variables effecting the nucleation, growth and morphology of diamond and the various growth mechanisms are discussed in the subsequent sections. Since the advent of reasonably fast deposition rates for diamond films, the cutting tool industry has been exploring their use for machining. Metal cutting applications take advantage of the high hardness, extremely good wear resistance and low coefficient friction of diamond. The last section of the chapter will discuss the development of these diamond coatings on cutting tools and the associated problems.

2.2 Historical Background

Sir Isaac Newton was the first to characterize diamond and determine it to be of organic origin (Newton, 1704). The first well documented experiment on diamond was conducted by two Italian academicians, G. Averani and C. D. Tarigioni, in 1694 (Blackey, 1977). They set up a large magnifying glass, and focused a beam of light on a small diamond and saw it "crack, coruscate and finally disappear," leaving

a minute quantity of black ash. Some years later, French chemist Lavoisier determined that the product of combustion of diamond was carbon dioxide. One of Lavoisier's most celebrated experiments was, to place a diamond in a bell jar filled with oxygen which rested in a basin containing mercury. The sun rays were then focused on the diamond by means of a large magnifying glass. After the diamond had been consumed, the bell jar was found to contain great quantities of carbonic acid, indicating that the diamond was composed principally of carbon (Lavoisier, 1772). English chemist Smithson Tennant showed that the combustion products of diamond were the same as those of coal and graphite (Tennant, 1797). Later with the discovery of X-rays, in the early 20th century, Bragg confirmed that diamond, graphite, and charcoal were the allotropes of carbon (Bragg, 1913). The quest for the synthesis of diamond began, since then. However, earlier efforts did not meet with much success, basically due to the lack of understanding of the chemical thermodynamics. The only intuition, which later worked out successfully was that diamond being the densest carbon phase, high pressures may have to be used. The development of chemical thermodynamics permitted a more scientific approach, and in 1939 the graphite diamond stability field was computed (Leipunski, 1939; Rossini and Jessup, 1938). Subsequent efforts were primarily directed towards exploring pressures and temperatures at which diamond is thermodynamically stable with respect to graphite (Angus et al., 1988). Of the same significance as many successful achievements in the history of making diamond was the failure of Bridgman's experiments (Bridgman, 1947). He compressed graphite to pressures well within the diamond stable region for a few seconds without producing diamond. This work led to the current understanding of the large kinetic barrier between

8

the diamond and graphite phases. All these efforts culminated when in 1955, researchers at General Electric company synthesized diamond for the first time using a molten transition metal solvent catalyst at pressures where diamond is thermodynamically stable (Bundy et al, 1955). This is known as the high pressure high temperature (HP-HT) process.

2.3 High Pressure High Temperature Process

The HP-HT process employs a belt apparatus where two opposed anvils are pressed inwards by a large press against a diamond growth cell surrounded by a belt to contain the high pressure (Bundy et al., 1955). A current is passed through the cell to heat it above 1200 °C and a pressure greater than 60 Kilobars is produced in the cell by the opposing anvils. At this pressure and temperature the cell is in the region of the carbon phase diagram where diamond is the stable phase. The metastable graphite dissolves in the liquid metal catalyst and precipitates out as diamond. The use of a liquid metal catalyst enables one to use relatively low pressures that are close to the diamond-graphite phase boundary. Pressures of ~ 120 kilobars and temperatures of ~ 2000 °C are required for direct graphite-to-diamond conversion without a metal catalyst. The static indirect process has other advantages including a high diamond growth rate up to 10,000 μm/hr and excellent crystal quality (Anthony, 1991). Plants in many countries use this HP-HT technique to produce about 30-40 tons of synthetic industrial grade diamond grit per year for a wide range of applications (Komanduri, 1993).

Despite many advantages, the HP-HT process has some limitations (Anthony, 1991). The very high pressure and maximum strengths of materials limits the size of the growth cells and hence the maximum size of diamond that can be made to less than several inches across. Secondly, small amounts of the liquid metal catalyst can become trapped as inclusions in the diamond crystal. These metal inclusions have a different thermal expansion coefficient than diamond and cause internal stresses to develop and weaken the diamond. This weakening of diamond by metal inclusions, is undesirable for some abrasive-tool applications.

The invention of the static HP-HT process was followed by the development of a dynamic high pressure process that uses high energy explosives to generate a high pressure high temperature shock wave that directly converts graphite to diamond (Anthony, 1991). Because of the short duration of the shock wave, this dynamic process produces very fine diamond powder (< 2 μm in diameter) that is useful mainly for polishing compounds. Consequently, 90 % of the industrial grade diamonds are produced by the HP-HT process where a variety of crystal sizes up to gem sized stones can be easily made.

2.4 Diamond Growth at Low Pressures

2.4.1 Theoretical Considerations

Since diamond is unstable from the thermodynamic point of view at atmospheric pressure and room temperature, synthetic as well as natural diamonds are typically formed under extreme conditions of high pressures

and high temperatures. However, this does not mean that the diamond crystallization cannot occur under normal conditions. Interest in the metastable growth of diamond at low pressures where graphite is thermodynamically stable has come a long way from Von Bolton's early attempt made in 1911 (Von Bolton, 1911) to the present widespread use of activated CVD processes to grow diamond.

From the temperature-pressure equilibrium diagram of diamond (Figure 2.4.1.1), it can be seen that diamond is stable at high pressures and metastable under atmospheric conditions (Bovenkerk et al., 1959). A careful examination of the P-T diagram (Bundy et al., 1973) of diamond shows that under normal atmospheric conditions, graphite is a stable form of carbon, because of its lower energy and higher entropy than diamond.
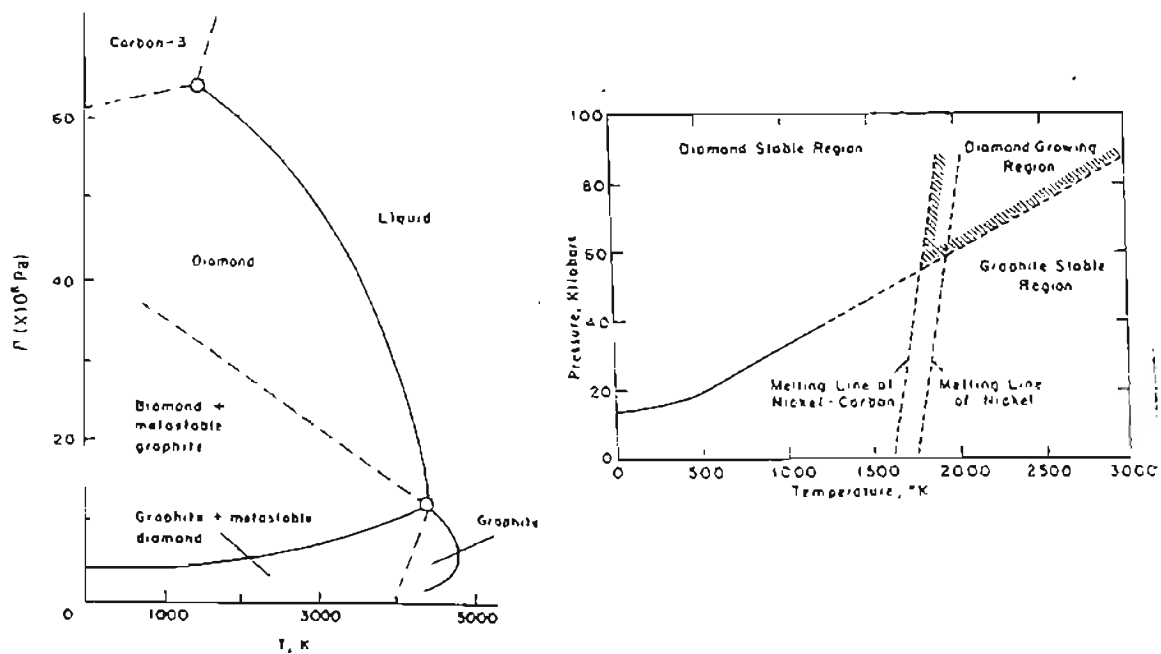
Figure 2.4.1.1   P-T diagram of Carbon Showing the Diamond Stable Region
(Bovenkerk et al., 1959)

The Gibbs free energy change for the transformation of graphite to diamond is positive for all temperatures at zero or atmospheric pressures (Bent, 1965).

$$Graphite \Leftrightarrow Diamond : \Delta G_{298K} = +693 \text{ cal/mol}$$
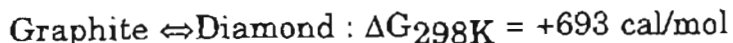
Since the Gibbs free energy difference of 693 cal/mole, which is about 0.016 eV is less than kT (0.025 eV) at room temperature, diamond, which is metastable at room temperatures co-exists with the more stable form (graphite) (Bent, 1965). The presence of large kinetic barrier prevents the spontaneous transformation to a more stable phase (Bundy et al., 1973).

From the thermodynamic point of view, in a system in which stable and metastable phases of various energy levels exist, the least stable phase will form first, with the others occurring step by step until the minimum energy level is reached (Bent, 1965). The free energy of carbon atoms in some compounds, such as methane (CH_4) and carbon monoxide (CO), may be higher than that of carbon in the diamond lattice (Bundy et al., 1973). During the decomposition of such compounds by suitable means, if it is possible to stabilize the carbon atoms at the metastable energy level corresponding to diamond instead of allowing them all the way down to a lower free energy of graphite, diamond could be crystallized. Bridgman, father of modern high pressure technology, who himself failed in attempting diamond growth at low pressures, predicted in a Scientific American article that diamond growth at low pressures should be equally achievable as at high pressures (Bridgman, 1955). However, achieving the appropriate conditions for low pressure diamond growth has taken decades of research.

2.4.2 Brief overview on the Development of Low Pressure Vapor Deposition Methods for Diamond synthesis

The production of synthetic diamonds from low-pressure gases was first reported by Von Bolton in 1911 (Devries, 1987). He claimed to have achieved growth on diamond seed crystals from illuminating gas (acetylene) decomposition at 100 °C in the presence of mercury vapor. However, little attention was given to these claims. Systematic studies of diamond vapor deposition techniques began primarily in the 1950's in the Soviet Union and the United States. The major Japanese effort began in 1970's (Devries, 1987). Deryagin et al., (1975) summarized the results of the first two decades of research on vapor-deposited diamond in the Soviet Union. They reported that the diamond growth rates were low (Angstroms/hour) and the simultaneous codeposition of graphitic carbon was always a problem. The early research primarily involved in the thermal decomposition of hydrocarbons and hydrogen-hydrocarbon gas mixtures. Under these conditions, the hydrocarbon gas was pyrolysized to form diamond and graphite and then hydrogen was used to etch the graphite away. The main reactions are as follows (Anthony, 1991):

$$CH_4 \xrightarrow{\text{heat}} \text{Deposit (Diamond \& Graphite)} + 2\,H_2 \tag{a}$$

$$H_2 + \text{Deposit} \xrightarrow{\text{heat}} \text{Diamond} + CH_4 \tag{b}$$
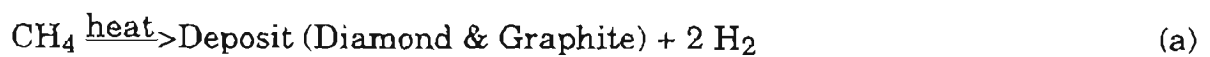
The synthesis process required many cycles of growth followed by hydrogen etching to remove excessive graphitic deposits. Similar research was also being conducted in the United States during the early time period. Eversole (1958) filed a patent on the low-pressure vapor synthesis process, but again

the growth rates were very low and graphitic carbon was deposited simultaneously. Angus and coworkers (1968, 1973, 1976), continued to pursue these techniques and obtained results similar to those of Eversole. Since the growth rates were extremely low the process was of scientific interest only.

In 1977, Deryagin's group reported that the gas activation techniques resulted in dramatic increases in diamond growth rates while eliminating much of graphitic codeposition. The same aspect was demonstrated by Angus and coworkers. If it is possible to obtain high concentration of atomic hydrogen by decomposing molecular hydrogen during deposition, it acts as a "solvent" for graphite, thereby suppressing the codeposition of graphite.

$$CH_4 \xrightarrow{\text{heat \& Atomic Hydrogen}} Diamond + 2H_2 \qquad \text{(Anthony, 1991)}$$

Following this breakthrough in the early 1980's, Japanese researchers began reporting dramatic successes in low-pressure diamond growth using a variety of new gas activation techniques. All methods are basically different ways of generating the atomic hydrogen required in reaction (c) (Anthony, 1991). The emerging new techniques of synthesis of diamond under low pressure conditions and the subsequent increase in the growth rates are shown in Figures 2.4.2.1 a and b respectively. At the time of Eversole's announcement the growth rate was only 20 Å/hr. However, following the demonstration by Russian researchers of the usefulness of atomic hydrogen (Spistyn et al., 1981) the growth rates have increased substantially to about 1000 µm/hr (Spear et al., 1989; Angus et al., 1991).

14
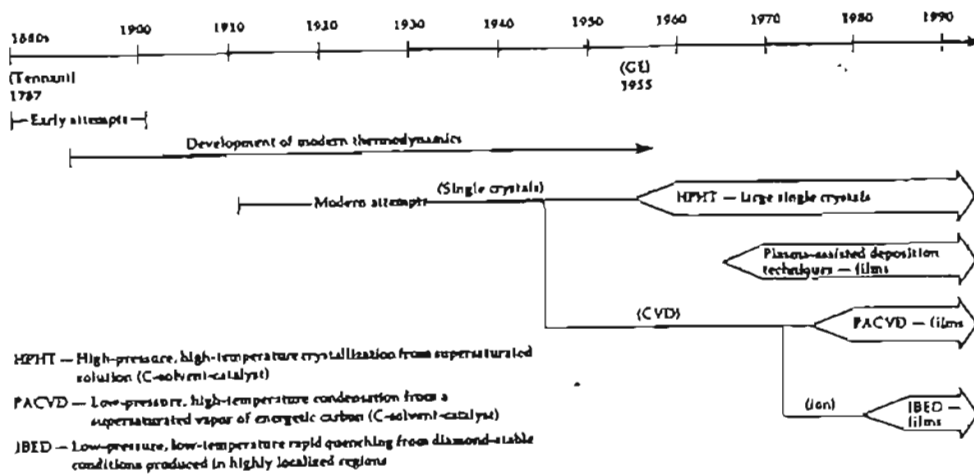
Figure 2.4.2.1a)   Attempts to Fabricate Synthetic Diamond
(Deutchman et al., 1989)
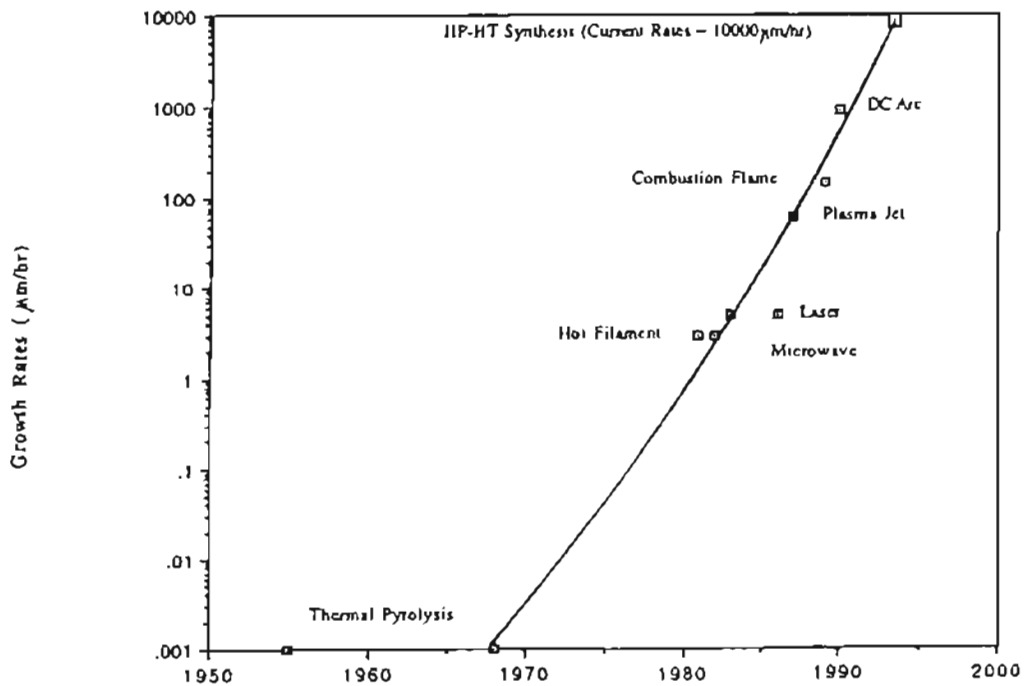
Figure 2.4.2.1 b)   Trends in Growth Rates (Komanduri et al., 1991)

The substantial increase in the growth rate rejuvenated interest among researchers all over the world and several methods such as RF or microwave plasma enhanced CVD, DC glow discharge CVD, hot filament CVD, AC discharge were devised for decomposing the precursor gases

15

(Matsumoto et al., 1982,1983, 1985; Kamo et al., 1983; Sawabe et al., 1985, 1986). Table 2.4.2.1 categorizes different deposition methods according to the specific way of initiating the chemical reactions that lead to the diamond formation.

Table 2.4.2.1 CVD Methods for the Preparation of Diamond

(Bachmann et al., 1991)

Thermal CVD	Thermal decomposition Chemical Transport Reaction (CTR) Hot Filament Technique Oxy-Acetylene Torch
DC Plasma CVD	Low Pressure CVD Medium Pressure DC plasma Hollow cathode discharge DC arc plasma DC plasma jet
RF Plasma CVD	Low pressure RF glow discharge Thermal RF plasma CVD
Microwave Plasma CVD	915 MHz plasma low pressure 2.45 GHz plasma atm. pressure 2.45 GHz plasma torch 2.45 GHz magnetized (ECR) plasma 8.2 GHz plasma

Karner et al., (1996) discussed a relatively new kind of CVD diamond deposition method. The high current DC arc (HCDCA) process is based on a high current arc discharge with a long discharge column (Figure 2.4.2.2). The plasma density in the column is extremely high, so that the substrates can be positioned at a relatively low plasma density at a large

distance from the intense discharge column. The main advantage of this process is that it is possible to generate a large surface area with uniform conditions for the deposition of high quality diamond films. Also, the substrates are mainly heated by the hydrogen recombination on the surface. The atomic hydrogen flow is adjusted so that the rate of substrate heating is compensated by an equal cooling rate by radiation. Hence no additional cooling is necessary. Using this method, they obtained good quality diamond coatings on a large number of WC tool inserts with arbitrary shapes.
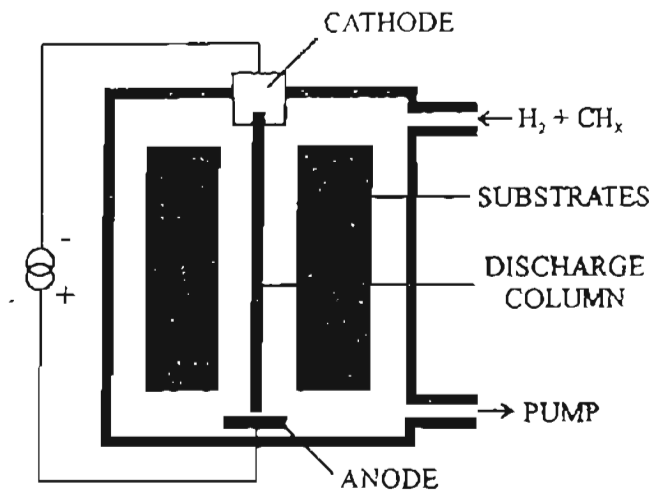
Figure 2.4.2.2   Principle of ReactorLay-out for HCDCA Process
(Karner et al., 1996)

Researchers from Argonne laboratories are currently exploring the use of bucky ball (C_{60} Fullerenes) as an alternate precursor for diamond growth (Dieter et al., 1997). C_{60} is the only form of carbon that does not contain oxygen or hydrogen and can be converted to gas phase by heating in a standard tube furnace. Initial reports indicate that in argon microwave

discharge these bucky balls produce smooth (~17 nm rms R_a) nano crystalline diamond films (~ 15 nm grain size). From quantum mechanical calculations they determined that the diamond growth rate is directly related to the concentration of the C_{60} dimer and therefore participation of atomic hydrogen is not required. However, they found that by addition of hydrogen to plasma it was possible to control the properties over a wide range.

Of all the techniques, microwave plasma assisted CVD, hot filament CVD, and combustion synthesis are widely employed for the diamond film synthesis. Each of these techniques will be discussed in the following sections.

2.4.3   Various CVD Techniques of Diamond Deposition

2.4.3.1   Hot Filament CVD (HF-CVD)

Hot filament CVD (HF-CVD) was first proposed by Matsumoto et al., (1982). The basic experimental setup of the hot filament reactor is shown in Figure 2.4.3.1.1. Important process parameters and their typical values employed in this method are given in Table 2.4.3.1.1. In this method, a filament, made of tungsten, tantalum or rhenium is heated to a temperature of 1,950°C - 2,300°C. Generally, the filament is made of tungsten, tantalum or rhenium.

Table 2.4.3.1.1   Typical Conditions for Diamond Deposition in HF-CVD (Klages, 1993)

Filament Temperature, ^oC	1950 -2300
Substrate Temperature, ^oC	700 - 1000
Pressure, Torr	20-50
Flow of rate CH_4/H_2 , sccm	0.5/99.5
Substrate - Filament Distance, mm	1- 20
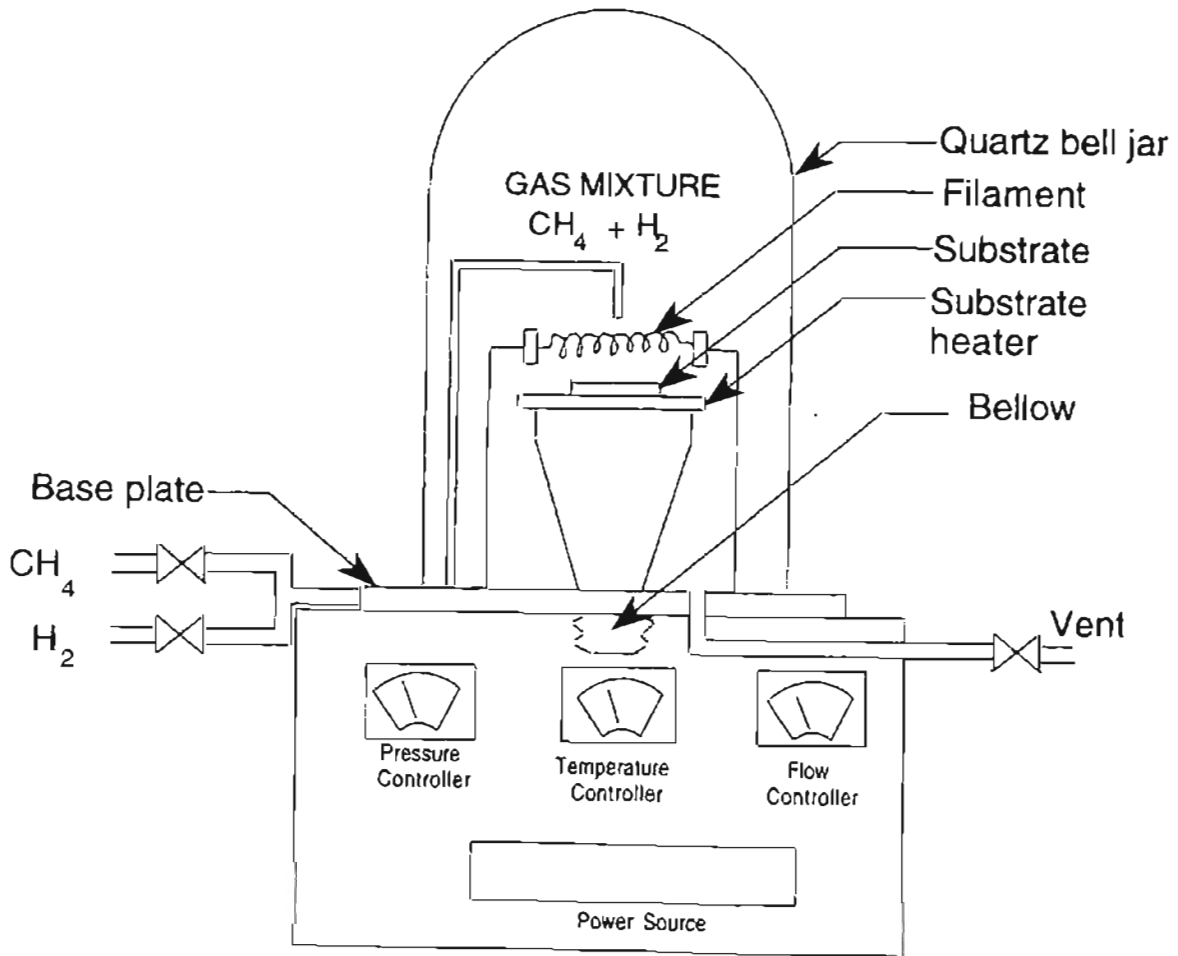
Figure 2.4.3.1.1   Experimental Setup of HFCVD (after Iyengar, 1995)

A heated (700°C - 1000°C) substrate is placed at a distance of 1 to 20 mm from the filament. A gas mixture of hydrogen and hydrocarbon (e.g. methane) is passed over the heated filament. The molecular hydrogen, present in the mixture, is converted to atomic hydrogen at high filament temperatures. The atomic hydrogen thus formed facilitates the formation of diamond by etching away graphite that is formed during the reaction. The growth rates in this method are in the range of 0.3-2 μm/hr (Bachmann et al., 1991). The growth rates can be further increased by providing a negative bias to the substrate. The area of deposition is dependent on the filament structure and is typically in the range of 2-100 cm^2. The main advantages of this method are the following (Haubner and Lux, 1993):

- inexpensive equipment (i.e. reactor and gas activation source)
- large areas of homogeneous deposition are possible by the use of multiple filaments
- deposition conditions can be easily controlled

The main disadvantages are the following

- diamond deposits may contain traces of filament material
- reproducibility lower than microwave deposition systems

2.4.3.2 Microwave-Plasma-Assisted CVD

Microwave-plasma-assisted CVD methods are more extensively used than any other methods for the growth of diamond films (Kamo et al., 1983; Saito et al., 1986, 1988, 1991; Badzian and Badzian, 1988; Mitsuda et al., 1987; Matsumoto et al., 1982, 1985, 1987; Haubner et al., 1993;Liu et al., 1995; Itoh et al., 1991, 1996,1997; Stiegler et al., 1996; Zhu et al., 1989, 1990). This specific deposition technique, along with hot filament technique, has moved

diamond thin films close to an industrially applicable technology (Ashfold et al., 1994). A majority of diamond related patents utilize this approach (Lux et al., 1996). Figure 2.4.3.2.1 shows a typical set up used for microwave assisted CVD diamond synthesis and Table 2.4.3.2.1 gives typical operating conditions.
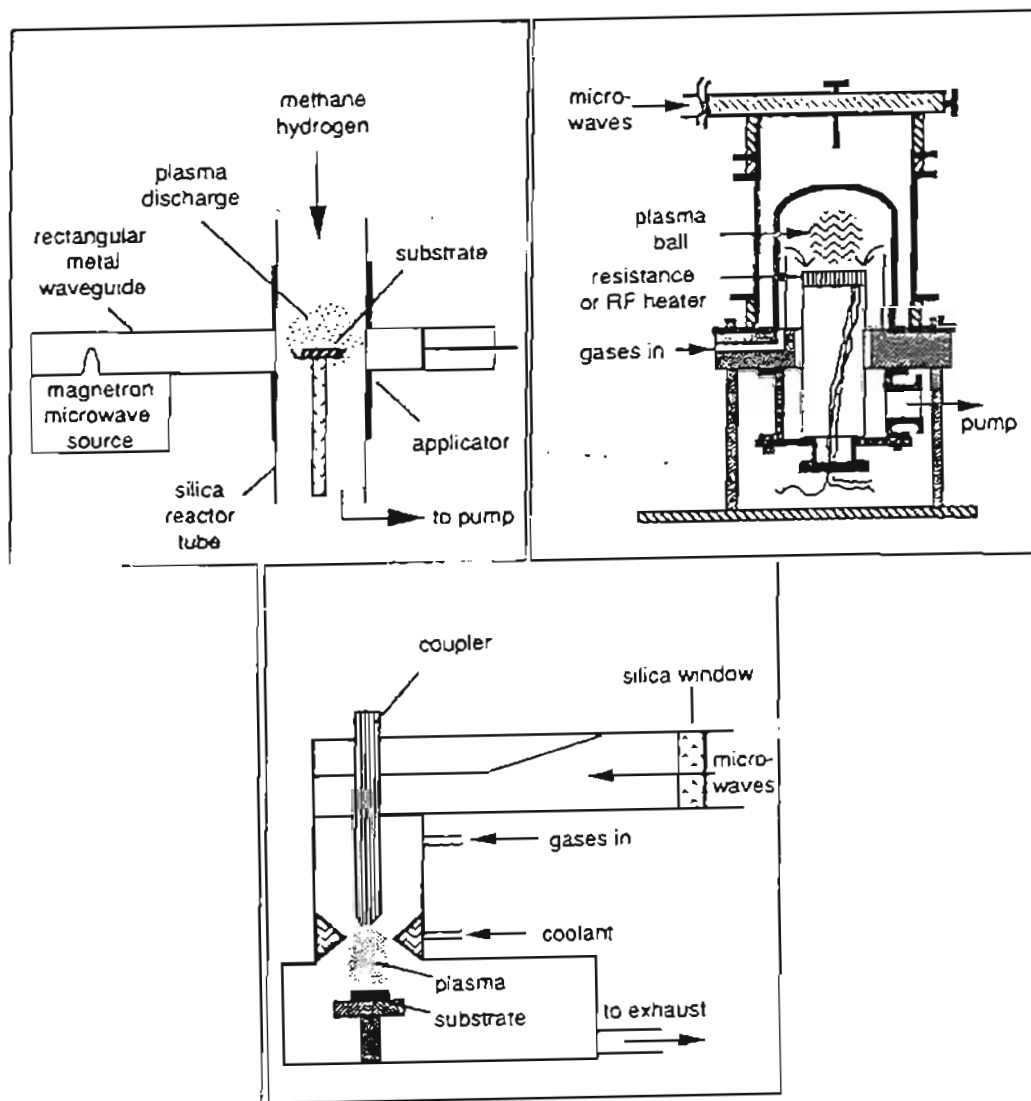
Figure 2.4.3.2.1   Different Setups for Microwave Plasma CVD of Diamond (after Bachmann et al., 1991)

Table 2.4.3.2.1   Typical Conditions for Diamond
Deposition in Microwave CVD (Klages, 1993)

Microwave Power, watts	100-1000
Substrate Temperature °C	800-1000
Pressure, Torr	20-50
Flow rate of CH_4/H_2, sccm	0.5/99.5

The chamber consists of a 2.5 GHz magnetron power source for generating the microwave. A mixture of hydrogen and hydrocarbon gas, such as, methane is introduced into the reaction chamber. The gas mixture is ionized and excited by microwave power leading to the formation of a ball shaped plasma discharge (Brewer et al, 1992). The role of the plasma is to generate atomic hydrogen and to produce proper carbon precursors for the growth of diamond. Important process parameters include gas composition, pressure, flow rate, substrate temperature, and microwave power. The diamond growth rates in this method are in the range of 1-2 $\mu m/hr$. This method has a number of distinct advantages over the other methods of film growth. (Bachmann, et al., 1991; Klages et al., 1993).

- Microwave deposition being an electrodeless process avoids contamination of the films due to electrode erosion
- Microwave discharge, being a higher frequency process, produces higher plasma density with higher energy electrons. This results in higher concentrations of atomic hydrogen and hydrocarbon radicals.

- Since plasma is confined in the center of the deposition chamber in the form of a ball, there is no carbon deposition on the walls of the chamber.

2.4.3.3   Combustion Synthesis

A relatively simple technique of growth of diamond at atmospheric pressures using an oxy-acetylene welding torch was reported by Hirose and Kondo (1988). Figure 2.4.3.3.1 shows a typical setup used for the combustion synthesis of diamond and Table 2.4.3.3.1 gives the process parameters and conditions employed in combustion synthesis. The flame, in a welding torch has two regions, namely, the oxidizing flame region and the reducing 'acetylene feather' region. The diamond deposition occurs directly under the acetylene feather. Instead of acetylene, ethylene or ethane can also be used as carbon source in this method. Generally, the ratio of oxygen to acetylene is in the range of 0.9 to 1.1, ethylene to oxygen is in the range of 1.18 to 1.125, and ethane to oxygen is in the range of 1 to 1.63 for diamond deposition (Butler et al, 1990). The morphology and quality of the synthetic diamond films produced by this method depend on several factors including the substrate temperature, gas flow rates and their ratios, and the substrate position (Nandyal, 1991; Bang 1994a). Morphology and quality of diamond films were shown to have a strong relation to the substrate temperature profile and nozzle size (Bang et al., 1994b). Typical growth rates of diamond by this method are in the range of 50 -150 $\mu m/hr$ which is significantly higher than that of microwave or hot filament assisted CVD. This method can be employed when high growth rates are required and the

23

contamination of the film is not a major consideration. The main advantages of this method are the following:

- simple set up
- high growth rates (50 - 150 μm/hr)

The main disadvantages are the following:

- control of substrate temperature is difficult
- inhomogeneous deposition and contamination

Table 2.4.3.3.1   Typical Conditions for Diamond Deposition by Combustion Synthesis (Klages, 1993)

Flame Temperature, ^oC	3000
Substrate Temperature, ^oC	400-1100
Pressure, bar	1
Flow rate of C_2H_4/O_2, sccm	1000-2000
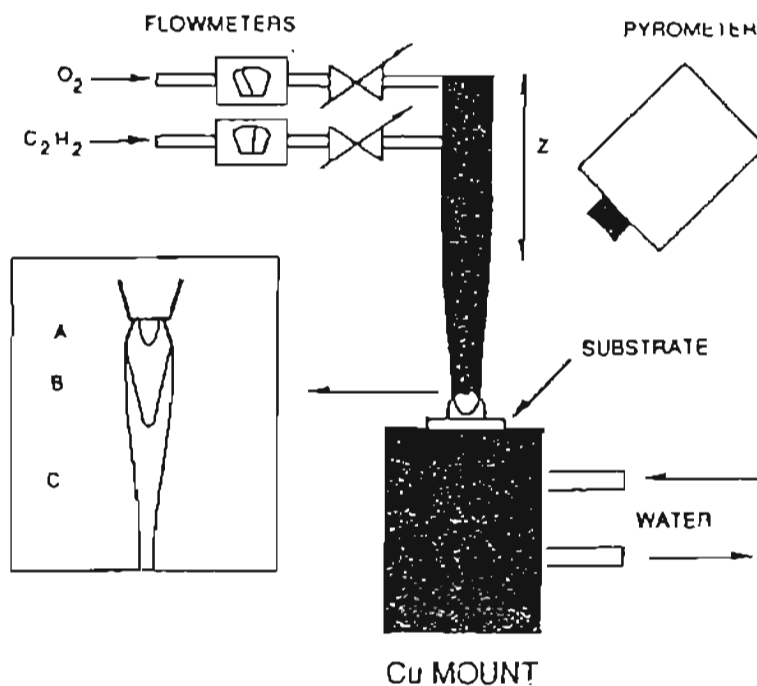
Figure 2.4.3.3.1   Schematic of the Apparatus for Combustion Synthesis (after Hanssen et al., 1988)

24

2.5   The C-H-O Phase Diagram for CVD diamond Growth

Bachmann et al., (1991) examined the low pressure CVD diamond data from various researchers, since the work of Eversole, and attempted to rationalize them. Hydrogen and one of the various hydrocarbons are the starting precursors in the low pressure diamond synthesis. Oxygen is frequently added, either directly (e.g. in the oxy-acetylene combustion synthesis) or as an integral part of the carbon carrier (e.g. CO). A common C-H-O ternary phase diagram is constructed by Bachmann et al., to provide a common scheme for the analysis of low pressure diamond synthesis (Figure 2.5.1). The phase diagram for all diamond CVD methods used shows a diamond growth region. Most of the combustion synthesis experiments were conducted along the acetylene line. Most of the plasma and hot filament experiments were conducted with highly diluted mixtures of hydrocarbon and hydrogen, sometimes with additional oxygen. The diamond region is very narrow in the hydrogen rich end of the phase diagram and broadens considerably on the C-O line. This diagram indicates that the low pressure diamond synthesis is feasible only within a well-defined field of the phase diagram, a 'diamond domain' with 'no growth' region on the oxygen-rich side and by a region where only 'non-diamond carbon' forms on its carbon rich side. It is possible to predict the starting precursors along with their compositions from this diagram. Figure 2.5.2 is an enlarged hydrogen-rich region of the phase diagram where most of the plasma and hot filament experiments were conducted. Using this diagram, Bachmann et al., pointed out that the upper concentration limit for diamond formation from methane and hydrogen mixture can be predicted to be between 3-4 %. They have also shown that for

higher values of methane in the CH_4-H_2 mixture, small additions of oxygen could shift from non-diamond carbon into diamond region.

They also suggested that the effect of the substrate temperature can be considered with the substrate temperature as the axis perpendicular to the C-H-O phase diagram (Figure 2.5.3). The width of the base of the triangular diamond domain narrows to zero above 1300 °C where graphitization of diamond predominates. This means, that as the substrate temperature increases the triangular diamond domain region in the C-H-O equilibrium diagram shrinks to almost a line at the highest temperature. They also explained for the large diamond growth rates for different CVD activated methods. Figure 2.5.4 shows the variation of the linear growth rate with the approximate gas phase temperatures of the various CVD methods. It can be seen from the figure that thermal decomposition methods yield low diamond deposition rates (0.01 μm/hr) due to the low gas phase temperatures, while the highest growth rates (~ 980-1000 μm/hr) can be obtained from high power d.c. arc discharges, in r.f. plasma torches or by d.c. jets where the gas phase temperature is ~ 5000 °C. Techniques such as microwave plasma or hot filament CVD where the gas phase temperatures are around 2000-2500 °C yield growth rates of ~1-2 μm/hr while for combustion synthesis where the temperatures are around 2900-3300 °C growth rates are around 50-150 μm/hr.
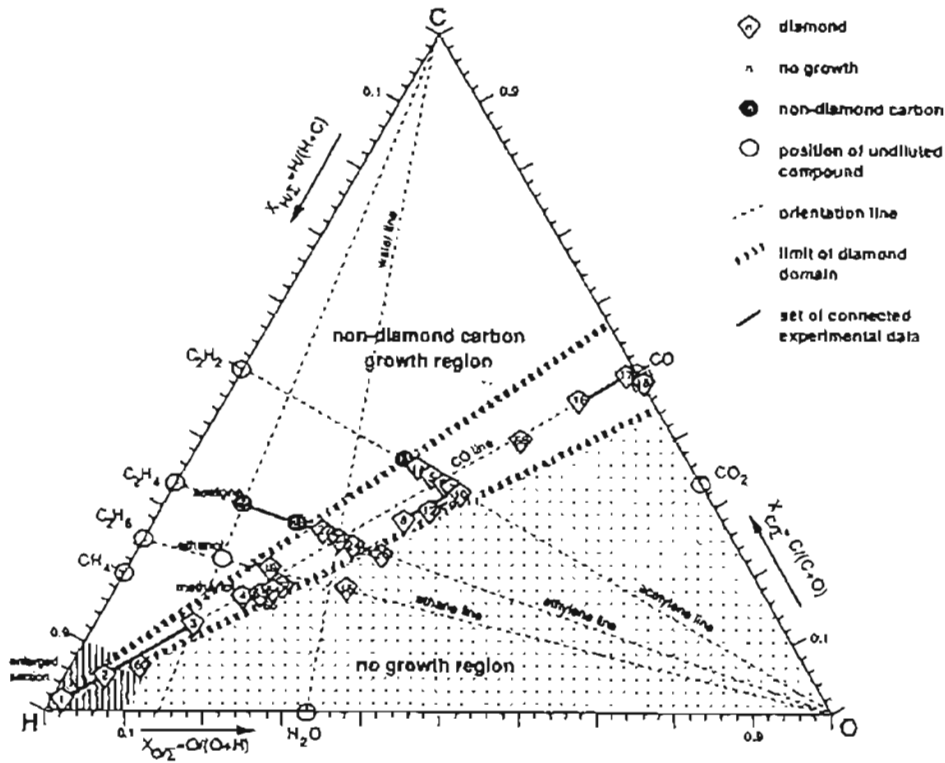
Figure 2.5.1   Atomic C-H-O Diamond Deposition Phase Diagram for
                 Various CVD Diamond Methods Used Showing a Definite
                 Diamond Growth Region (after Bachmann et al., 1991)
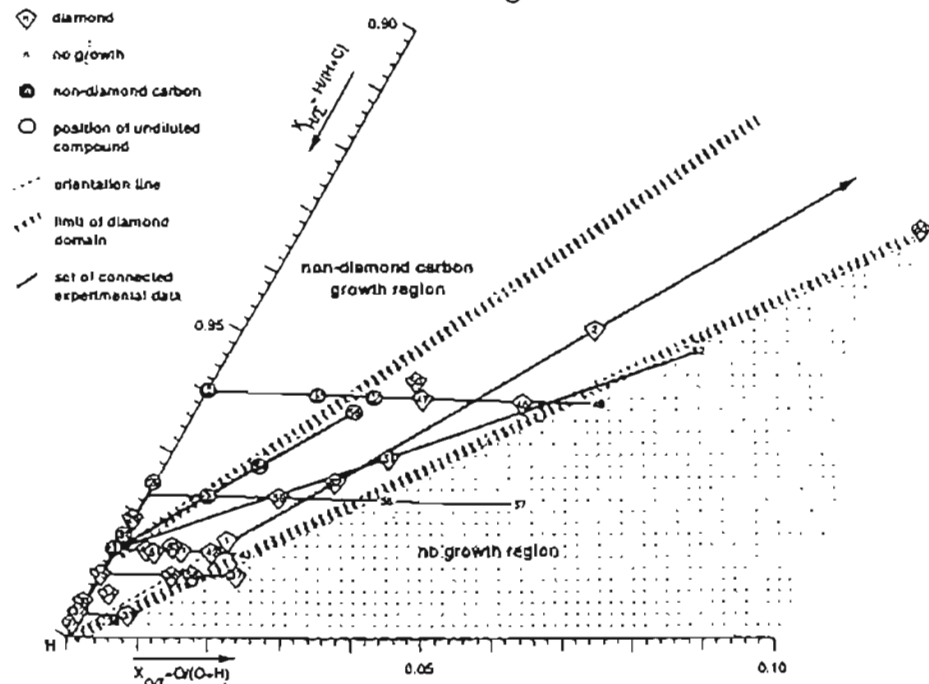
Figure 2.5.2   Enlarged Hydrogen-Rich Region of the Phase Diagram
                 where most of the Plasma and Hot Filament
                 Experiments are Conducted (after Bachmann et al., 1991).
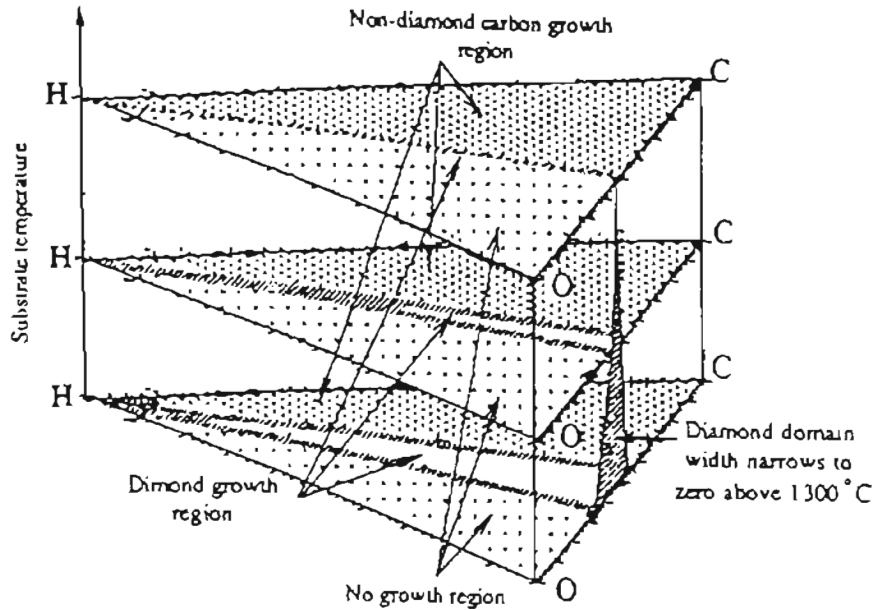
Figure 2.5.3   Effects of the Substrate Temperature on the Diamond
Domain in the C-H-O Phase Diagram
(after Bachmann et al., 1991)
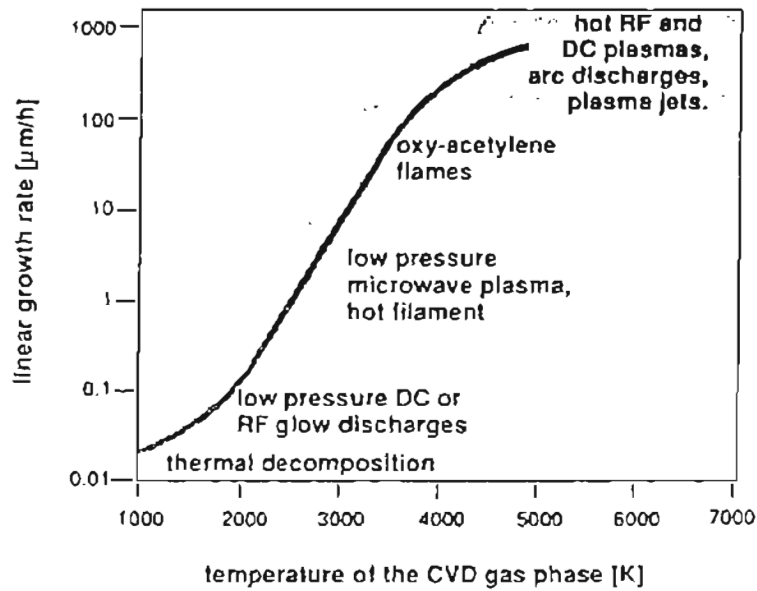
Figure 2.5.4   Variation of the Linear Growth Rate with Gas Phase
Temperatures (after Bachmann et al., 1991)

2.6   Role of Atomic Hydrogen

A major breakthrough in developing both the science and the technology of low-pressure diamond growth occurred when Russian scientists experimentally determined the importance of atomic hydrogen for enhancing the rates of diamond growth and reducing or eliminating graphite codeposition. They found that the addition of excess hydrogen to the hydrocarbon precursor gas led to less graphite codeposition, just as Chauhan et al., (1976) had determined, but the Russian scientists also discovered that "activating the gas prior to deposition increased the diamond growth rates from Å/hr to μm/hr. An electron discharge in the system and a hot filament over which the gas flows before encountering the lower temperature deposition region were the two mechanisms that were used to activate the gas (Spear, 1989).

Deryagin et al., (1977) proposed that a super equilibrium concentration of atomic hydrogen at the growth surface is responsible for the major reduction of graphite codeposition. They argued that atomic hydrogen behaves like a "solvent" for graphite. Their studies of the relative etching rates of diamond and graphite showed that the removal of graphite by activated hydrogen was orders of magnitude faster than that for diamond. As a part of their diamond growth studies Angus et al., (1968) had previously determined that molecular hydrogen would thermally etch graphite at a rate almost 500 times faster than it would etch diamond, but this graphite removal process was performed in a separate cycle from the diamond growth process.

Setaka (1987) reported etching rates of graphite, glassy carbon, and diamond in a hydrogen plasma under typical activated growth conditions for diamond to be 0.13, 0.11, and 0.006 mg/(cm^2.hr) respectively. Saito et al., (1988) also showed much greater etching rates for graphite than for diamond when subjecting the materials to microwave plasmas of either hydrogen or hydrogen-1.6 mol% water mixtures. Oda et al., (1986) reported that the growth rates and quality of diamond films were enhanced by the H atoms generated by a microwave plasma. They noted that impurities such as C and O were efficiently removed by active H-atom reactions and that the dangling bonds on the surface of epitaxial films were effectively passivated by H atoms.

2.7 Role of Hydrocarbon Precursor

Sato et al.,(1987) deposited diamond films from gaseous mixtures of various hydrocarbons and hydrogen by plasma-assisted deposition and found that the nature of the hydrocarbon precursor had little effect on the deposition behavior. Both saturated and unsaturated hydrocarbons were used and similar growth features were noted for all hydrocarbons when comparisons were made as a function of the C/H ratio in the input gas. The density of nucleation and the growth rates were found to be essentially the same as those observed with the more commonly used CH$_4$.

The relative independence of diamond growth on the nature of the input hydrocarbon species is consistent with the fact that most hydrocarbon sources tend to transform to common product species (such as acetylene, one of the most stable of such gaseous products) under environments such

as those found in high temperature pyrolysis, combustion, plasmas and other typical methods used for the activating precursor gases in diamond deposition (Spear, 1989). Supporting this is the observation that approximately the same growth conditions (temperature, pressure, concentrations of precursors) are needed for the crystalline diamond growth, regardless of the method of activation. The method of activation influences the rate of diamond growth, but not the general structure of the deposited crystallites. This also supports the conclusion that the same general growth species are produced by all activation methods that produce crystalline diamonds (Spear, 1989).

2.8 Diagnostics of Activated Gas

Matsumoto et al., (1985, 1987), Saito et al., (1986), Mitsuda et al.,(1987), and Harnett (1988) have all conducted emission spectroscopic analyses of microwave-plasma activated hydrogen-hydrocarbon mixtures and detected the species of H_2, atomic H, C_2, and CH. Matsumoto et al. (1985) examined a hydrogen plasma with no hydrocarbon in the gas and no substrate and observed the emissions of molecular and atomic hydrogen. Upon placing a graphite substrate in the hydrogen plasma, emissions corresponding to CH, C_2, and H were observed. Mass spectroscopy measurements of the plasma showed C_2H_2 to be the main reaction product of the chemical etching of the carbon.

Attempts have been made by Mitsuda et al., (1987) to correlate the emission spectroscopy intensity ratio of CH-H radicals to diamond formation and C_2 radical concentrations to graphite formation. However,

other species, such as CH_3 radicals and C_2H_2, which cannot be detected by the emission spectroscopy techniques, are probably the main precursors to diamond growth. Therefore correlation between CH and C_2 emission spectroscopy intensities and relative concentrations of CH and C_2H_2 in the activated gas are needed.

IR diode laser absorption spectroscopy was employed as an insitu method to examine gas-phase species present during filament-assisted deposition of diamond films by Cecil et al., (1988). From a reactant gas mixture of 0.5 mole % methane in hydrogen, acetylene (C_2H_2), methyl radical (CH_3), and ethylene (C_2H_4) were detected above the growing surface, while ethane (C_2H_6), various C_xH_y hydrocarbons, and methylene (CH_2) radical were below their sensitivity levels. These authors noted that their findings were consistent with the Frenklach-Spear growth model (1988) for propagating (111) planes through the addition of acetylene to activated surface sites.

Harris et al., (1988a, 1988b) obtained similar results from the mass spectral data in a hot filament assisted diamond growth system as a function of filament to substrate distance. In addition to the mass spectral sampling of the gas, they also performed detailed chemical kinetic calculations and suggested that diamond growth came mainly from acetylene and/or methyl radical precursors, but that the contributions from methane and ethylene could not be ruled out. Subsequent research by other workers established that the about 90 % of the diamond film was produced from methyl radicals and the remainder from acetylene (Wei et al., 1995).

2.9   Deposit morphologies

The morphologies of CVD diamond crystal obtained by transport (Spitsyn et al., 1981), filament (Matsumoto, et al., 1982), rf plasma (Matsumoto, et al., 1985), and microwave plasma (Kamo, et al., 1983) techniques show striking similarities and analogous temperature dependencies of the crystal habit (Badzian et al, 1988). The morphology of vapor-deposited diamond crystallites is dominated by cubic {100} and octahedral {111} surfaces and {111} twin planes. Cubo-octahedra exhibiting both {100} and {111} surfaces are common. Matsumoto et al., (1983) utilized electron microscopy to examine the structures of diamond crystals grown in a hot filament assisted CVD system and observed that the typical crystal habits were cubo-octohedra and singly and multiply twinned particles. Utilizing microwave plasma assisted CVD, Kobashi et al (1987, 1988a, 1988b) found that {111} faces dominated for substrate temperatures of about 800 °C and methane concentrations of < 0.4 mol%. When the CH_4 concentration was between 0.4 % and 1.2 mol% {100} surfaces dominated, but at higher concentrations the deposits were structureless. Badzian et al., (1988), reported that, at temperatures of 900 °C and lower, {111} faces dominate the crystallite morphology, and at 1000 °C and higher, {100} faces are predominant. At low CH_4 concentrations, {111} faces are predominant, and, at high concentrations, {100} faces are predominant. This observation is consistent with those of Kobashi and co-workers, and the earlier work reported by Spistyn et al.,(1981). The latter authors observed octahedral crystals with {111} faces with growth temperatures of 800 °C and regular cubo-octahedra with {111} and {100} faces at 1000 °C. However, Haubner et al.,(1987) observed morphological results that are not consistent with the

above observations. They reported that in their microwave-plasma assisted deposition system, cubic crystals with {100} surfaces dominated at low CH_4 concentrations (0.3%), low substrate temperatures (600 ºC), and medium plasma intensity. At higher plasma intensities, but the same concentration and substrate temperature, cubo-octahedra ({100} and {111} surfaces) were observed. At 750 º to 800 ºC and medium to high plasma intensities, octahedral crystals with {111} surfaces dominated. Low plasma intensities led to spherulitic crystallites at both lower and higher temperatures.

Barrat et al., (1993) correlated the diamond morphology with physical parameters of the deposition procedure such as gas composition, temperature variation and pretreatment of the silicon substrate. Diamond films with minimum structural defects such as stacking faults and twin planes were obtained by decreasing the substrate temperature. Substrate temperature was lowered by decreasing the microwave power. However, they found that lower microwave power resulted in a lower plasma density and decreased the concentration of active species and resulted in the deterioration of the film quality. Therefore, they suggest that good quality diamond films can be obtained by a compromise between a low substrate temperature and good plasma reactivity.

Ashfold et al., (1994), demonstrated that surface morphology is very sensitive to the gas ratio and substrate temperatures. Based on the parametric studies, Asfold et al., (1994) developed a schematic diagram of film morphology as a function of deposition temperature and methane concentrations for CVD between 20-80 Torr (Figure 2.9.1). It can be seen from the figure that triangular {111} facets, with many twin boundaries

tend to be most evident at low CH_4 ratio and low substrate temperatures. {100} facets, appearing both as square and rectangular forms, begin to dominate as the relative concentration of CH_4 in the precursor gas mixture, and/or the substrate temperature is increased. At still higher CH_4 concentration, the crystalline morphology disappears altogether.
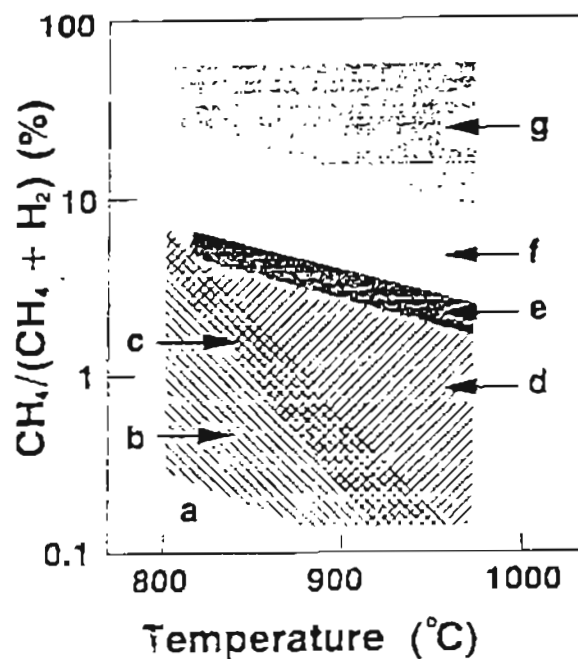
Figure 2.9.1   Schematic Diagram of Film Morphology as a Function of Deposition Temperature and Methane/Hydrogen Ratio for CVD Between 30-80 Torr. The Regions Correspond to Different Observed Morphologies: a) Little or no Deposition b) {111} c) {111} and {100} d) {100} e) {100} f) Disordered Graphite and/or nanocrystals of Diamond g) Fibrous Deposits of Soot or Disordered Graphite (Ashfold et al., 1994)

In addition to the cube and octahedral morphologies, flat hexagonal platelets and complex multiply twinned forms (e.g. decahedrons and icosdedrons) are also observed (Badzian et al., 1988; Angus et al., 1991, 1992). Twinned clusters, with many re-entrant surfaces, are the most common form, especially when in a regime that gives {111} octahedral

facets. Re-entrant corners arise from the intersection of (111) twin bands or stacking faults with the surface and were found to play a major role in enhancing diamond nucleation and growth rates (Angus et al., 1993). Sunkara (1992) found that many complex morphologies can arise from the enhancement of the growth rates by re-entrant corners arising from multiple stacking errors. Many other morphologies commonly observed , can be explained by the interaction of various combinations of stacking errors . They are summarized in Table 2.9.1 (Angus et al , 1993).

Table 2.9.1   Various Morphologies Observed During CVD of Diamond

Angus et al., (1993)

Type of Error	Morphology
Two stacking errors on parallel planes (intrinsic or extrinsic stacking fault or micro twin)	Hexagonal platelet
Three stacking errors on parallel (111) planes	Truncated hexagonal platelet
Two stacking errors on non-parallel (111) planes	Decahedral (pseudo five-fold symmetry)
Three stacking errors on non-parallel (111) planes	Icosahedral
Single stacking error	Triangular (macle)

2.10   Substrate Materials

Diamond has been vapor deposited on a wide variety of substrate materials, though the dominant substrate has been single-crystal silicon. Examples of substrate materials used are Si, Ta, Mo, W, SiC, WC and

diamond (Nishimura et al., 1987), Au, Si, Mo, W, and diamond (Spistyn et al., 1981) and diamond, graphite, Si, SiC, SiO_2, and Ni (Badzian et al., 1988). In their review on diamond thin films by various CVD methods, Asfold et al., (1994) summarize the properties required of a substrate to be able to support an adherent film of diamond. The substrates must a high melting point , higher than the temperature range (1000-1400 K) required for diamond growth. This precludes the use of existing CVD techniques to diamond coat plastics or low melting metals like Al. They also suggested that the tendency of the substrate to form a carbide might be helpful, though not essential. Also the substrate material should have a low coefficient of thermal expansion. Figure 2.10.1 is a bar graph showing typical values of thermal expansion coefficient for a variety of substrate materials at 300 K. Since the CVD growth takes place at elevated temperatures it is almost the case that upon cooling back to room temperature, the substrate will have contracted more than diamond film. As a result, the latter will be under compressive stress. This is manifested by the shifting of the Raman peak from 1332 cm^{-1} (Knight et al., 1989). Thus the mismatch in the coefficients of thermal expansion for diamond and the substrate is an important factor in determining the adhesion of the diamond film to the substrate.

Lux et al, (1996) reviewed the possible interactions at the diamond - substrate interface and classified the substrates into three classes

1. Little or no C solubility or reaction: These include metals such as Cu, Sn, Pb, Ag, and Au as well as non-metals such as Ge, sapphire, diamond itself, and graphite, although in the latter case etching will occur concurrently with diamond growth.

2. C diffusion: Here, the substrate acts as a carbon sink, whereby deposited carbon dissolves into the metal surface to form a solid solution. This causes large amounts of carbon to be transported into the bulk, leading to a temporary decrease in the surface C concentration, delaying the onset of nucleation. Metals such as Fe, Co, Ni, Pt, Pd, Rh belong to this class. For these substrates, carbon diffusion occurs until the entire substrate is saturated and the nucleation starts after the substrate surface is saturated.

3. Carbide Formation: These include metals such as Ti, Zr, Hf, V, Nb, Ta, Mo, W, and Cr) and non-metals such as B, or Si, and Si-containing compounds such as SiO_2 and Si_3N_4. Substrates composing of carbides themselves, such as, SiC, WC, and TiC are also particularly amenable to diamond deposition.
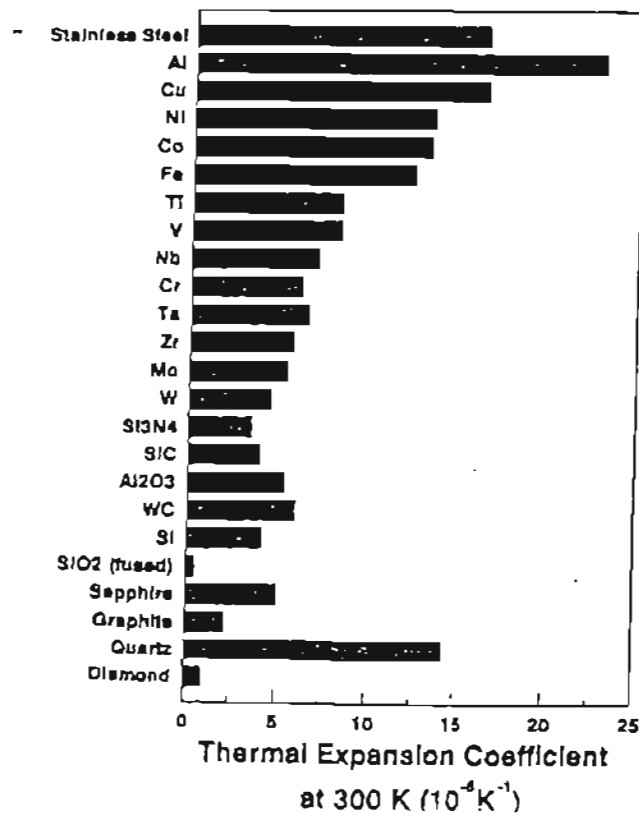
Figure 2.10.1   Bar Graph Showing Typical Values of Thermal Expansion Coefficients for a Variety of Substrate Materials (Ashfold et al., 1994)

2.11 Energetics of Gas-Solid Growth Interface

The heart of the hypothesis on "metastable' diamond growth rests on the fact that the diamond growth process occurs at the gas-solid interface in the carbon-hydrogen system (Spear, 1989). The vapor-growth process does not involve just elemental carbon, the one component which is represented on the phase diagram, but it also involves hydrogen. A diamond carbon surface saturated with sp^3 C-H bonds is more stable than a carbon surface free of hydrogen. Once a surface carbon is covered by another diamond growth layer, then the covered carbon possessing four sp^3 C-C bonds is metastable w.r.t to a graphitic carbon. Thus, according to Spear an upper temperature limit for vapor growth of diamond is determined by the kinetics of the diamond-graphite solid-state transformation.

A diamond structure with puckered {111} planes stacked in their ABCABC... sequence above the stacking of the hexagonal planes of graphite is shown in Figure 2.11.1. Lander et al.,(1966) were the first to hypothesize that hydrogen can stabilize a diamond surface by forming sp^3 C-H bonds with the surface carbons. Without the hydrogen's maintaining the sp^3 character of these surface carbon atoms, it is easy to imagine the {111} diamond planes collapsing into the more stable planar graphite structure during the growth process (Spear, 1989). In the absence of hydrogen, the surface atoms on cleaned bulk diamond crystals will reconstruct from their bulk-related surface sites at about 900 ° - 1000 °C (Badzian, 1988; Field, 1979; Pandy, 1982; Pate, 1986). However, in the presence of hydrogen, the reconstruction reverses as dangling surface sp^3 bonds become satisfied by C-H bonding (Landel et al., 1966).
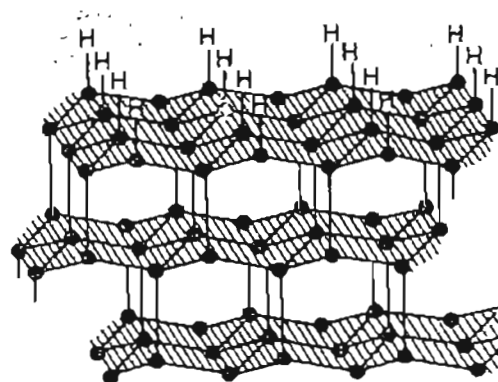
DIAMOND

GRAPHITE

Figure 2.11.1   Schematic Diagrams Showing the Similarities in the Crystal Structures of Diamond and Graphite (Spear, 1989)

The net saturation of a C=C double bond with hydrogen has a favorable negative enthalpy change (ΔH^0 (reaction) = -126 kJ).
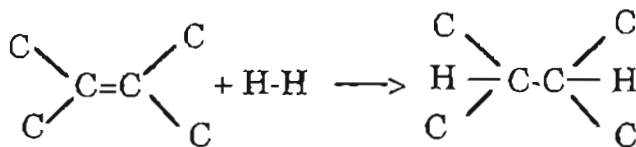
However, an activation energy to produce either a carbon or a hydrogen radical will be required to get a net reaction to proceed at a significant rate. Likely mechanistic radical reactions are (Spear, 1989):

$$\begin{array}{ccc}
\text{C} & & \text{C} \\
\diagdown & & \diagup \\
& \text{C=C} & \\
\diagup & & \diagdown \\
\text{C} & & \text{C}
\end{array} \quad + \text{ H}\cdot \quad \longrightarrow \quad
\begin{array}{ccc}
& \text{C} & \text{C} \\
& \diagdown & \diagup \\
\text{H} & \text{C-C} & \cdot \\
& \diagup & \diagdown \\
& \text{C} & \text{C}
\end{array}$$

$$\begin{array}{ccc}
& \text{C} & \text{C} \\
& \diagdown & \diagup \\
\text{H} & \text{C-C} & \cdot \\
& \diagup & \diagdown \\
& \text{C} & \text{C}
\end{array} \quad + \text{ H-H} \quad \longrightarrow
\begin{array}{ccc}
& \text{C} & \text{C} \\
& \diagdown & \diagup \\
\text{H} & \text{C-C} & \text{H} \\
& \diagup & \diagdown \\
& \text{C} & \text{C}
\end{array} \quad + \text{ H}\cdot$$
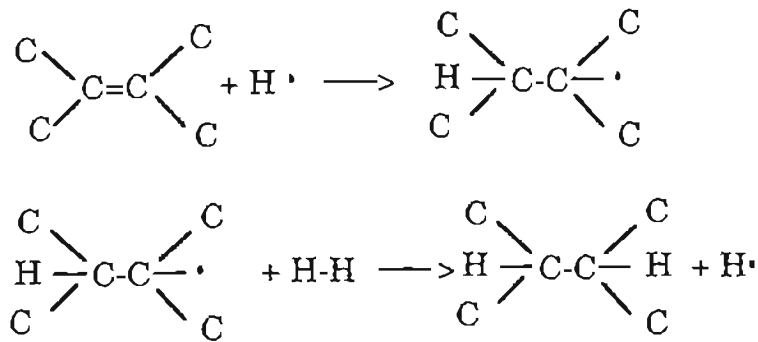
A hydrogen radical attacks the C=C double bond to produce a carbon radical, which then reacts with a hydrogen molecule to complete the saturation and regenerate a hydrogen radical. This is in agreement with the fact that only when gas activated vapor deposition methods were first employed in the 1970s did the growth rates of crystalline diamond become large enough to be of technological interest. The source of hydrogen atoms can serve the dual role of hindering graphite growth as well as etching away any that does not nucleate on the growing diamond surface.

The thermodynamics of the deposition process may place a lower limit on the deposition temperature for given total pressures and gas concentrations. Lander et al (1966) indicate that the mobility of carbon on a (111) diamond surface is appreciable at 1000 °C. Figures 2.11.2 show the plots of the output of equilibrium calculations to illustrate how the deposition limits depend on experimental parameters. Similar calculations were performed by other researchers and the following important observations were made (Bichler et al., 1987; Sommer et al., 1988):

1. The fraction of carbon deposited changes from practically zero at lower temperatures to close to 100 % over 200 °C.

2. High pressures and /or low methane concentrations increase the lower temperature limit to obtain any deposit.

Thus, thermodynamic considerations set a lower limit on diamond growth of about 400 ° to 600 °C, depending on specific pressure-composition conditions, unless "non equilibrium" bombardment techniques are used. These techniques always produce some diamond-like carbon (DLC), or some defective form of carbon along with crystalline or microcrystalline diamond (Messier et al, 1987).
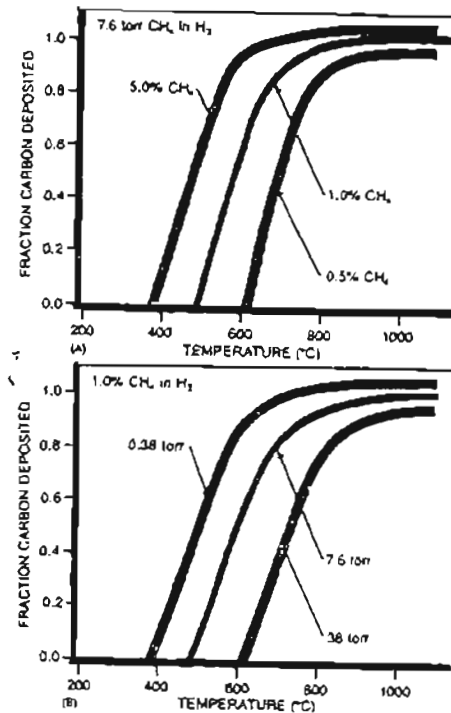
Figure 2.11.2   Equilibrium Plots of the Fraction Carbon Deposited from Methane-Hydrogen Mixtures as a Function of Temperature a) Constant Total Pressure b) Constant Methane Content (Landler et al., 1966)

Angus et al., (1993) summarized the basic energetics of the entire diamond deposition process.   Table 2.11.1 gives the principal reactions along with an estimate of their standard enthalpy and free energy changes.

Table 2.11.1 Principal Reactions occurring during CVD (Angus et al., 1993)

Reaction		T(K)	ΔH^o (kcal/mol)	ΔG^o (kcal/mol)
	on filament /plasma discharge			
1	$H_2 \longrightarrow 2H$	2500	+109	+37
	in gas phase			
2	$H + CH_4 \longrightarrow CH_3 + H_2$	1800	0	-11
3	$H + H + M \longrightarrow H_2 + M$	1800	-108	-57
4	$CH_3H + H + M \longrightarrow CH_4 + M$	1800	-108	-45
5	$CH_3 + CH_3 + M \longrightarrow C_2H_6 + M$	1800	-86	-26
6	$C_2H_x + H \longrightarrow C_2H_{x-1} + H_2$	1800	small	small
	on Substrate (S)			
7	$H + S \longrightarrow S\text{-}H$	1200	-94	-68
8	$S\text{-}H + H \longrightarrow S + H_2$	1200	-13	-6
9	$CH_3 + S \longrightarrow S\text{-}CH_3$	1200	-81	-47

Reaction 1 has a very positive enthalpy change. The atomic hydrogen, once formed undergoes several spontaneous , highly exothermic reactions. It can react with hydrocarbons in the gas phase, abstracting hydrogen to form methyl radicals (reaction 2), or can recombine with another atomic hydrogen to form molecular hydrogen (reaction 3). However, since it is a three body reaction, its rate is slow at low reactor pressures and often can be ignored despite the favorable free energy change (Angus et al, 1993). Methyl radical destruction can take place by

recombination with atomic hydrogen (reaction 4) or by diffusion out of the reaction zone to the walls of the reactor. Reaction 5 represents the possibility of formation of higher molecular weight species. A spectrum of C_2H_x species can be formed by subsequent hydrogen atom abstraction reactions of the general type shown in reaction 6. Reaction 7 represents the hydrogenation of a bare diamond surface. Hydrogen can also abstract hydrogen from a hydrogen covered surface as shown in reaction 8. This reaction is thermodynamically favored because of the strong H-H bond. The fractional coverage of the surface at typical substrate temperatures is dominated by the competition between reactions 7 and 8.

Assuming the reactions to be of first order the steady state concentration of free radical sites, fs, is given by the relation

$$f_s = k_8/(k_8 + k_7) \hspace{3cm} \text{(Angus et al., 1993)}$$

where, k_7 and k_8 are the first order rate constants for reactions 7 and 8. f_s can be estimated using kinetic constants for analogous gasphase reactions. At temperatures of 1000 and 1750 K, f_s was estimated to be 0.12 and 0.37 respectively (Kuczmarski, 1992). According to Angus and coworkers (1993), these sites are where free radicals such as CH_3 (reaction 9) or acetylenic species, C_2H_x, can add to the surface. The hydrogen atom recombination could be direct through reaction 3 where the surface plays the role of the third body or it could result as the net reaction from the two step process of reactions 7 and 8.

2.12 Diamond Nucleation

Matsui et al., (1983) proposed, on the basis of symmetry arguments, that hydrocarbon cage compounds might serve as diamond precursors. It was also proposed that a more likely precursor for diamond nucleation would be graphitic intermediates, which are subsequently hydrogenated by atomic hydrogen to saturated structures that can act as sites for diamond growth (Angus et al., 1988; Sunkara et al., 1990). Belton et al., (1990) studied the nature of carbon bonding at different stages of nucleation on platinum substrates using X-ray photoelectron spectroscopy. They found that a carbon phase with graphitic bonding is first formed, followed by a hydrogenated carbon phase and finally diamond. Microbalance studies of diamond nucleation and growth on platinum show an initial induction period in which an oriented graphite deposit forms (Wang et al., 1993). Subsequently, this deposit disappears and the final deposit contains only polycrystalline diamond. In an attempt to understand diamond nucleation, Angus et al (1991) used graphite flakes as seed crystals. They observed that the (111) diamond plane was parallel to the basal (0001) plane of the graphite. Subsequent experiments by Li et al., (1992) showed that in addition to the (111) diamond ‖ (0001) graphite, there is also a directional orientation within the planes, i.e. [$1\bar{1}0$] diamond ‖ [$11\bar{2}0$] graphite. This relation would mean that the puckered six-membered rings in the diamond (111) planes would retain the same orientation as the flat six-membered rings in the graphite basal (0001) plane. Figure 2.12.1 shows the transmission electron micrograph of one of the oriented diamond crystals on graphite, and the geometric relationship between the two structures.
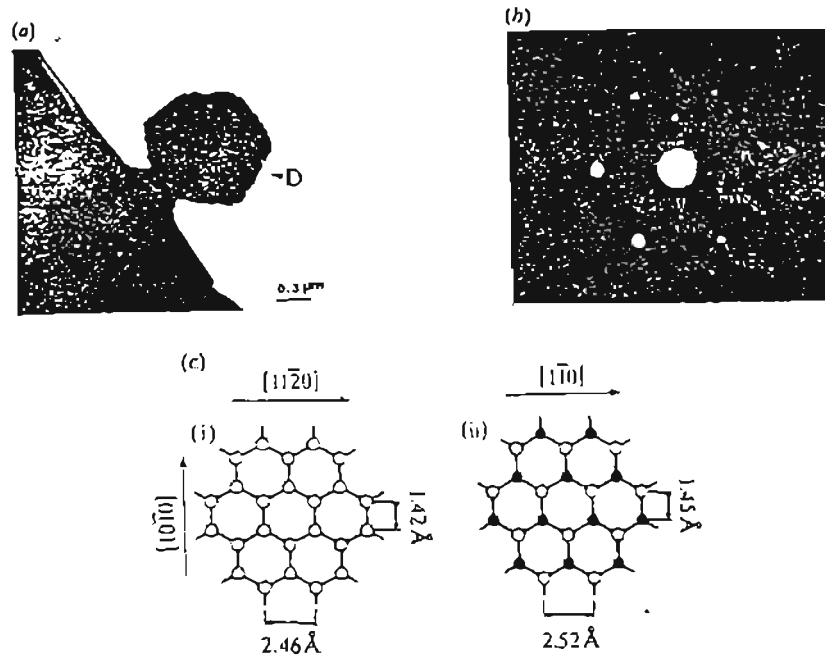
Figure   2.12.1   TEM of Oriented Diamond Crystals on Graphite along with Corresponding Electron Diffraction Pattern and the Geometric Relationship Between the Two Structures (Li et al., 1992)

Badziag et al., (1990) pointed out that hydrogen terminated 'diamonds' less than 3 nm in diameter have a lower energy than hydrogen terminated graphitic nuclei with the same number of carbon atoms. This means that in an environment rich in atomic hydrogen, the sp^3, tetrahedrally coordinated nuclei are energetically favored over the sp^2, trigonally coordinated nuclei. Stein (1990) criticized the above work and pointed out that the correct parameter to consider is the free energy change for the appropriate reaction. However, Stein neglected to account for the fact that the active reagent under diamond growing conditions is atomic hydrogen, H, not molecular hydrogen H_2. The enthalpy and free energy

46

changes for the sequential hydrogenation of graphite to naphthalene and decalin by atomic hydrogen were calculated as (Badziag, et al., 1990):

Graphite $+ 8 H \longrightarrow$ Naphthalene $+ 10 H \longrightarrow$ Decalin

$$\Delta G^0 = -904.6 \text{kJmol}^{-1}$$
$$\Delta G \leq -356.4 \text{kJmol}^{-1}$$

$$\Delta G^0 = -1338.3 \text{kJmol}^{-1}$$
$$\Delta G \leq -653.1 \text{kJmol}^{-1}$$
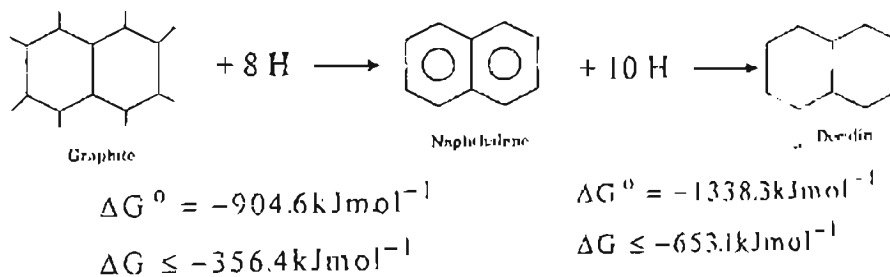
The estimated free energy changes at reaction conditions are strongly negative for these model reactions, which show that graphite nuclei can indeed be converted into hydrogen saturated structures similar to diamond. Molecular orbital studies of the hydrogenation of single graphite sheets also support this conclusion (Angus et al., 1991; Mehandru et al., 1992a, 1992b;Walter et al., 1993; Jung Nickel et al., 1996).

The nucleation sequence may start with the formation of high molecular graphitic and polynuclear aromatic hydrocarbons (PAH) by the sequential polymerization of acetylene (Frenklach et al., 1985). These high molecular weight materials are sufficiently non-volatile so that they remain on the substrate until they become hydrogenated by atomic hydrogen forming the saturated edge structure that is attractive to diamond nucleation. The atomic hydrogen plays a multiple role in this process. By terminating the dangling surface bonds it stabilizes the tetrahedrally coordinated sp^3 nuclei with respect to the trigonally coordinated, sp^2 nuclei. It also serves as a reactive solvent which permits the conversion of

graphitic nuclei into diamond nuclei, thereby circumventing the large activation barrier separating graphite from diamond. (Angus et al., 1993). The mechanism is consistent with the observations of Lux and coworkers, who showed that induction time for nucleation are shortest on those metals that can achieve a supersaturation of carbon on the surface most rapidly (Lux et al., 1991, 1993, 1996).

2.13 CVD Diamond Growth Mechanisms

Significant advances have also been made towards the understanding of CVD diamond growth mechanisms (Wei et al, 1995; Heggie et al., 1996).

Tsuda etal. (1987) conducted quantum chemical computations in order to determine the lowest energy path for a proposed mechanism of diamond growth on {111} surfaces. According to them the reaction proceeds in two steps. In the first step the {111} plane of the diamond surface is covered by the methyl groups via methylene insertion or hydrogen abstraction followed by the methyl radical addition. In the second step, following the attack of a methyl cation and the loss of three hydrogen molecules, three neighboring methyl groups on the {111} plane are bound together to form the diamond structure. Constant supply of methyl radicals should be ensured and the surface should maintain a positive charge to sustain epitaxial growth. However the critical effect of hydrogen atoms on the growth is not explained by this mechanism.

Frenklach and Spear (1988) have proposed an alternative mechanism for the growth of diamond on {111} surface of diamond. Acetylene was the

main monomer growth species in this mechanism. The mechanism basically consists of two alternating steps : The first step is the surface activation by H-atom removal of a surface-bonded hydrogen .

$$C \atop H\bullet + \underset{\displaystyle C}{\overset{\displaystyle\backslash}{C\text{-}H}} \text{------}> H_2 + \underset{\displaystyle C}{\overset{\displaystyle C \backslash}{C\bullet}}$$
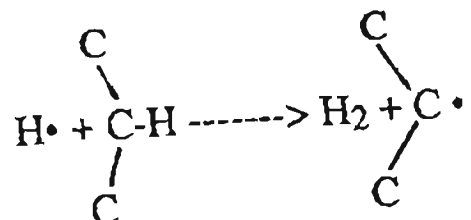
In the second step, this surface activated carbon radical acts as a site for adding more carbons to the structure by reacting with acetylene.

$$\underset{\displaystyle C}{\overset{\displaystyle C\backslash}{C\bullet}} + H\text{-}C\text{=}C\text{-}H \text{-----}> \underset{\displaystyle C}{\overset{\displaystyle C\ \ H\ \ H}{C\text{-}C\text{=}C\bullet}}$$
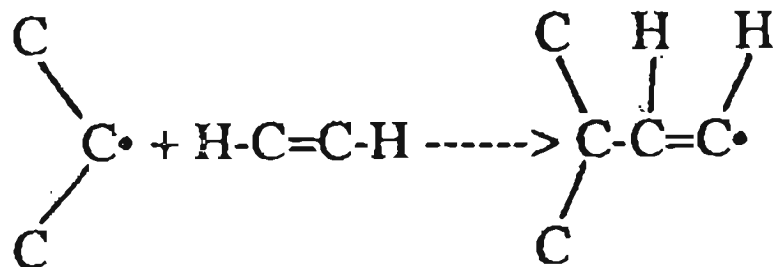
The propagation of a growth step on the [111} plane then proceeds by additional radical reactions. The propagation results in the addition of two acetylene molecules for one hydrogen abstraction step, with the resulting regeneration of the hydrogen atom which was consumed in forming the activated surface site.

Kobashi et al., (1988) conducted detailed investigations on the growth of diamond films in microwave plasma. With methane concentrations of 1.2 % and growth periods spanning about 60 hours, periodic observations on SEM revealed cyclic growths of micro-crystallites of diamond along with the already developed facets. As these microcrystallites grew and developed

into facets, new microcrystallites began to evolve and this process repeated. This suggested that diamond films grew cyclically through micro-crystal formation due to the higher order growth followed by the formation of well-defined diamond faces. They explained the restructuring process as follows:

- Increase in the areas of primary diamond faces
- overgrowth of small crystallites on well defined faces
- "fusion" of a group of small crystallites to form well-defined larger faces, and finally
- "absorption" of small crystallites into larger faces.

Peploski et al (1992) reported the elementary reactions involved in the low pressure synthesis of diamond using MD studies. They modeled the C(111) surface with an ensemble of 127 atoms and adopted the velocity reset procedure to incorporate the thermal effects of the bulk. Brenner potential for hydrocarbons was employed in all calculations for both the surface and incident gas phase molecules. Their calculations support the suggestion advanced by Belton and Harris (1992) that if acetylene is involved directly in the growth process, it probably incorporates into the lattice by the formation of 2 C-C bonds. However their results suggested that ethynyl radical C_2H may be an even more important growth species. They found that the sticking coefficient of acetylene on a clean C(111) surface lie in the range 0.25-0.33 for incident translational energies between 1.5-2.0 eV with surface temperatures in the range 1000-1500 K. Chemisorption of acetylene most frequently involves the formation of two $C_{(s)}$-C single bonds to adjacent adsorption sites on the C(111) surface. The addition of a second acetylene molecule to form an ethenyl radical is a very low probability process for all

surface structures investigated. When such chemisorption does occur, the probability of subsequent desorption is large unless the ethenyl radical is able to subsequently form a second C-C bond to the surface. Addition of a $C\equiv CH$ radical to a chemisorbed acetylene proceeds with a much higher probability than is the case for C_2H_2. The ethynyl radical is also chemisorbed readily to the other surface structures with a low probability of subsequent desorption. The authors suggest that C_2H is an important diamond-growth species even in experiments where its concentration is one or two orders of magnitude less than that of acetylene.

Chang et al (1993) calculated the reaction probabilities, cross sections, rate coefficients, frequency factors, and activation energies for hydrogen-atom abstraction from a hydrogen-covered C(111) surface. The authors employed classical trajectory and quantum wave packet methods on the empirical hydrocarbon potential hyper surface developed by Brenner (1990) for their calculations. The activation energies for the hydrogen atom abstraction were found to vary from 0.0 to 1.063 eV. They found that some sp^2 bonded hydrogen atoms can be removed in a barrierless process if they are adjacent to a carbon radical. Abstractions that produce a methylene carbon are associated with much larger activation energies in the range 0.49-0.82 eV. Hydrogen abstraction from sp^3 carbon atoms are found to have activation energies ~ 0.4 eV. Based on the results they suggest that hydrogen abstraction rates are strongly dependent on the bonding structure involved and the development of an accurate phenomenological model for diamond-film growth needs a careful examination of the expected rates for each of the elementary reactions that might contribute to the process.

Subsequently, Chen et al (1993) calculated the minimum-energy paths for the important elementary reactions that include hydrogen atom abstraction and migration, C_2H_2, C_2H and hydrogen atom addition to a carbon radical site and six-membered, carbon ring closure. They found that the reaction barrier for addition of C_2H_2 or C_2H via C_s-C single bond formation is within the range of thermal energies available at temperatures typical of diamond CVD experiments. Chemisorption of ethynyl radicals (C_2H) was found to lead to a more stable surface product which is much less likely to undergo subsequent desorption than in the case for the corresponding addition of C_2H_2. The reaction barriers to the creation of a carbon radical site via abstraction of a surface sp^3-bonded hydrogen atom and via hydrogen migration were calculated to be 0.529 eV and 1.62 eV respectively. They suggest that the diamond growth mechanism involves either the formation of two radical sites via hydrogen atom abstraction or the chemisorption of a radical species such as C_2H instead of C_2H_2, with hydrogen abstraction being the rate-determining step.

Perry et al (1994) calculated the rate coefficients, event probabilities and dissociation probabilities for several elementary chemisorption reactions on a diamond (111) terrace structure at 1250 K. The chemisorbing molecules and radicals that were investigated include C_2H_2, C_2H, CH_3, CH_2, C_2H_4, C_2H_3, C, C_2, C_3, C_3H and H. They found that the ethylene chemisorption plays only a minor role in diamond film formation on a terrace. They also observed that acetylene chemisorbed more readily on a terrace than on ledge structure while CH_3 preferentially chemisorbs at edges and corners rather than on terraces. Though CH_3 radical was found to be least reactive, since it is present in large concentration in most CVD

experiments they suggest that CH_3 is an important growth species along with C_2H_2. Atomic carbon was found to have the largest chemisorption rate coefficient of all the species investigated. The authors suggest that atomic carbon will be an important growth species in plasma experiments where its concentration is sufficiently high.

A kinetic Monte Carlo simulation of diamond film growth from acetylene and hydrogen has been carried out by Xing et al (1993). In this work acetylene and hydrogen were impacted in a ballistic manner on a diamond [111] surface covered with hydrogen. Surface reactions were modeled by barrier-hopping Monte Carlo moves and energies were calculated from the Brenner potential. They observed that deposition occurs more readily at terraces as opposed to ledges. The fact that the surface that evolved from the simulations was rougher than the observed surface led them to conclude that acetylene alone was not likely to produce high-quality diamond films.

Clark et al (1996) report the results of the kinetic Monte Carlo simulations of early stages of diamond film growth from a C[111] substrate via methyl radical and Hydrogen. They observed that the surface growth primarily consists of the formation of linear bonded chains, which may close off into rings for short time intervals. The simulation was conducted as a function of time for the first 20 ms of CVD diamond film growth. At this early stage they found that stable ledges of tetrahedral carbon was just beginning to form. They observed that the substantial overlayer will subsequently occur over the substrate before large-scale relaxation into the crystalline phase can begin. Hence they suggest that this should occur on a time scale of seconds since an experimental growth rate of 0.5 μm/hour

corresponds to about 1.5 Å of vertical growth, which corresponds to roughly one layer per second.

A hybrid Monte Carlo simulation method consisting of kinetic and equilibrium methods was developed by Clark et al (1996). The authors applied this hybrid method to investigate the early stages of CVD diamond growth. After 0.60 ms of kinetic Monte Carlo simulation they observed the formation of elongated chains of bonded chemisorbed carbons and closed rings and after 22.63 ms some surface ledges with diamond [111] symmetry. They explained the evolution of the surface morphology as follows. After the bare surface is sufficiently covered pair bonds are formed rapidly between adjacent chemisorbed methyl radicals, with strained surface bonds. After the methyl radicals approach closely to form a bond three-carbon "bridges " form, where a third carbon bridges the gap between two carbons chemisorbed to the original surface. These structures are required for the formation of a second diamond [111] layer. After sufficient pairs and triplets have formed on the surface, these clusters link into larger, linear clusters. Since these diamond like structures have formed from CH_3 radicals alone, they conclude that methyl is an important growth molecule for diamond films.

Mehandru et al (1992) investigated the structures and energetics for the sequential addition of hydrogen atoms to the extended {$10\bar{1}0$} zigzag edge of a graphite sheet using the atom superposition and electron delocalization (ASED) band technique. Their calculations showed that H can chemisorb strongly on the unsaturated rings located on the edge of a graphite sheet, transforming them to their fully saturated analogues. They

observed that the all-chair conformation structure is consistent with a general tendency for the diamond nuclei thus formed to have their {111} planes parallel to the basal plane of graphite. They suggest that the primary function of the graphitic ring structure may be simply to provide a thermally stable, nonvolatile substrate on which diamond precursor structures can form.

Angus et al (1993) proposed a mechanism to explain the nucleation of diamond from the gas phase through a graphitic intermediate. The corrugated hexagonal rings in the diamond (111) plane have the same spatial orientation as the flat hexagonal rings in the graphite (0001) plane. By energy minimization calculations they determined the relative energies of various interface models. They observed that a low energy interface is formed when three (111) diamond planes are joined to two (0001) graphitic planes. They also found that the interface energies are low compared to the surface energies even in the presence of dangling bonds on every three diamond layers and that when the dangling bonds are saturated with hydrogen, the interface energy is further reduced. The model reactions proposed by the authors involve the sequential conversion of monatomic gas phase carbon species to aromatic sp^2 bonded species, to saturated sp^3 bonded species by reaction with atomic hydrogen. In the presence of hydrogen, the system can further reduce its energy by further condensing from sp^2, trigonally coordinated nuclei to the sp^3, tetrahedrally coordinated nuclei. Also, by application of empirical rules, the authors proved that in the absence of hydrogen, the system remains trapped as graphite and in the presence of hydrogen subsequent thermodynamically favored

transformations can take place that would result in hydrogenated diamond nuclei.

2.14 Diamond Coatings on Cutting Tools

Two approaches are generally taken for CVD diamond coatings on cutting tools (Komanduri, 1993). One is to grow thick (1-1.5 mm), free standing polycrystalline diamond and braze then on to the cemented carbide substrate. However, these tools have to be finished before use. In concept, this type, is not very different from the polycrystalline diamond made by HP-HT process. The other process is to develop thin coatings (2-5 μm) on cutting tools. This, in fact, is unique to the CVD diamond process as it is not possible and/or economical by the HP-HT process. Microwave CVD, hot filament CVD, combustion synthesis, and plasma torch are some of the techniques used either individually or in combination to deposit diamond coatings on cutting tools. The considerable advantage of this technique is that no subsequent finishing of the tool is required , thus saving considerably on the finishing costs. A review on the development of diamond coatings on cutting tools is given by Hintermann (1996). Flexibility in insert design is a big advantage of thin-film diamond coated inserts. Compared to the limited cutting edge geometry's of PCD tools, a diamond coated insert has multiple cutting edges (Koepfer, 1996).

Thin-film diamond coated carbide inserts are among frontier expanding tools. While the ability to deposit a thin layer of pure diamond on a carbide substrate has been a reality for many years, commercialization of the process is relatively recent. Al-Si alloys, copper, fiber-reinforced

56

composites, titanium, ceramics, and laminates are a few material candidates for these diamond coated tools (Koepfer, 1996).

Adhesion of the diamond coating on the WC substrate is a challenging problem. The cobalt binder used to hold together the carbide grains in an insert substrate creates a problem in achieving high adhesion between the diamond coating and the substrate (Okoli et al., 1989). To reduce the occurrence of cobalt, specially formulated carbide substrates (cobalt content less than 6 % or less) are used for diamond-coated inserts (Koepfer, 1996). However, the problem here is the lack of toughness. CVD diamond coatings are brittle when deposited on low cobalt substrates, and are not robust enough to endure high mechanical shock. Hence they are not always the best choice for heavy metal removal and interrupted cutting. However, when compared to the non-diamond inserts, a tool-life increase of 10 to 50 times is common (Koepfer, 1996).

Kennametal one of the major tool manufacturing company in the United States, developed a commercially available, 25 μm thick layer diamond coated insert (Vasilash, 1995). This insert was found to perform well in terms of both tool life and resulting part surface finish, in machining hypereutectic Al alloys. Kennametal also reported that in machining metal matrix composites (MMC s), such as Duralcan (Al with 22 % SiC particles dispersed throughout), a CVD diamond coated insert performed better then the PCD tool. In order to improve adhesion of diamond coatings, Kennametal has adopted the following techniques (Vasilash, 1995, Quinto, 1996):

1. Use a lower-cobalt substrate material to minimize the diamond-cobalt interaction.

2. Roughen the substrate surface.

3. Lower substrate temperatures during the deposition process.

4 High rate of diamond deposition during the process.

Crystallume claimed to be the first U. S. company to develop CVD diamond coatings on standard grades of tungsten carbide (Mason, 1990). Crystallume has also been active in the production of diamond coated carbide drills for circuit boards and diamond coated drill bits (Conner, 1994). The diamond coated Si_3N_4 ball bearings developed by Crystallume were found to last 100 times longer than the conventional steel ball bearings in high temperature and high load applications (Drory, 1997).

Norton company compared the tool wear between a free-standing diamond film produced by DC arc jet CVD and brazed to WC substrate and several grades PCD cutting tools in machining Al-18 % Si alloy (Hay et al., 1991). They found that the wear mechanisms of PCD's vary from that of CVD diamond in that the PCD's preferentially wear at the cobalt grain boundaries while the CVD diamond wears down by diamond itself by chipping away and wearing individual grains. They also claimed that a CVD thick diamond film had 2.25 X the wear life of 25 μm grain size PCD, when turning Al-18 % Si alloy. They also found good abrasion and crater wear resistance when turning abrasive non-ferrous materials such as A390 alloys.

The potential of CVD diamond as a cutting tool material has also been demonstrated by Yazu et al.,(1991) and Leyendecker et al., (1991). Three Japanese companies, namely, Mitsubishi, Toshiba, and Idemitsu

have been actively involved in producing diamond coated inserts (Mason, et al., 1990).

Mitsubishi Materials Corporation developed diamond coated WC throw away inserts (Kikuchi et al., 1991). The WC substrate was etched with dilute HNO_3 prior to the deposition in order to improve adhesion. Kikuchi et al., (1991) reported that the tool life of these inserts was 3-18 times longer than that of uncoated WC substrates, when used for milling Al-Si alloys.

Toshiba Tungaloy, another major tool manufacturing company in Japan, reported an improvement in adhesion of the diamond coatings by decarburizing the WC substrate in an H_2-O_2 plasma prior to the deposition (Saijo et al., 1991). They found that these diamond coated tools performed better than uncoated WC, in milling Al-18 % Si alloy in the speed range of 200-350 m/min. However, due to the interaction of the hard Si particles with the rough diamond surface, they observed microchipping of the diamond coating. Saiji et al., found that polishing of the diamond film was effective in prolonging the tool life as well as in improving the surface finish of the work material.

Idemitsu Petrochemical Company, has been developing diamond coated tools using microwave plasma CVD and test marketing these inserts in Japan. In an attempt to overcome the adhesion problem of diamond coatings on WC substrates, they replaced WC with Si_3N_4 (Mason et al., 1990). Diamond coated Si_3N_4 inserts developed by Idemitsu had a tool life 5-10 times more than uncoated Si_3N_4 inserts (Ito et al., 1991). Norton Company also reported that thin film diamond coated Si_3N_4 tools were

found to show considerable improvement in wear life over tungsten carbide inserts when machining abrasive materials(Stephen et al., 1992). Similarly, Sandvik an European based tool manufacturing company overcame adhesion problem by replacing WC tools with Si_3N_4 or SiAlON (Soderberg, 1991).

Shen (1996) assessed several thin film diamond coated inserts and drills obtained from several sources. He tested these inserts in machining hyper-eutectic 390 Al alloy containing 16-18 % Si and noticed a wide difference in the adhesion strengths of the diamond coatings on various Si_3N_4 and WC substrates. Figure 2.14.1 shows the comparison of performances of various tools. He noticed inconsistency in performance within a batch or among batches by the same coating source and comments that a good statistical process control method may be required to eliminate the inconsistency in the tool performance.
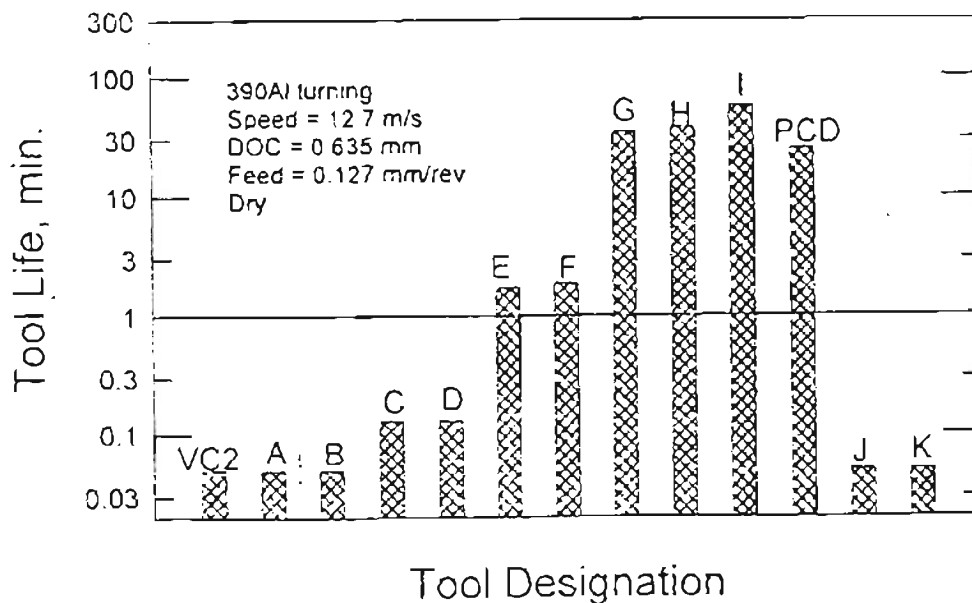
Figure 2.14.1 Performance Comparison Between a PCD Insert, an Uncoated Carbide (VC2), and CVD Diamond Coated Inserts from Various Sources (A-K) (Shen, 1996)

Cappelli et al., (1996) studied diamond deposition on different substrate materials such as cemented carbides (WC-6 % Co), Ceramics (SiAlON, Al_2O_3 + TiC) and whisker reinforced ceramics (Al_2O_3 + SiO_2, ZrO_2). They found that SiAlON substrates were the most suitable substrates for diamond deposition. Good quality adherent diamond coatings were also obtained on SiC/ZrO_2 whisker reinforced ceramic. They attributed the adhesion in this case, to the SiC whiskers acting as anchoring agents overcoming the large thermal mismatch between diamond and Al_2O_3. Even though the authors could obtain diamond coatings on other substrates (TiC + Al_2O_3, TiN), they found that the adhesion was not good on these substrates.

Ikeda et al.,(1996) compared the adhesion of diamond coatings on WC-6% Co and SiAlON substrates when machining Al-16%Si alloys and found that adhesion was better on SiAlON substrates.

CHAPTER 3

PROBLEM STATEMENT

The low pressure diamond synthesis technique for coating on cutting tools is still far from full development to meet the needs of large scale industrial applications. A thorough understanding of the CVD process, better control of the diamond deposition to reduce or eliminate structural imperfections in the films, and improving the quality and adhesion of diamond coatings on various substrate materials are some of the important areas requiring further investigation.

Low pressure diamond synthesis, being a relatively simple and inexpensive technique offers a great potential for diamond coated tools. Ceramics (Si_3N_4, SiAlON) and cemented carbides are the two candidate materials which are considered as the substrates. Thermal stresses are greatly reduced for diamond coatings on Si_3N_4 generated due to the closer matching of the thermal expansion coefficients . However, the total residual stress of the coating is the sum of thermal stresses and intrinsic stresses developed during the deposition process. If the deposition conditions are not properly chosen intrinsic stresses can develop which will deteriorate both the quality and the adhesion. While limited literature is available on the effect of various process variables on the quality and adhesion of diamond coatings on Si_3N_4 substrates, not much has been reported on the effect of process variables on the residual stresses.

Much of the literature on cemented carbides reports the detrimental effects of the cobalt binder in achieving good adhesion. The effect of cobalt seems to be strongly dependent on the deposition temperature. Based on the literature review it was also observed that there is some contradiction regarding the deposition temperatures. Some researchers suggest that the effect of cobalt can be reduced at low substrate temperatures (~ 750-800 ºC) while others claimed that high temperatures (~ 900-950 ºC) are more favorable for diamond deposition on WC-Co tools. Also, most of these experiments were conducted with WC- 6%Co. Very little has been published on the effect of deposition temperatures on cemented carbides with higher cobalt content. The results obtained for WC-6%Co may or may not be valid when the cobalt content in the tool is changed. Also, removal of surface cobalt is routinely adapted to reduce its adverse effects. However, the existence of surface cobalt on WC tools has not been established by any characterization technique. In this investigation efforts have been made to address some of these issues.

Better control of the deposition process requires the evaluation of various process variables and identifying the crucial parameters which would have maximum influence in diamond formation. In particular, for a given substrate, deposition conditions affect the film quality and adhesion through their influence on the content of diamond and non-diamond carbon components in the diamond film, the film morphology, and the residual stresses in the film.

Substrate material is itself another important variable. Diamond deposition has been reported on various substrate materials and the ease of formation of diamond on a substrate is related to its tendency of forming

stable carbides. However, the structure and stability of carbides is related to the electronic structure in particular to the 3d electrons. Chemical nature of the substrate is found to play an important role in determining the diamond growth. Limited literature is available on the role of the chemical nature of the substrate.

The present investigation was aimed at addressing some of the above issues, in specific:

1.   A systematic study on the effect of process variables on the nucleation, growth and quality of diamond coatings on cutting tools.

- Evaluation of the effect of various process parameters on the quality of diamond coatings on Si_3N_4.

- Characterization of the diamond coatings on Si_3N_4 using μ-Raman spectroscopy to determine the phase purity, relative amounts of diamond and non-diamond carbon phases, both qualitatively and quantitatively.

- Estimation of the residual stresses of the diamond coatings on Si_3N_4 by using μ-Raman spectroscopy.

- Investigation of the effect of process variables on the quality of the diamond coatings obtained on Si_3N_4 in order to determine the range of deposition parameters to produce high quality diamond coatings on a given substrate. This could be used as a basis for determining the optimum deposition conditions for a specific CVD reactor.

2. Investigation of the role of cobalt on the adhesion of diamond coatings on cemented WC cutting tools. WC cutting tools with different cobalt content (3 to 12%) are chosen for this purpose.

- Identification of surface cobalt by XRD.

- Investigation of various surface pretreatment techniques for the improvement of quality and adhesion of diamond coatings on cemented WC tools.

3. Qualitative evaluation of the adhesion of the diamond coatings on Si_3N_4 and cemented WC tools by indentation testing.

4. Investigation of the chemical nature of the substrate in relation to the low pressure CVD diamond growth. This involves diamond growth studies on various transition elements as substrate materials. A mechanism for the diamond growth based on the electronic structure of the substrate materials will be proposed.

CHAPTER FOUR

EXPERIMENTAL SETUP

4.1 Description of the Reaction Chamber

The microwave CVD system used for the diamond film deposition in this investigation incorporates the ASTEX S-1500, 1.5 kW microwave power generator operating at powers of 0.125 to 1.5 kW at 2.45 GHz. Figure 4.1.1 is the schematic of the experimental setup. Microwave energy is coupled by the symmetric plasma coupler to produce a ball of plasma at, or slightly above the substrate surface in a stainless steel chamber. Samples of up to 4 inches in diameter can be produced in this system. A motorized stage is used to raise or lower the substrate for altering the plasma proximity, and the substrate can be heated up to 1200 °C. Thermal power is delivered by a 3.5 kW induction heater operating at 60 Hz. This provides uniform heating of the 4 -inch diameter graphite susceptor at typical operating pressure in a hydrogen plasma. Current through the induction coil is supplied by a IPX-3750 induction power supply operating at 60 Hz.

The induction coil is made up of nine turns of 3/8" O. D. copper tubing with a 1/16" wall thickness. The turns are placed 5/16 " apart so that the span of the coil is 5 7/8". The coil design is such that it matches the frequency range of the power supply and the susceptor material resulting in maximum efficiency in terms of power conversion into heat. The hollow copper coil and the walls of the reactor chamber are cooled by circulating water.
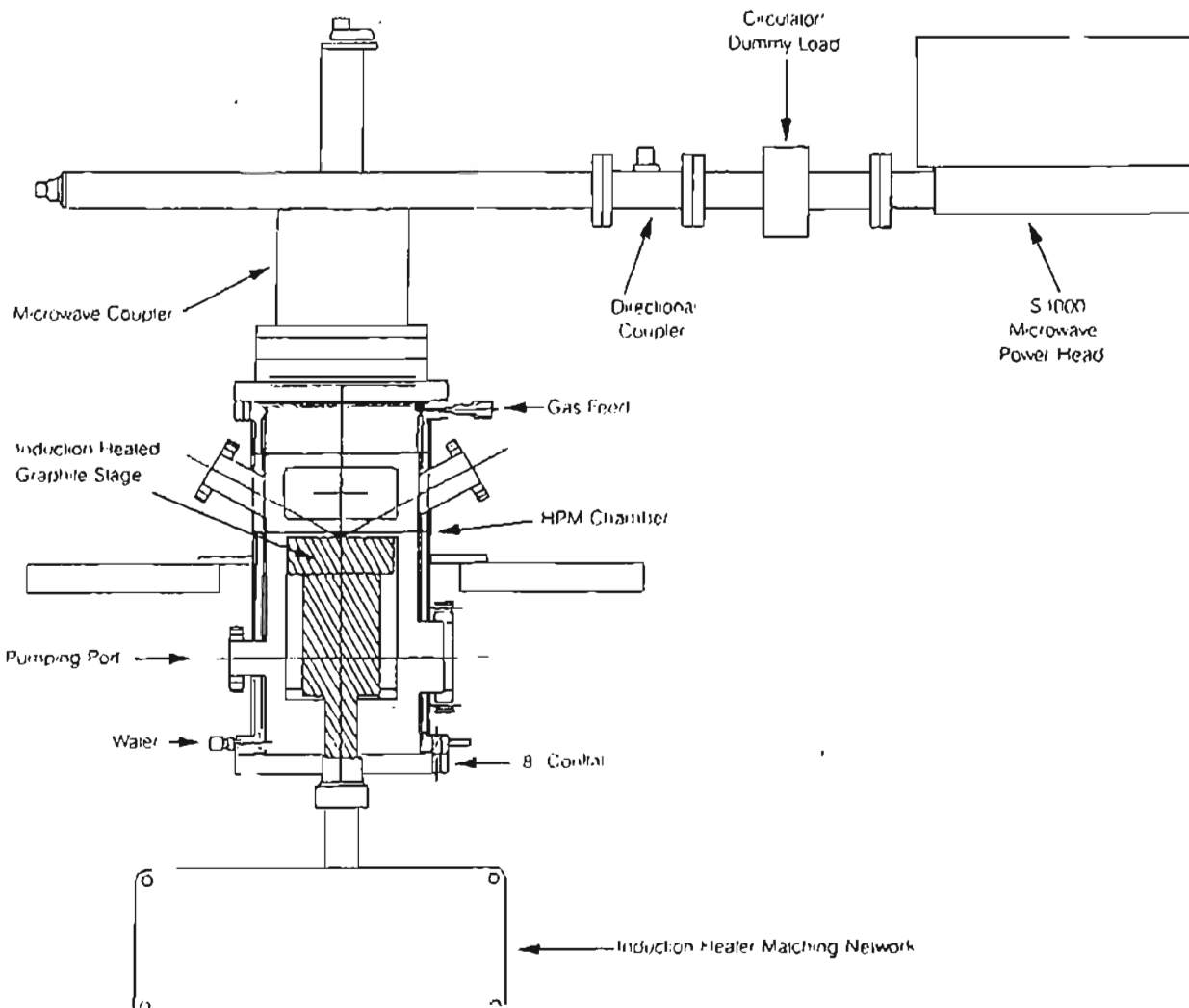
Figure   4.1.1   Schematic of the Microwave CVD Experimental Setup

Substrate temperature is monitored by a thermocouple (K-type) embedded in the backside of the susceptor block. Type K thermocouples are most linear between 700 -1200 °C. Since the temperature range in this investigation is between 700-1000 °C a K-type thermocouple was utilized. The thermocouple was calibrated at four reference points, namely, ice at 0 °C, boiling point of water at 100 °C, melting point of tin at 232 °C and melting point of zinc at 420 °C. The calibration result indicated an error of ± 1 % in the thermocouple reading. The substrate temperature is controlled by a Eurotherm temperature controller. It is a microprocessor based closed loop PID controller with an ON/OFF feature to maintain the substrate temperature at a particular set point. The substrate temperature was maintained at a desired set point with an accuracy of ± 0.5 °C of the reading (refer Appendix B for more detailed specifications). A Williamson dual-wavelength optical pyrometer is used to monitor the substrate temperature. The dual-wavelength optical pyrometer features a rotating chopper carrying four narrow-band pairs of spectral filters of different wavelengths and determines the temperature by computing the ratio of the radiant energies emitted by the target in these wavebands. The wavebands selected for the measurements are adjacent to each other in the electromagnetic spectrum so that they will be equally affected by the target emissivity. Thus, these dual wavelength pyrometers can accurately measure the temperature of materials with low or constantly changing emissivities. The accuracy of the pyrometer was ± 1% of span (Appendix B). Calibration was checked periodically by slowing heating a copper block in the reactor until it melted. A record of the temperature difference between the measured melting point and the true melting point was maintained and the temperature of each coating run adjusted accordingly. The measured

melting was generally on the order ~ 10 °C above the actual melting point. The stainless steel chamber is equipped with two sapphire viewports for observation of the progress of the deposition and the measurement of the substrate temperature with a pyrometer.

4.2   Gas Flow and Control System

The gas handling system was composed of mass flow meters (MKS Type 247C) along with mass flow controllers (MKS Type 1159B), a Baratron pressure transducer (MKS Type 127), a pressure controller (MKS Type 250), stainless steel tubing, hand operated valves, and a mechanical pump (Alcatel), for the control and monitoring of chamber pressure and gas flow rates.   The stainless steel tubings were connected with Swagelog fittings and routine leak checks were conducted for integrity. CH_4 and H_2 were used as the main reactant gases in the present investigation. UHP grade gases were used and were introduced into the chamber through a gas inlet port.   The gas flowed downstream against the substrate surface, and pumped out the bottom of the tube by the vacuum pump. Its inlet could be shut off with a throttle valve, and in order to control the pressure in the reactor, its conductance was effectively controlled by means of feedback actions of a solenoid actuated butterfly valve, a pressure transducer and pressure control units.   The required pressure is maintained using a pressure controller and monitored by means of a pressure transducer. The accuracy of the pressure transducer was ± 0.15 % and that of the pressure controller was ± 0.25 % respectively.   Details of the instrument specifications are given in Appendix B.

The flow rates of gases are monitored and controlled using mass flow meters along with Mass Flow Controllers (MFC). Over time, the measured flow may drift due to the electronic drifting and/or contamination of the flow tubes in an MFC. The mass flow controllers are equipped with "scaling pots" which allow the user to adjust the reading to match the flow when calibrating the system.

Typically, calibration is accomplished by flowing a gas through a pipette or bubbler (a larger tube with volumetric markings). Soapy water is placed in a rubber bulb attached to the bottom of the tube. When the bulb is squeezed, a soap bubble is formed and the gas from the MFC forces the bubble to rise in the bubbler. The gas flow (F, in standard cubic centimeters per minute (sccm) is calculated by timing the bubble's passage through a known volume and dividing the volume (V, in centimeters) by time (t, in minutes)

$$F = V/t$$

The actual flow (F in the above equation) should match the reading on the MFC's display. If these values do not agree, the scaling pot for this particular MFC is adjusted so that reading matches the flow. Calibration is an iterative process, so the above steps are repeated until the actual flow matches the flow reading. The calibrated accuracy of the MFC's is $\pm 1.0\%$ of the full scale. (refer Appendix B).

4.3   Deposition Procedure

1. Insert the substrate into the reaction chamber and place it on the graphite/quartz plate on the graphite susceptor.

2. Turn on the vacuum pump and evacuate the system to a pressure less than 5×10^{-3} torr. Set the desired pressure and the flow rate. Typically, pressures in the range of 20-60 Torr and total flow of 100 sccm of hydrogen with 0.5-5% of methane are used for diamond deposition. Turn on the water supply.

3. Set the substrate temperature by the Eurotherm controller and switch on the power supply. Flush the chamber with hydrogen.

4. Switch on the microwave power generator and ignite the hydrogen plasma.

5. Center the plasma ball and minimize the reflected power by tuning the wave guides, and the substrate position.

6. Adjust the optical pyrometer to measure the temperature of the substrate

7. Once the set temperature is reached, introduce methane into the chamber. Monitor any temperature fluctuations on the substrate surface and the plasma stability and make the corresponding adjustments if necessary.

8. Continue the deposition for the required time.

9. After the deposition is complete, shut off the microwave generator and the substrate heater. Switch off the methane flow after the deposition. However, hydrogen flow is maintained during the cool down period.

10. After cooling, switch off all the gas flows, water supply and vent the system. Remove the sample and perform necessary characterization.

CHAPTER 5

CHARACTERIZATION TECHNIQUES

5.1 Introduction

In order to have a better understanding of the nucleation and growth mechanisms of diamond films on various substrates and to improve the quality of the diamond films for different applications, researchers have used many analytical techniques to characterize the diamond films chemically, structurally and morphologically. Assessment of the film quality is important because of the existence of another class of films known as diamond-like carbon (DLC) films, which have properties close to that of diamond. These DLC coatings are characterized by a high degree of sp^2 bonding and consist of a variety of non crystalline carbonaceous materials ranging from amorphous to microcrystalline (Angus, 1988). It is therefore a necessity to differentiate between diamond and DLC films and identify techniques to characterize these materials. Messier et al.,(1991) have suggested a working definition of diamond coatings produced by vapor deposition techniques as follows:

1. having a crystalline morphology discernible by electron microscopy

2. having a single crystalline structure identifiable by X-ray and electron diffraction and

3. displaying a Raman peak typical of crystalline diamond.

Much attention has also been devoted to the characterization of the interface between the diamond film and the substrate, since the chemistry,

microstructure and stress state of the substrate near its interface and up to the surface of the film determine the suitability of a sample for a particular application. A variety of techniques currently used by various researchers include: μ-Raman spectroscopy, Scanning electron microscopy (SEM), X-Ray diffraction (XRD), Auger Electron Spectroscopy (AES), Secondary Ion Mass Spectroscopy (SIMS),X-Ray Photo Electron Spectroscopy (XPS), Electron Energy Loss spectroscopy (EELS), Low Energy Electron Diffraction (LEED) and Transmission Electron Microscope (TEM). Scanning electron microscopy, Raman spectroscopy and X-Ray diffraction techniques are employed for the characterization of the diamond films in the present investigation. Each of these three techniques will be discussed in the following sections. Methods of measuring adhesion strength of coatings are also discussed.

5.2   Scanning Electron Microscopy (SEM)

Scanning electron microscopy (SEM) is a widely used technique for characterization of morphologies of surfaces, interfaces and crosssections of various materials. Electrons from the tungsten filament are accelerated by a voltage in the range of 5-30 kV and are focused by a series of converging magnetic lenses to a beam diameter of about 10 nm. The interaction of the electron beam with the specimen gives rise to a number of signals, each of which provides valuable information about the structure and the composition. The inelastic collisions between the electrons gives rise to the emission of secondary electrons. However because of their limited range only those secondary electrons, arising within the top 50-100 Å of the surface have enough energy to escape from the surface and are the most

73

commonly used signal for SEM image formation. Depending on the surface topography a number of these secondary electrons reach the detector. The brightness of a corresponding spot is modulated depending on the number of electrons reaching the detector. The electron beam is made to scan an area on the specimen surface to produce a magnified image of the surface.

An ABT-32 scanning electron microscope with a resolution of 5 nm is used in the present investigation. The SEM, with an accelerating voltage range from 2 to 30 KV, has a 6" specimen chamber and accommodates a tilt from -10° to +90°. The accelerating voltage can be adjusted depending on the sample and the depth of the field required. Magnifications from 15X to 300,000X can be achieved. A built-in Polaroid camera is used for taking the micrographs of the specimens. The SEM is also equipped with a KEVEX X-ray microanalyzer for elemental X-ray analysis and mapping.

The morphology of diamond films exhibit highly developed facets of different crystallographic orientations when observed under the scanning electron microscope. These morphological features are not discernible on a DLC film which mainly consists of an amorphous structure. Thus, the SEM is a powerful tool to identify the crystalline nature of the deposited film. In this investigation SEM is used to examine the morphology, grain size and the thickness of the diamond coatings under various deposition conditions on different substrates. The morphology of the substrates and the substrate/coating crossections are also studied. The elemental composition of the coating/substrate interface is examined with the KEVEX X-ray microanalyzer.

5.3   μ-Raman Spectroscopy

5.3.1 Background

Raman spectroscopy is probably the most commonly used characterization tool for diamond film analysis (Yoshikawa et al., 1988, 1989, 1993; Bachmann et al., 1994; Wang et al., 1996). This technique measures the energy changes in photons of light which have interacted inelastically with molecules in a material. An important advantage of Raman spectroscopy is that it is nondestructive for most inorganic materials, including diamond.

When a sample is irradiated with monochromatic radiation, the incident radiation may be absorbed, transmitted, reflected or scattered. Of the radiation scattered by a sample, most will be scattered elastically whence the incident and the scattered photons have the same energy. The strongest form of elastic scattering is Rayleigh scattering, in which the electrons and nuclei within a molecule are displaced in opposite directions by the oscillating electric field of the incident radiation. A dipole moment is induced in the molecule, oscillating at the same frequency as the incident radiation. However, monochromatic radiation may also be scattered inelastically by a molecule, when incident and scattered photons do not have the same energy. The energy of the molecule changes in this kind of scattering. This effect was theoretically predicted by Smekel in 1923 and experimentally demonstrated by Raman (1928) and Landsberg and Mandelstam almost simultaneously (Bulkin, 1991)[*].

---

[*]Raman received the Nobel prize in physics in 1930 for his efforts.

In Raman scattering, a photon with initial energy $h\upsilon_0$ interacts with a molecule to produce a scattered photon of energy $h\upsilon_s \neq h\upsilon_0$ By the law of conservation of energy, $h\upsilon_0$ must be equal to $h\upsilon_s + h\upsilon$ where $h\upsilon$ is the change in the energy of the molecule. In a Stokes transition, $h\upsilon_s < h\upsilon_0$ and the molecule gains energy hv while in anti-Stokes transition $h\upsilon_s > h\upsilon_0$ and the molecule gives up energy $h\upsilon$. The difference in the frequency observed in the Raman effect is caused by the energy exchange between the incident radiation and one of the normal modes of the scattering material. Figure 5.3.1.1 shows the three kinds of transitions. The normal modes involved could be a vibrational or rotational mode in the molecule, a lattice mode in a crystal, or a mixture of these modes in amorphous materials.
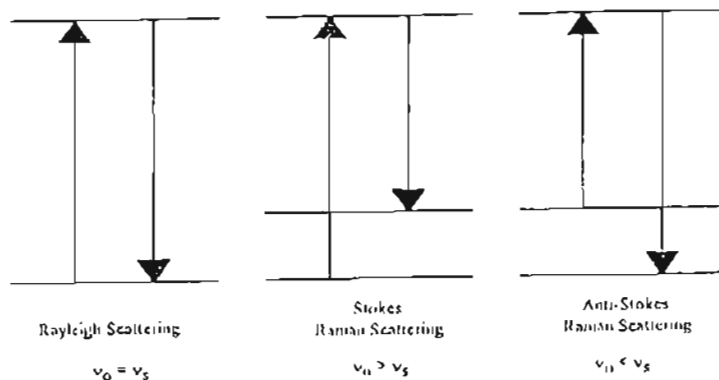
Figure   5.3.1.1   Energy Level Diagrams of Rayleigh Scattering,
Stokes Raman Scattering and Anti-Stokes
Raman Scattering (Bulkin, 1991)

Raman spectroscopy is the most commonly used technique to evaluate the purity of diamond films. Since the allotropes of carbon all have unique structure, each also has its own characteristic signature. As a result, position of the Raman peaks distinctly specify what forms of carbon are present in the sample. The full width at half maximum (FWHM) gives a qualitative estimate of the crystal quality, since the width of the peak may be broadened by localized strains produced by defects and impurities. Table 5.3.1.1 summarizes the reported peak positions and widths of the crystalline forms of carbon.

Table 5.3.11 Summary of Raman Peak Positions and Widths for Several Allotropes of Carbon (Buckley et al., 1989)

Form of Carbon	Peak Position(s) (cm^{-1})	Peak Width(s) (cm^{-1})
natural diamond	1332.5	2
diamond with 15% ^{13}C	1328	2
diamond with 36% ^{13}C	1319	2
lonsdaleite on sawed diamond	1319	2.2
shock-induced lonsdaleite	1316 to 1325	30
graphite	1580	20
typical CVD diamond	1332	10 - 20
amorphous carbon	1355, 1580, sometimes 1470-1490	both broad very broad
diamond-like carbon	1300 to 1350, 1540 to 1580	both broad

Knight et al., (1989), analyzed various forms of graphitic carbon, amorphous carbon, natural and artificial diamond, and diamond-like carbons. In addition to presenting Raman patterns for each of these materials, their work outlines the changes on Raman spectra due to bonding, structure and stress. For example, ordered carbons with sp^2 carbons (i. e. graphite) show two features: a sharp peak at 1580 cm^{-1} and a smaller band at 2710-2724 cm^{-1}. As crystallite size decreases another feature appears at 1357 cm^{-1}. This last band along with a broad band in the range of 1580 -1600 cm^{-1} occurs for disordered or amorphous sp^2 carbons. As the level of disorder increases, these peaks become broader and less well defined.

Diamond films generally contain a mixture of diamond and non-diamond carbon and the relative peak heights associated with each type of material indicate their relative amounts. Also, the scattering efficiency of graphite is 50 times that of diamond (Nemanich et al., 1979). Therefore μ-Raman spectroscopy is a sensitive test for the presence of graphite and disordered sp^2 carbon.

5.3.2 Measurement of Residual Stresses

Cubic diamond has a single first order Raman line at 1332 cm^{-1} (Solin and Ramdas, 1970). . These phonon frequencies are however sensitive to the lattice deformations caused by mechanical stress (Nemanich et al., 1991). An arbitrary stress tensor can be decomposed into a hydrostatic component and a deviator, inducing a volume change of the

78

unit cell and a distortion of the bond angles respectively. The volume change of the unit cell due to hydrostatic stress results in a linear shift of the triply degenerate Raman line (Grimsditch et al., 1978; Cerdeira et al., 1972). The Raman shift $\Delta\omega_H$ relative to the stress-free state is related to the magnitude of the hydrostatic stress σ by

$$\Delta\omega_H = \frac{\omega_0 \gamma}{B} \sigma \qquad \text{(Grimsditch et al., 1978)} \qquad \text{(a)}$$

where γ is the Gruneisen parameter = 1.06 at room temperature and B is the Bulk modulus = 442 GPa. Substituting these values in the above equation a value of -3.20 cm^{-1}/GPa is obtained for the hydrostatic piezo Raman coefficient.

The triple degeneracy of the zone-center optical phonon is lifted when deviatoric stress distorts the bond angles. This causes the splitting of the single Raman line into either three singlets or into a singlet and a doublet. However, it was observed that the centroid position of the split line does not change under deviatoric stress. In particular cases, the splitting of the singlet is twice that of the doublet and opposite in sign (Grimsditch et al., 1978). The centroid position of the Raman split line is thus entirely determined by the hydrostatic stress.

For CVD diamond coatings on substrates it is reasonable to assume a balanced biaxial stress state in the coating plane. The stress tensor can be represented in the [001] plane of the cubic lattice by the sum of a hydrostatic and deviatoric component as :

$$
\begin{pmatrix} \sigma & 0 & 0 \\ 0 & \sigma & 0 \\ 0 & 0 & 0 \end{pmatrix} = (2/3) \, \sigma \begin{pmatrix} 1 & 0 & 0 \\ 0 & 1 & 0 \\ 0 & 0 & 1 \end{pmatrix} + (1/3) \sigma \begin{pmatrix} 1 & 0 & 0 \\ 0 & 1 & 0 \\ 0 & 0 & -2 \end{pmatrix} \qquad \text{(b)}
$$

The Piezo-Raman coefficient of the centroid is then evaluated as -2.13 cm^{-1}/Gpa by multiplying (a) with a factor 2/3. Since the hydrostatic component is invariant of rotation, this coefficient remains the same for any crystal orientation (Mohrbacher et al., 1996). The Raman line splitting caused by the stress deviator can be calculated from perturbation theory using the deformation potential constants of diamond (Ager and Drory, 1993). Grimsditch et al., (1978) obtained split values of 0.73 and 2.20 cm^{-1}/GPa along the [001] and [111] lattice planes of diamond respectively.

In polycrystalline diamond coatings, crystallites of various orientations may contribute simultaneously to the measured Raman intensity. In the presence of a homogeneous biaxial coating stress, they induce a distribution of line splitting around a common centroid position. Because of the finite Raman line width, however, the line splitting cannot be resolved for small stress values. The FWHM of single crystal diamond is generally below 3 cm^{-1} while the line width of most of the CVD diamond coatings range between 4- 12 cm^{-1} (Mohrbacher et al., 1996). Ager and Drory (1993) also demonstrated that the line splitting becomes apparent only at a sufficiently large deviatoric stress in diamond coatings.

The position of any Raman band is sensitive to a number factors such as temperature, pressure or stress and domain or finite crystal size (Bachmann et al., 1994). The Raman signal from a crystal of finite size exhibits a smaller Raman shift and has a larger FWHM than that from an

infinite crystal lattice. The position of a Raman band can be used to determine the residual stress after taking into the account effects of temperature (this becomes significant at temperatures above 200 °C) and finite crystal size. A phonon confinement model can be utilized to measure the line width of the diamond peak to determine the domain size, so that the effects of the crystal size can be corrected. Since, the branch of a phonon dispersion curve of interest is a decreasing function , the average scattered phonon will have a lower frequency than the phonon in an infinite crystal. The Raman peak from microcrystallite domains exhibits a smaller Raman shift.

$$\Delta\omega_{stress} = \Delta\omega_{obs} - \Delta\omega_{domain} \qquad . \qquad (c)$$

Some investigators considered this correction in stress measurement of diamond coatings (Oslon et al., 1996; Nemanich et al., 1991; Bachmann et al., 1994). They derived the domain-size induced line shift from the measured line width. Ager et al., (1993) showed that this can lead to erroneous results when other effects such as stress gradients or line splitting contribute to the broadening of the Raman line. Yoshikawa et al., (1993) also demonstrated that stress free diamond powder samples showed only a small line shift even for particle sizes below 0.1 μm. Since the grain size of the CVD diamond coatings obtained in the present investigation is of the order of few microns domain size correction was not taken into consideration and the stress magnitudes were calculated using the relation . -2.13 cm^{-1}/GPa.

5.3.3 Instrumentation and Collection Optics

The Raman spectra is recorded using a SPEX 500 M double monochromator, equipped with a Lexel 95 Argon ion laser with a variable power from 50 mW to 2 W. The Argon laser line at 5145 nm is passed through a 1450 Tunable Excitation Filter, to filter the non-lasing plasma lines. The laser beam on exit from the 1450 filter is reflected by three folding mirrors, in a beam steering tower towards the beam splitter housing in the vertical illuminator of the microscope. The beam splitter reflects some of the laser radiation towards the objective, while simultaneously allowing the Raman radiation collected by the same objective to pass through and continue towards the spectrometer entrance. The incident laser light is focused, on the sample, through a Olympus BH-2 microscope using a 80 X objective. The Olympus microscope is equipped with a Sanyo CCD camera , which is connected to a Panasonic color video monitor (CT 1030 M), allowing both viewing and positioning of the laser beam on the sample surface.

The scattered radiation is reflected by the two mirrors in the microscope output selector box. Then it passes through the confocal apertures, and is focused on to the entrance slit of the spectrometer, by a lens. The scattered light is collected in a 180° back-scattered geometry by a CCD detector, which is cooled to a temperature of 140 K by liquid nitrogen. The detector is interfaced with an IBM compatible PC, for data acquisition.

5.3.4 Procedure

Several alignment and calibration procedures were performed each day the Raman spectrometer was used. The laser beam was focused on a silicon wafer through the 80 X objective of the microscope. With the image of the beam on the monitor, the microscopic stage was moved up and down to check the symmetry of the beam. If the beam did not focus symmetrically, mirrors leading into the microscope were adjusted, until it did, thus assuring the backscattering configuration. Next, with monochromator slit width of 100 µm, and a laser power of 100 mW, a single crystal diamond sample was aligned with the laser beam, the mirror directing scattered light into the monochromator was adjusted to maximize the intensity of the 1332 cm^{-1} peak of diamond. The peak maximum was determined by a quick scan with an increment of 0.1 cm^{-1} and the integration time of 0.2 s. If the peak position was not located at 1332 cm^{-1}, the peak maximum was recalibrated to this value within the DM5000 software.

Since Raman line widths were very important in this investigation, the width of the single crystal diamond was determined as a function of slit width. Scans were taken with slit widths of 200, 150, 100, 50 and 30 µm in 0.2 cm^{-1} increments with an integration time of 1.0 s. The peak width was found to decrease linearly with slit width until reaching 30 µm, where diffraction becomes a problem. By plotting peak width Vs. slit width, the zero-slit width (intrinsic) diamond peak width was found to be 1.7 cm^{-1}. The actual width of the diamond peak as reported in literature is 1.65 cm^{-1} (Solin et al., 1970). This ensured that the instrumental broadening is

minimal. The purpose of this calibration was to determine the absolute minimum peak width which could be expected for CVD diamond films while using large slit widths. In this way, resolution could be sacrificed to obtain an improved signal to noise ratio.

Before the scans were taken, the sample was visually inspected using the 80 X objective of the Raman microscope. Next, preliminary scans were done on several regions of interest. These scans extended over the broad range of 900 to 1600 cm^{-1} in 1.0 cm^{-1} increments, each integrated for 0.2 seconds. This was done to check for different carbon structures. Further evaluation was done every 1 to 2 mm across the surface, radially outward from the center of the sample to the corners. These are more focused scans and extended from 1200 to 1700 cm^{-1} in 0.5 cm^{-1} increments with integration times of 0.2 s. These scans were repeated 5 -10 times to check the consistency and repeatability. All spectra were recorded at a constant laser power of 50 mW.

It was already mentioned that the shift in the diamond peak is correlated to the internal stresses. However, peak shifts might also be due to the heating effects (Bulkin, 1991; Chen et al., 1995). Since peaks shifts were very important for this investigation for the calculation of internal stresses, the shifts observed a particular laser power were confirmed by changing the laser power and observing whether the shift is maintained. This would rule out the possibility of the shifts being associated with the laser heating effects. In order to examine the distribution homogeneity of the residual stress inside the diamond films, Raman spectroscopy analysis was performed at fifteen different positions for each diamond films. The

shift of the diamond line from 1332 cm^{-1} was in the range of $\pm$ 1 cm^{-1}, corresponding to a stress fluctuation of $\pm$ 0.47 Gpa.

After the scans were taken, they were converted from DM 5000 to ASCII files and were loaded into Jandel's Scientific Peak fit for further analysis. While relative peak intensities are of primary interest, absolute values can also be obtained, by subtracting the photoluminescence background. A model shape function was developed to fit the background of the spectra (discussed in Chapter 6).

Raman spectroscopy is extensively used in this investigation to extract the following information:

1. Identification of phases: diamond, graphite, amorphous carbon and DLC.

2. Intensity ratio of the 1332 cm^{-1} peak to background, which gives a general insight of lattice disorder of the diamond phase.

3. Frequency shift of the 1332 cm^{-1} line, which is indicative of strain in the diamond lattice

4. Profile of the 1332 cm^{-1} line, which is related to the distortion of the lattice both of the first (short range) and the second kind (long range order), is connected to the frozen displacement of atoms from their equilibrium sites. The half width of the line is a relative measure of these distortions.

5. background level, which is connected to the luminescence by particular types of lattice defects; and

6. luminescence bands, which are connected to impurity atoms and/or vacancies.

5.4   X-Ray Diffraction

5.4.1 Background

When a monochromatic X-ray beam strikes parallel crystal planes at an angle θ to the planes, the beam is scattered over all directions of space. However constructive interference occurs, at certain angles when all the rays scattered by the atomic planes, reinforce, leading to a formation of a diffracted beam.

This process can be described by Bragg's law as :

$$n\lambda = 2d\sin\theta$$

where λ= wavelength of the incident beam

   d= interplanar spacing

   - θ= angle of incidence or diffraction angle

   n = order of reflection

Bragg's Law establishes the relationship between the direction of the diffracted beam and the crystal planes. The intensity of the diffracted beam, provides valuable information about the crystal structure.

5.4.2 Equipment and Data Collection

In the present investigation a Siemens X-ray diffractometer equipped with low angle facilities is used. The diffractometer employs a 3.0 kW sealed-tube X-ray generator, with a 3-circle goniometer for sample positioning, and a radiation safety enclosure. Copper is used as a target of X-ray source. Graphite is used to monochromatize the Cu radiation from the tube, after which the radiation is collimated with pinhole optics. A

Nickel filter is used to filter the K-β Cu radiation. Samples are mounted on a three circle goniometer and can be precisely positioned in the χ and ω axes. A two-dimensional, position-sensitive area detector is mounted on the 2θ arm of the goniometer, for the measurement of diffracted X-rays. Standard runs were made from 10° to 90° 2θ, with a step size of 0.05°. Samples were mounted on the goniometer in a fixture which held the surface of interest at a proper height for the exposure of the beam. The sample is held on the fixture with wax. The sample is positioned by placing a clean glass slide against it and pressing it until the sample surface is flush with the top surface of the aluminum fixture. It is important to clear any wax around the fixture or around the sample to avoid extraneous peaks on the XRD spectrum.

- Frames of the scattering data from the sample are collected and processed by GADDS software. In this investigation, the quality of the diamond film deposited, crystalline phases present, and the thickness of the deposited film were investigated by XRD. The glancing angle facility was used to study the interface between the diamond films and various substrates.

5.5   Adhesion Measurements

Adhesion measurements are made in a variety of ways. The testing method chosen for a particular system must meet two criteria: it must apply a tensile or shear force to the coating and it must cause failure at the interface or determine that the interface is stronger than the cohesive strength of the substrate and/or the coatings (Steinmann et al., 1989). Steinmann et al., (1989) reviewed some of the test methods including pull-

off, topple, acceleration and shock wave tensile tests and adhesive tape, direct shear, and peel shear tests. They concluded that all of these tests are limited to weakly adherent coatings. They considered the scratch test as the only method capable of generating stresses which exceed the interfacial bond strength of thin and well-adherent coatings.

The Scratch test is a widely used test for measuring the adhesion strength of diamond films and other hard coatings (Drory et al., 1995). The test essentially consists of drawing a diamond indentor across the coating surface with various uniform loads or with a gradually increasing load. The minimum load at which stripping of the coating occurs is called the critical load and is representative of the coating adhesion. The critical load can be determined by acoustic emission, optical or scanning electron microscopy and by tridimensional force recording (Perry, 1983). However it has been shown that the critical loads vary from one diamond film to another deposited under identical conditions (Huang et al., 1992). In order to have a better interpretation of the values of the critical load in terms of adhesion strength, many test parameters, such as loading rate and scratching speed, substrate hardness and roughness, coating thickness, just to mention a few have to be considered. This makes the accurate explanation of the results very difficult.

Indentation adhesion testing is a related measurement technique first described by Chiang and coworkers (Jindal et al., 1987). This technique utilizes a diamond indentor pressed into the surface of a coating at static loads. There is a critical load, P_{cr}, below which no delamination occurs. At loads lower than P_{cr}, the coating and the substrate are deformed together. Some cracking may occur under the indentor, but damage

outside of the indentation scar is difficult to observe. At the critical load, lateral crack first emerges on the coating surface (Figure 5.5.1) (Jindal et al., 1987). Loads higher than the critical load create lateral cracks with larger diameters. There are also radial cracks which extend from the indent edge outward as far as the lateral cracks extend. As long as the cohesive energies of the substrate and the coating are higher than the adhesive force in the interface between them, these cracks are an indication of the adhesive strength at the interface. As with scratch testing, this is an inexpensive and quick test. It has the following advantages relative to scratch testing: the critical load is independent of the condition of the indentor tip and damage to the tip occurs less readily, thus results are not as sensitive to substrate hardness, the stress state is less complicated and there are no frictional forces to complicate the results. In addition, each indent requires a very small area on the sample, so a range of loads and/or statistical sampling can be done on one sample. This type of data can provide information on the uniformity of the coating. One factor which cannot be separated from the results is the residual stress. Residual stresses may include buckling in the film, which then creates an additional driving force for crack growth (Jindal et al., 1987).

The original test developed by Chiang et al., used a Vickers pyramidal indentor. A variation of Chiang's test was developed which utilizes a conical Brale indentor on a Rockwell hardness tester (Jindal et al., 1987).
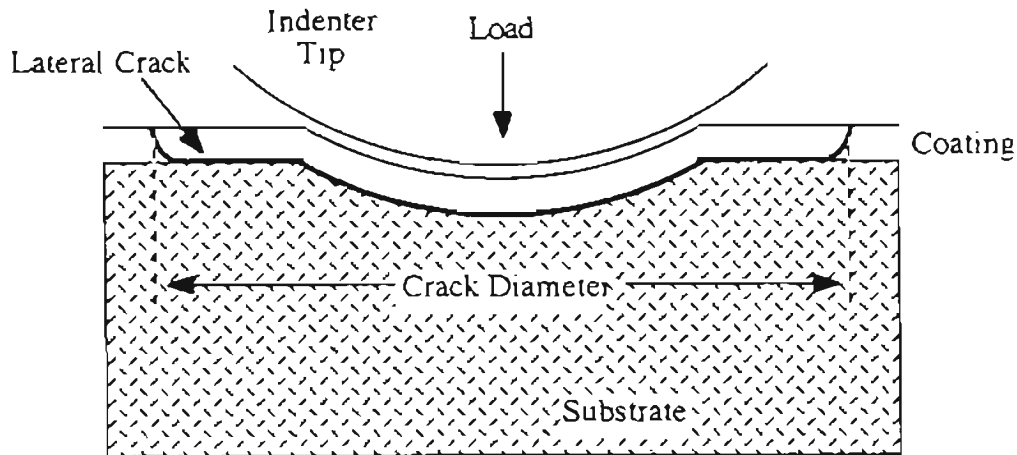
Figure   5.5.1   Schematic Drawing of the Cross Section of an Indent
Showing the Crack Pattern along the Coating-Substrate
Interface (Jindal et al., 1987)

The reason for the switch was "to facilitate its use in a production environment," specifically in coating facilities for the cutting tool industry. This variation of the indentation adhesion test is most widely used for diamond coatings on cutting tools. A disadvantage of the test is that Rockwell hardness testers have discrete loads. Critical load determinations must therefore be interpolated between the load where the lateral cracks first appear and the next lowest load. The data collected is generally presented on a plot of crack area or diameter versus the indentation load. In its present form, indentation testing is a qualitative measure of coating adhesion. However the slope of the indentation load-lateral crack length function provides a good measure of relative adhesion of hard coatings on different substrates and was found to be more discriminating than the approximate measurement of the crack initiation load P_{cr} (Jindal et al., 1987).

Indentation adhesion testing has been studied for diamond films on various substrates. Huang et al., (1993) tested samples with W, WC-5.7% Co and SiAlON substrates which had undergone different surface pretreatments prior to diamond deposition. They measured lateral crack diameters on SEM micrographs after the indented pieces were ultrasonically cleaned in ethanol to remove the delaminated portions on cutting tools. This removal step is necessary because the delaminated portions of the diamond films do not flake off completely. They found that the WC-Co had critical loads of 10-20 kgf regardless of the length of the pretreatment. Oakes et al., (1991), Saito et al., (1993), Zhu et al., (1994), Nesladek et al., (1995), Singh et al., (1996) have also evaluated the adhesion of diamond coatings using Rockwell hardness tester. The slopes of the indentation load versus the lateral crack diameter are generally used to evaluate the adhesion of the films, because they reflect the ease with which the lateral cracks are propagated, and are proportional to $1/G_c$, where G_c is the critical strain energy release rate. Higher slopes indicate poorer adhesion (Drory et al., 1995; Zhu et al., 1994).

In the present investigation, a Wilson Rockwell hardness tester was used for Brale indentation tests. This tester has discrete loading capability and loads of 15, 30, 45, 60, 100, 120 kgf were utilized. At each load level, at least three indentations were made on the sample. The crack diameter was measured with an optical microscope and re-examined with SEM.

CHAPTER 6

Diamond Coatings on Silicon Nitride

6.1 Introduction

Thermal stresses generated due to differences in the thermal expansion coefficients of diamond and the substrate material are detrimental to the adhesion and quality of the diamond coatings. Choice of materials with similar thermal expansion coefficients to diamond is necessary to decrease the thermal stresses. Si_3N_4 has a linear thermal expansion coefficient very close to that of diamond ($\alpha_{Si3N4} = 3.5 \times 10^{-6}$ /°C and $\alpha_{Diamond} = 3.1 \times 10^{-6}$/°C). In addition, owing to its superior mechanical properties, such as high hardness, strength, and good wear resistance, Si_3N_4 is emerging as a potential candidate material for diamond coatings (Soderberg et al, 1991; Sprow, 1995). Sandvik Coromant in Sweden and Norton Company in the US have been active in the development of commercially available diamond-coated Si_3N_4 inserts (Sprow 1995, Quinto, 1996). However, limited literature is published on the effect of process variables on the diamond coatings on Si_3N_4.

Peng et al., (1995) deposited diamond films on Si_3N_4 substrates using a d.c plasma jet CVD. They found these coatings to exhibit much smaller values of thermal stresses compared to the coatings deposited on WC-8% Co and Si coated cemented carbide coatings. The diamond films deposited on Si_3N_4 did not flake under severe thermal shocks caused by the rapid heating and cooling rates in the d.c plasma jet CVD process.

Xu et al., (1996) coated Si (111) with Si_3N_4 films ~ 400 nm thick and used them as substrates for diamond deposition by hot filament assisted chemical vapor deposition (HFCVD). They obtained good quality diamond films at only lower CH_4 concentrations (~ 0.5 %) and at 800 °C substrate temperature. At substrate temperatures above 850 °C, they noticed a degradation in the Si_3N_4 layer.

Itoh et al., (1996, 1997) obtained good adherent coatings on Si_3N_4 inserts at substrate temperatures between 850 °C-900 °C. Microwave plasma assisted CVD process was utilized for the deposition and the precursor gases used were carbon monoxide and hydrogen. The Si_3N_4 specimen was microflawed for 30 minutes by immersing it in ethanol containing diamond powder (0.25 μm) in an ultrasonic bath, prior to diamond deposition. This microflawing treatment was found to increase nucleation sites and a thick (~ 30 μm) diamond coating was obtained. These diamond coated Si_3N_4 tools were found to perform well in milling tests of Al-20 % Si alloys. No peeling of the diamond coating was observed even after the normal flank wear up to 0.15 mm was attained.

Much of the parametric studies conducted using microwave assisted CVD were confined to single crystal Si as substrate material. (Glass et al, 1988; Badzian et al, 1988; Zhu et al., 1989; 1990; Hirai et al, 1991;Liu et al, 1995). Temperature, pressure, ratio of CH_4/H_2 in the gas mixture and gas flow were identified as main parameters affecting growth rate and quality (Badzian et al., 1988). Based on the experimental results, they indicated that optimal conditions occur in the following range of parameters (Table 6.1.1).

Table 6.1.1   Range of optimum deposition conditions
(Badzian et al., 1988)

Temperature	975-1000 °C
CH_4/H_2	0.2-0.5 %
Pressure	40-90 Torr
Flow	~ 100 sccm

Hirai et al., (1991) studied the effect of microwave power on the hydrogen content in diamond films deposited on Si. They conducted experiments at 850 °C substrate temperature and 30 Torr pressure and observed that at higher microwave powers {111} surfaces dominated while at lower powers the morphology was a mixture of {100} and {111}. The size of the crystals was found to increase with increase in the microwave power. From secondary ion mass spectroscopic (SIMS) measurements and Raman measurements they found that both hydrogen count and the amount of amorphous carbon decrease logarithmically with increase in the microwave power.

Glass et al., (1988) studied the effect of varying CH_4 % on the morphology of diamond films on Si using microwave plasma assisted CVD and observed that {111} planes predominate for less than 0.4 % CH_4 concentration and {100} planes dominate between 0.5 and 1.2 % CH_4. For methane concentrations greater than 1.6 %, no specific orientation was observed and particles became microcrystalline with no facets.

Rats et al.,(1995) studied the influence of the total pressure on the diamond deposition domain from a C-H-O containing microwave plasma and observed that diamond films of good quality are difficult to obtain at pressures < 5 Torr.

Kikuchi et al.,(1988) investigated the effects of deposition parameters on morphologies and crystal structures of diamond films. They observed that with increase in CH_4 concentration the morphology changes from well faceted crystals to fine grained coagulated ball like structure.

Wolden et al., (1996) attempted to suggest the pressure limits for diamond CVD, by examining the data from a variety of conventional CVD reactors (HF, ECR plasma, d.c arc jet, rf plasma). They found that pressure limits are strongly dependent on the reactant composition and substrate temperature. For systems containing only carbon and hydrogen, high quality diamond deposition has not been obtained below a total pressure of 15 Torr. Based on the chemical kinetics calculations, they demonstrated that CVD of diamond is not possible in systems where the partial pressure of atomic hydrogen is less than 20 mTorr.

Phillip et al., (1997) demonstrated that an interfacial SiC layer is intimately involved in the heteroepitaxial growth on [100] Si. By Infrared measurements they concluded that the interfacial layers between Si and randomly oriented diamond may comprise amorphous phases of SiC, SiO_2, C or non-aligned crystalline SiC.

From the above literature review it can be observed that nature of the substrate and CVD diamond deposition conditions are major factors that influence the quality of the diamond films. In particular, for a given substrate, deposition conditions affect the film quality and adhesion through their influence on the content of non-diamond carbon components in the diamond film, the film morphology and the residual stresses in the

film. The amount of non-diamond carbon in a diamond film is again a function of deposition conditions and substrate material (Saito et al., 1990).

Hence, this part of the research focused on the study of effect of various process variables on the surface morphology, film thickness, crystallinity and the amount of non-diamond carbon of diamond films deposited on Si_3N_4 substrates. Raman spectra are presented as a measure of the relative structural changes of the films under different deposition conditions. The effect of these parameters on the quality of the diamond films was quantitatively investigated in order estimate the range at which deposition parameters have to be set, to produce high quality diamond films on this particular substrate. This would facilitate in a better understanding of the optimal deposition conditions.

6.2 Experimental Approach

Initial base line experiments were conducted to determine the appropriate deposition conditions. As mentioned earlier, most of the parametric studies were done using Si wafer as a substrate material. Substrate material is itself a variable parameter in influencing the diamond deposition. Also, the configuration of each reactor is different. Though some general trends may be observed, the range of parameters are specific for each reactor. Hence, a matrix of deposition experiments were conducted initially to investigate the trends.

A fractional factorial design developed from the theory of orthogonal design was used to study the four variables at three levels each (four -factor, three-level design). The interaction between the process variables was not

considered in these preliminary set of experiments. This design allows the analysis of the effect of each variable on the observed film characteristics. Pressure, substrate temperature, methane concentration and microwave power were the four variables studied. Table 6.2.1 summarizes the experimental design parameters.

The lower and the upper limits of pressure depend on the reactor design. For the reactor used in this investigation, when the pressure is < 20 Torr, the plasma discharge becomes very unstable. Instead of a plasma ball forming over the substrate at the center of the chamber, discharge occurs at the microwave window near the top. This can lead to the damage of the window and/or the seal. On the other hand, when the pressure is greater than 60 Torr, the plasma ball shrinks to a very small volume, almost to a point, leading to non-uniform deposits over a very small area of the substrate. Hence the low level was chosen at 20 Torr and the high level at 60 Torr. Accuracy in controlling the pressure was ± 0.4 Torr (refer to Appendix B). The range of other deposition conditions were chosen based on the review of literature (Badzian et al., 1988; Zhu et al., 1990; Barrat et al., 1993; Klages et al., 1993). The total gas flow rate was kept constant in this investigation at 100 sccm. The methane concentration is measured as the ratio of flow rate of methane divided by the total flow rate of hydrogen and methane. Accuracy's in controlling the flow rates of methane and hydrogen were ± 0.5 sccm and ± 1 sccm of the full scale respectively (refer Appendix B).

Commercially available Si_3N_4 tool inserts were used as substrates. The substrates were initially polished with a 240 grit SiC paper and ultrasonically cleaned in acetone for 30 minutes to remove any dirt prior to

the deposition. Details of the experimental procedure are given in Chapter
4. The deposition time for these set of experiments was ~ 8 hrs.

Table 6.2.1   Four factor three level experimental design
for Si_3N_4 substrates

	Level		
Variable	Low	Middle	High
Chamber pressure ($\pm$ 0.4 Torr)	20	40	60
Substrate temperature $\pm$(1% of set point + 0.5) $^{\circ}$C	800	850	900
Microwave power ($\pm$ 1 W)	500	750	1000
% CH_4 concentration ($\pm$ 1% of the set point)	0.5	1.0	2.0

The microstructures and morphologies were characterized using
optical and scanning electron microscopes. Nucleation density was
measured using the KEVEX image analysis software, equipped with the
SEM. μ-Raman was used to examine the quality of the deposits. Readings
were taken at about 15 points per sample. The variation in the values of the
nucleation density was ~ 5 %. Hence, average values were used as a
representative value.

ANOVA (analysis of variance) of the experimental data was conducted
to evaluate the degree of influence of the factors. The variance is calculated
by the following formula:

$$V_G^2 = m/f \sum_{i=1}^{n} (\sum_{j=1}^{m} \frac{y_{ij}}{m} - \bar{y})^2 \qquad (a)$$

where V_G^2, is the variance, y_{ij} is the measured value (surface coverage), f is the free degree, n is the level number and m is the repeat number of each level. $\bar{y}$ is the arithmetic mean, which is obtained from the equation :

$$\bar{y} = 1/mn \sum_{i=1}^{n} \sum_{j=1}^{m} y_{ij} \qquad \text{(b)}$$

6.3   Results and Discussion

Measurements of the substrate surface coverage with diamond nuclei are given in Table 6.3.1. The variance of the factors is calculated according to equation (a) and is shown in Figure 6.3.1.

Table 6.3.1   Surface coverage of diamond after ~ 8 hrs deposition

Sample	Pressure (±0.4 Torr)	Temperature (± 1 % of the set point + 0.5) °C	Microwave Power (± 1 W)	CH$_4$ (±1% of the set point)	% surface covered with diamond nuclei (Average value)
SN1	20	800	500	0.5	52.6
SN2	40	800	750	1.0	73.8
SN3	60	800	1000	2.0	17.3
SN4	20	850	750	2.0	83.7
SN5	40	850	1000	0.5	25.6
SN6	60	850	500	1.0	19.7
SN7	20	900	1000	1.0	75.7
SN8	40	900	500	2.0	58.8
SN9	60	900	750	0.5	4.5

From the above table, it is evident that the nucleation density varies with deposition conditions.
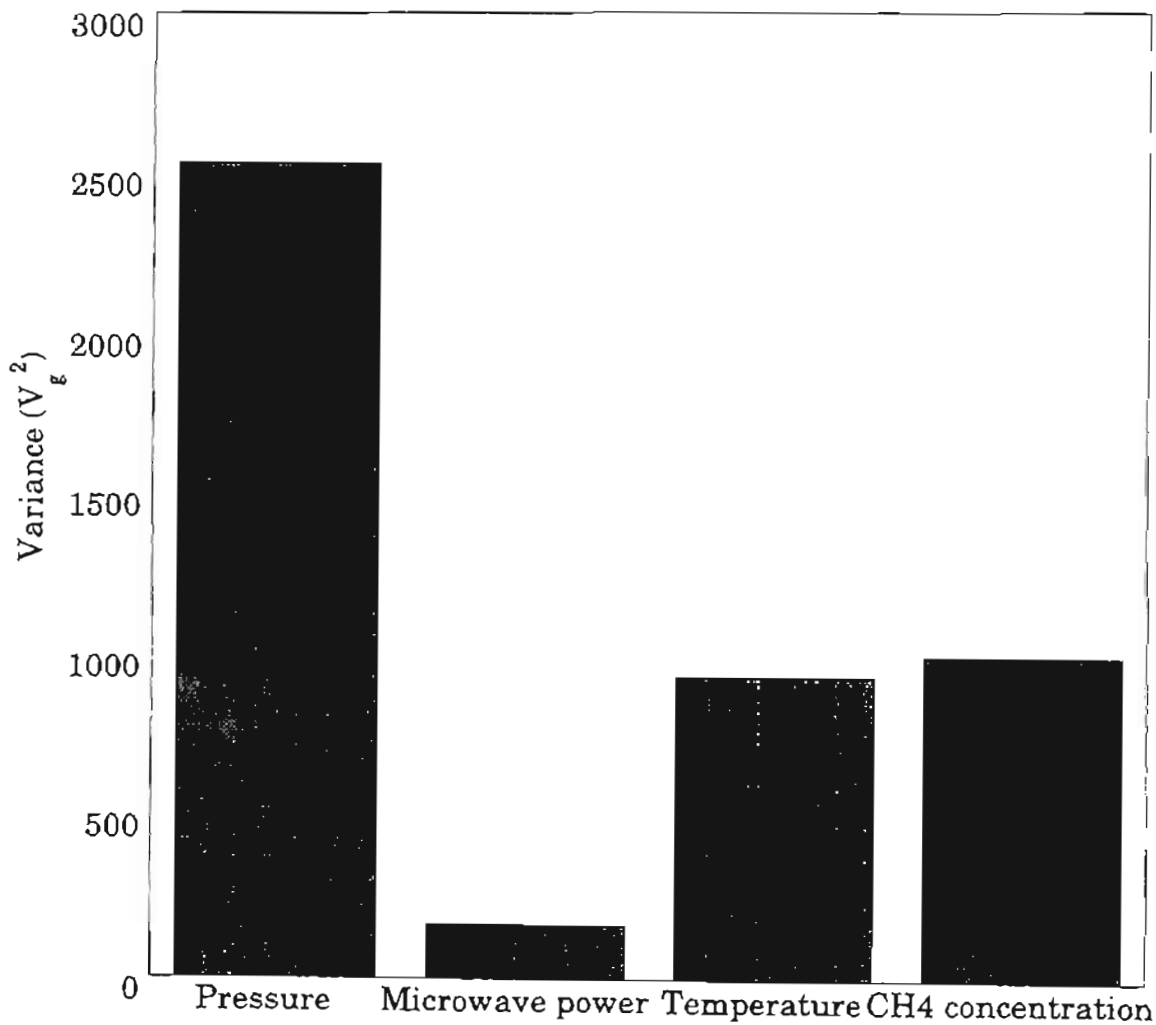
Figure   6.3.1   Variance Analysis of the Parameters on Nucleation

The values of the variance (Figure 6.3.1) indicate that the reactor pressure has the strongest influence on nucleation, followed by temperature and methane concentration. Microwave power was found to have a minimum influence.
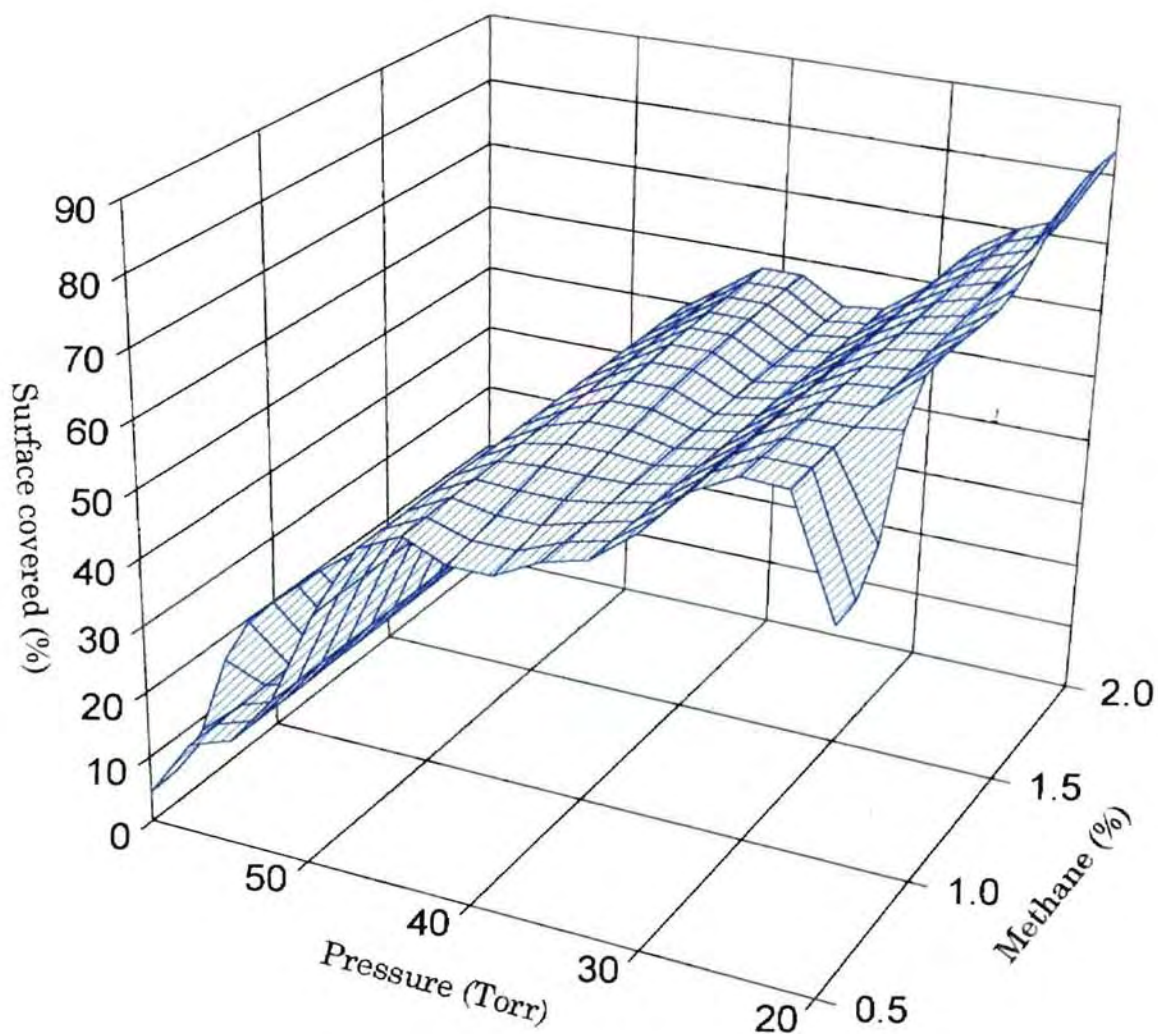
Figure 6.3.2   Surface Coverage w.r.t Dependence on Pressure and Methane Concentration
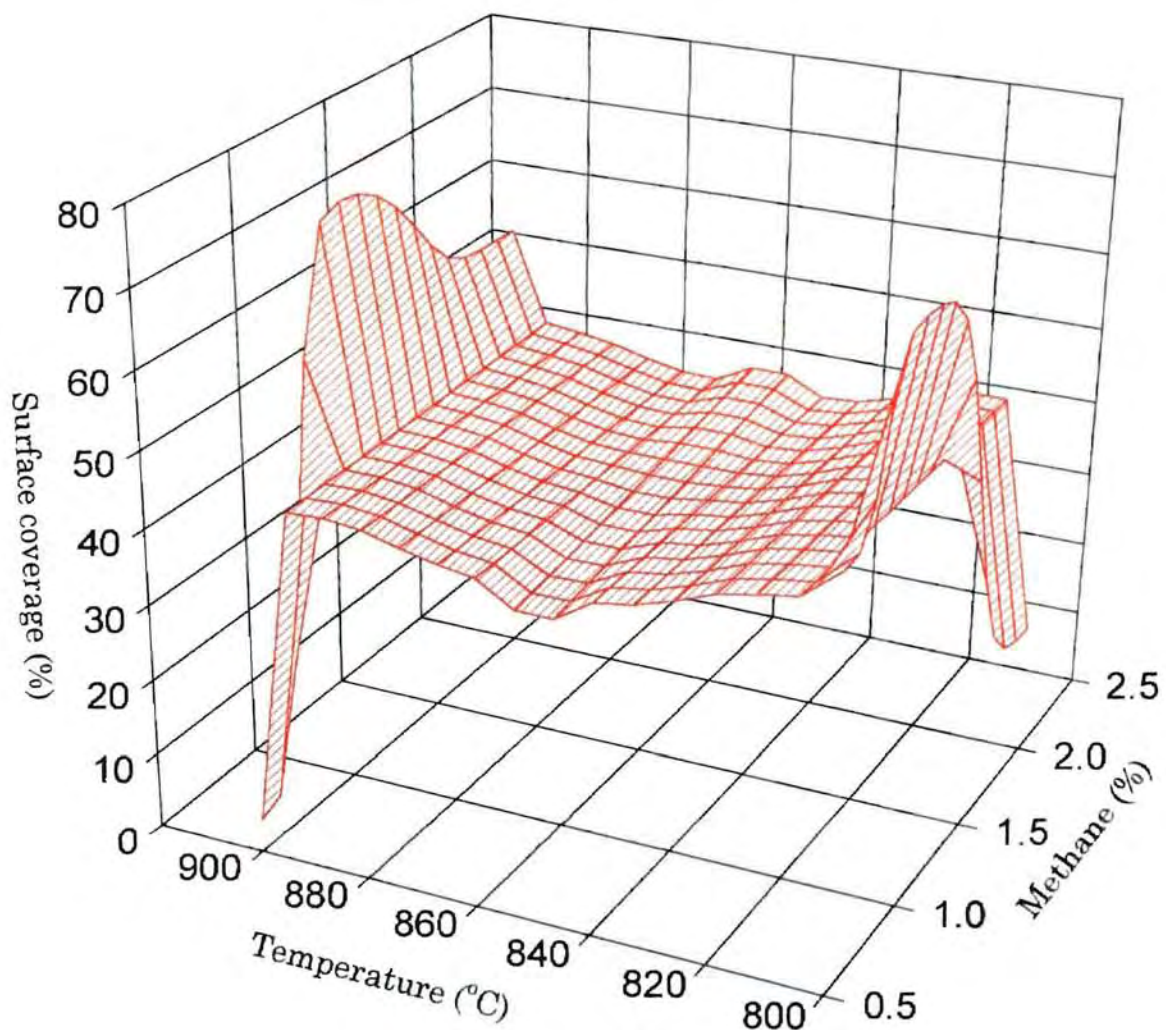
Figure 6.3.3 Surface Coverage w.r.t Dependence on Temperature and Methane Concentration

It can also be observed that nucleation density decreases with increase in pressure (Figure 6.3.2), while it increases with increase in CH_4 concentration (Figure 6.3.3). Each experiment was repeated two or three times at each level to ensure reproducibility of results.

Lux et al., (1991) pointed out that the substrate surface must be stable to promote diamond growth. However, Si_3N_4 substrate is reactive to the hydrogen plasma especially at high pressures (Stephen et al., 1992). This can lead to the disturbance in the diamond nucleation. Figures 6.3.4 a, b and c show the SEM micrographs of the substrate surfaces at different pressures with 1% CH_4.
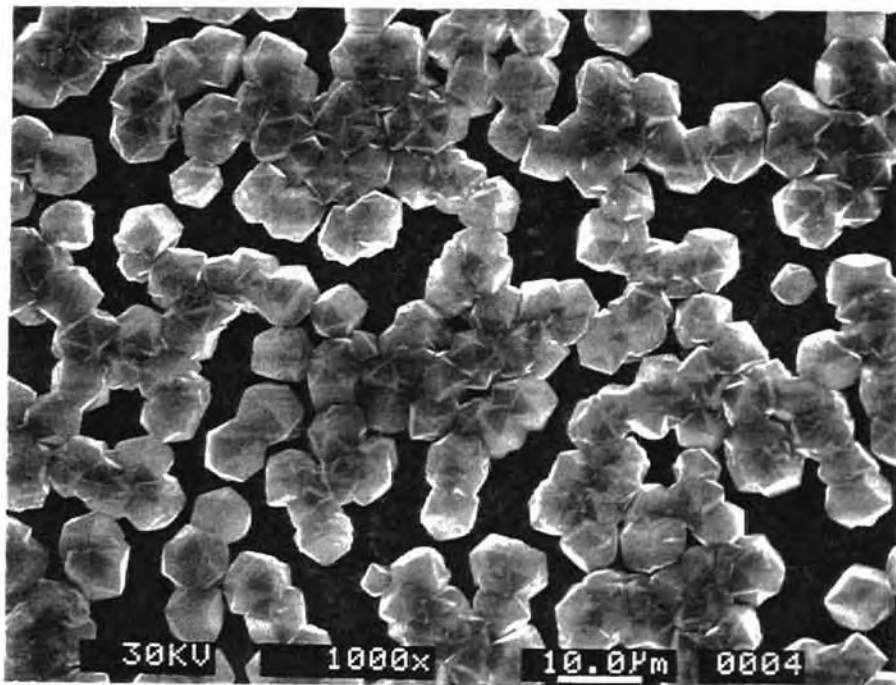
Figure 6.3.4 a) SEM Micrograph Showing Uniform Nucleation of Diamond on Silicon Nitride at 20 Torr Pressure
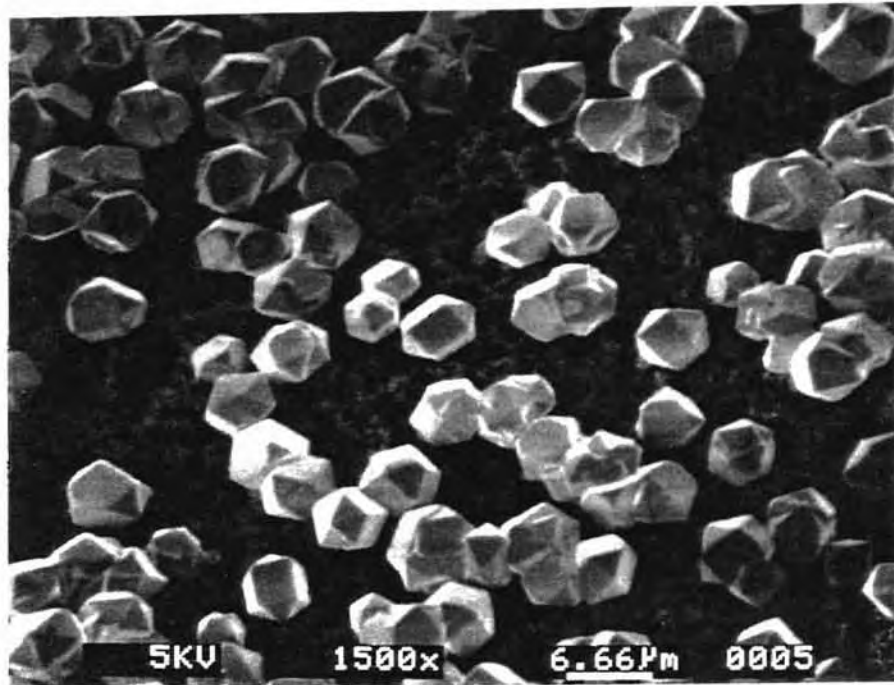
Figure   6.3.4 b)   SEM Micrograph Showing the Slight Etching of the
Silicon Nitride Substrate by Plasma Species at
40 Torr Pressure
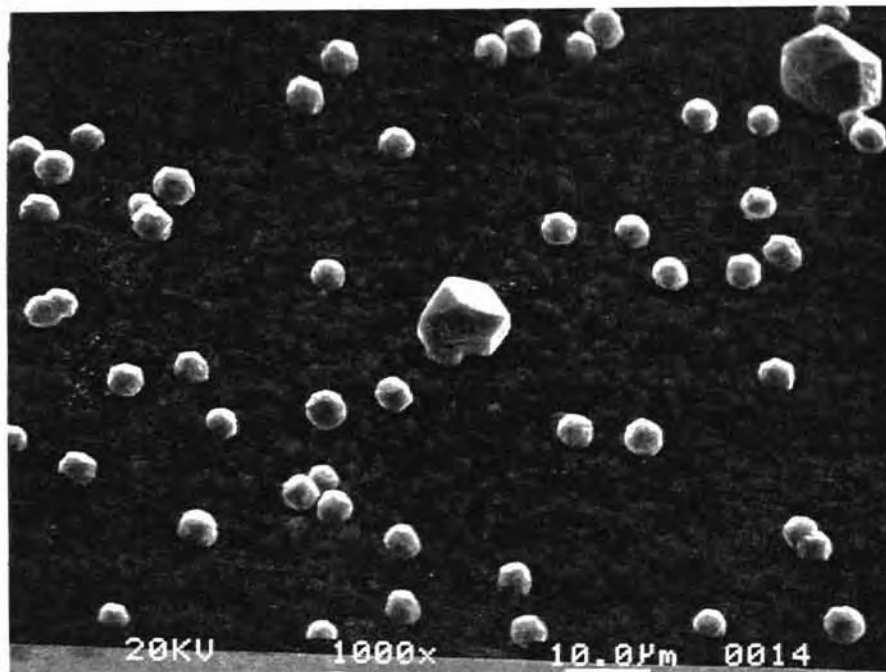
Figure   6.3.4c)   SEM Micrograph Showing the Damaged Substrate
Surface due to the Pronounced Etching by
Plasma Species at 60 Torr Pressure

Diamond nucleation is uniform at 20 Torr (Figure 6.3.4a). At 40 Torr, the substrate seems to be etched by plasma species and sparse nucleation is observed (Figure 6.3.4b). Figure 6.3.4c shows the damaged surface of the sample deposited at 60 Torr . Liu et al., (1995) reported that at high gas pressures, along with the substrate surface, pronounced etching of the diamond nuclei is also observed.

In the microwave chamber the plasma ball shrinks with increase in pressure. The reactive species in the plasma discharge are confined to a smaller volume. Hence nucleation is confined only to a very limited region (around the center of the tool) at 60 Torr. Figure 6.3.5 shows the Raman spectra of the samples deposited at various pressures.
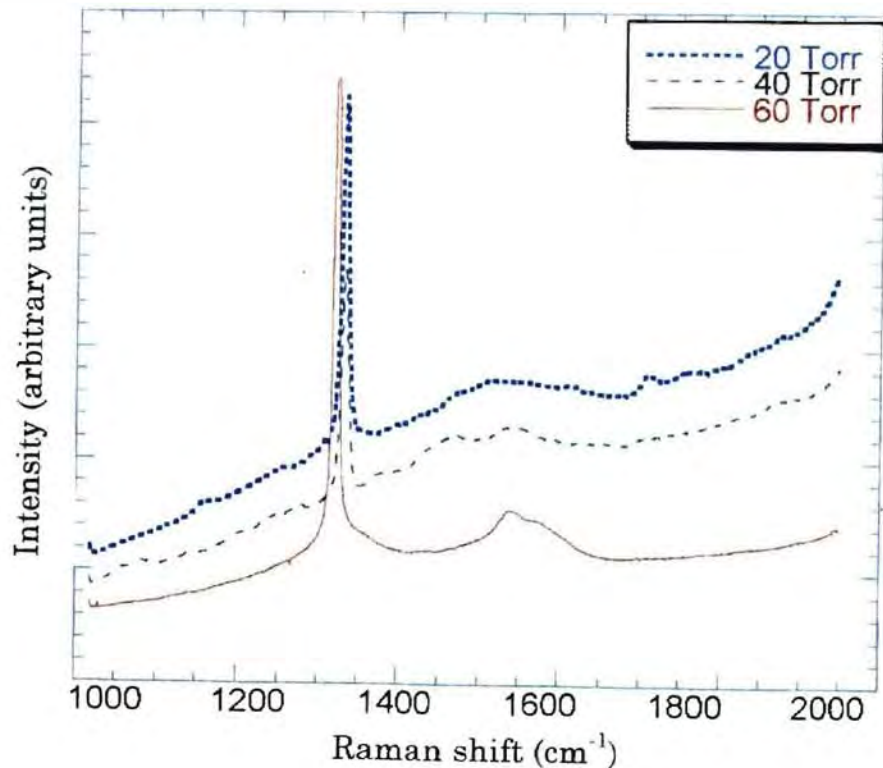
Figure 6.3.5 Raman Spectra Showing Diamond and Non-diamond Peaks on Si_3N_4 Substrates at Different Pressures

It can be seen from the above figure that the relative intensity of the non-diamond to the crystalline diamond decreases with the increase in pressure. Raman spectra of the diamond deposited at 60 Torr contains almost none or very little non-diamond carbon impurity.

At higher pressures the mean free path between the electrons and the molecules decreases. This results in an increase in the collision frequency of electrons and molecule. Also the number of electrons in the plasma discharge increases with increase in pressure (Sharda et al., 1996). Both these factors get multiplied in order to enhance the production rate of atomic hydrogen. This in turn leads to the reduction in the non-diamond content at high pressures.

Zhu et al.,(1990) pointed out that the quality and morphology of the diamond films are not sensitive to pressures. Pressure limits are dictated by the design of the reactor. Also, low pressure plasma occupies a large volumetric space than higher pressure plasma, more uniform films can be produced on a larger substrate area under low pressure conditions.

Methane percentages in the range 0.5-1.0 % enhance diamond formation because of an increasing number of carbonaceous reactant species in the plasma, which are necessary for the generation of possible amorphous layers (SiC, a-C) and also for the carbon saturation at the substrate surface (Liu et al., 1995). Further increase in CH_4 up to 2.0% enhances the nucleation slightly, but its influence depends on the selected temperature.

The microwave power was found to have the least influence on the nucleation. High microwave powers however help in the reduction of non-

diamond content (Figure 6.3.6). This observation is consistent with that of Hirai et al., (1990).
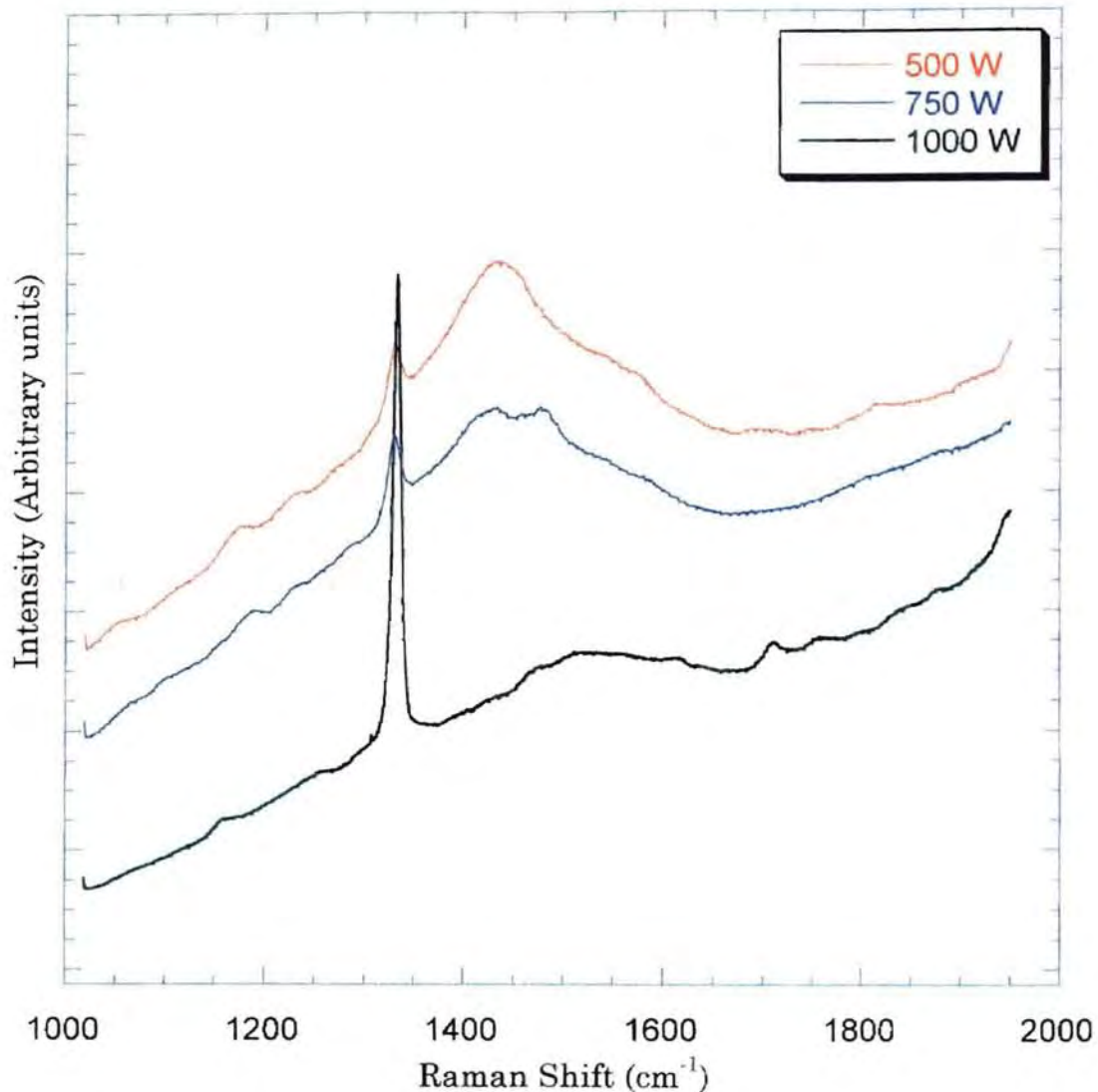
Figure   6.3.6   Raman Spectra at Different Microwave Powers Showing the Decrease in the Non-Diamond Peak Intensity at High Microwave Powers

Substrate temperature is perhaps one of the most important variables determining the film growth rate, since it closely relates to many growth phenomena such as the supersaturation of the gas phase on or near the

surface and the mobility and residence time of the adatoms. Zhu et al., (1990), reported that the growth rate is not appreciable until the substrate temperature is around 800 °C. As the temperature is increased further, the growth rate increases and reaches a maximum at about 1000 °C (Spistyn et al., 1989). Further increase in the temperature were found to result in the reduction of growth rate (Zhu et al., 1990). Substrate temperatures at ~ 850 °C were found to be favorable for nucleation.

These baseline experiments facilitated in identifying the important process variables influencing nucleation. Statistically, pressure and the microwave power were found to have a minimal influence on the nucleation. Substrate temperature and methane concentration were found to play a crucial role in the nucleation process. The decision as to which set of conditions to be chosen for further investigation was based on the results of these base line experiments along with the perception for the optimum film characteristics. Dense uniform nucleation covering the whole substrate was obtained at low pressure (~ 20 Torr). The diamond film whose Raman spectrum gives a sharp and narrow band around 1332 cm^{-1} and the smallest sp^2 bonded carbon band around 1550 cm^{-1} and with a very small photoluminescence background is quantified as a good quality diamond film. From Raman spectra obtained at different microwave powers (Figure 6.3.6), it was found that increase in the microwave power helps in improving the quality of diamond films. Hence, it was decided to choose a value of 1000 W for the microwave power.

Substrate temperature and methane concentration are the most crucial parameters dictating the overall growth rate as well as the quality of the diamond films. Zhu et al., (1990) reported that substrate temperature and

the methane concentration affect the morphology and the growth rate of the diamond films deposited on Si. Increase in CH_4 concentration was found to increase the growth rate but at the expense of the quality. With increase in methane concentration the diamond film became more defective and contained graphitic inclusions. They found that pressure has a minimal effect on the morphological development.

In order to obtain good quality diamond films, it is necessary to choose the right combination of both substrate temperature and methane concentration for a given substrate. It has already been pointed out that substrate itself is a variable. Hence, the next set of investigations were conducted to study the effect of methane and substrate temperature on the quality of diamond. The effects of these two important deposition parameters on the quality of the diamond films was investigated in order to have a better understanding of the optimal deposition conditions for quality and adhesion improvements.

6.4   Influence of substrate temperature and methane concentration

6.4.1   Experimental details

Commercially available Si_3N_4 tool inserts were chosen as substrate materials. These substrates were initially polished with 240 grit SiC paper. and then with 0.1 μm diamond powder for 15 minutes to enhance nucleation density. All the substrates were ultrasonically cleaned in acetone for 30 minutes to remove any debris/dirt prior to the deposition. The substrate was then placed in the microwave chamber. Details of the

experimental procedure is given in Chapter 4. The substrate temperature was monitored by a K-type thermocouple (accuracy $\pm$ 1 %) and was set by the Eurotherm temperature controller (accuracy $\pm$ 0.5 ºC). A 2 color optical pyrometer (Williamson Model) was used to monitor the substrate surface temperature. The accuracy of the pyrometer is $\pm$ 1%. Due to the plasma discharge the substrate surface temperature was ~ 50 ($\pm$10) ºC higher than the substrate temperature. This is referred to as tool temperature. Since the plasma discharge was uniformly spread over the tool (1/2 inch square inserts), the recorded temperature is taken as the representative temperature of the sample. The total pressure, microwave power and the gas flow were set at 20 Torr, 1000 W and 100 sccm respectively. Raman spectroscopy and scanning electron microscopy were used to characterize the diamond films. Detailed descriptions of the instruments and procedures for their use were given in Chapter 5. Table 6.4.1.1 gives the experimental designation.

Table 6.4.1.1   Sample Designations and Deposition Conditions

CH_4 ($\pm$ 1 % of the set point)	$800 \pm (1\% \, T_s + 0.5)$ ºC (Tool temperature ~ 850 ± 10 ºC)	$850 \pm (1\% \, T_s + 0.5)$ ºC (Tool temperature ~ 900 ± 10 ºC)	$900 \pm (1 \% \, T_s + 0.5)$ ºC (Tool temperature ~ 950 ± 10 ºC)
0.5	SN11, SN12, SN13	SN14, SN15, SN16	SN17, SN18,SN19
1	SN21,SN22, SN23	SN24, SN25, SN26	SN27, SN28, SN29
1.5	SN31,SN32, SN33	SN34, SN35, SN36	SN37, SN38, SN39
2	SN41, SN42, SN43	SN44, SN45, SN46	SN47, SN48, SN49

6.4.2 Results and Discussion

6.4.2.1 Scanning Electron Microscopy

The SEM micrographs of diamond films of the 12 samples deposited under different experimental conditions are shown in Figure 6.4.2.1.1. Most of the films are well faceted with preference towards [111] orientation. Zhu et al., (1989) developed a morphology "field map" describing the influences of the deposition temperature and methane concentration on the film morphology. They reported that with the increase in temperature from below 900 °C to above 1000 °C the morphology of the diamond films on Si substrates would change from the "hill and valley type" to {100} face dominating to {111} face prevailing type. From Figure 6.4.2.1.1, it can be noticed that the deposition temperatures in the present investigation did not seem to effect the morphology very much. It may be because of the different substrate materials used (Si and Si_3N_4) and that the temperature range used in the experiments is relatively small.

However, with the increase in CH_4 concentration the grain size tends to decrease and there is gradual loss in crystallinity. At 2 % CH_4 concentration, the morphology of the films is entirely different. Spherical shaped submicron crystallites aggregates appeared at all deposition temperatures and the diamond films become entirely structureless. This observation of morphology behavior at different methane concentrations is consistent with the results reported in literature irrespective of the substrate material used for the deposition (Kobashi et al., 1988 (Si substrate); Zhu et al., 1989, 1990 (Si substrate); Barrat et al., 1993 (Si

111

substrate); Lu et al., 1991 (Si, Mo and W substrates); Zhu et al., 1994 (W substrate); Xu et al., 1996 (Si_3N_4 substrate)}.
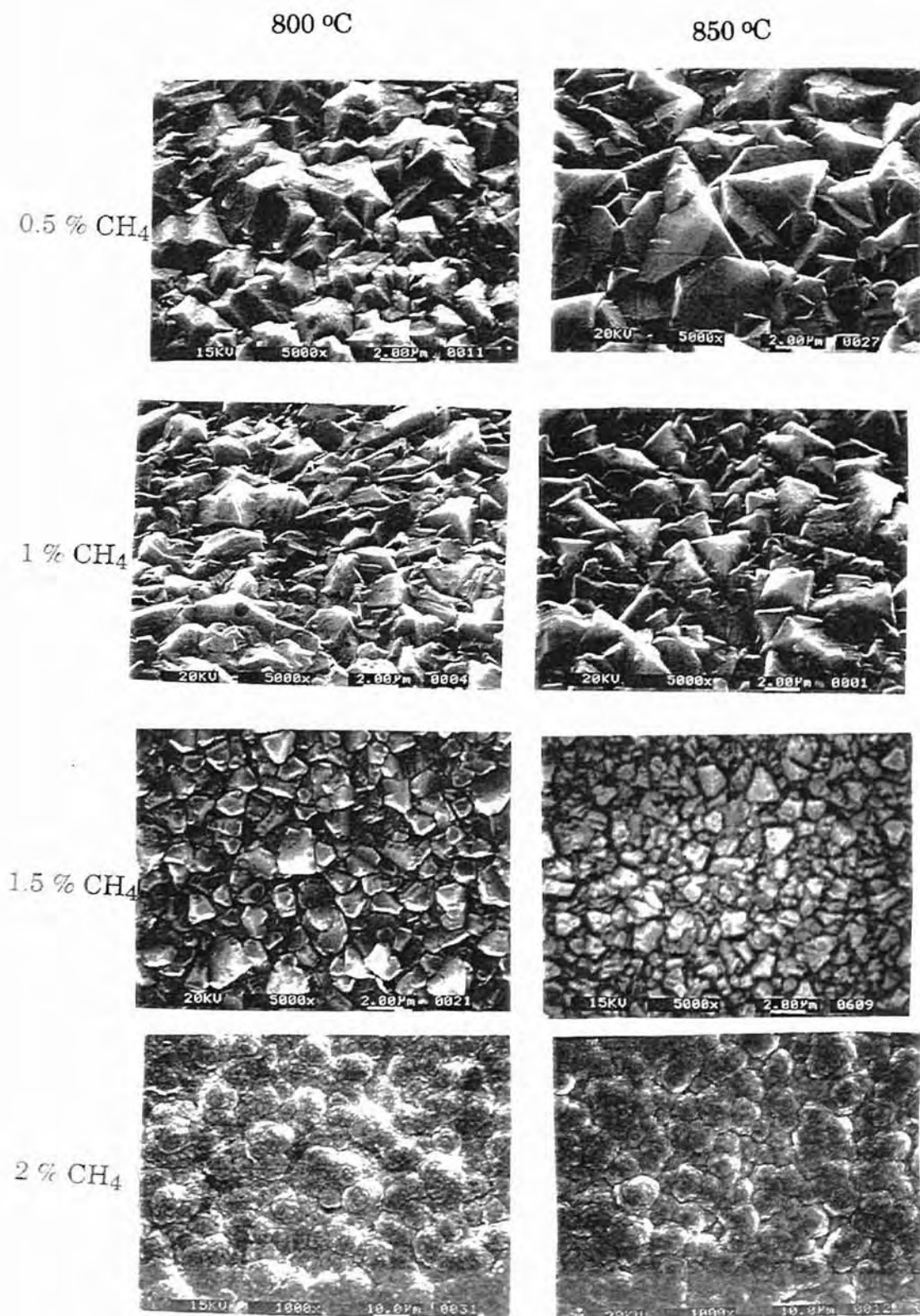
900 °C
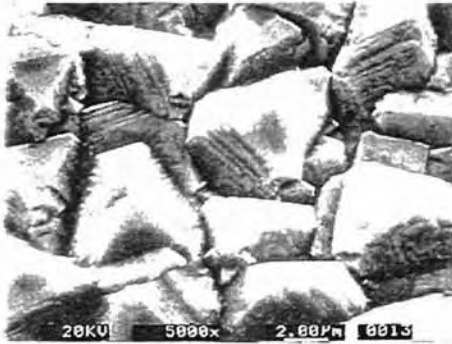
0.5 % CH$_4$
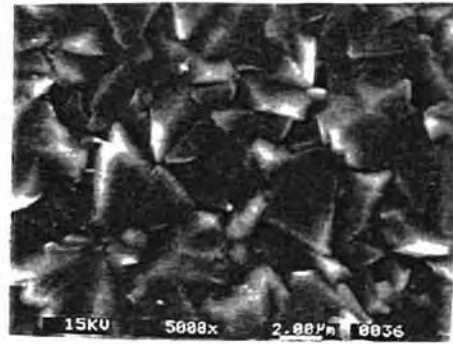
1 % CH$_4$
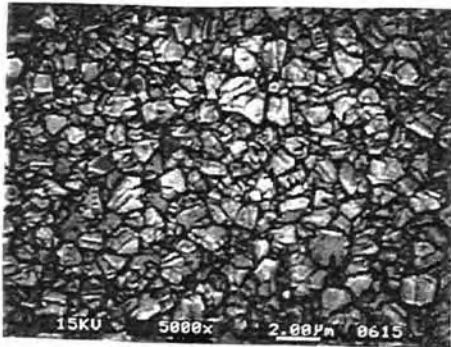
1.5 % CH$_4$
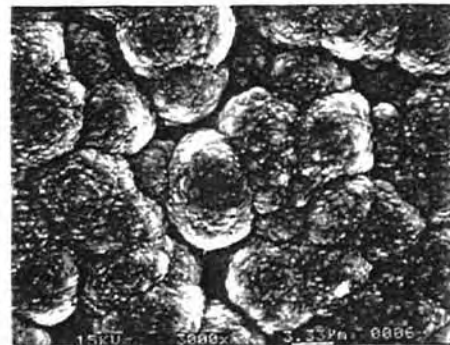
2 % CH$_4$

Figure   6.4.2.1.1 SEM Micrographs of Diamond Films of 12 Samples
Deposited Under Different Experimental Conditions

The increase in the methane concentration in the gas phase would lead to the increase in secondary nucleation. The secondary nucleation on the existing diamond facets prevents the existing crystals from growing completely thus leading to the decrease in the grain size. This also implies that a carbon supersaturation in the gas phase dominates the entire deposition process, by increasing the nucleation density.

6.4.2.2 μ-Raman spectroscopy

Raman spectra from the 12 samples showed a sharp peak at ~ 1332 cm^{-1} corresponds to that of diamond and the broad peak around ~ 1550 cm^{-1} corresponds to that of non-diamond carbon. In order to get a quantitative data from Raman analysis, concerning the phase purity, crystallinity and to determine the residual stresses the collected Raman spectra were subjected to the following data reduction procedure.

6.4.2.2.1 Analysis of Raman Spectra

In their investigation on the line shape analysis of the Raman spectrum, Robins et . al (1990) designed a model shape function with a minimum number of free parameters, and then used a nonlinear least squares method to fit the model to the data. They have represented the photoluminescence (PL) background by a quadratic polynomial. In the present investigation, initial curve fitting was attempted using a similar quadratic polynomial, for the background. However, since the shape of the PL background is more complex, a simple quadratic polynomial was a inappropriate model and the results obtained were not satisfactory.

114

Hence, it was decided to model the PL background as a combination of an exponential and a Gaussian function, given by the following expression:

$$I_{Background} = C_0 + a_0 e^{-x/a_1} + b_0 e^{-\frac{(x-x_0)^2}{2\sigma^2}}$$

The total function developed to fit the experimental Raman spectrum is a sum of two symmetric lines, representing the diamond Raman line and the sp^2 bonded carbon Raman band, and a PL background given by the above expression.

$$I_{fit}(k) = I_{Background}(k) + I_{diamond}(k) + I_{non\text{-}diamond}(k)$$

This background function was loaded into Jandel's Scientific Peakfit. The diamond peak was fitted to a Lorentzian shape function and the broad non-diamond peak was fitted to a Gaussian shape. Computations were continued through atleast one hundred iterations to ensure a good fit. The coefficient of determination, r^2, provided a measure of accuracy for the computer-generated curve. This number, which ranges from zero to one (with one indicating a perfect fit), was normally 0.99 or better. Figure 6.4.2.2.1.1 shows the fitted Raman spectra. Following this curve fitting procedure, the FWHM of the diamond Raman line, intensity ratio of the diamond to the non-diamond, and the shift of the Raman peak were obtained. Residual stresses were evaluated from the peak shift using the formula $-\delta/2.13$ [Mohrbacher et al., 1996]. Table 6.4.2.2.1.1 summarizes the results of the Raman analysis.
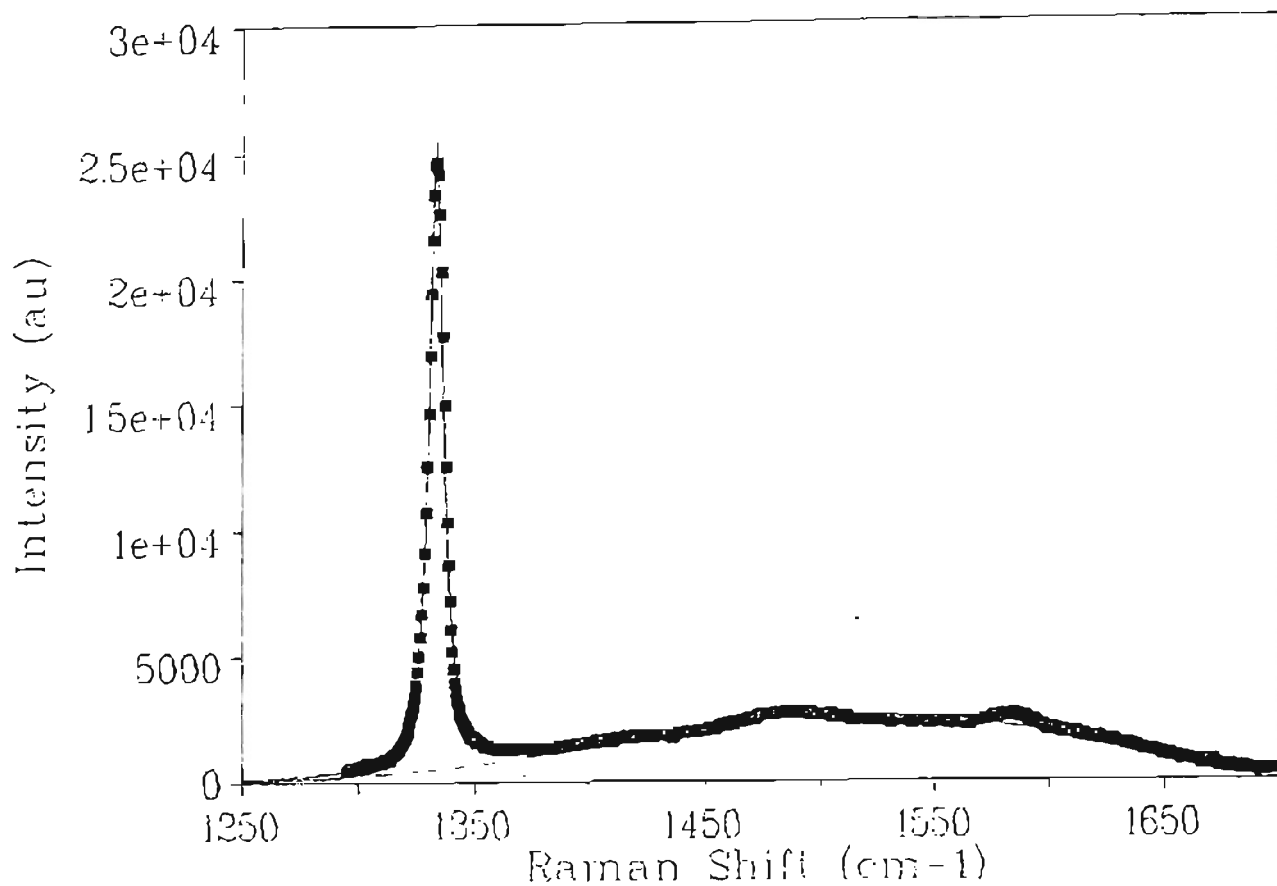
Figure 6.4.2.2.1.1 Deconvolution of the Raman Spectrum of Diamond on Si_3N_4 using Curve Fitting

Table 6.4.2.2.1.1   Results from the Raman Analysis

CH$_4$	800 ºC			850 ºC			900 ºC		
	Δ*	R**	δ***	Δ*	R**	δ***	Δ*	R**	δ***
(%)	cm^{-1}		cm^{-1}	cm^{-1}		cm^{-1}	cm^{-1}		cm^{-1}
0.5	4.56	0.85	-1.91	4.12	0.90	-2.04	3.99	0.92	-2.25
1	4.99	0.83	-1.49	4.67	0.87	-1.66	4.59	0.89	-1.75
1.5	6.11	0.78	1.31	5.35	0.79	1.53	5.15	0.81	2.12
2	7.17	0.69	1.53	6.82	0.70	1.82	6.14	0.72	3.35

*Δ = FWHM; **R = Intensity ratio $I_d/(I_d+I_{nd})$; ***δ = Peak shift

Figures 6.4.2.2.1.2 and 6.4.2.2.1.3 show the variation of the intensity ratio with methane concentrations and deposition temperatures respectively.
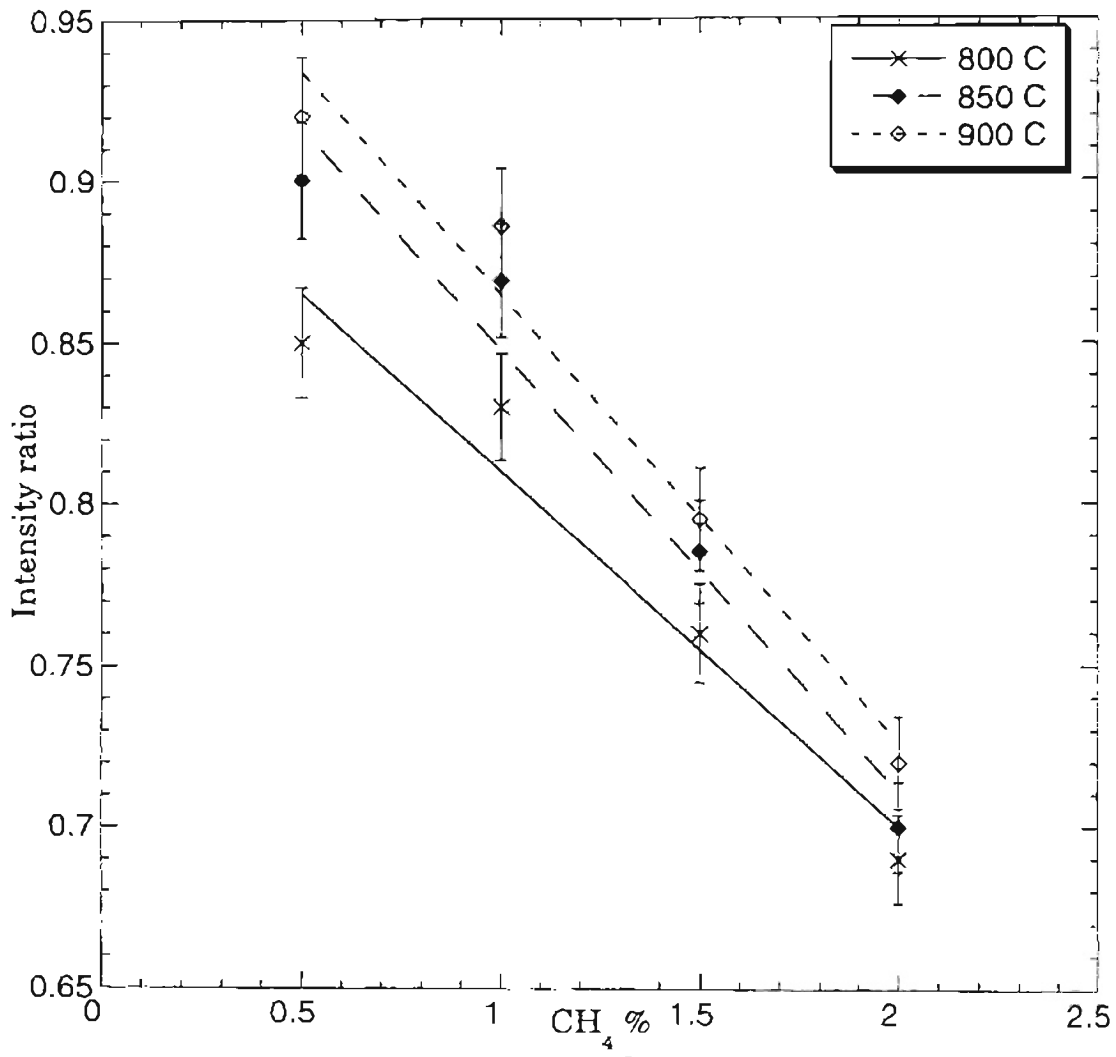
Figure   6.4.2.2.1.2   Variation of the Intensity Ratio of the Diamond to the Non-Diamond Peaks as a Function of Methane Concentration
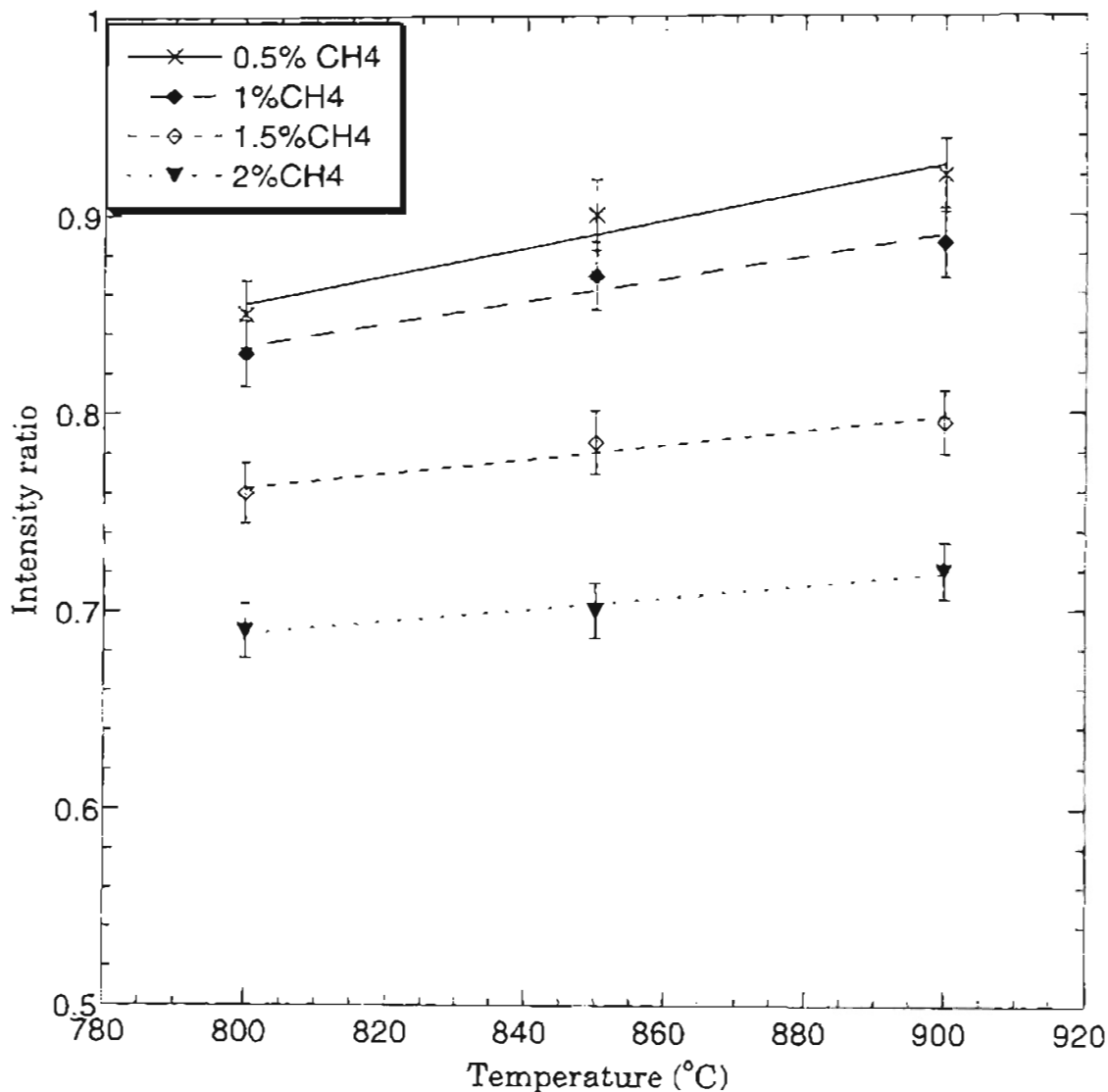
Figure   6.4.2.2.1.3   Variation of the Intensity Ratio of the Diamond to the Non-Diamond Ratio as a Function of Deposition Temperature

It can be seen from Figure 6.4.2.2.1.2 that the phase purity of the diamond films decreases with increase in the methane content (~0.93 at 0.5% CH_4 to ~ 0.70 at 2% CH_4). The trend appears to be the same at all deposition temperatures.   However the intensity ratio increases with deposition temperatures (Figure 6.4.2.2.1.3).

Wang et al.,(1996) showed that carbon deposits with a high sp^3/sp^2 ratio can be obtained in a definite range of substrate temperatures and that the diamond to non-diamond ratio has a maximum at a given temperature, whose value depends on deposition parameters. It has been proposed in growth models (Angus et al., 1993) that at temperatures < 800 °C the deposition of amorphous sp^2 -carbon is due to the condensation of aromatic hydrocarbons formed in the thermally activated gas phase. At high temperatures (~800-1000 °C), the decomposition of hydrogenated sp^3 carbon atoms of the diamond surface leads to the formation of π-bonds and to the codeposition of an amorphous sp^3/sp^2 carbonaceous net work. Therefore, the increase in the phase purity of diamond films at the temperature range investigated here may be attributed to the increase in the atomic hydrogen concentration, which stabilizes the dangling bonds from condensing into an amorphous carbon phase.

Figures 6.4.2.2.1.4 and 6.4.2.1.5 show the variation of the FWHM of the diamond peak with methane and deposition temperatures respectively. The FWHM generally reflects the amount of disorder or defect density incorporated in the material. The increase in the FWHM of diamond with increase in the methane concentration is significant (~3 cm^{-1}). However, with increase in deposition temperature, it can be seen that the decrease is quite small (~ 1 cm^{-1}). i.e. the FWHM of the diamond Raman line more or less remains stationary with the increase in the deposition temperature.
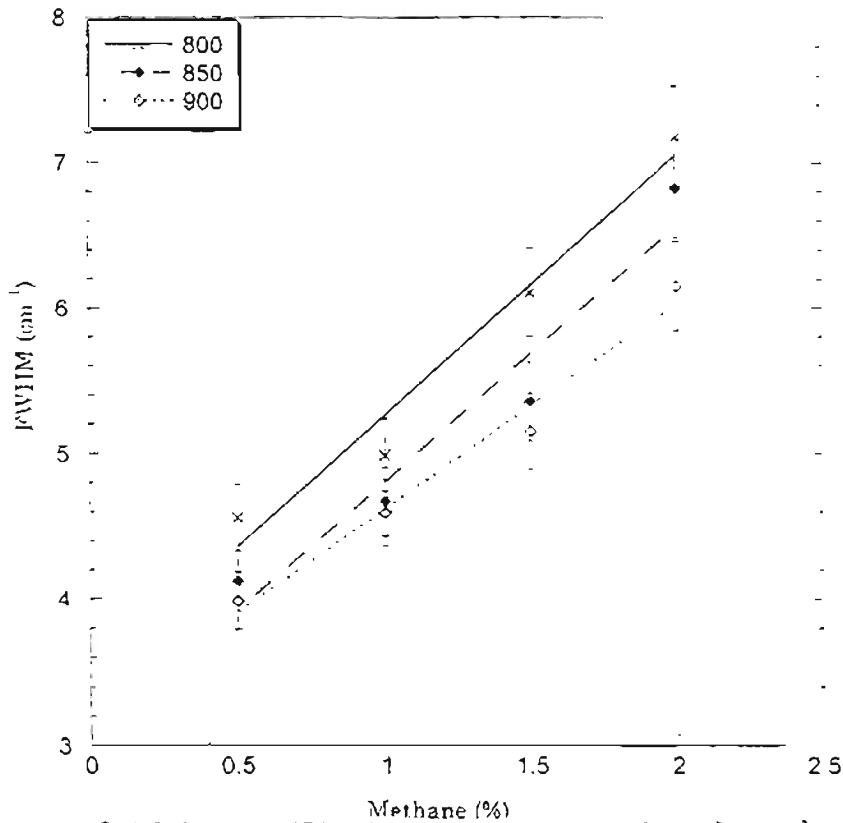
Figure   6.4.2.2.1.4   FWHM of the Diamond peak as the Function of
Methane Concentration
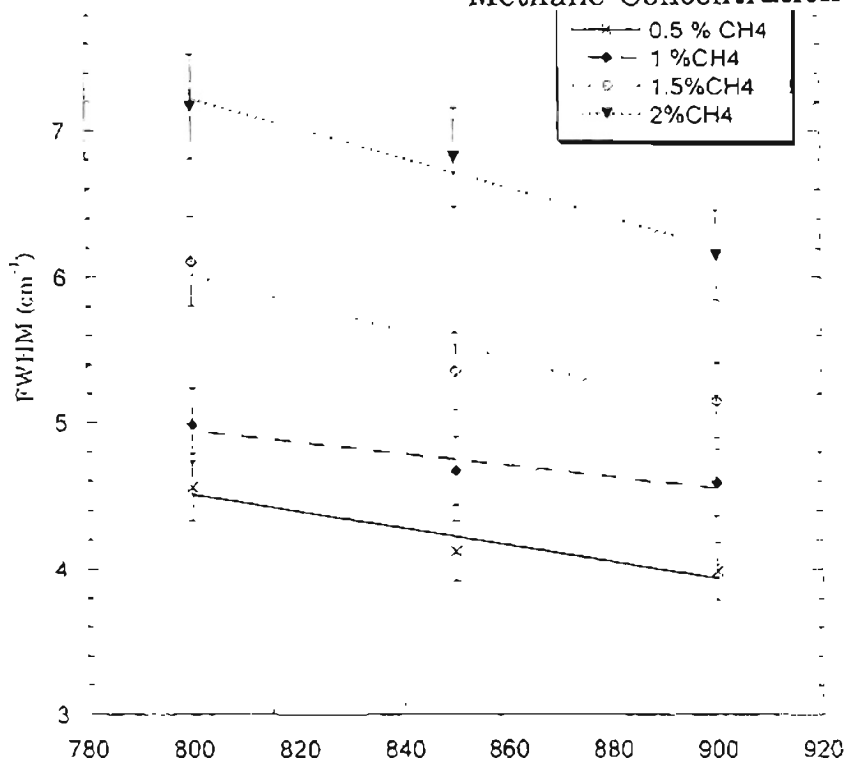
Figure   6.4.2.2.1.5   FWHM of the Diamond Peak as a Function of
Substrate Temperature

The increase in the FWHM can be attributed to the increase in the defects and the non-diamond contents with increase in methane concentration. The Raman line for diamond is fitted to a Lorentzian shape, and the Raman signal is controlled by the phonon life time. Thus, a decrease in FWHM implies an improvement in the crystalline quality and vice versa. Defects and local impurities decrease the phonon life time and increase the FWHM. Therefore, the FWHM of the Raman line increases as the defect concentration increases. Since increase in the CH_4 concentration leads to an increase in the deposition of non-diamond and graphitic phases an increase in FWHM can be explained.

6.4.2.3 Residual Stresses

Figures 6.4.2.3.1 show the variation of residual stresses with the methane concentration. It can be seen from the figure that the residual stresses of diamond films deposited on Si_3N_4 substrates change from tensile (associated with a peak shift towards lower wave numbers i.e. < 1332 cm^{-1}) to compressive (associated with peak shifts towards higher wave number > 1332 cm^{-1}) with increase in the methane concentration.

Peng et al., (1995) reported that the diamond films deposited on silicon nitride samples have tensile stresses (~0.7 Gpa). Mohrbacher et al., (1996) reported that the residual stresses of diamond films on WC-Co and SiAlON are compressive and tensile in nature respectively. Windischmann et al., (1991) investigated the effect of deposition temperature and methane on residual stresses of diamond films deposited on Si.
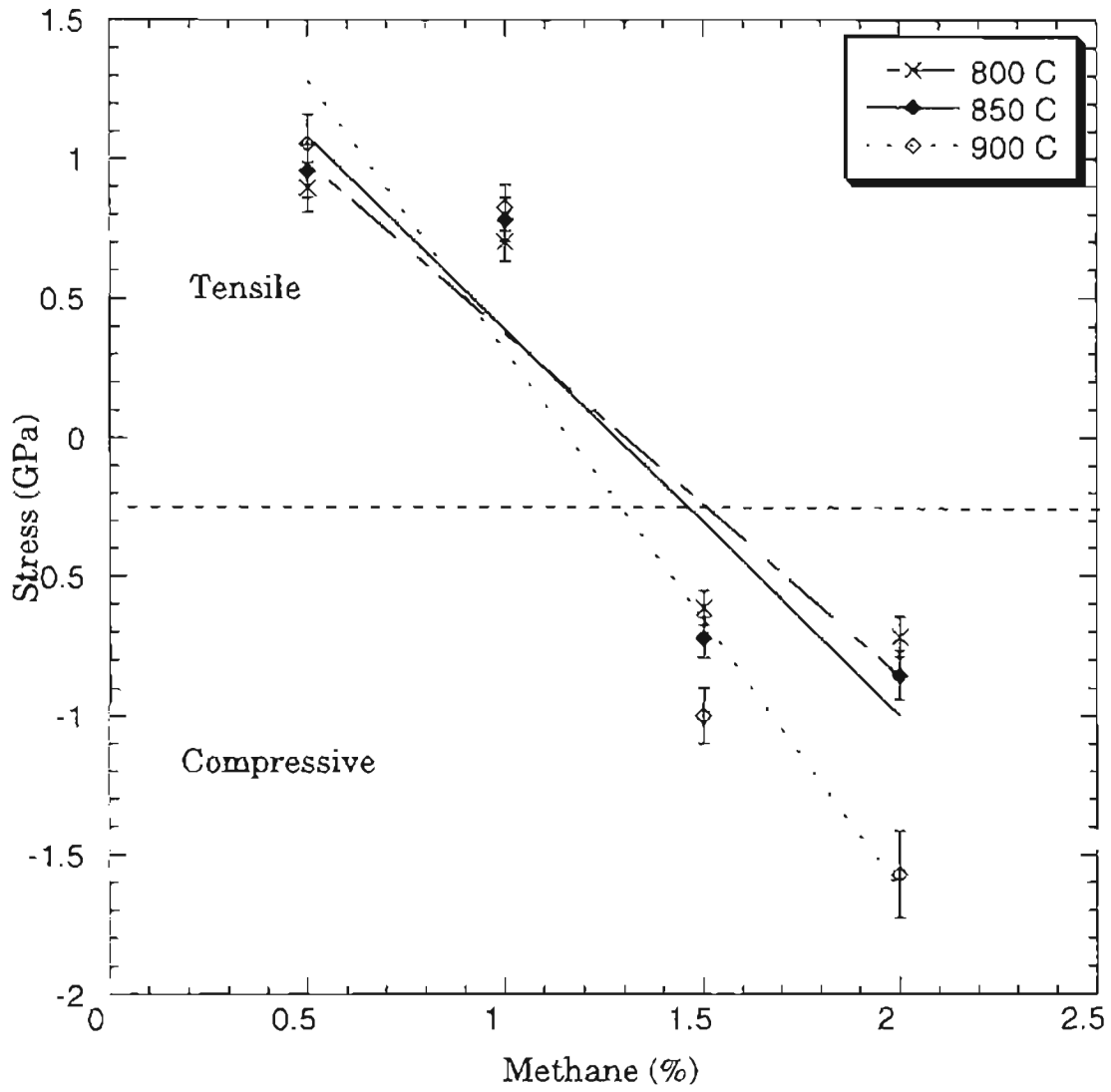
Figure 6.4.2.3.1 Variation of Residual Stresses with Methane Concentration, Showing a Change in the Stress State

They indicated that the thermal stresses were relatively constant for deposition temperatures from 550 °C to 900 °C. However, they found that the intrinsic stresses are tensile and interpreted its origin in terms of a grain boundary relaxation model due to a fine-grained and porous microstructure. The decrease in the intrinsic tensile stress values with increasing methane concentration was attributed to the impurities such as sp^2 bonded carbon and hydrogen incorporated in the diamond films. Kuo et al., (1996) contradicted the above model. They obtained comparable values of residual stresses for both diamond crystals and diamond films formed on Si, WC and quartz substrates. Hence, they suggest that the contribution from the grain boundary relaxation is small and the intrinsic stress due to the transformation of non-diamond carbon to a more stable graphite phase may be a significant factor for the residual stresses of the diamond films. A greater non-diamond content in the films would therefore give rise to a greater compressive stress. They found that the residual stresses were compressive for both Si and WC substrates, and tensile for quartz substrates.

The lattice constant of diamond is 3.567 Å and that of Si_3N_4 is a = 7.59-7.61 Å and c = 2.71-2.92 Å. When diamond film is deposited on Si_3N_4, the lattice may expand in diamond and shrink in Si_3N_4 because of lattice mismatch. Consequently, diamond films on silicon nitride substrates should be under a tensile stress which is observed in the present case. The thermal stress σ_{th} is calculated from the formula (Windischmann, et al., 1991):

$$\sigma_{th} = [E/(1-\nu)] \int_{T_1}^{T_2} (\alpha_s - \alpha_f) dT$$

where, α_s and α_f are the thermal expansion coefficients of the substrate (Si_3N_4 in this case) and diamond respectively, E/1-v is the biaxial Young's modulus (1345 Gpa for diamond) (Field et al., 1979), T_1 is the deposition temperature and T_2 is the room temperature. Table 6.4.2.3.1 shows the calculated values of the thermal stresses at various deposition temperatures:

Table 6.4.2.3.1 Thermal Stresses at Various
Deposition Temperatures

Temperature(^{o}C)	Thermal Stresses (GPa)
800	-0.419
850	-0.456
900	-0.473

The residual stress in the coating is the sum of the intrinsic stresses induced during the growth phase and the thermal stresses. Thermal stresses are evaluated from the above expression and the biaxial residual stress is calculated from the peak shift of the Raman diamond line. The intrinsic stresses can be calculated from

$$\sigma_{intrinsic} = \sigma_{total} - \sigma_{thermal}$$

In this case the thermal stresses which are compressive are smaller than the intrinsic stresses which are tensile in nature, thus making the overall stress tensile in nature. It has been reported in the literature that the voids and dislocations produce tensile stresses, whereas hydrogen clusters and impurity phases produce compressive stresses (Buckel, 1969). Windischmann et al., (1991) related the origin of the intrinsic tensile stresses in the diamond films deposited on Si, to the grain boundary

124

relaxation phenomenon. Diamond deposited by those researchers was a fine grained (~ 0.12 μm grain size) porous microstructure containing a high density of grain boundaries and voids. The authors argued that these films are under tensile stresses due to the attractive atomic forces acting across grain boundary or micropore gaps which induce an elastic strain in the anchored grains due to a constrained relaxation. This is referred to as grain boundary relaxation model. In the present investigation the above model is not applicable, since the films obtained at 0.5 and 0.1 % CH_4 concentration consisted of well defined crystallites (~2-4 μm). In addition the FWHM of these diamond films was between ~ 3-4 cm^{-1}, which also is an indication that the defect density incorporated in the films is much less. Hence the origin of the observed tensile stress in the present investigation might be related to the heteroepitaxial growth conditions arising from lattice mismatch.

It can be seen from Figure 6.4.2.3.1 that the residual stress changes from tensile to compressive at about 1.5 % CH_4. Since the thermal stresses are always compressive and are negligible in this case, it follows that the intrinsic stress is compressive. This might be attributed to the compressive stresses produced by graphitic and other non-diamond phases.

With increase in methane concentration it was noticed that the amount of non-diamond carbon incorporated in the films increases. The increase in CH_4 concentration leads to the decrease in the grain size. It has been reported that non-diamond phase will be co-deposited preferentially along the grain boundaries (Bachmann, et al., 1994; Partridge et al., 1996). It can be postulated that the decrease of the crystal size leads to the precipitation of amorphous carbon at the grain boundaries. Non-diamond carbon produces

a compressive stress field owing to its large specific volume (1.5 X that of diamond) (Windischmann et al., 1991). The idea that graphitic carbon defects are responsible for the compressive stress has been put forward by Yoshikawa et al., (1989). Hence, at high CH_4 concentrations the increase in the non-diamond carbon introduces a compressive stress field, which overrides the tensile growth stress and changes the overall residual stress to compressive.

It follows that the stress in the diamond films on Si_3N_4 substrates is sensitive to the deposition conditions. Tensile or compressive stresses can be achieved depending on the methane fraction and deposition temperature. The deposition conditions can be chosen so that the coatings have a minimum residual stress at methane concentrations between 0.5 - 1%.

6.4.3 Evaluation of Adhesion

The diamond films deposited on Si_3N_4 substrates were tested for adhesion. Indentation tests were carried out using a Wilson Rockwell hardness tester with a Brale diamond indentor at discrete loads of 15, 30, 45, 60, 100 and 150 kgf. At each load, atleast 3 indentations were made. The crack diameter was measured with an optical microscope and reexamined under the SEM. Figures 6.4.3.1 a - d show the micrographs of the diamond films after indentation tests at 15, 45, 60, and 100 kgf respectively.
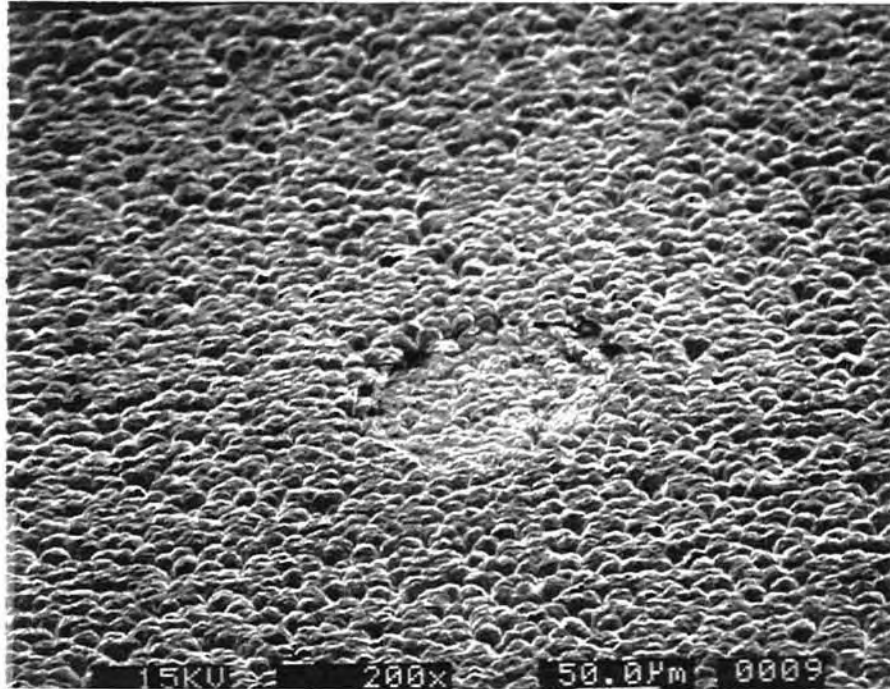
Figure   6.4.3.1 a) SEM Micrograph of Diamond Coating Showing
an Indentation Imprint (Load = 15 kgf)
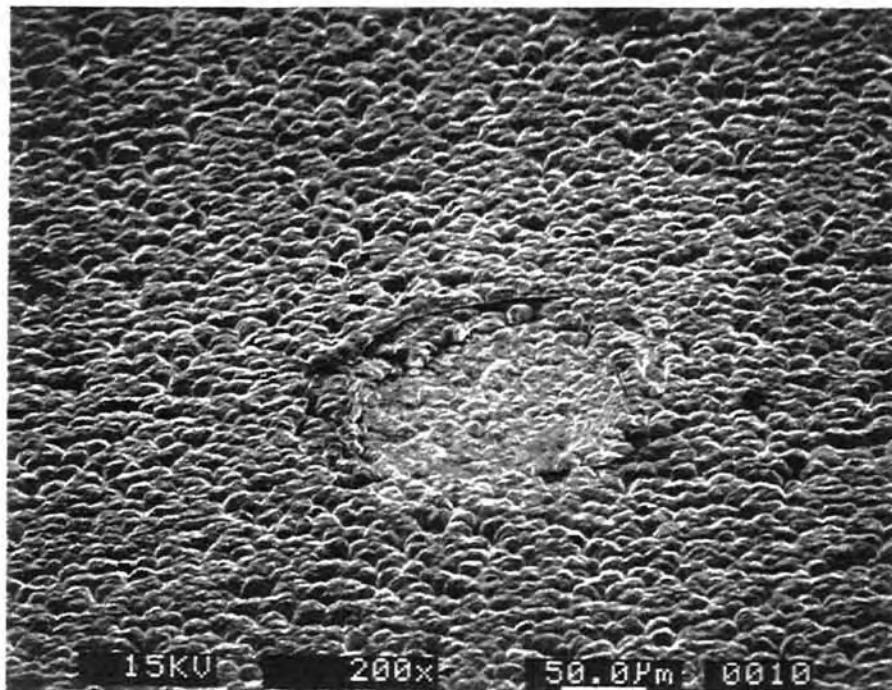
Figure   6.4.3.1 b) SEM Micrograph of Diamond Coating Showing
an Indentation Imprint (Load = 45 kgf)
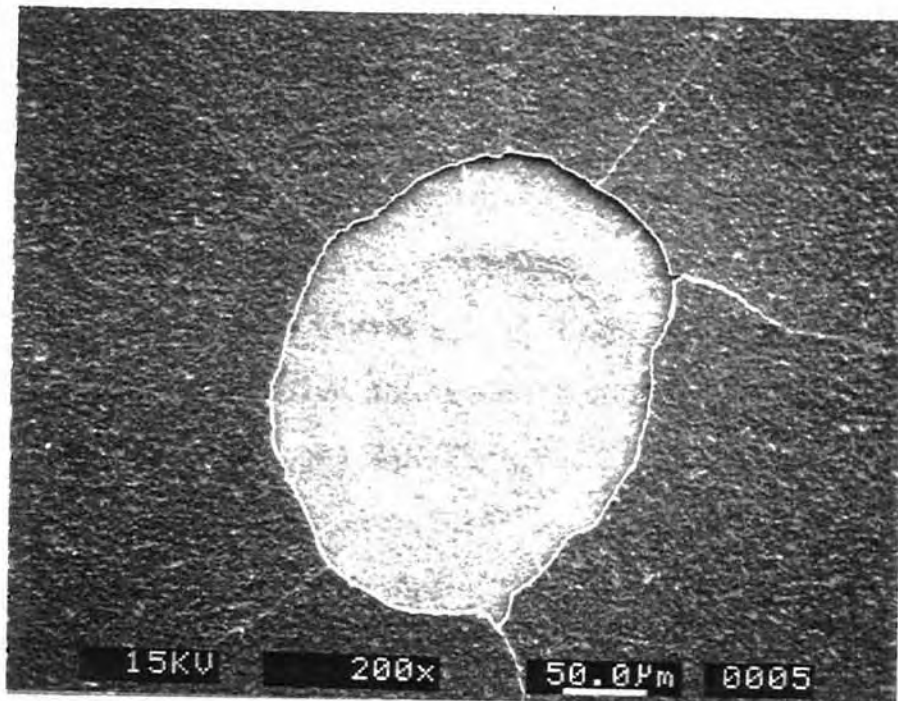
Figure   6.4.3.1 c) SEM Micrograph showing the Cracks in the
Si₃N₄ substrate (Load = 60 kgf)
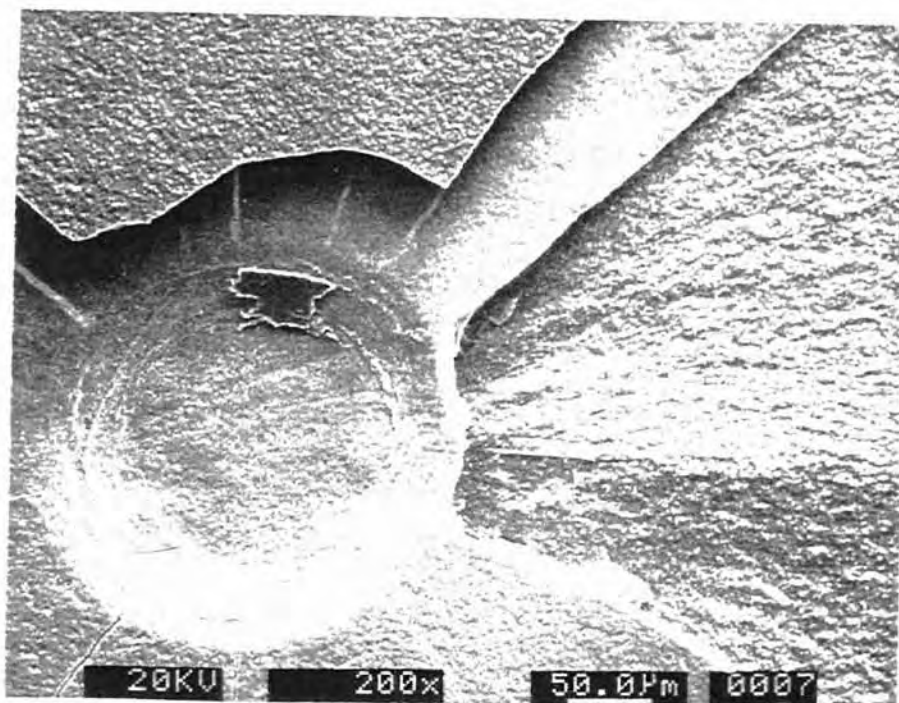
Figure   6.4.3.1 d) SEM Micrograph showing the fracture of the
Si₃N₄ substrate (Load = 100 kgf)

128

It can be seen that the diamond films and the silicon nitride substrate crack around the indentation center for load of 60 kgf (Figure 6.4.3.1c). Peng et al., (1995) encountered the same situation while testing the adhesion of the diamond films deposited on silicon nitride. They reported that the diamond films spalled even under a load of 31.25 kgf (the lowest limit of the apparatus). However, the diamond films deposited in the present investigation survived upto a load of 45 Kgf (Figure 6.4.3.1b). It can be seen from the micrographs (Figures 6.4.3.1c and d) that cracks propagate in the substrate and result in the fracture and peeling off of the silicon nitride pieces. The fracture of the silicon nitride could lead to the chipping and loss of the diamond films.

Figure 6.4.3.2 shows the plot of lateral crack diameter versus indentation load for the diamond coatings on Si_3N_4 substrates. The relative error in the measurement of the lateral crack was ~ 10 %. The reciprocal of the slope dP/dx was evaluated as an index for the cracking resistance, and adhesion strength of the film as discussed in section 5.5. The crack resistance of the diamond coatings on Si_3N_4 is calculated as ~ 238 Kgf mm^{-1}. Huang et al., evaluated the crack resistance of diamond coatings on Si-Al-O-N and SiC as ~ 243 and 226 kgf mm^{-1} respectively. Yen et al., (1990) obtained poor adhesion of diamond coatings on SiAlON substrates. They obtained a value of ~ 162 kgf mm^{-1} for diamond coatings on SiAlON substrates.
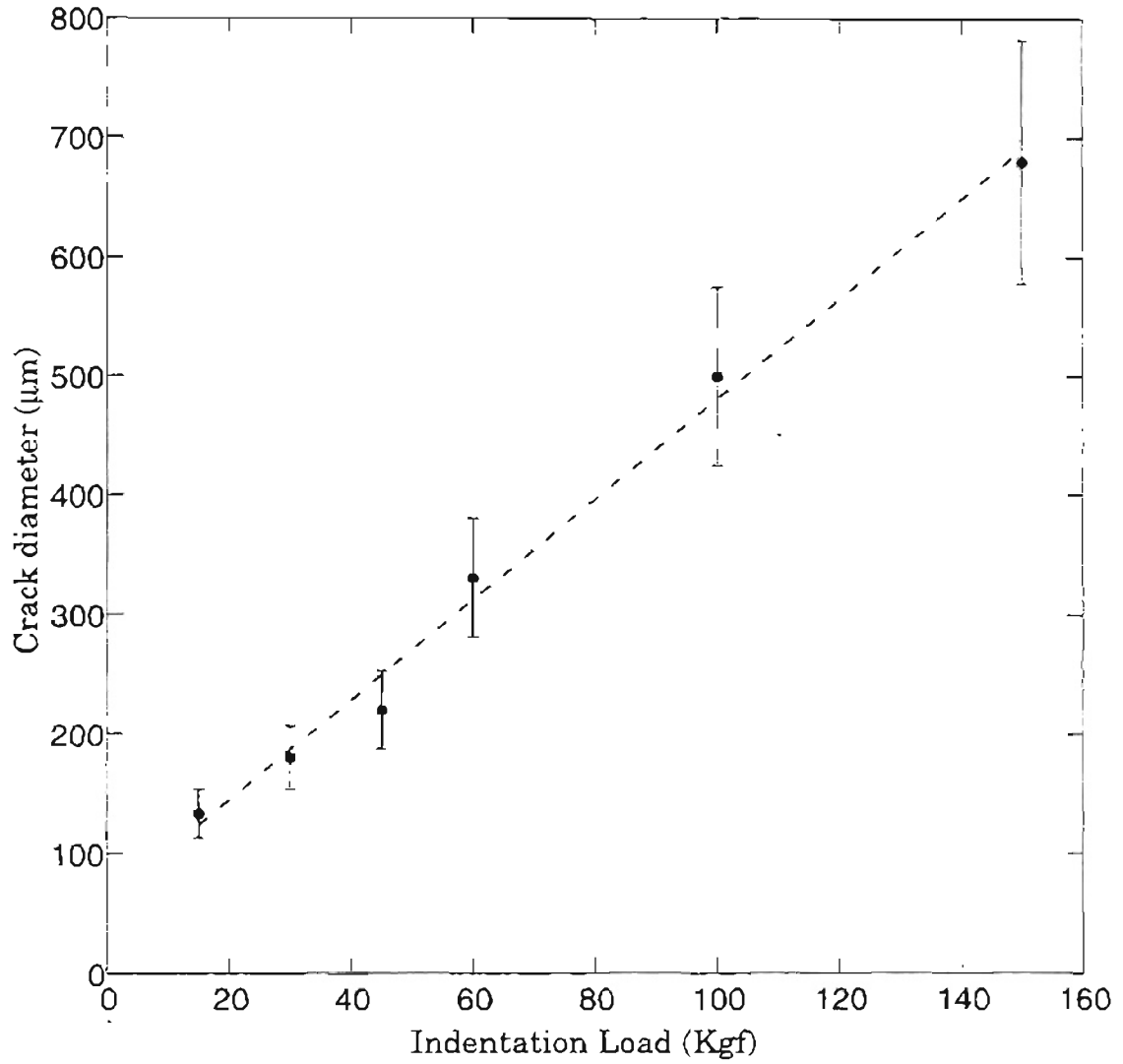
Figure   6.4.3.2   Crack Diameter Vs Indentation Load for Rockwell
Indentation of the Diamond Coating, Deposited on
Si_3N_4 Substrate.

It must be noted that these indentation test results do not necessarily mean poor adhesion of diamond to Si_3N_4. It may not be an effective method to evaluate the diamond film adhesion to Si_3N_4 because of the low fracture toughness of Si_3N_4. Hence, a second method was used to test the adhesion of the diamond coatings, consisting of polishing the diamond films against 6μm diamond paste. This method was originally employed by Fan et al., (1996) and Weihnacht et al (1996). The setup was modified for this investigation and is shown in Figure 6.4.3.3.

The diamond coated tool was held on the force dynamometer and held in place by a fixture as shown in Figure 6.4.3.3. Diamond paste (~ 6 μm) was applied to the spindle of the milling machine which was covered with a polishing cloth (Buehler). Abrasion force was applied through the spindle locked in place over the diamond coated tool. The value of the force used for these wear tests was selected at 50 N based on the literature review. The force was monitored by the data acquisition system connected to the force dynamometer. Minor changes in the force values during the abrasion process was corrected with the spindle pressure on the coated tool. The spindle coated with the diamond paste was rotated against the diamond coated tool for specific period of time.

Rotating Spindle

Spindle end
coated with diamond paste

Diamond coated Tool

Force Dynamometer

Charge Amplifier

Data Acquisition System
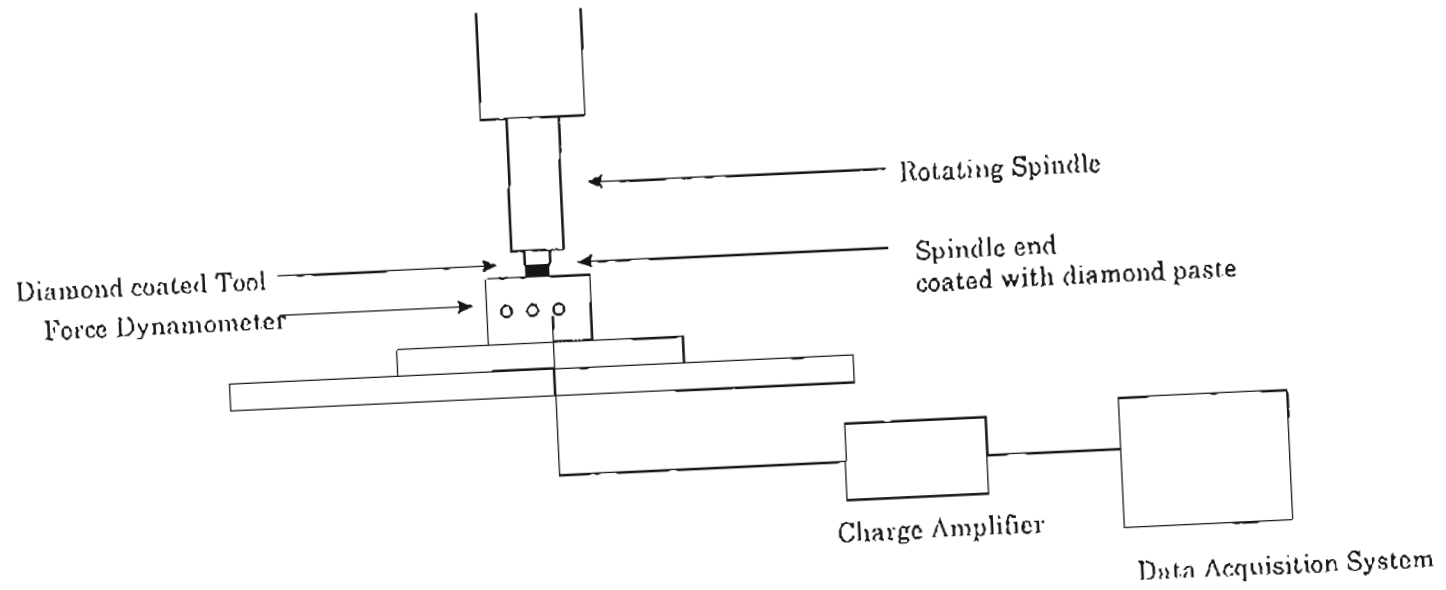
Figure   6.4.3.3   Setup to Measure the Adhesion of Diamond Coatings

The wear surface of the diamond coated tool was examined after every 30 minutes inside the SEM and the amount of diamond retained on the surface estimated. Figures 6.4.3.4a and 6.4.3.4b show the micrographs of the diamond coating prior to the wear test and wear surface of the diamond after one hour.

Figure   6.4.3.4 a)   SEM Micrograph Showing the Diamond Coating before the Wear Test
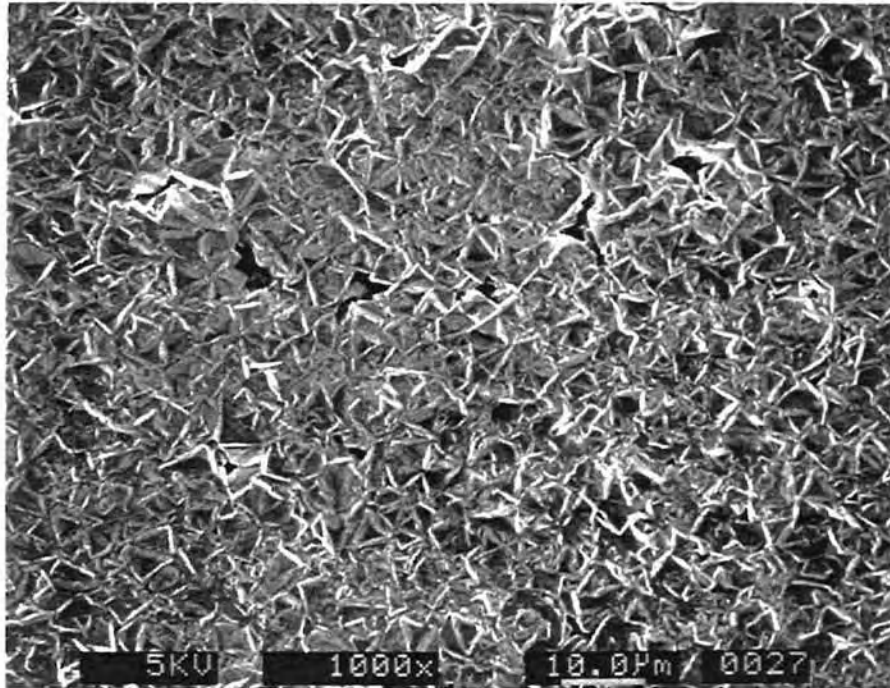
Figure   6.4.3.4 b)   SEM Micrograph Showing the Wear Surface of
Diamond after One Hour

Complete coverage of the diamond film can be noticed even after one hour of polishing. The eroded surface (Figure 6.4.3.4b) appears to be smooth, which is an indication of the wear of the original flat crystallites of diamond by grinding. Thus, the wear process appears to be grinding and is not related to the cleavage of the crystallites. The low force applied might be responsible for the wear mechanism by grinding. Figures 6.4.3.4c and 6.4.3.4d show the wear surfaces of the diamond after 2 hours and 4 hours respectively.
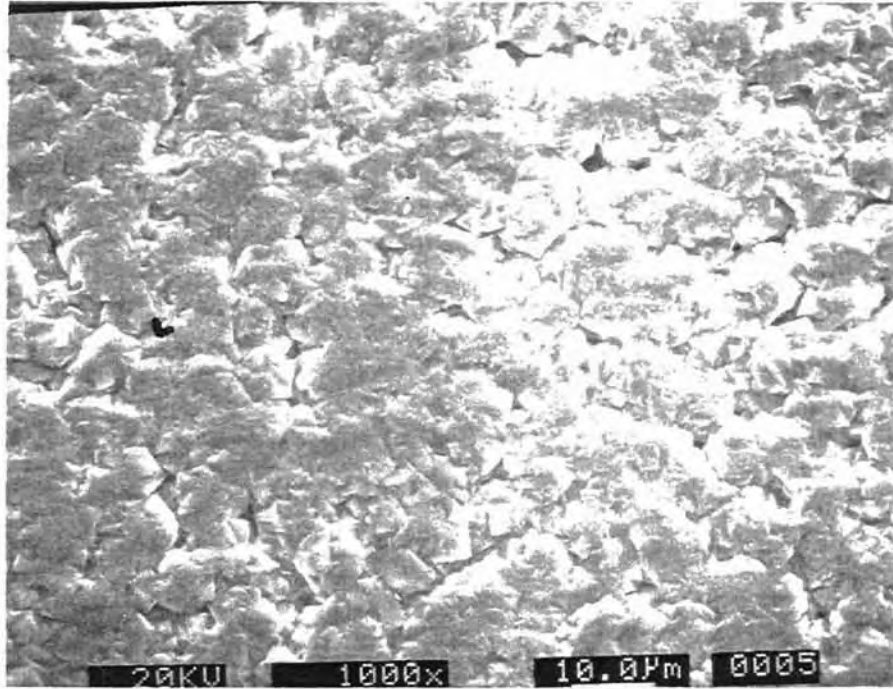
Figure   6.4.3.4 c)   SEM Micrograph Showing the Wear Surface of
Diamond after Two Hours
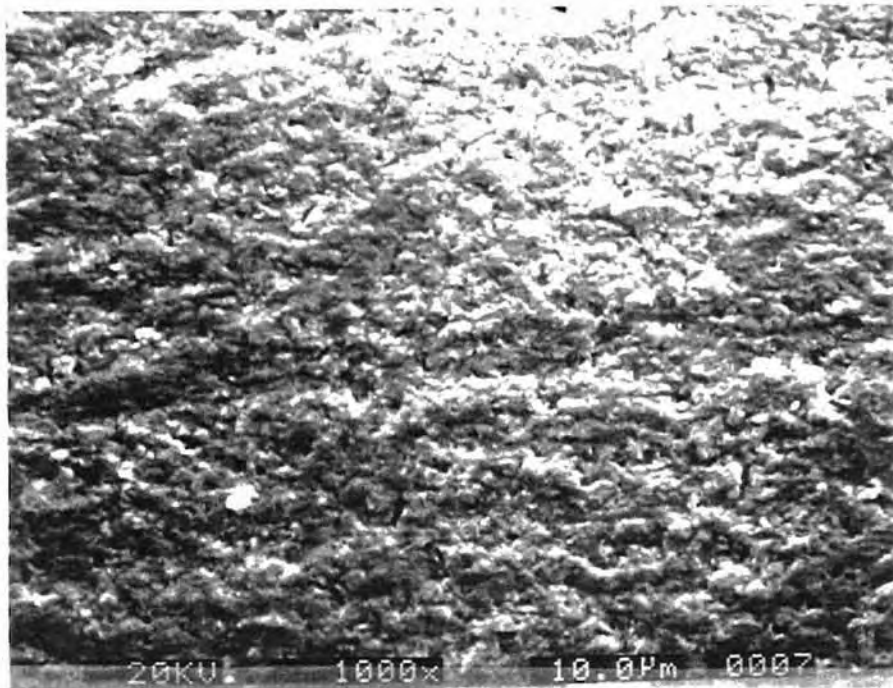
Figure   6.4.3.4 d)   SEM Micrograph Showing the Wear Surface
after Four Hours

The wear surface after 2 hrs (Figure 6.4.3.4c) appears to be smooth. A few voids observed on the surface can be associated with the non exposed surfaces of diamond crystallites to wear. Figure 6.4.3.4d shows the wear surface after 4 hours. It can be observed that the diamond film is completely removed from the surface after 4 hrs. The removal of diamond must be due to the abrasion process, than poor adhesion because the wear surface is smooth. The mechanism is erosion of diamond by grinding and agglomeration of the diamond wear debris to the surface of the diamond (Weihnacht et al., 1996). Figure 6.4.3.5 is another wear surface of diamond coating on silicon nitride deposited at 1.5% CH_4 concentration.
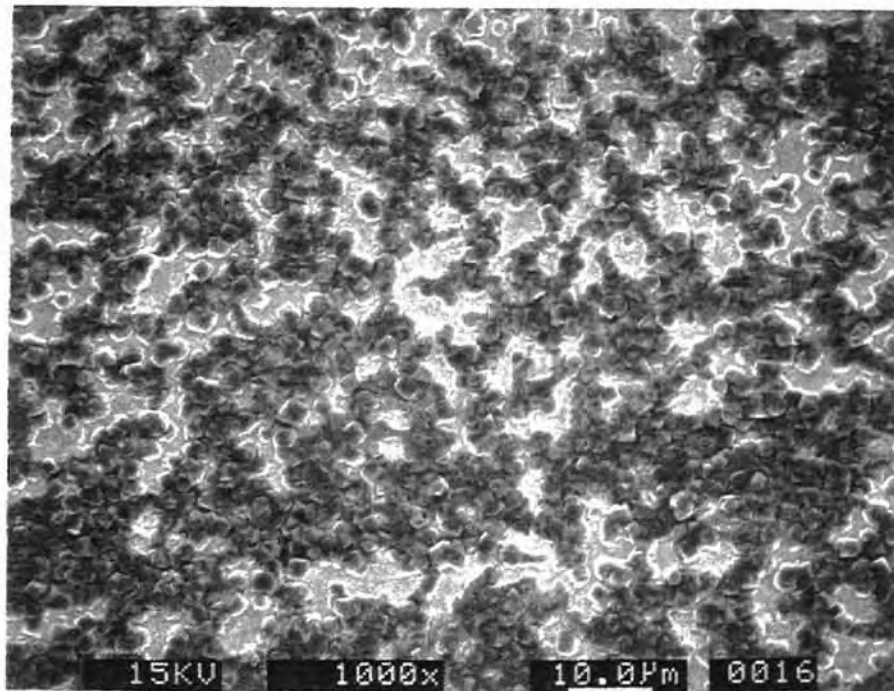
Figure   6.4.3.5   SEM Micrograph Showing the Wear Surface of
Diamond Coating on Si_3N_4 at 1.5% CH_4 Concentration

It can be seen from the figure that surface is covered with diamond only at a few places and at other places there are no crystallites. In this case the wear is related to the cleavage of diamond and can be attributed to the poor adhesion between the diamond and the substrate. High methane concentrations lead to the increase in the non-diamond deposits which deteriorate the quality and also adhesion. Diamond coatings deposited at high methane concentrations showed delamination at the lowest load (15 kgf) during indentation tests.

Thus, both wear and indentation tests emphasized the importance of the choice of process parameters on the adhesion of diamond coatings to the substrate. Deposition conditions affect the film quality and adhesion through their influence on the content of diamond and non-diamond carbon components in the diamond film, the film morphology, and the residual stresses in the film.

CHAPTER 7

Diamond Coatings on Cemented Carbides

7.1 Introduction

Considerable research efforts are focused on the development of diamond coatings on cutting tools (Shen 1996; Vashilash, 1995; Stephan et al., 1992; Quinto, 1996; Leyendecker et al., 1991; Konyashin et al., 1996; Komanduri 1993; Koepfer, 1996; Hintermann, 1996; Guseva et al., 1997; Jagannadham et al., 1997). Cemented carbides, which have excellent properties for applications in the areas of wear protection and low frictional applications could be further improved by diamond coatings especially for machining abrasive Al-Si alloys and glass reinforced composites (Oslon et al., 1996; Oles et al., 1996; Alam et al., 1997). However, the main problem is the lack of good adhesion between the diamond coating and the cemented tungsten carbide substrate (Haubner et al., 1989; Shuji et al., 1991).

Soderberg et al., (1991) cited three reasons for this problem, namely, 1. void formation at the interface, 2. non-diamond material at the interface, and 3. high residual stresses. Each of these factors must be overcome or compensated for in order to produce adherent diamond films on WC-Co substrates. Voids form because of low nucleation density. As the nuclei grow (approximating spheres) and eventually coalesce, pores are left at the carbide surface between the bases of the ball-like grains. Secondary nucleation is very limited, so the voids are not filled during growth.

The second problem is generally considered to be the most deleterious to diamond film deposition and adherence on cemented carbide materials. For cemented carbides, cobalt is the only suitable binder holding the carbide grains together during sintering. Non-diamond carbon phases form during diamond film deposition due to high solubility of carbon in cobalt at the deposition temperatures (Haubner et al., 1993) and because graphite is the thermodynamically stable carbon phase at these conditions. It is likely that soot and graphite form at the interface between the diamond film and the cobalt in the substrate during cooling from the deposition temperature. As the temperature decreases, the solubility of carbon in cobalt decreases and the dissolved carbon diffuses to the surface where it forms a non-adherent graphite like film. Figure 7.1.1 is the phase diagram for the C-Co system after Kosolapova (1971) which illustrates this phenomenon. The shaded region shows the temperature range in which diamond deposition is commonly performed. At any composition within the solubility range of C in Co, graphite will precipitate out as the temperature is dropped.

Finally, high residual stresses may result from the large thermal expansion mismatch between diamond and the cemented carbide substrate. The linear thermal expansion coefficient of diamond is 3.1 X 10^{-6} /°C . while that of WC-Co ranges between 4.5-7.1 X 10^{-6}/°C depending on the cobalt content (Touloukian et al., 1975). As a result, the deposited diamond is under a residual compressive stress and the substrate is under a residual tensile stress (Clausing et al., 1990).
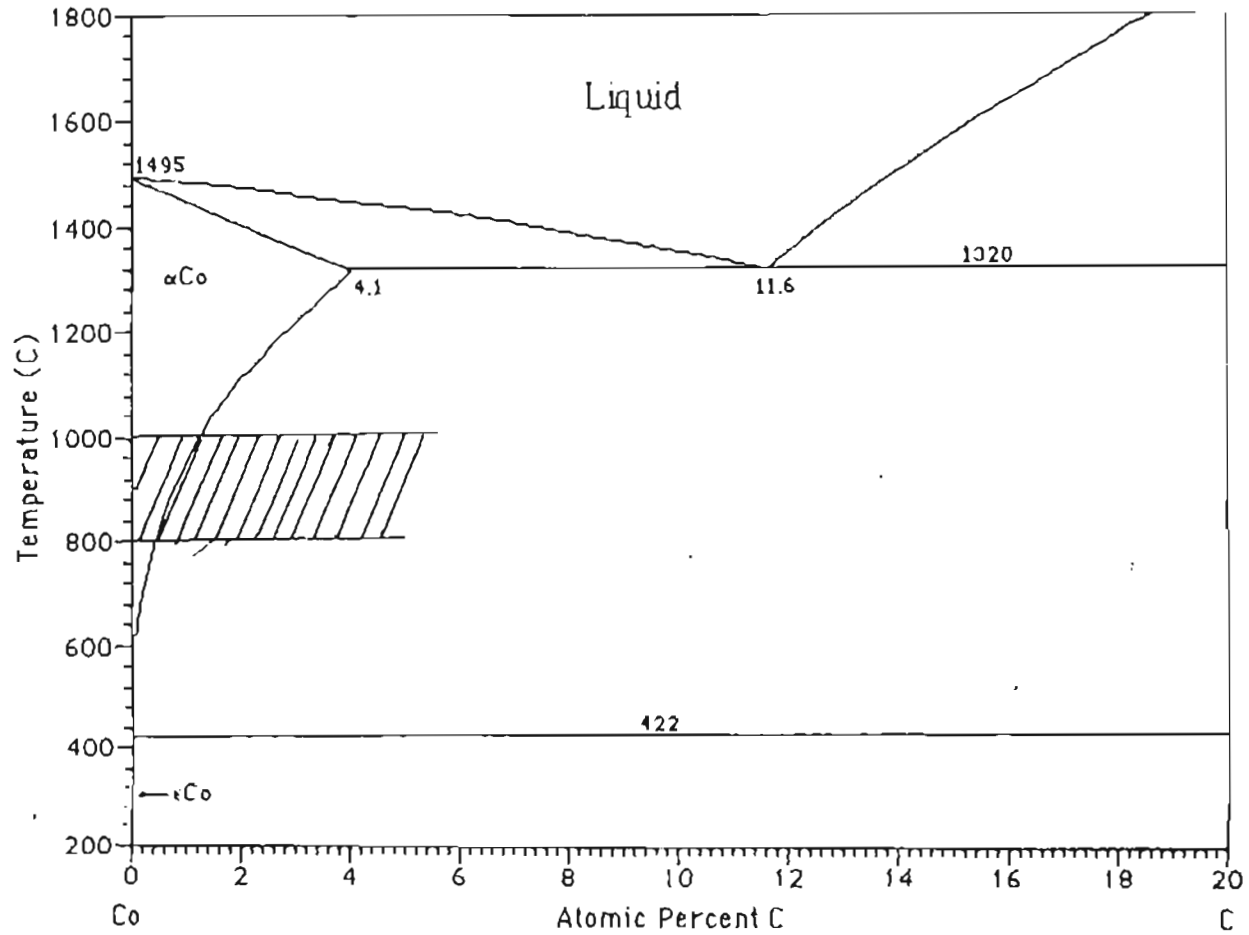
Figure   7.1.1   Phase Diagram for the C-CO System (Kosalapava, 1971)

Of the three problems outlined above, the effect of cobalt is considered to be the most detrimental to diamond nucleation, growth, quality, and adhesion. Hence, this part of the investigation is focused on the effect of cobalt on the quality and adhesion of diamond coatings on cemented carbides. A review of the role of cobalt and the techniques usually adopted to improve the adhesion of diamond coatings on cemented carbides is presented in the first section. Experimental work and discussion of the results are presented subsequently.

7.2 Role of Cobalt

Haubner et al., (1993) observed that direct deposition of diamond on a pure cobalt substrate encounter two basic problems. High carbon dissolution into cobalt during the diamond deposition and the high vapor pressure of cobalt at the deposition temperatures ~ 800 ^{o}C favoring the formation and deposition of amorphous carbon. They reported that diamond deposition is feasible only at low CH_4 concentrations (0.4%). At methane concentrations > than 0.4 %, they could only deposit amorphous carbon.

The influence of cobalt content in cemented WC on the growth of continuous diamond coating was studied by Haubner and Lux (1989). Cemented carbides with 0, 0.3, 1, 2, and 3 wt% Co were prepared by hot pressing. The specimens were polished with SiC (240 grit) abrasive and ground with diamond prior to diamond deposition using hot filament technique. Though the growth and nucleation rates of diamond on cemented carbides were not influenced by the amount of cobalt, they

observed that higher cobalt contents led to the secondary nucleation of diamond and affected the morphology of the diamond coatings.

Bichler (1987) studied the effect of cobalt in cemented carbides on diamond nucleation rates. He found the nucleation rate of diamond on cemented carbides without prior diamond treatment to decrease with increase in cobalt concentration in the range of ~ 3-10% with minimum nucleation at cobalt > 6% (Figure 7.2.1).
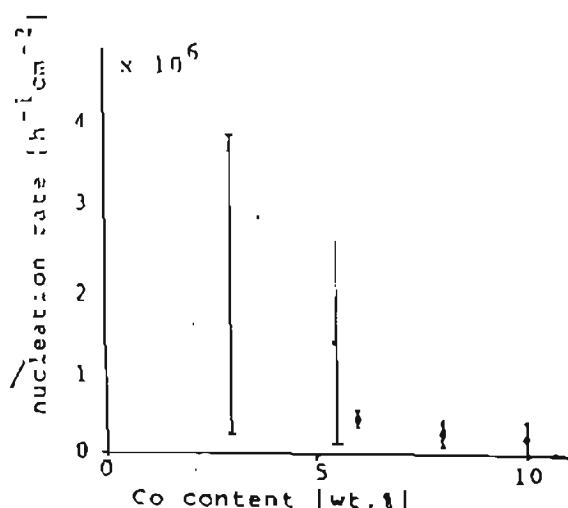
Figure 7.2.1 Influence of Cobalt Content on Diamond Deposition
(Bichler, 1987)

In addition to carbon diffusion into the cobalt binder in the cemented carbide tool during diamond deposition, several studies have noted that cobalt diffused into the growing carbon layer and effected the diamond growth. Mehlmann et al., (1992) reported the formation of ball-shaped particles in several regions after the diamond deposition. By EDXA analysis, they found that these particles were cobalt particles saturated with carbon. They attribute the formation of these particles to the

interaction of cobalt with the growing diamond nuclei. In a subsequent investigation Mehlmann et al.(1994) reported the etching of cobalt at high temperatures in activated atomic hydrogen. Two WC (6% Co) substrates were heated separately in activated 1 % CH_4 / H_2 mixture at different substrate temperatures. The specimens were later analyzed by Auger electron spectroscopy (AES). It can be seen from Figure 7.2.2, that at low substrate temperatures (~ 750-800 °C), there was no change in the cobalt content, while the cobalt content decreased when the substrate was heated to high temperatures (~900 - 950 °C) in the activated gas mixture. The authors attribute this effect to the reaction of cobalt with atomic hydrogen, leading to the formation of gaseous cobalt hydride.
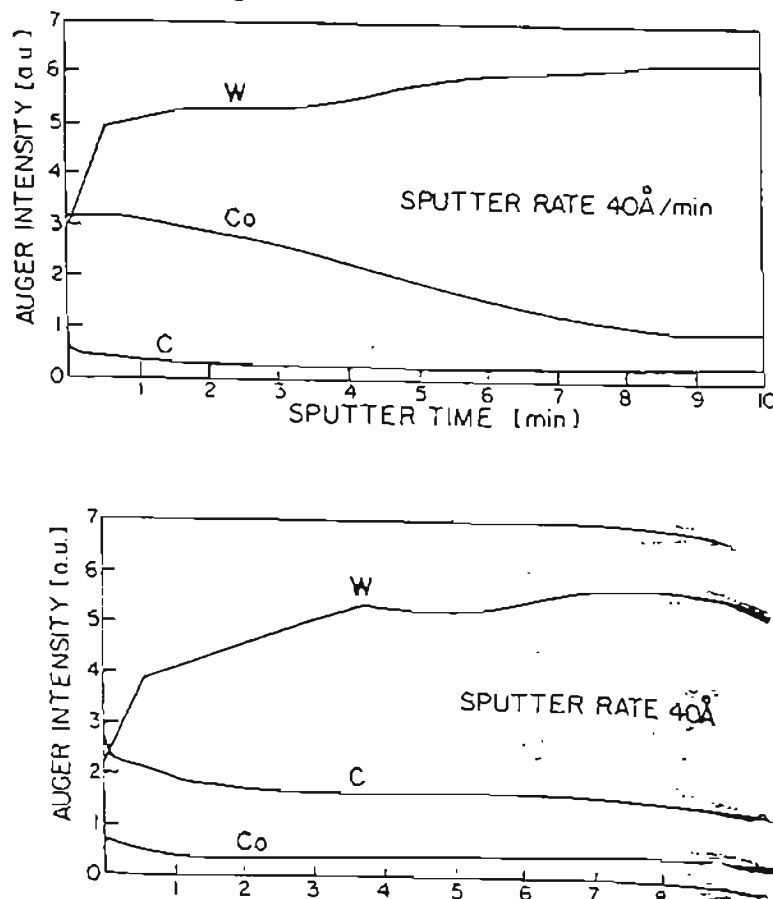
Figure   7.2.2   Auger Spectrum Showing the Decrease in Cobalt Content, when the Sample is Heated at High Temperatures in an Activated Gas Mixture (Mehlmann et al., 1993)

Cobalt in the WC-Co substrates also gets included in the diamond coatings as the deposition time is increased. Due to the presence of cobalt in the diamond film, even after the full coverage of the substrate surface is accomplished, it is difficult to grow high quality diamond. Mehlmann et al., (1994) observed this effect to be more pronounced at lower substrate temperatures. They also observed a large number of cobalt containing particles at lower substrate temperatures (around 750 °C). At high temperatures (940 °C) the number of cobalt containing particles was reduced . The authors attribute this effect to the *in situ* etching effect of cobalt.

This observation contradicts some of the earlier results (Saijo et al., 1991; Oakes at al., 1991), namely, low substrate temperatures (~750-800 °C) during diamond deposition lessens the mobility of cobalt and result in a more adherent film.

Pan et al. (1994) confirmed diffusion of cobalt from the bulk to the surface during the CVD process by AES and Cross-sectional Transmission Electron Microscopy (XTEM) studies. WC with 6% Co was pretreated with a mixture of HNO_3+H_2O to remove the surface cobalt. The deposition was carried out with a hot filament CVD system. From the line shapes of the C (KVV) peaks from the AES spectrum, the authors infer the presence of an amorphous carbon layer with an average thickness < 120 Å, at the interface. They suggest that the diffusing cobalt under CVD conditions plays a key role in the formation of amorphous carbon layer.

Park et al (1993) observed a difference in the surface morphology of the diamond films deposited on WC (5% Co) for etched and unetched substrates. Figure 7.2.3 shows the measured roughness change of the diamond films on both substrates. They attribute the roughness of the films to the movement of the cobalt rich binder phase during deposition. They reported that during the diamond deposition process, the cobalt rich binder phase comes out rapidly and covers some of the growing particles, and inhibits their growth. They also showed that binder phase is mobile during the deposition process. This continuous movement of the binder phase covers new nucleating particles, and reduces the density of the nucleating particles. Park et al., suggest that the reduced particle density causes nonuniform growth and surface irregularity, leading to the roughness and voids in the film.
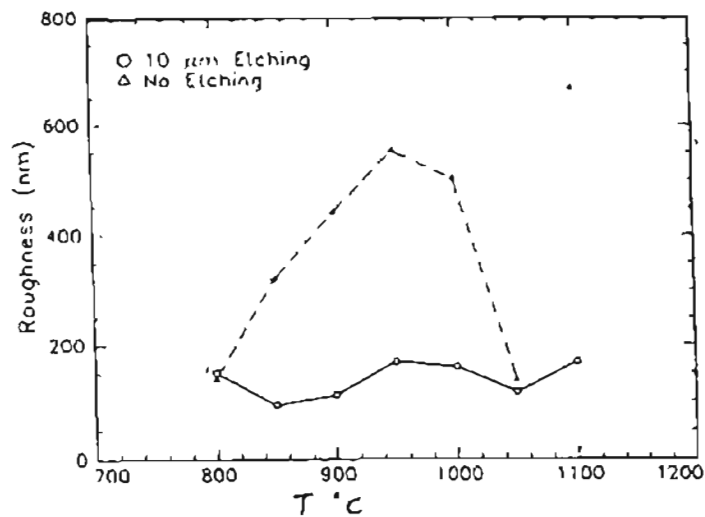
Figure 7.2.3 Variation in the Roughness of the Diamond Films Deposited on As-Polished and Etched Specimens (Parks et al., 1993)

Kubelka et al (1994) reported that the carbon solubility in cobalt continues during diamond deposition till the cobalt binder in the substrate become saturated with carbon. The high temperatures cause the diffusion of carbon into the substrate and the cobalt binder becomes saturated with carbon during diamond deposition. However, they observed that the dissolution of carbon in cobalt continues even after the beginning of diamond growth on the substrate. This was verified as the lattice parameter of the cobalt binder phase continually changed with the degree of carbon dissolution, during the deposition. The authors suggest that this carburization proceeds by the dissolution of the diamond coating itself at the diamond-substrate interface. Thus, they conclude that the changing interface conditions during deposition would influence the adhesion of the diamond coating on the substrate. Scardi et al., (1996) confirmed the increase in the lattice parameter of cobalt due to the dissolution of carbon.

7.3   Techniques adopted to improve adhesion

Cobalt readily dissolves in sulfuric, hydrochloric and nitric acids forming cobaltous salts (Young 1961). This chemical property has been widely adopted by many researchers to remove cobalt from the cemented carbide substrates, in an attempt to obtain good adhesion. Oakes et al., (1991) etched WC substrates (94% WC, 5.5% Co, 0.5% (Ta,Nb) C) in a solution of $HNO_3:H_2O(1:1)$ for 10 minutes and carried diamond deposition using the hot filament CVD technique. They found the substrate surface temperature to effect cobalt mobility. At low substrate temperatures (~ 760

146

ºC), they could obtain diamond coatings on unetched substrates. The influence of cobalt was found to increase with temperature and at high temperatures (900-1000 ºC), diamond coatings were obtained only by etching the substrate.

One of the standard etchants for cemented carbides is a solution of potassium ferricyanide and potassium hydroxide (1:1:10). This reagent is referred to as Murakami reagent (Bleecker, 1950). Murakami reagent attacks WC grains leaving the surface cobalt unaffected. Peters and Cummings (1993) reported improved adhesion of diamond on WC (6% Co) using Murakami agent. The tools were then treated in a solution of either $H_2SO_4+ HNO_3$ (30:70) or diluted solution of HNO_3 to remove the surface cobalt. These tools were then coated using microwave CVD. They were then used in turning of 390 Al alloy. They reported that these diamond coatings had better adhesion when compared to the coatings obtained on unetched substrates.

Another common way to alleviate the effect of cobalt is to alter the composition of the substrate, either throughout the tool or just the surface. The change in composition is aimed at reducing the contact between cobalt and carbon and invariably involves reducing the cobalt from the substrate. Decarburization of the substrate surface prior to the deposition in a $H_2 - 2\%$ O_2 gas is adopted to expose the tungsten grains which would improve the contact area between the diamond and substrate thereby improving the adhesion (Takastu et al. 1991; Saijo et al., 1991; Nesladek et al., 1995).

Another hybrid method of diamond film adhesion enhancement was developed by Saito et al., (1993), which combines a change in the substrate

composition with a heat treatment step prior to diamond deposition to create an *in situ* interlayer. This process was a refinement of the author's previous work with ion-plated group IV a, V a and VIa metals and/or their compounds (such as nitrides or carbides) (Isozaki et al., 1993). When one or more of these metals was incorporated into the substrate during powder processing and the cutting tool material heat treated in an inert gas prior to diamond film deposition, the metal was found to diffuse to the surface of the tool. The metal essentially encapsulated the tool and became an interlayer suitable for depositing diamond. The interlayer apparently blocked diffusion of cobalt and resulted in a significant increase in adherence over a standard WC-Co tool coated with diamond. The treated tool outperformed the untreated tool in a machining test, but did not last as long as a sintered polycrystalline compact tool.

On similar lines, Oles et al., (1996) reported that adhesion of the diamond coatings on WC substrates can be improved by heat treating the carbide prior to the deposition. By heat treating, they noticed an increase in the surface roughness of the WC without the formation of subsurface porosity. They found that the surface cobalt was eliminated by evaporation. The increase in the surface roughness provided anchoring sites for the mechanical interlocking of the diamond thereby improving the adhesion of the film.

Surface modification by using a laser prior to the deposition of diamond has been investigated (Singh et al., 1996). Multiple nano second laser pulses with energy densities near the ablation threshold of the substrate material were used to create a microrough surface morphology of WC - 10% Co and diamond coatings were obtained by HFCVD. By Rockwell

indentation tests, they found that the diamond film did not show any visible delamination for loads up to 150 kg, thus confirming good adhesion.

Murakawa et al., (1988) obtained good adhesion of diamond on WC-6% Co by using ethanol as a diamond source gas. The authors observed that ethanol removes the cobalt layer exposing the bare WC substrate, hence no substrate pretreatment is required for the removal of cobalt.

Studies have been reported concerning the use of interlayers between diamond films and a variety of substrates for the purpose of improving adherence. Kubelka et al (1994) pretreated cemented carbides with boron and silicon by packing the samples in B or Si powder in evacuated and sealed silica ampules. The samples were heat treated at 700 $^{\circ}$C to diffuse B or Si into the WC-Co surface and then diamond coated. While diamond nucleation density and film growth rates were enhanced by these pretreatments, cobalt was still present on the surfaces of the diamond films until the grains coalesced. The mobility and vapor pressure of cobalt were reduced, but cobalt was still present in the film and therefore its deleterious effect was not eliminated. There was a range of thicknesses between grain coalescence (the film thickness required for this to occur was not reported) and 20 μm where adherence was claimed to be improved over untreated cemented carbide substrates. Alam et al., (1997) obtained good adhesion of diamond on WC-6% Co by boron incorporation into the coating during the growth of diamond.

Nesladek et al., (1993) reported an improvement in adhesion by developing a complex interlayer configuration on the WC-Co substrate. Between thin layers (0.04 μm each) of the refractory metals (W and/or Nb),

they deposited a 2-25 μm thick film of Ag. The W and/or Nb layers served as diffusion barriers and bonded well with both the substrate material and the diamond film, while the Ag layer absorbed interfacial stresses. The stress reduction was accomplished by a process similar to brazing, in which diamond coated samples were heated above the melting point of Ag. The silver flowed and wetted the refractory metals and adherence of the diamond film was increased.

Refractory metals which form stable carbides have been found to be good substrates for diamond growth in terms of ease of growing continuous films (Lux et al., 1996). Many authors have taken this one step further and deposited their diamond coatings directly on carbide interlayers. Konyashin et al., (1996) deposited a multilayer (TiN-TiCN-TiN) coating on WC-Co substrate prior to diamond deposition by CVD and obtained good adhesion of the diamond coatings. Guseva et al.,(1997) obtained good adhesion of diamond on WC-10% Co by depositing an Ti based interlayer. Ti based underlayer (TiC_xNy) ~ 500 nm thick was deposited on WC substrates using arc-evaporation PVD. This layer was seeded with nano-grained diamond particles by laser ablation coupled by ultrasonic treatment. Diamond coatings were obtained on this substrate by d. c. plasma CVD. They found that the interlayer was effective in preventing the diffusion of cobalt and thus an increase in adhesion was achieved.

By introducing a interposing layer of TiC or TiN; Fan et al., (1996) achieved good adhesion of diamond on these SiC substrates. In these multilayer coatings diamond was initially deposited by HFCVD for 2 hours to obtain a discontinuous layer of small crystallites 0.5 - 1 μm. The interposing TiC/TiN (1 μm) was deposited by laser physical vapor deposition

technique. The second layer was deposited to obtain a continuous film. Although the differences in the thermal expansion coefficients between diamond and the interposing layers is large, Fan et al., conclude that the net effect of the interposing layer is to reduce the thermal stresses. They argue that the differences in the thermal expansion coefficients of SiC and the interlayer compensate for the difference in the thermal expansion coefficients between the SiC and the diamond film thus improving the adhesion.

Endler et al., (1996) investigated the suitability of various coatings such as Si_3N_4, SiC, SiC_xN_y, TiN, TiC, and a-carbon as interlayers on WC-6% Co. They employed various Plasma assisted CVD (PACVD) processes to deposit interlayers (~5-15 μm) thick on WC-6 % Co and carried out diamond deposition using HFCVD in the temperature range (600-950 ^{o}C). Adherent diamond coatings were obtained on TiC, SiC, Si_3N_4, and Si_xN_y interlayers over the total temperature range. However on TiN and $(Ti,Si)N_x$ diamond coatings were obtained only at higher temperatures (> 800 ^{o}C). From Auger spectroscopic investigations, Endler et al., determined the formation of a TiCN (titanium carbo nitride) layer at the interface between diamond and TiN. They did not observe such a carburized zone at low temperatures. The non-diamond carbon as indicated by the broad peak at 1550 cm^{-1} by Raman spectroscopy was higher for TiN as compared to the other interlayers. By scratch tests they determined that the best adhesion was obtained for the interlayers of SiC and Si_3N_4.

Development of WC tools with alternate binder materials has also been addressed as a means of improving the adhesion. Two such studies have been reported. Zhu et al.,(1994) deposited diamond films on a W-Mo

composite carbide substrate. This substrate material consists upto 96 wt % WC and about 4 wt % molybdenum carbide employed as a binding agent. The WC grains are reaction bonded by the molybdenum carbide phase. Though the intention of exploring this substrate was to eliminate the adverse effects of the cobalt binder, the authors found that cobalt which is present as an impurity (< 0.1 wt %) segregates to the surface during deposition. The adhesion of diamond as measured by Rockwell indentation tests on these substrates was comparable to that on WC-6% Co.

Weihnacht et al., (1996) developed a WC tool with NiAl and Ni$_3$Al binders. They found that NiAl suppressed graphitization completely and Ni$_3$Al has less tendency for graphitization compared to Co. The high temperature strength and toughness of Ni$_3$Al were found to increase with temperature by a factor of 3 at 850 °C over room temperature value and remained fairly constant to 900 °C for NiAl. Owing to these factors the authors suggest that these tools offer a high temperature limit up to which they can be used, as well as promote adhesion of the diamond coating.

7.4 Experimental Approach

From the literature review, it can be seen that the net effect of cobalt is to deteriorate the quality and adhesion of diamond coatings. The effect of cobalt seem to be strongly dependent on the deposition temperature, although there is some contradiction regarding the deposition temperature. Some researchers suggest the detrimental effect of cobalt can be reduced at low substrate temperatures (~ 750 - 800 °C) while others showed that high temperatures (~ 900 - 950 °C) are favorable for diamond deposition. Most of

these experiments were conducted with WC- 6%Co. Very little has been published regarding the effect of deposition temperatures on cemented carbides with a higher cobalt content. The results established for WC-6%Co may or may not be valid if the cobalt content in the tool is changed.

The surface of a WC-based cemented carbide substrate is composed of WC grains bound together by cobalt or a cobalt alloy (Oles et al., 1996). Cobalt is present not only between the WC grains but is smeared over the entire surface of the tool due to grinding. This fact has been accepted by default and several techniques are routinely employed to etch the surface cobalt. However, the presence of the surface cobalt has never been established by any characterization technique.

Commercially available WC tool inserts with different cobalt contents (3, 6, 12 %) were selected for this investigation. Seimen's low angle diffractometer equipped with a glancing angle facility was employed to identify the surface cobalt. XRD patterns were collected using Cu K_α radiation produced at 40 kV/40mA, in 0.05° step in the 2θ region from 30 - 100°.

The first set of experiments were conducted to establish the effect of deposition temperature. Table 7.4.1 gives the deposition conditions. The tools were scratched with diamond powder (< 1μm) to provide nucleation sites. All the tools were ultrasonically cleaned in acetone for about 15 minutes to remove any chemical residue and dirt prior to the conduction of experiments. The deposition conditions were kept constant for all the experiments.

Table 7.4.1   Typical Deposition Conditions

Pressure	20 ± 0.4 Torr
Microwave Power	1000 ± 1 W
Substrate heater temperature	650 - 850 ±(1% of T_s + 0.5) ºC
Substrate surface (tool) temperature	750 - 950 ºC (± 10 ºC)
Duration	6-8 hours
Total gas flow rate CH$_4$ (vol. %)	100 sccm 0.5 (± 0.005 sccm)

The samples were characterized by SEM and μ-Raman spectroscopy. Details of the equipment were covered in Chapter 5.

7.5   Results

7.5.1   Identification of Surface Cobalt

Figure 7.5.1.1 show the XRD pattern of a WC-12% Co sample prior to diamond deposition collected at a glancing angle, showing the peaks corresponding to cobalt and WC. This XRD pattern of the WC-Co substrate presents a complex overlap between peaks from WC (hexagonal) and α-cobalt (hexagonal). The 100 % intensity peak corresponding to WC is at 2θ - 48.307º while that of Cobalt is at 47.610º. Both these reflections are (101) reflections. Hence, XRD patterns taken at wide angle showed only the peaks corresponding to WC. The reflections from cobalt are most of the

154

time hidden by WC peaks. Another factor which needs to be considered is the scattering efficiency of tungsten compared to that of cobalt. WC scatters X-rays very strongly compared to Co. Hence, it was extremely difficult to separate the overlapping peaks of WC and surface cobalt for WC 3 and 6 % cobalt. However, the surface cobalt could be identified for the case of 12% cobalt.

7.5.2 Effect of Cobalt at Low Substrate Temperatures

Figures 7.5.2.1a, b and c show the micrographs of the diamond deposited at low substrate temperatures (~ 750 ºC). It can be seen that groups of isolated diamond crystals are formed on WC-3% Co (Figure 7.5.2.1a), while scattered octahedral crystals are observed on WC-6%Co (Figure 7.5.2.1b). Portions of the crystals appear to be black. This may be attributed to the effect of cobalt. The effect is more pronounced in WC-12% Co (Figure 7.5.2.1c). A dome shaped particle can be noticed in the micrograph. EDXA analysis revealed the particle to be cobalt. Thus surface cobalt seems to effect the diamond growth in the early stages. The effect was prominent for WC- 6%Co and 12% Co. It is also possible that this cobalt covers the growing diamond crystals and dissolves some of the carbon, thereby extending the incubation period. However, with continued deposition, it was possible to obtain continuous diamond coatings on all the samples.

Counts

20201.06

0.00

30   35   40   45   50   55   60   65
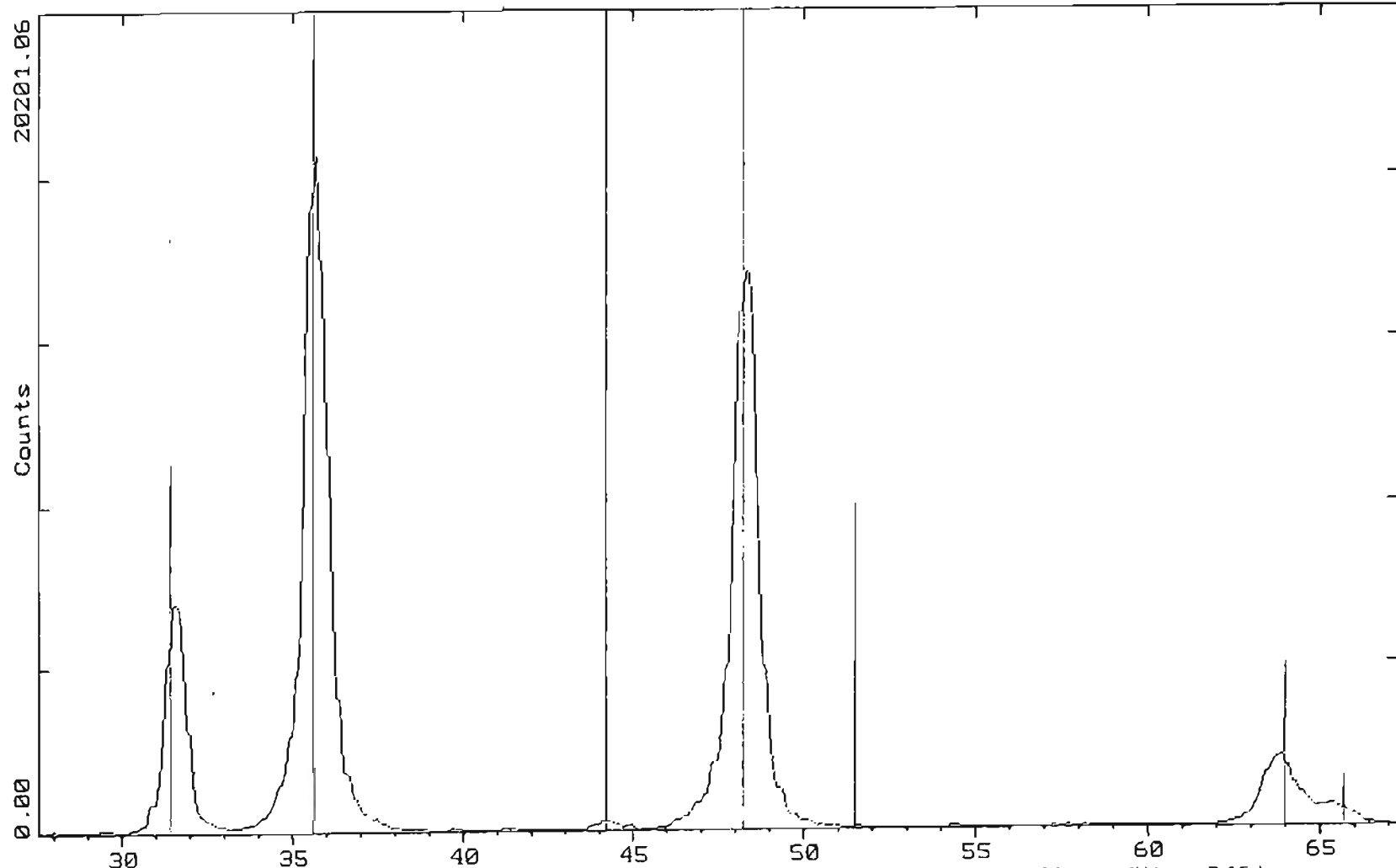
C:\USERS\MALLIKA\JCG3.RAW neground (CT: ..., SS:0.100dg, WL: 1.5406Ao, DX:-.249)

15-0806 ... Co

Figure   7.5.1.1   XRD Pattern of Ground WC-12% Co Showing the Peaks
Corresponding to Cobalt and WC
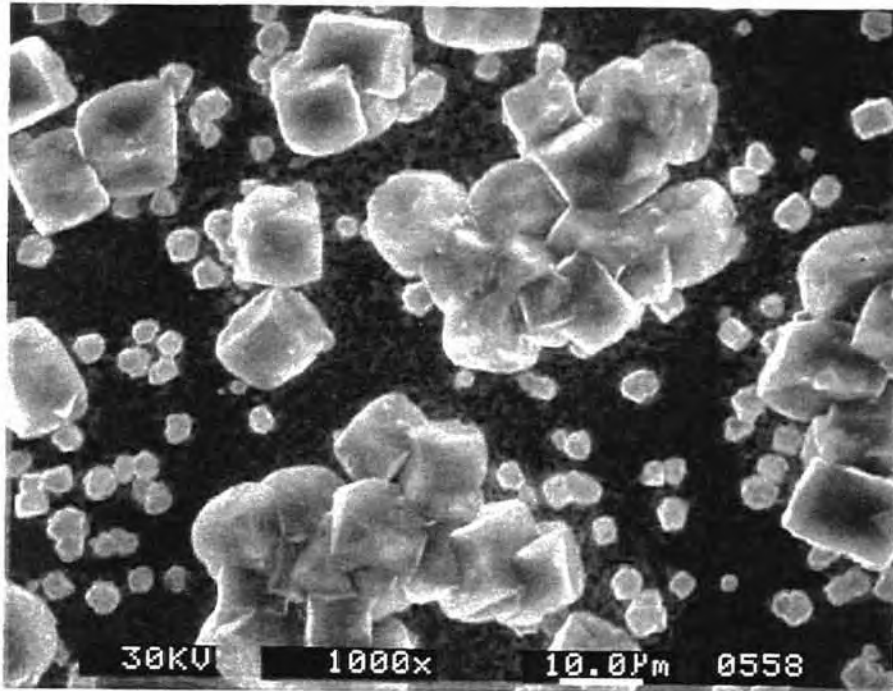
Figure   7.5.2.1a) SEM Micrograph Showing Isolated Crystals on
                 WC-3% Co at Low Substrate Temperatures
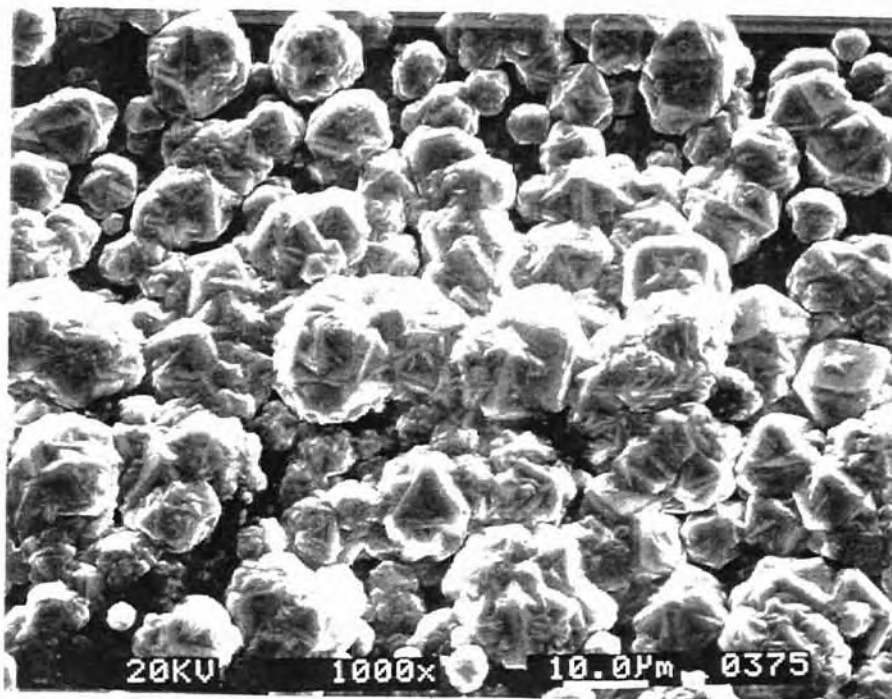
Figure   7.5.2.1 b) SEM Micrograph Showing Scattered Octahedral
                 Crystals on WC-6%Co at Low Substrate Temperatures

157
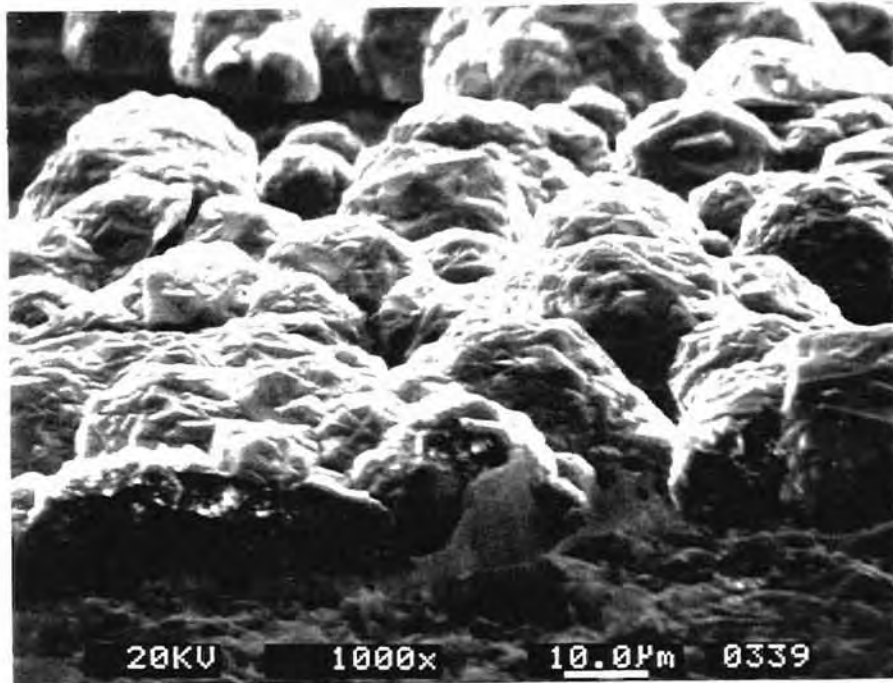
Figure   7.5.2.1c) SEM Micrograph Showing Dome Shaped Cobalt Particle
on WC-12%Co at Low Substrate Temperatures

7.5.3   Effect of Cobalt at High Substrate Temperatures

7.5.3.1   In-situ etching of cobalt

Park et. al., (1992) reported, that at higher temperatures (~ 950 °C), the
effect of cobalt can be reduced to some extent. This has been attributed to
the insitu etching effect of cobalt (Mehlmann et. al., 1992). Experiments
were conducted to verify this effect

At higher pressures the plasma ball is concentrated over a certain
region of the tool rather than being evenly distributed along the tool. This
leads to the confinement of the active growth species and atomic hydrogen
to a small region typically near the center of the tool.   Experiments

conducted at 40 Torr did not give a continuous film. Scattered islands of octahedral diamond crystals were formed throughout (Figure 7.5.3.1.1). A spongy porous mass was observed near the edges. EDXA analysis confirmed that the spongy mass observed near the edges was cobalt (Figure 7.5.3.1.2). X-maps near the center showed a very little amount of cobalt, in contrast to the X-ray map at the edges. High concentration of the plasma near the center might have led to the etching of the cobalt effectively at the center (Figure 7.5.3.1.3). This confirms that the surface cobalt is effectively etched away by the atomic hydrogen in the plasma when the temperatures are ~ 950 °C.
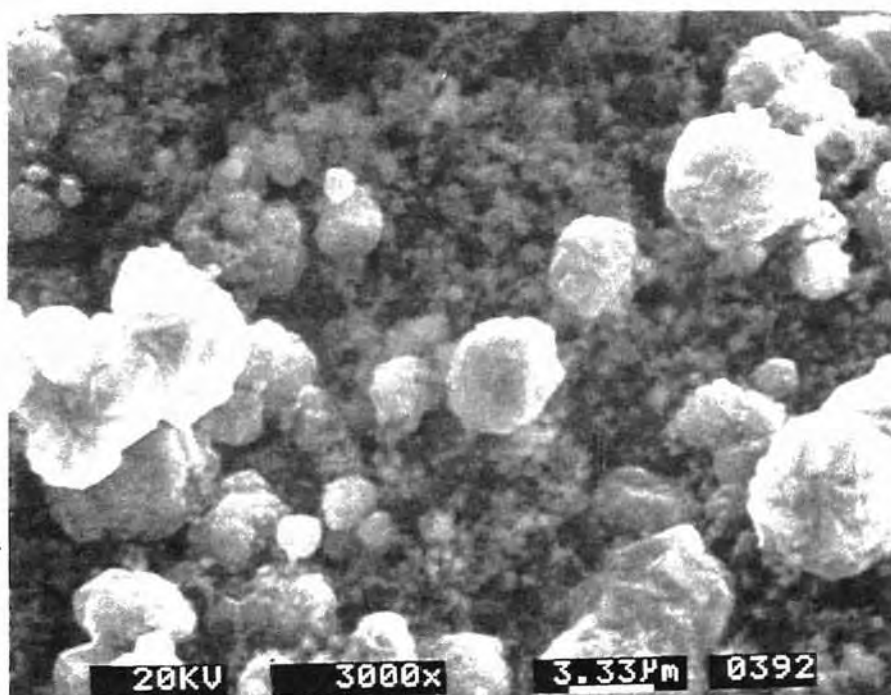
Figure   7.5.3.1.1 SEM Micrograph Showing Isolated Crystals of Diamond along with a Spongy Porus Mass Which is Identified as Cobalt by EDXA

Figure 7.5.3.1.2 EDXA Map near the edge of the Tool Showing
the Presence of Cobalt
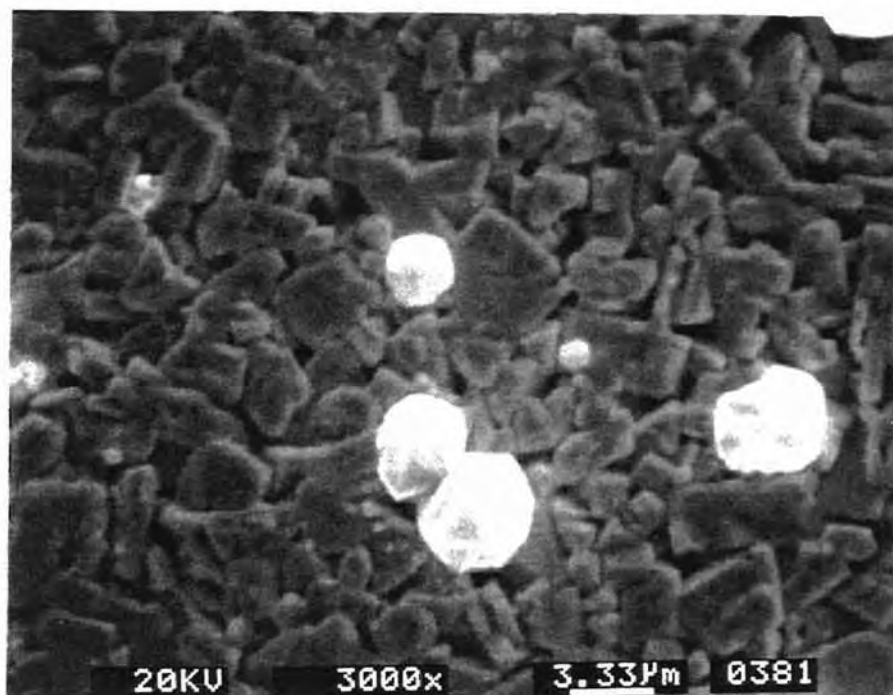
Figure   7.5.3.1.3 SEM Micrograph Showing a Few Diamond Crystals
along with WC Grains

7.5.3.2   Diffusion of Cobalt from the Bulk

It was shown in the earlier section that the surface cobalt will be etched away by the hydrogen plasma at high temperatures (~ 950 °C). Therefore it should be possible to get good quality continuous coatings on all the three samples at high temperatures. Figures 7.5.3.2.1a, b, and c show the micrographs of the diamond coatings obtained on WC 3, 6 and 12% cobalt substrates respectively after ~ 24 hrs deposition time. It can be noticed from the micrographs that a continuous coating is obtained on all the substrates.
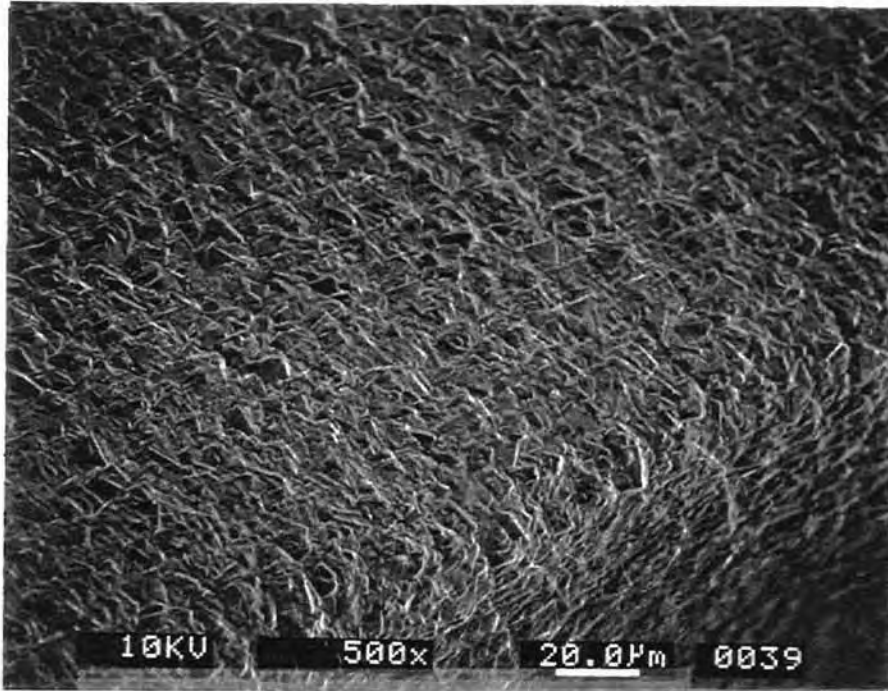
Figure   7.5.3.2.1 a)   SEM Micrograph Showing a Continuous Diamond
Coating on the Rake and Clearence Face of
WC -3% Co Tool at High Substrate Temperatures
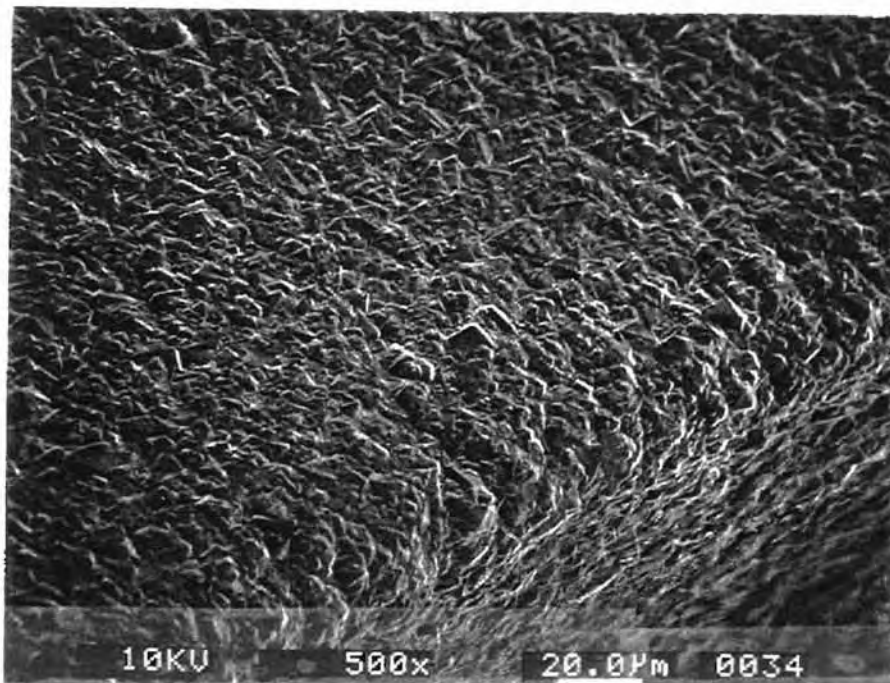
Figure   7.5.3.2.1 b)   SEM Micrograph Showing a Continuous Diamond
Coating on the Rake and Clearence Face of
WC -6% Co Tool at High Substrate Temperatures
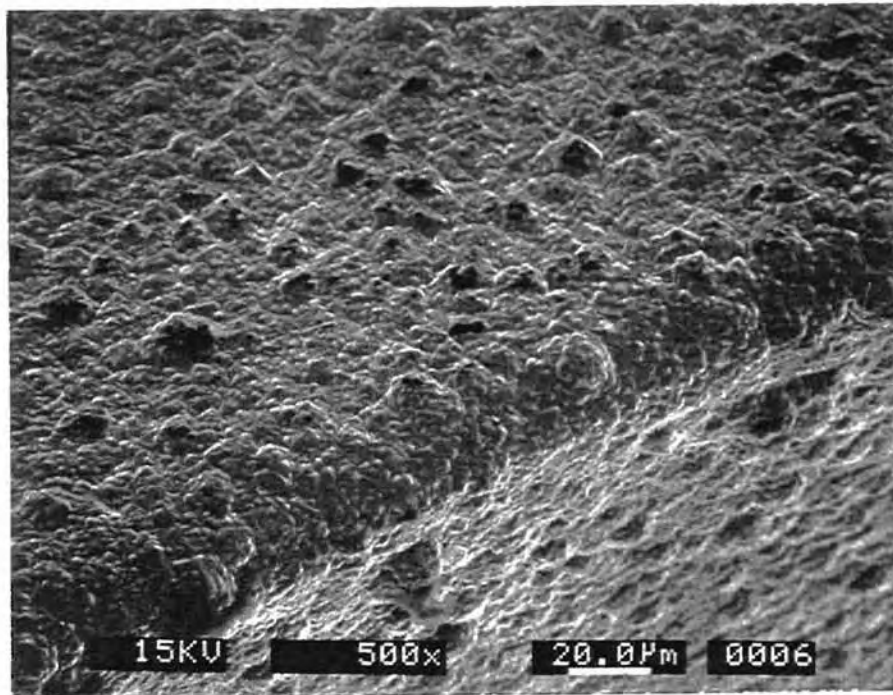
Figure   7.5.3.2.1 c)   SEM Micrograph Showing a Continuous Diamond
                          Coating on the Rake and Clearence Face of
                          WC -12 % Co Tool at High Substrate Temperatures

Figure 7.5.3.2.2a shows the micrograph of the diamond coating on WC
3% Co. Some of the crystals appear to be black. Figures 7.5.3.2.2b and
7.5.3.2.2c show the micrographs of the diamond on 6 and 12% cobalt
respectively. A similar black layer can be noticed on some crystals.
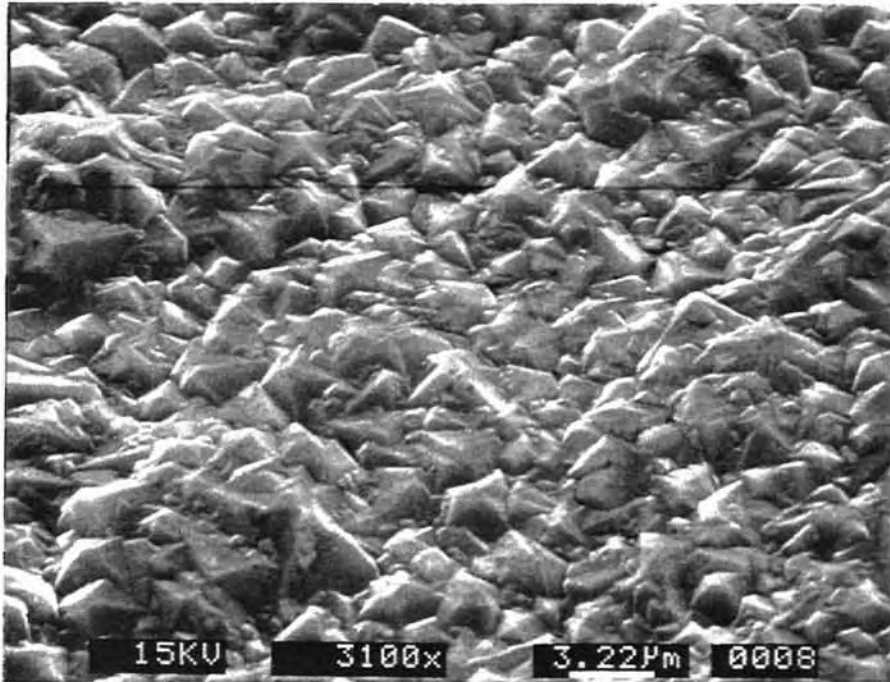
Figure   7.5.3.2.2 a)   SEM Micrograph of the Diamond Coating on
WC-3% Co Showing a Black Layer Covering
Some Crystals
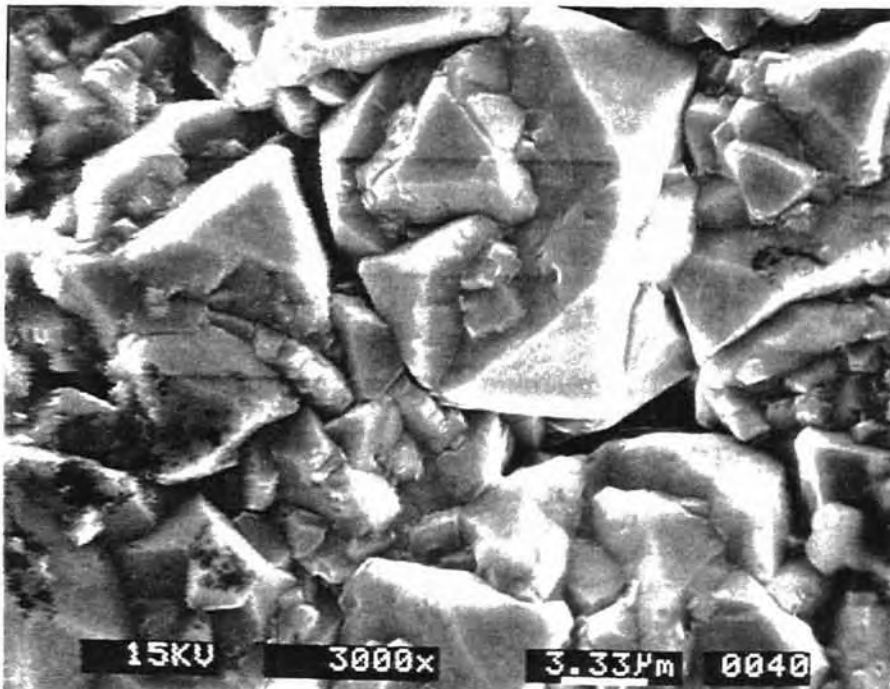
Figure   7.5.3.2.2 b)   SEM Micrograph of the Diamond Coating on
WC-6% Co Showing a Black Layer Covering
Some Crystals

164
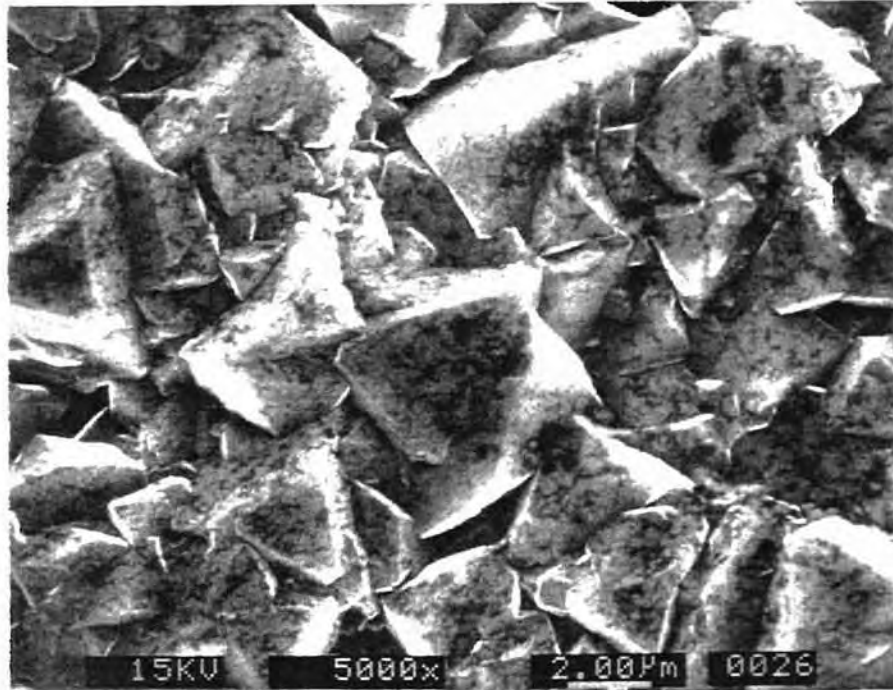
Figure   7.5.3.2.2 c)   SEM Micrograph of the Diamond Coating on WC-12%
Co Showing Black Spots on all the Crystals

It has been reported that cobalt can dissolve carbon and enhance the formation of graphitic and amorphous phases (Haubner et al, 1989; Park et al., 1993; Kubelka et al., 1994). It seems probable that the black layer is formed due to the effect of cobalt. Since high temperatures lead to the etching of the surface cobalt, it seems likely that the cobalt from the bulk diffused to the surface during deposition. This diffusing cobalt from the bulk attacks the growing diamond crystals and promotes the formation of graphitic phases. This would in turn deteriorate the quality of the diamond. Diffusion of the cobalt to the surface has already been demonstrated by Park et al., (1993). However, it has been demonstrated in this investigation that diffusion occurs even at high substrate

temperatures. XRD patterns were collected at both wide angle and glancing angle for 3 and 12% cobalt.

Peaks corresponding to WC and diamond can be observed in the XRD plot collected at wide angle (Figure 7.5.3.2.3), while peaks corresponding to cobalt, WC and diamond were prominent in the XRD plot collected at glancing angle (Figure 7.5.3.2.4). This confirms the above argument that even though surface cobalt is removed by insitu plasma etching at high temperatures, cobalt does diffuse from the bulk and affects the coating as well as the interface.
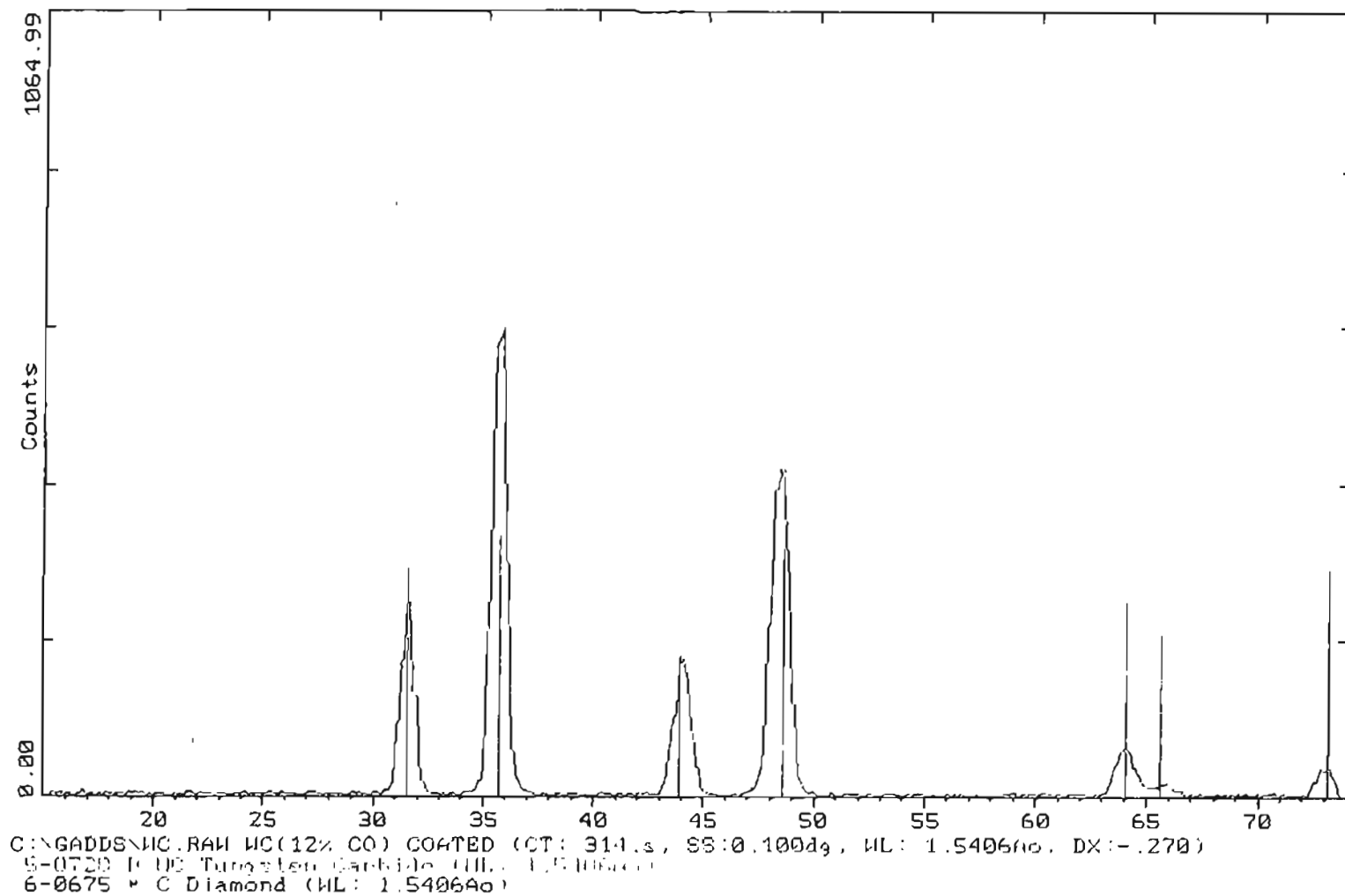
Figure   7.5.3.2.3 XRD Pattern of Diamond Coated WC-12% Co at Wide
Angle, Showing Peaks Corresponding to
Diamond and WC

C:\GADDS\OSUOF8B.RAW OSU Compax (Diamond Side) (CT: 120.s, SS: 0.100dg, WL: 1.5406Ao)
6-0675 * C Diamond (WL: 1.5406Ao)
25-1047 * WC Unnamed mineral, syn [NR] (WL: 1.5406Ao)
15-0806 * Co Cobalt (WL: 1.5406Ao)
27-1125
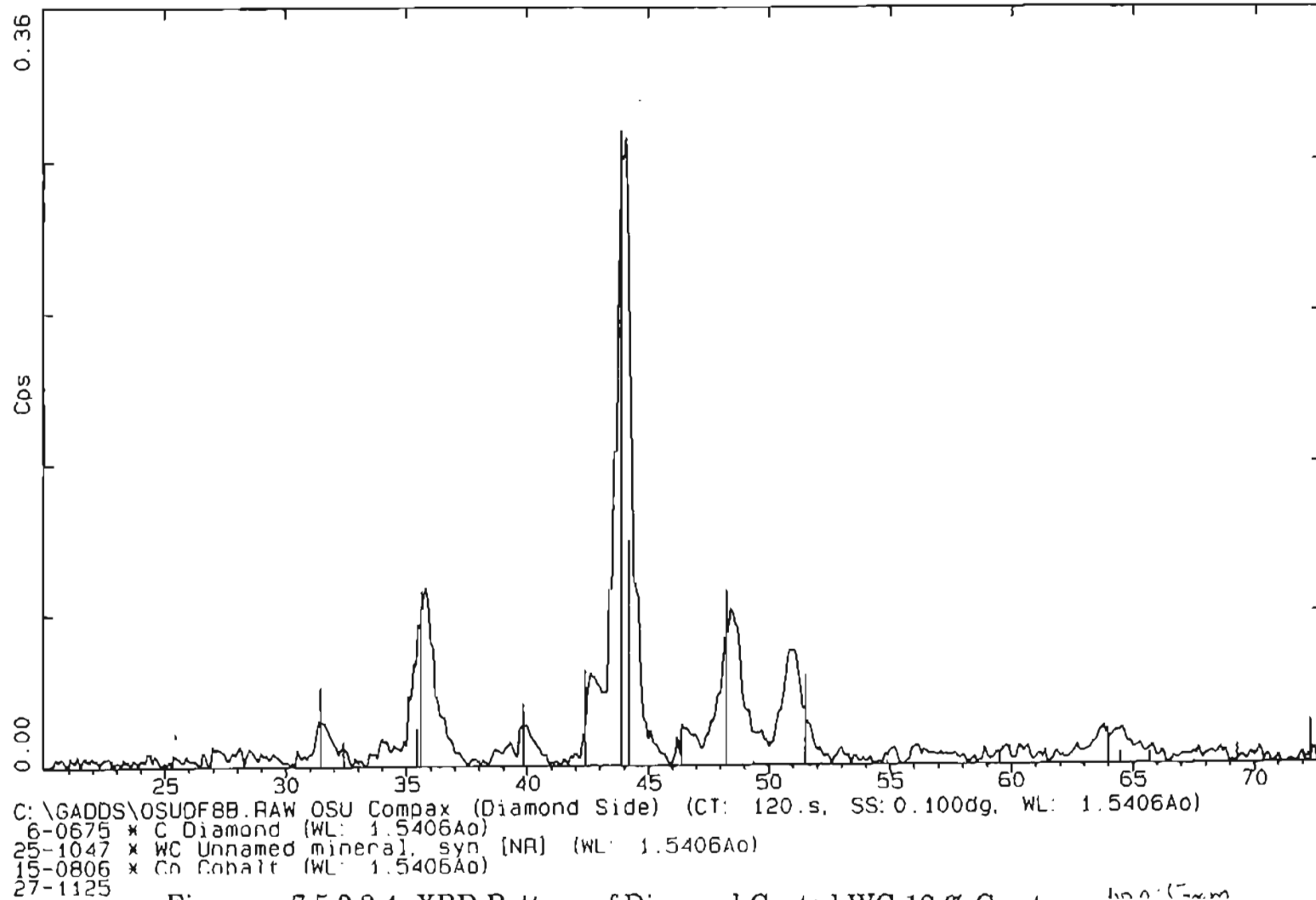
Figure   7.5.3.2.4 XRD Pattern of Diamond Coated WC-12 % Co at
Glancing Angle Showing the Peaks Corresponding
to Cobalt at the Interface

7.5.3.3 μ-Raman Analysis

Figure 7.5.3.3.1 shows the μ - Raman spectra of the three samples at 950 °C. μ-Raman at the other temperatures showed a similar trend. All the diamond coatings showed a relatively strong diamond peak around 1337 cm^{-1}, and a broad band centered around 1550 cm^{-1}. A characteristic photoluminescence background is associated with all the spectra. A shift in the diamond Raman line is noticed in all cases. This shift corresponds to the residual stresses in the diamond films. The thermal stress (σ_{th}) is calculated from the formula (Windischmann, et al., 1991) :

$$\sigma_{th} = [E/(1\text{-}v)] \int_{T_1}^{T_2} (\alpha_s \text{-} \alpha_f) dT$$

where, α_s and α_f are the thermal expansion coefficients of the substrate (WC in this case) and diamond respectively, E/1-v is the biaxial Young's modulus (1345 Gpa for diamond) (Field et al., 1979), T_1 is the deposition temperature and T_2 is the room temperature. Using the average values of α_d = 3.1 X10^{-6} /°C and α_s = 5.0 , 5.5 and 6.2 X 10 $^{-6}$/°C for 3, 6, and 12% Co substrates respectively, the thermal stresses were estimated (Table 7.5.3.3.1).

Table 7.5.3.3.1   Thermal Stresses for WC-3, 6, 12% Co
at different temperatures

Substrate Temperature (°C)	Thermal stresses (Gpa)		
	WC-3%Co	WC-6%Co	WC-12%Co
750	-1.85	-2.34	-3.02
950	-2.36	-2.98	-3.86
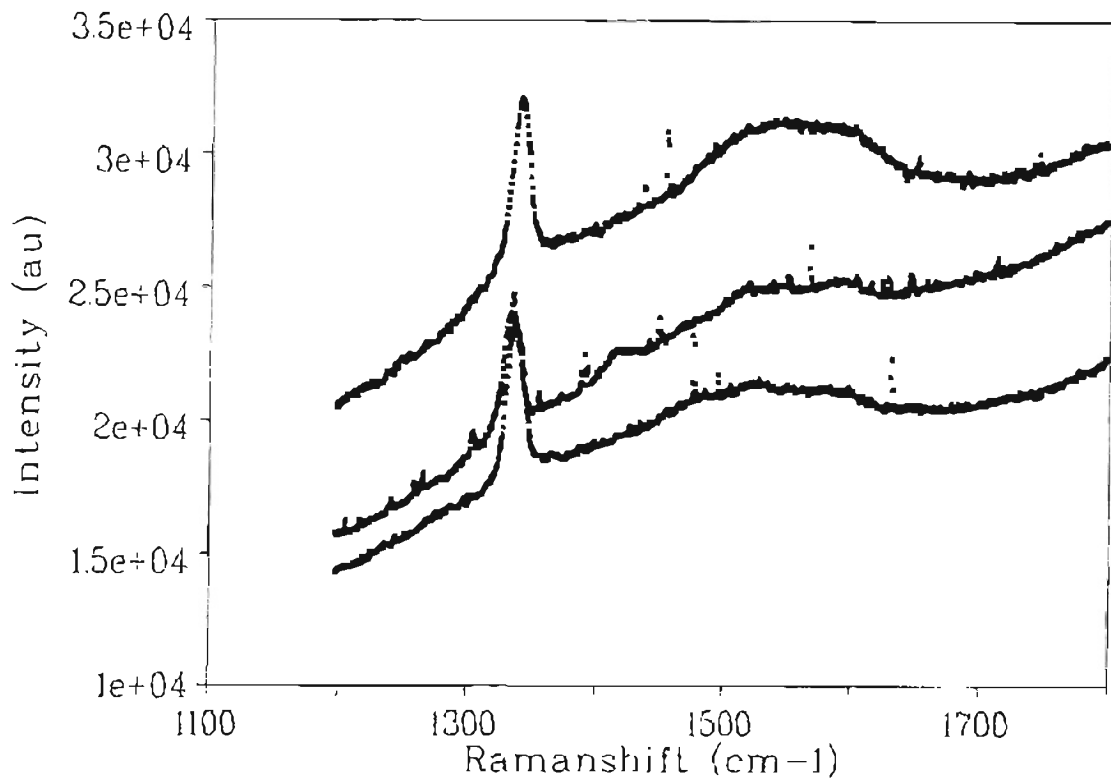
Figure   7.5.3.3.1 μ-Raman Spectra of Diamond Coatings on 3, 6 and
12% Co Showing Peaks Corresponding to Diamond
(~1337 cm^{-1}) and Diamond-Like Carbon (~ 1550 cm^{-1})

The residual stress of the coating is the sum of the intrinsic stresses
induced during the growth phase and the thermal stresses.   Thermal
stresses are evaluated from the above expression and the biaxial residual
stress is calculated from the peak shift of the Raman diamond line.
Residual compressive stresses of ~ 1.96, 2.53, and 4.50 GPa were obtained
for WC-3,6 and 12%Co respectively. Due to the experimental uncertainty in
measuring Raman band positions (± 1 cm^{-1}), it was not possible to

distinguish between stress states for different deposition temperatures. The intrinsic stresses which are the differences between the total residual stress and thermal stresses are estimated as ~ -0.11, -0.19, -1.06 Gpa, for WC-3, 6 and 12% Co respectively. It can be seen that the intrinsic stresses increase with the increase in the cobalt content in the tool.

The ratio of the relative intensities of the peaks is a measure of the phase purity of diamond films and it was found that the amount of amorphous carbon generally associated with a sp^2 structure seems to increase with the increase in the percentage of cobalt in the WC tools. Also, the peak width which is a measure of crystallanity in the structure was found to increase in the case of diamond and decrease in the case of the amorphous carbon. It appears that cobalt in the WC tools tends to favor the formation of amorphous carbon and an increase in the cobalt content seems to increase orderliness in the sp^2 bond, thereby resulting in the decrease of peak width of amorphous carbon. This would obviously deteriorate the quality of the diamond as observed in the gradual broadening of the diamond peak with the increase in Co content.

Figure 7.5.3.3.2 shows the effect of deposition temperatures on the phase purity of diamond films deposited on WC-3, 6, and 12% Co. A similar trend is observed for all the three samples. The intensity ratio decreases with increase in temperature from 750 to 900 °C. This implies that abundant codeposition of non-diamond carbon occurred with the increase in temperature.
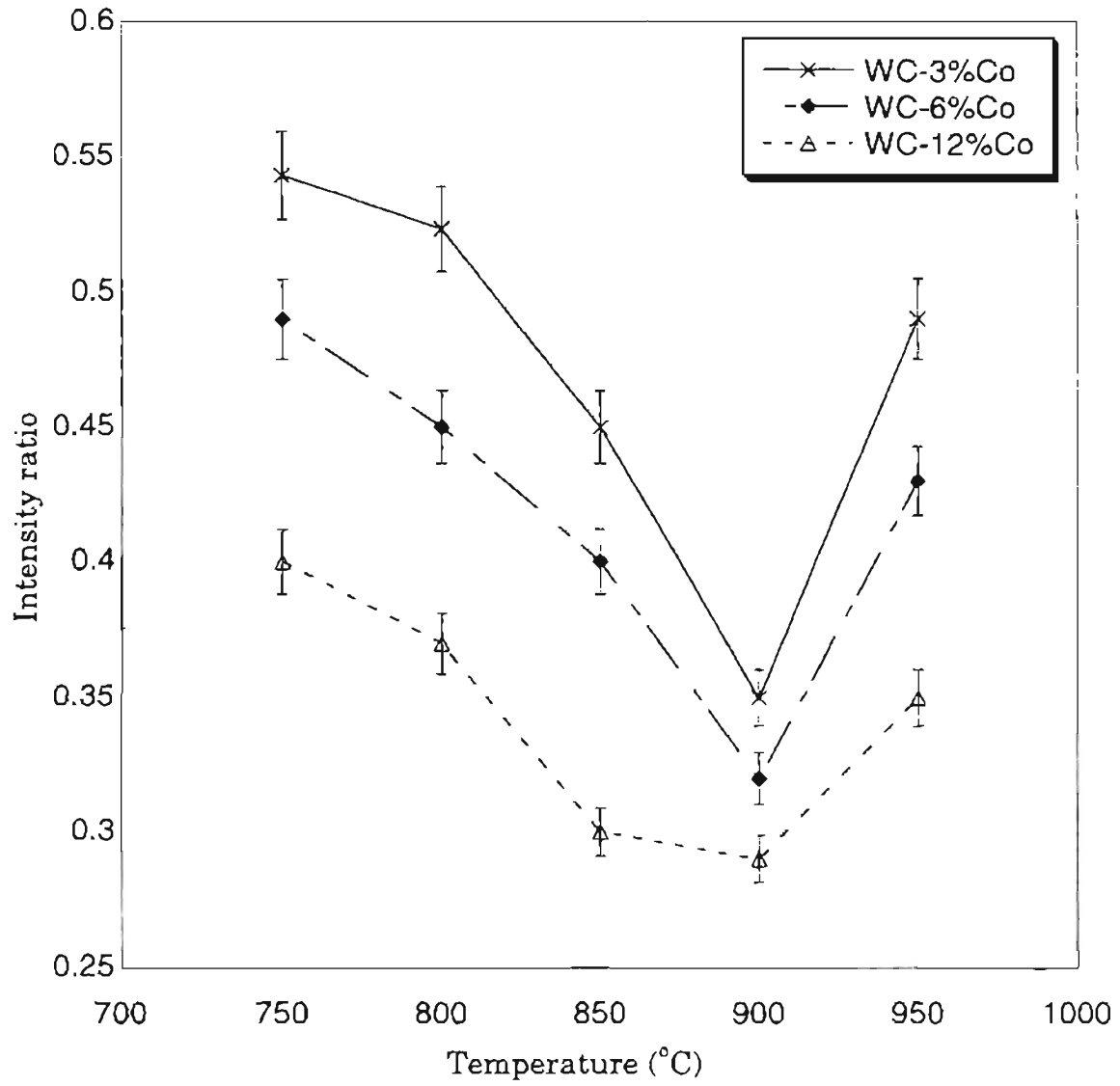
Figure   7.5.3.3.2   Effect of Deposition Tempertures on the Phase Purity of
Diamond Films Deposited on WC-3, 6 and 12 % Co

172

The trend was opposite for Si_3N_4; the intensity ratios increased with increase in deposition temperature. Similar results were reported in the literature (Wang et al., 1996). The decrease in the phase purity from 750 °C and the increase at 950 °C are apparently in contrast with the reported results and the results obtained on silicon nitride. The behavior of the cobalt binder phase and its interaction with the diamond needs to be considered to explain this trend.

Mehlmann et al., (1992, 1994) reported the presence of cobalt particles surrounded by disordered graphite in the diamond films deposited at low temperatures. These particles were not so abundant at higher temperatures and this was attributed to the *in situ* etching effect of cobalt (Mehlmann et al., 1994). Even in the present investigation, it was observed that at low temperatures the cobalt binder phase covers the diamond particles and prolongs the incubation time (Figure 7.5.2.1b). This effect was more pronounced for WC-12%Co. Removal of surface cobalt by atomic hydrogen in the plasma at high temperatures (Figure 7.5.3.1.2) was also observed. It seems probable that the trend in the intensity ratios is related again to the cobalt binder phase. At low temperatures this effect is more pronounced, while at high temperatures the effect is somewhat reduced due to the insitu etching effect. However, the diffusion of cobalt from the bulk still affects the quality of the diamond coatings at high temperatures. This is observed by the relatively low intensity ratios (~0.5-0.6) obtained for WC-Co samples compared to the very high intensity ratios (~0.93) obtained for silicon nitride samples, under similar deposition conditions.

Figure 7.5.3.3.3 shows the variation of the FWHM of the diamond peak with substrate temperatures for the three samples. The diamond Raman line

width is found to increase with the increase in the deposition temperature. It can be observed that the diamond deposited on WC-12%Co exhibits a maximum FWHM. It was mentioned in Chapter 6 that FWHM reflects the amount of disorder or defect density. Increase in the FWHM with increase in temperature might be attributed to the detrimental effect of cobalt in deteriorating the quality and crystallinity of the deposited diamond.

The above analysis indicates that cobalt does have an adverse effect on the quality of the diamond coatings at both low and high substrate temperatures. Though the effect is somewhat reduced at high substrate temperatures the diamond coatings obtained were still of inferior quality. Hence, it was required to address some of the surface modification techniques, in order to remove the surface cobalt prior to diamond deposition and to investigate the effect of various surface pretreatments.
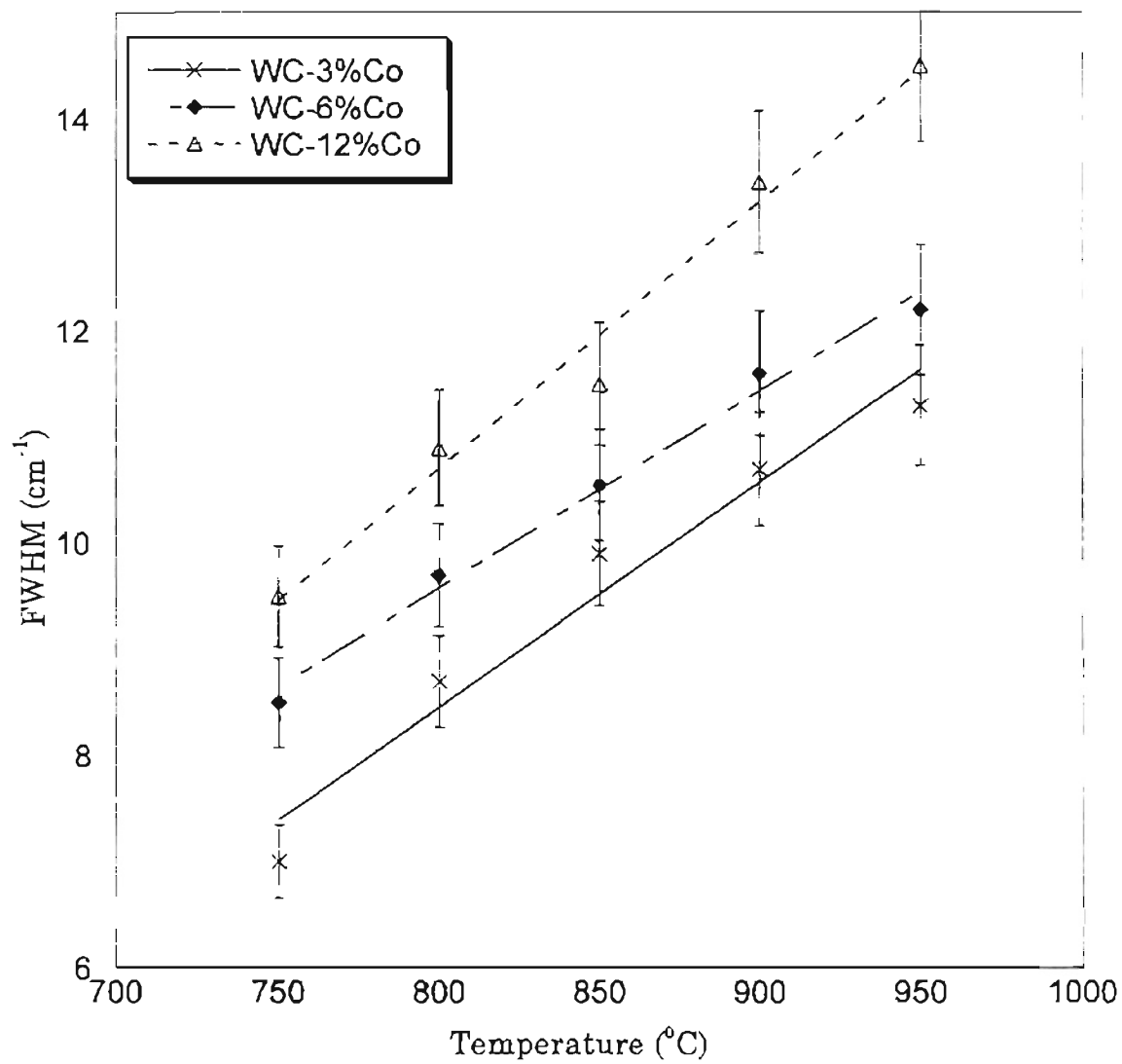
Figure   7.5.3.3.3 Variation of FWHM of the Diamond Peak with
Deposition Temperatures for WC-3, 6 and 12% Co

7.6 Surface Pretreatment Techniques

7.6.1 Experimental Details

Commercially available WC tool inserts with different cobalt content (3, 6, 12 wt%) from Carboloy were used in these experiments. The following pretreatments were used:

1. Removal of surface cobalt with aquaregia (1HNO3 + 3 HCl) for 10 minutes

2. Murakami treatment

This treatment comprised of treating the tools in a solution of Potassium Ferricyanide and potassium hydroxide (1:1:10) for 10-15 minutes, followed by a treatment in a solution of $H_2O_2:H_2SO_4$ (70:30) for 15-20 seconds. Murakami treatment attacks the WC grains leaving the binder phase unaffected. Treatment in a solution of $H_2O_2:H_2SO_4$ (70:30) removes the residual cobalt from the surface.

3. Murakami treatment followed by ultrasonic microscratching

The additional treatment in this case consisted of dispersing fine diamond powder (< 0.1 μm) in a iso-proponal solution in an ultrasonic bath and immersing the tool in the suspension for about 20 minutes. This would enhance the nucleation density.

All the tools were ultrasonically cleaned in acetone for about 15-20 minutes, to remove any chemical residue and dirt prior to the conduction of experiments. The deposition conditions were maintained constant at Pressure : 20 ± 0.4 Torr; Total gas flow : 100 sccm; Substrate temperature : 850 ± 9.5 °C (which corresponds to the tool temperature of ~950 ± 10 °C); and

%CH$_4$ = 0.5 ± 0.005. Deposition was carried for ~ 24 hours. The deposits were characterized by SEM, μ-Raman and X-Ray Diffractometer. Table 7.6.1.1 gives the sample designations and the corresponding pretreatments.

Table 7.6.1.1   Specimen Designations and Pretreatment

Specimen	Substrate	Pretreatment
wc311	WC-3%Co	AQUA
wc312	WC-3%Co	MUR
wc313	WC-3%Co	MUR+DIA
wc611	WC-6%Co	AQUA
wc612	WC-6%Co	MUR
wc613	WC-6%Co	MUR+DIA
wc1211	WC-12%Co	AQUA
wc1212	WC-12%Co	MUR
wc1213	WC-12%Co	MUR+DIA
wc321	WC-3%Co	MUR
wc621	WC-6%Co	AQUA
wc1221	WC-12%Co	MUR+DIA
wc322	WC-3%Co	AQUA
wc622	WC-6%Co	MUR+DIA
wc1222	WC-12%Co	MUR
wc323	WC-3%Co	MUR+DIA
wc623	WC-6%Co	MUR
wc1223	WC-12%Co	AQUA

where, AQUA = treatment with aquaregia; MUR = Murakami treatment; MUR+DIA = Murakami + ultrasonic treatment with diamond suspension;

7.6.2 Results and Discussion

Figures 7.6.2.1a, b and c show the ground surfaces of WC-3,6 and 12% Co respectively. The marks left by the grinding treatment are quite evident from these micrographs.
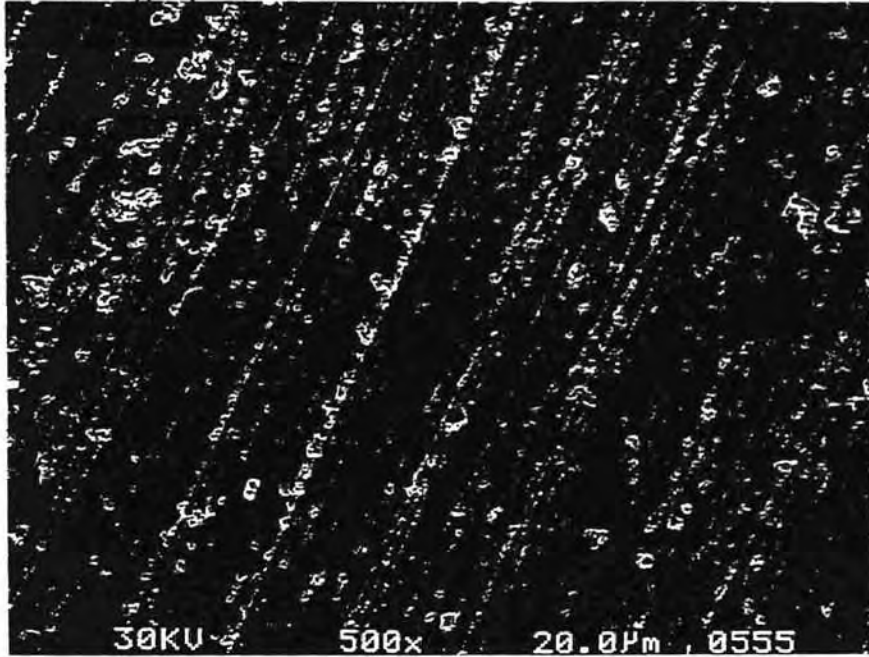
Figure   7.6.2.1 a)   SEM Micrograph of WC-3% Co Showing
Grinding Marks
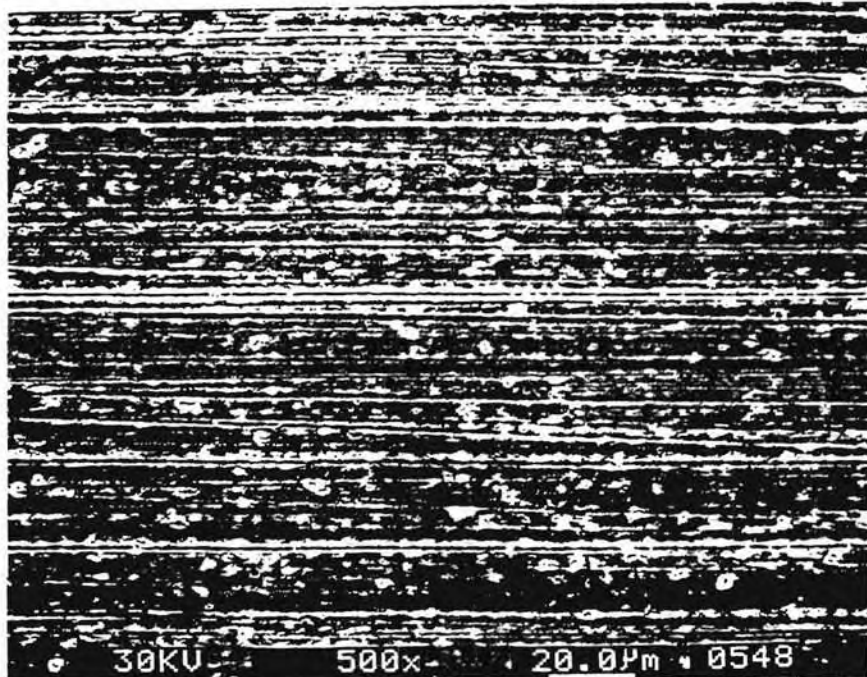
Figure   7.6.2.1 b) SEM Micrograph of WC-6% Co Showing
Grinding Marks
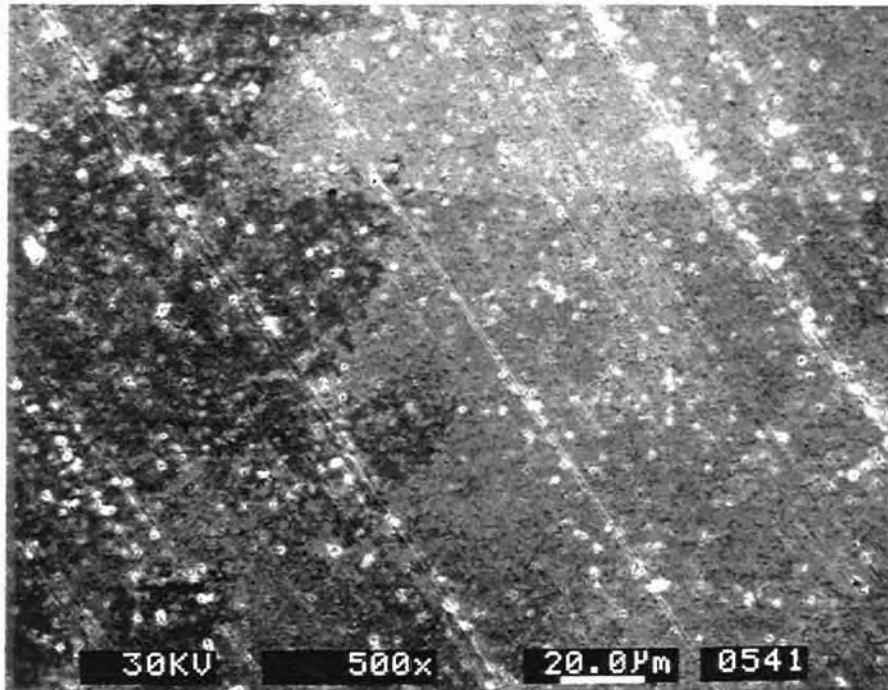
Figure   7.6.2.1 c) SEM Micrograph of WC-12% Co Showing
Grinding Marks

Figure 7.6.2.2a shows the micrograph of WC-12%Co etched with aquaregia for 15 minutes. It can be observed from the micrograph that the binder phase is selectively removed only at some regions exposing the WC grains, while at several other regions it can be seen that cobalt is covering the WC grains.   Figure 7.6.2.2b shows the micrograph of the same substrate after prolonged etching (~3-4 hrs).   It can be seen from the micrograph that the cobalt binder phase is etched completely leaving an anisotropic rough WC surface.   Similar results were observed on WC-3 and 6% Co samples.
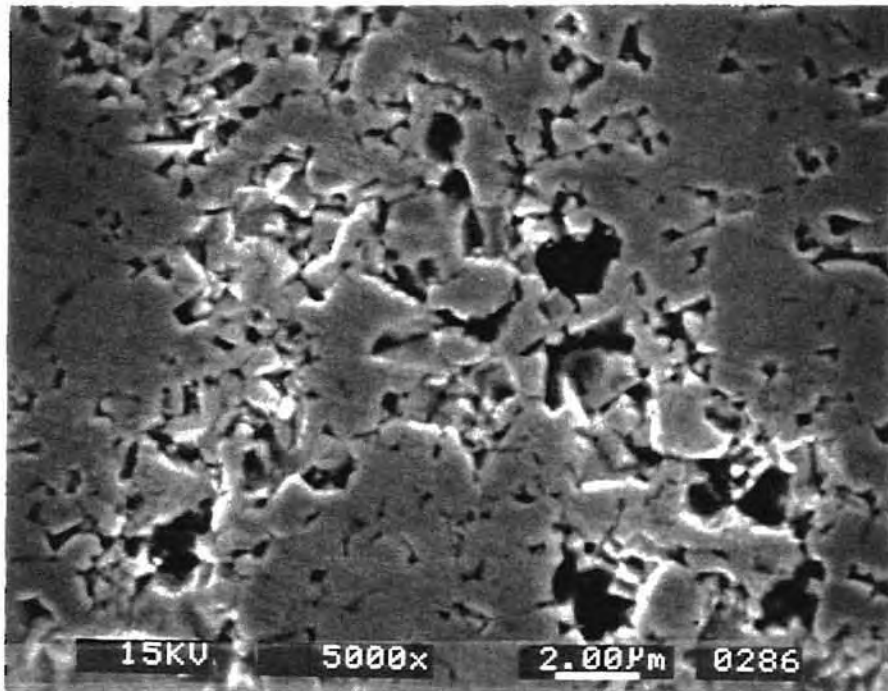
Figure   7.6.2.2 a)   SEM Micrograph of WC-12% Co Following Etching in
Aquaregia Showing Partial Removal of the Cobalt
Binder
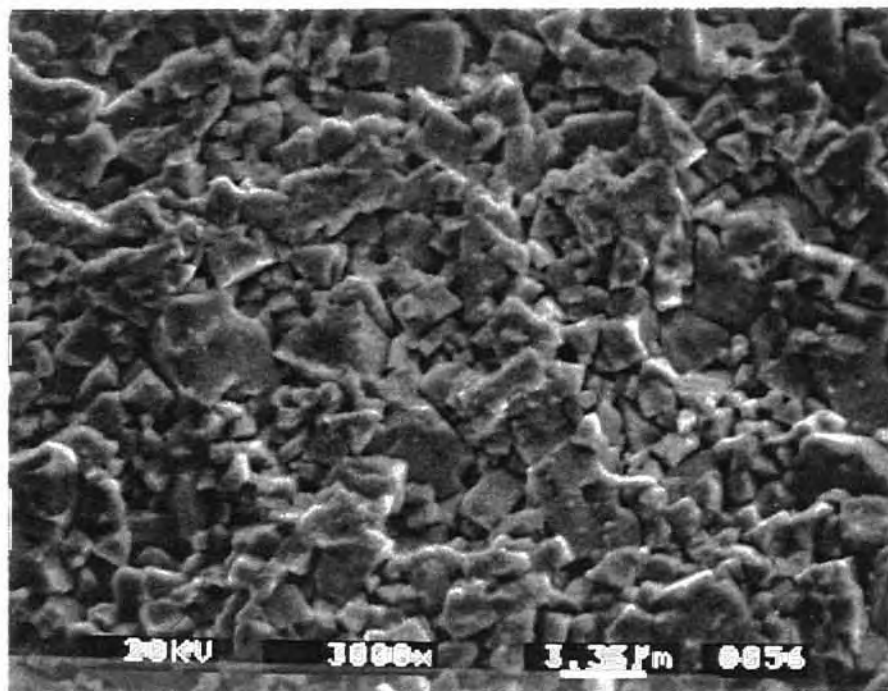
Figure   7.6.2.2 b)   SEM Micrograph of WC-12% Co After Prolonged
Aquaregia Etching Showing Faceted WC Grains

Figures 7.6.2.3 a, b and c show the micrographs of the three samples following Murakami treatment. It can be seen that an Murakami agent etches the WC grains uniformly leaving an isotropically rough surface. This method combining Murakami followed by H_2SO_4/H_2O_2 etching is found to reduce the surface cobalt as well as establish stable surface conditions. Etching by Murakami alone merely increases the cobalt concentration at the substrate surface by removing WC.
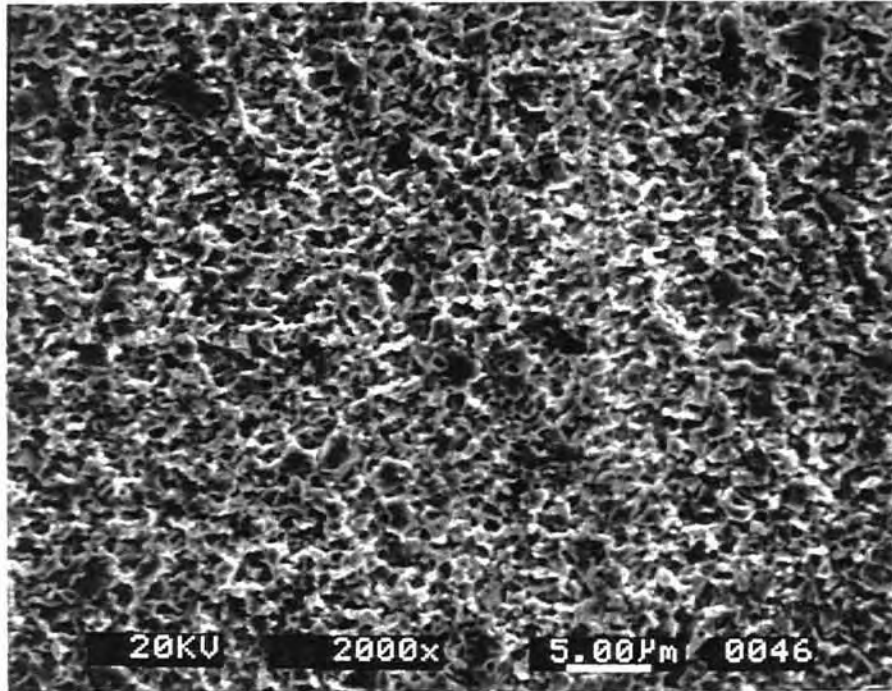
Figure 7.6.2.3 a) SEM Micrograph of WC-3 % Co Following Murakami Treatment Showing an Isotropically Rough WC surface
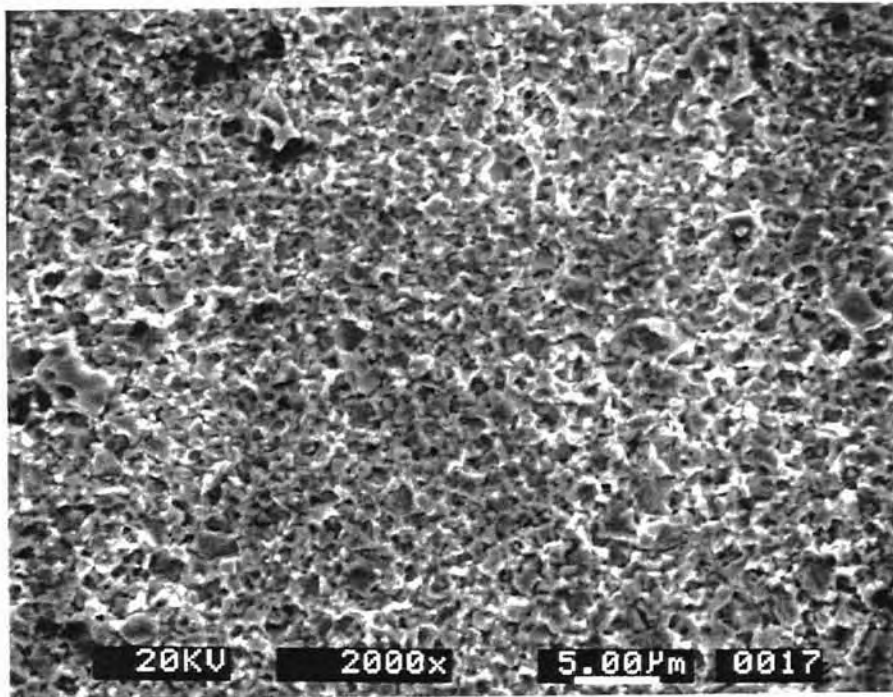
Figure   7.6.2.3 b) SEM Micrograph of WC-6 % Co Following Murakami
           Treatment Showing an Isotropically Etched WC surface
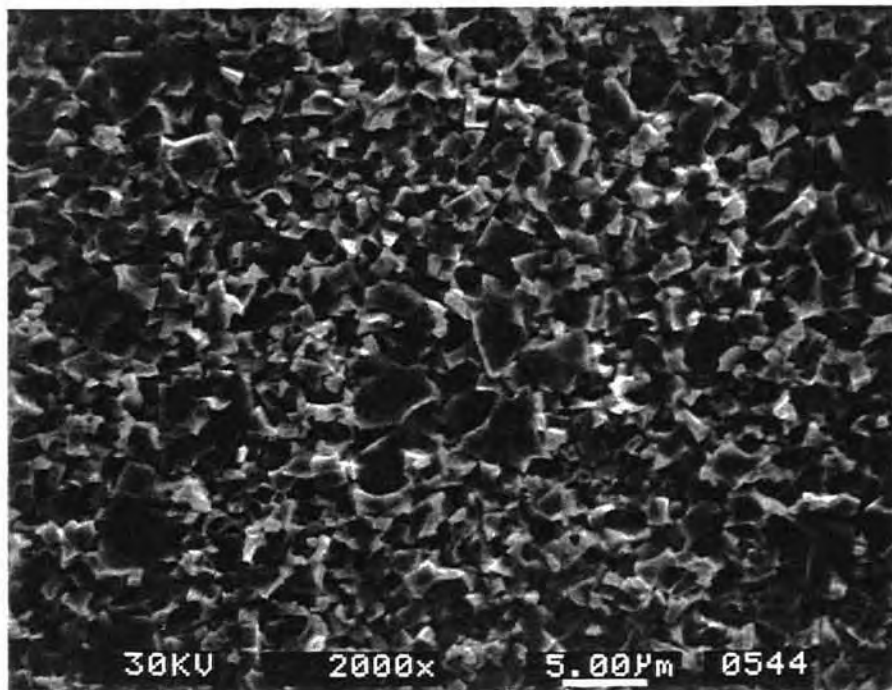
Figure   7.6.2.3 c) SEM Micrograph of WC-12 % Co Following Murakami
           Treatment Showing anIsotropically Rough WC surface

182

Etching by H_2SO_4/H_2O_2 alone also results in much less removal of surface cobalt due to the smooth surface. However etching by Murakami as a first step increases the substrate surface roughness, and provides a larger surface area which can be easily attacked by the H_2SO_4/H_2O_2 solution. The Co network is then easily dissolved by the acid. Comparing the two chemical etching procedures (Figures 7.6.2.2b and 7.6.2.3c), it can be seen that while WC grains appear to be faceted in the case of etching by aquaregia, the substrate surface appears to be isotropically rough without any faceted WC grains since Murakami etching removes the WC crystal facets that were present.

Figures 7.6.2.4a, b, and c show the micrographs of the wc311, wc621, and wc1211 substrates after diamond deposition. This substrate has been treated with aquaregia. Discrete faceted diamond crystals are observed on this substrate with crystal sizes ranging from 2-5 μm. The nucleation density on these substrates appears to be very low. Scattered crystals with octahedral morphologies were observed throughout. Similar results were obtained for wc322, wc611, and wc1223 substrates.
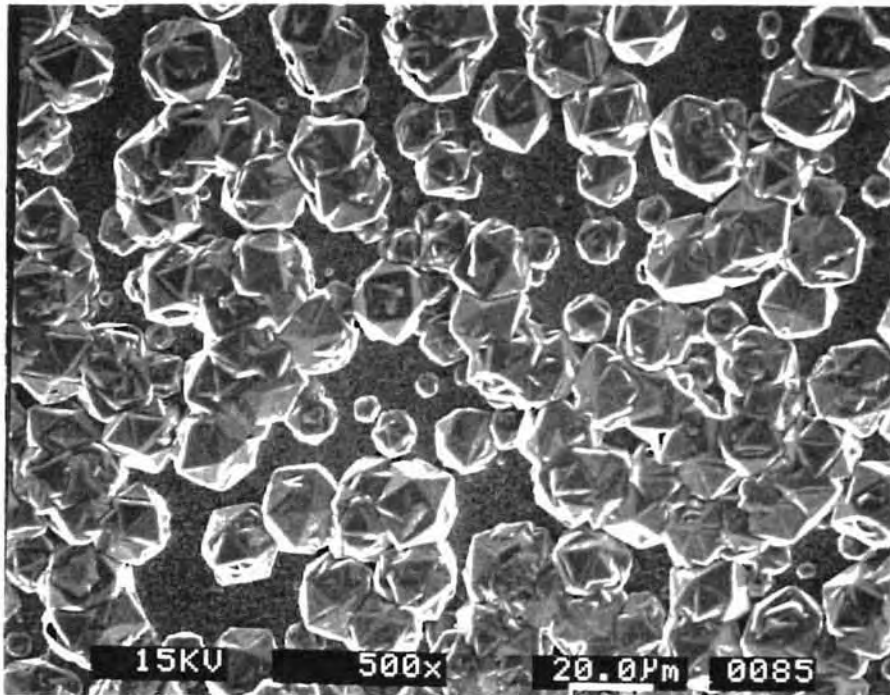
Figure   7.6.2.4 a)   SEM Micrograph Showing Scattered Diamond
Crytals on WC311

Figure7.6.2.4 b)   SEM Micrograph Showing Island of Cubo-Octahedral
Diamond Crystals on WC621
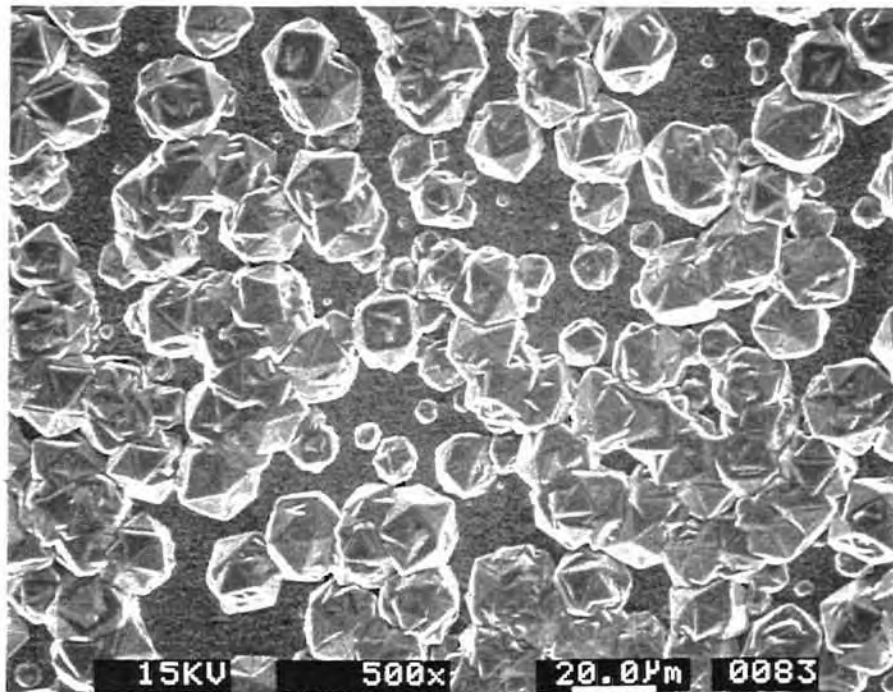
Figure   7.6.2.4 c) SEM Micrograph Showing Sparse Growth of
Cubo-Octahedral Diamond on WC1211

Figures 7.6.2.5a, b and c show the micrographs of the diamond coatings
on wc312, wc612 and wc1222 respectively. These substrates are treated with
Murakami treatment. Continuous diamond films are formed on all the
three substrates with octahedral morphology. The size of these crystals
range from 2-4 μm respectively. Murakami treatment produced a rough
topography on all these substrates. Researchers have established that
nucleation can be promoted by topographical features alone and nucleation
occurs preferentially on locations that protrude from substrate surfaces
(Liu et al., 1995). The changes in the substrate topography induced by
Murakami's reagent seem to have promoted the nucleation resulting in a
continuous diamond film. Similar results were obtained on other samples
prepared by this route.
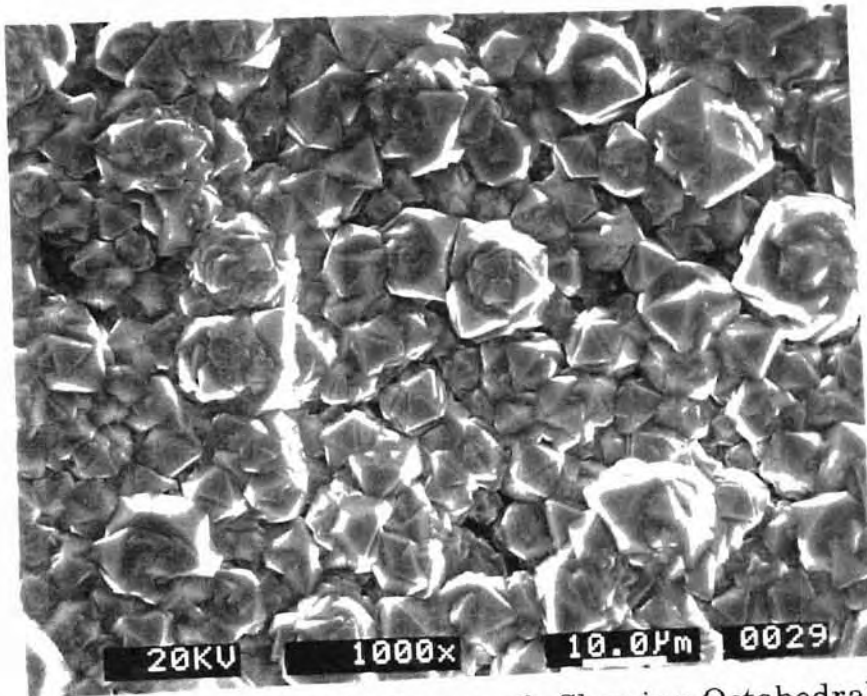
Figure 7.6.2.5 a) SEM Micrograph Showing Octahedral Morphology of Diamond on WC312
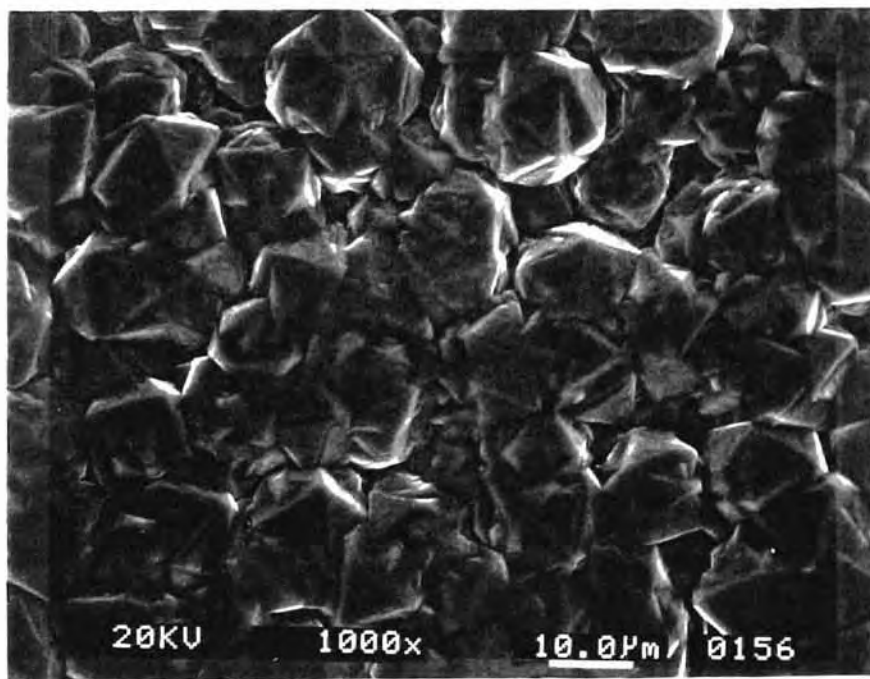
Figure 7.6.2.5 b) SEM Micrograph Showing Octahedral Morphology of Diamond on WC612
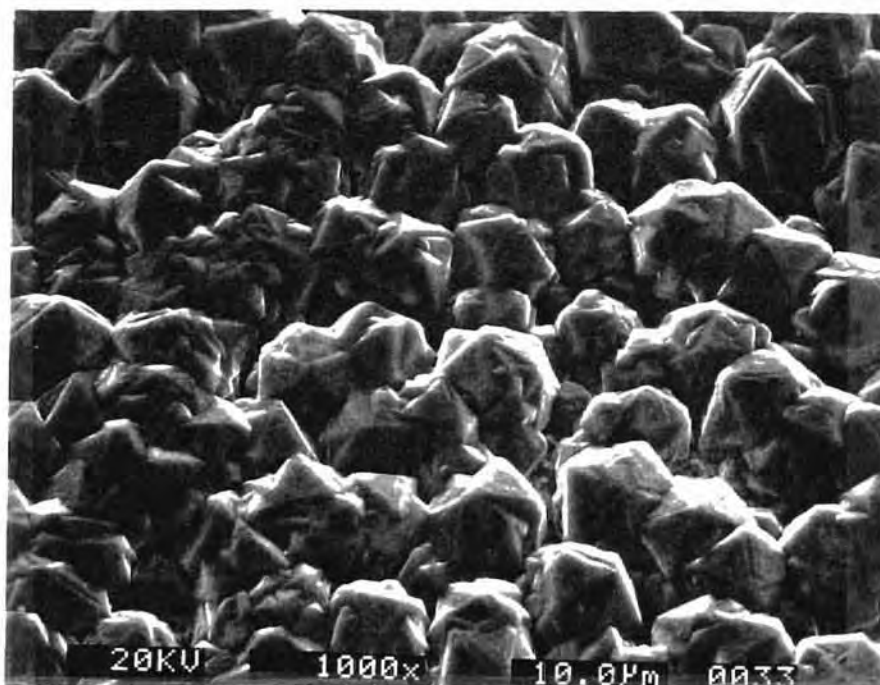
Figure   7.6.2.5 c) SEM Micrograph Showing Octahedral Morphology of
Diamond on WC1222

Figures 7.6.2.6 a, b and c show the micrographs of the diamond coatings
on wc313, wc1221, and wc622 respectively. It can be noticed that uniform
coatings with octahedral morphology are obtained on all the samples.
Figures 7.6.2.7a, b, and c are the micrographs showing that a dense
continuous coating is obtained on the cutting edges of the tool in all three
cases. A slight preference towards {111} orientation can be observed.
Similar results were obtained for other samples.

Raman spectra of these coatings showed a sharp peak at ~ 1334 cm^{-1}
corresponding to diamond, and a relatively broad peak   ~ 1550 cm^{-1}
corresponding to non-diamond carbon. These films appear to be of high
quality as revealed by the intensity ratios (~0.80-0.85) and good crystallinity .

XRD data was collected at both wide angle and grazing angles for the samples in order to investigate the interface composition. XRD spectra at a wide angle revealed the presence of WC and diamond. XRD spectra collected at a glancing angle indicated the presence of WC, W_2C and diamond. No peaks corresponding to cobalt were detected at the interface in these samples.
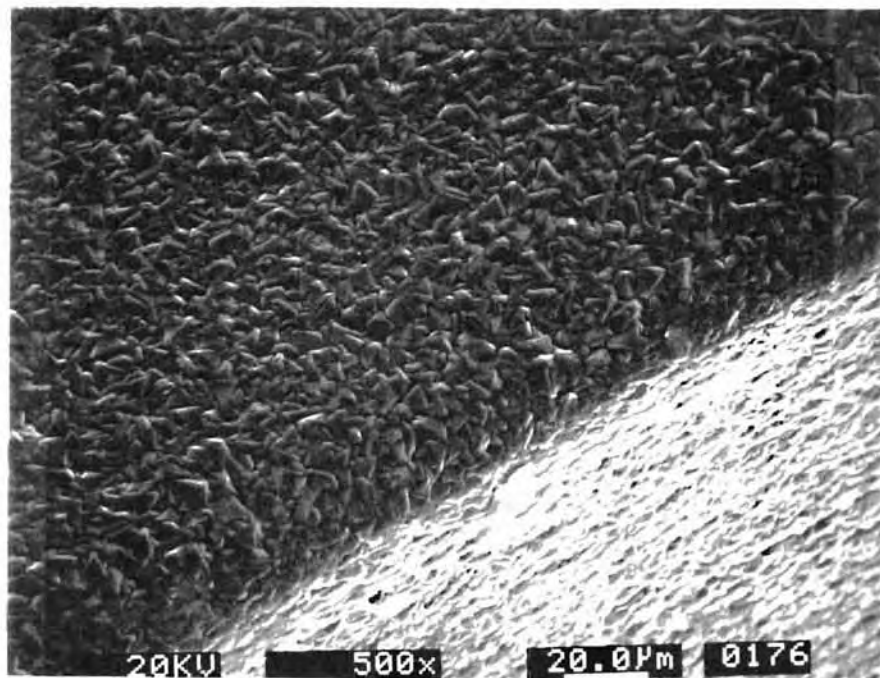
Figure   7.6.2.6 a)   SEM Micrograph Showing a Uniform Dense
Diamond Coating along the Rake and the
Clearence Face of WC313
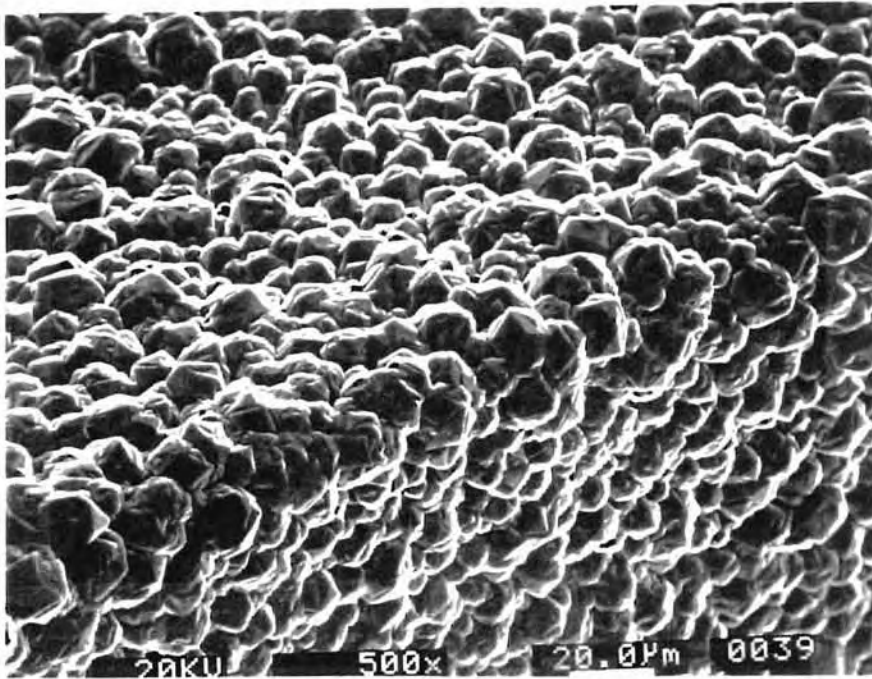
Figure   7.6.2.6 b) SEM Micrograph Showing a Uniform Dense
Diamond Coating along the Rake and the
Clearence Face of WC1221
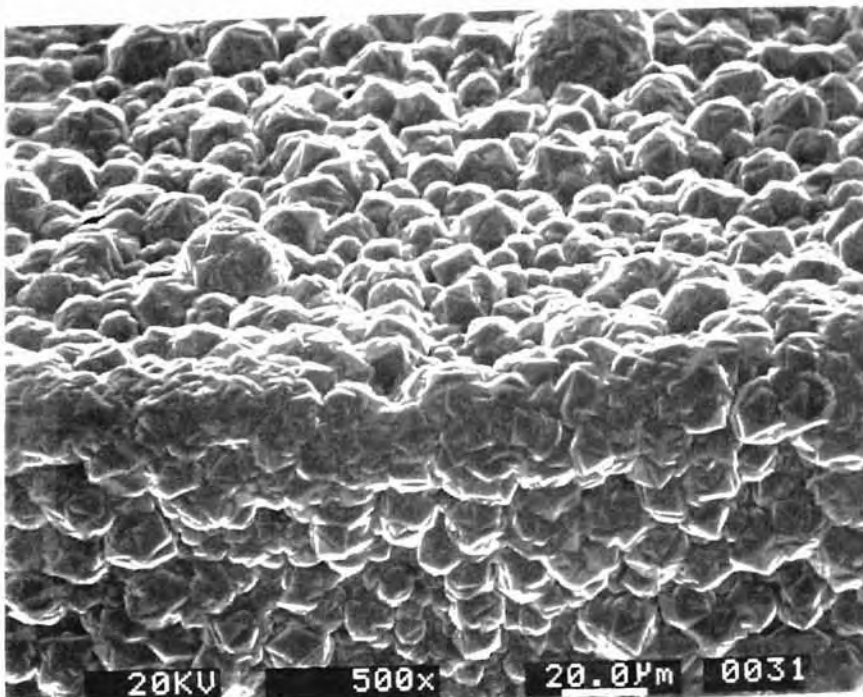
Figure   7.6.2.6 c) SEM Micrograph Showing a Uniform Dense Diamond
Coating along the Rake and the Clearence Face of
WC622
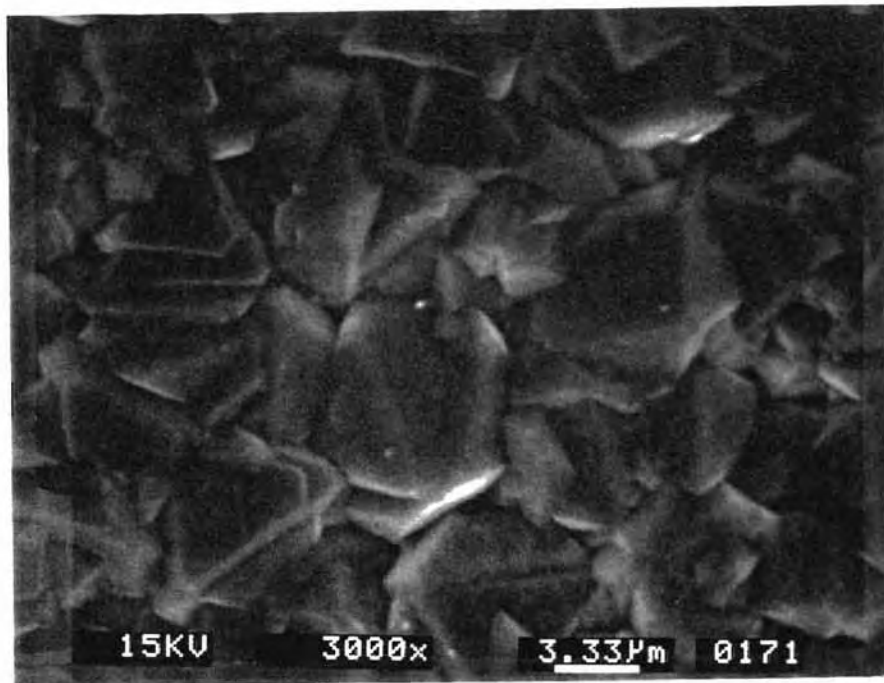
Figure 7.6.2.7 a) SEM Micrograph Showing a Octahedral Morphology of Diamond on WC313
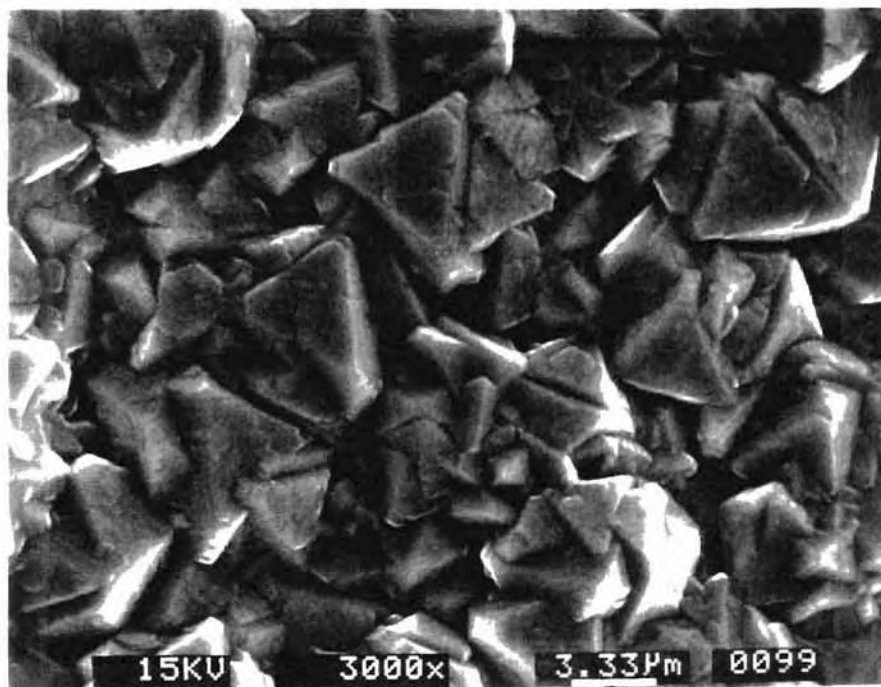
Figure 7.6.2.7 b) SEM Micrograph Showing a Octahedral Morphology of Diamond on WC1221

190
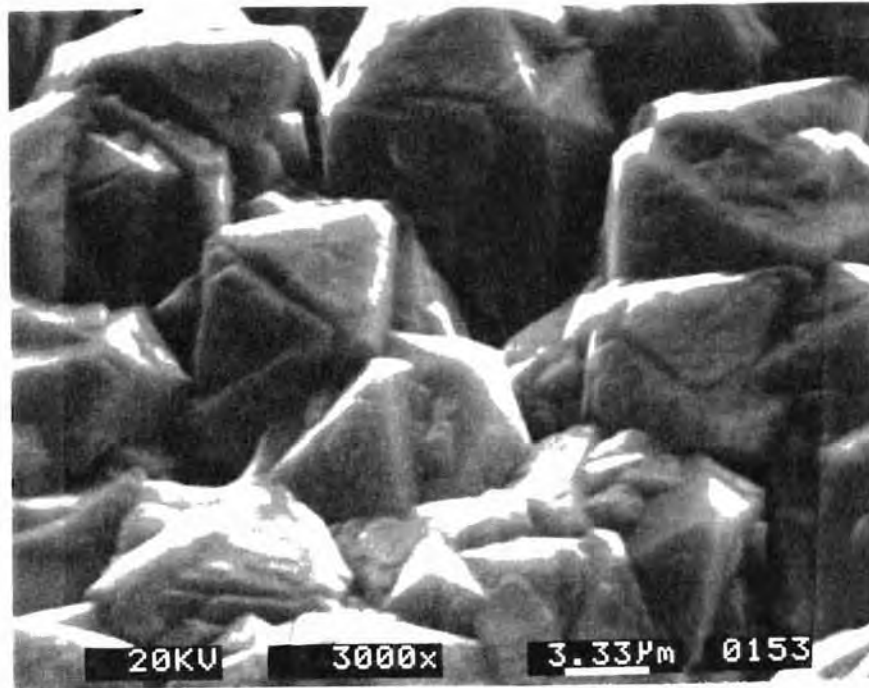
Figure   7.6.2.7 c) SEM Micrograph Showing a Octahedral Morphology
of Diamond on WC622

Formation of stable cobalt compounds during the deposition might reduce the adverse effects of cobalt and prevent its migration to the surface (Kubelka et al., 1994). Cobalt reacts with H_2SO_4/H_2O_2 to form $CoO/CoSO_4$ (Young, 1961). $CoSO_4$ can be further reduced to form more stable oxides or sulphides (Young, 1961). It seems probable that the sulphates and the oxides of the cobalt formed due to etching might be further reduced by atomic hydrogen and/or carbon in the plasma to form a more stable cobalt sulphide and/or oxides during diamond synthesis. This layer may have acted as an barrier layer and prevent the migration of cobalt to the surface.

The diffusion of cobalt to the surface is also closely related to the depth of acid etching (Alam et al., 1997). Treatment by Murakami might have

yielded an optimum depth, so that diffusion of cobalt to the surface is not possible.

7.7   Evaluation of Adhesion

The diamond films deposited using various substrate treatments were tested for adhesion using a Rockwell hardness tester with a Brale indentor. Discrete loads of 15, 30, 45, 60, 100 and 150 Kgf were used. Atleast 3 indentations were made at each load level. In a Brale indentation test, the substrate is deformed plastically to introduce delamination in the film. This condition was found essential by Jindal et al., (1987) for the case of very hard and adherent coatings on more compliant substrates. When the load is sufficiently high, lateral cracks are initiated and propagate between the film and the substrate. Lateral crack diameters were measured with an optical microscope and SEM. The slope obtained from the plot of indentation load versus the lateral crack diameter reflects the ease with which the lateral crack propagates. It is also proportional to $1/G_c$, where G_c is the critical strain energy release rate for crack propagation (Drory et al., 1995) and therefore can be used as a measure of adhesion. Higher slopes indicate poorer adhesion. Figure 7.7.1 shows the lateral crack diameter versus indent load for WC-3, 6, 12%Co with only diamond powder scratching. The relative error in the measurement of lateral cracks is estimated to be about 10%.
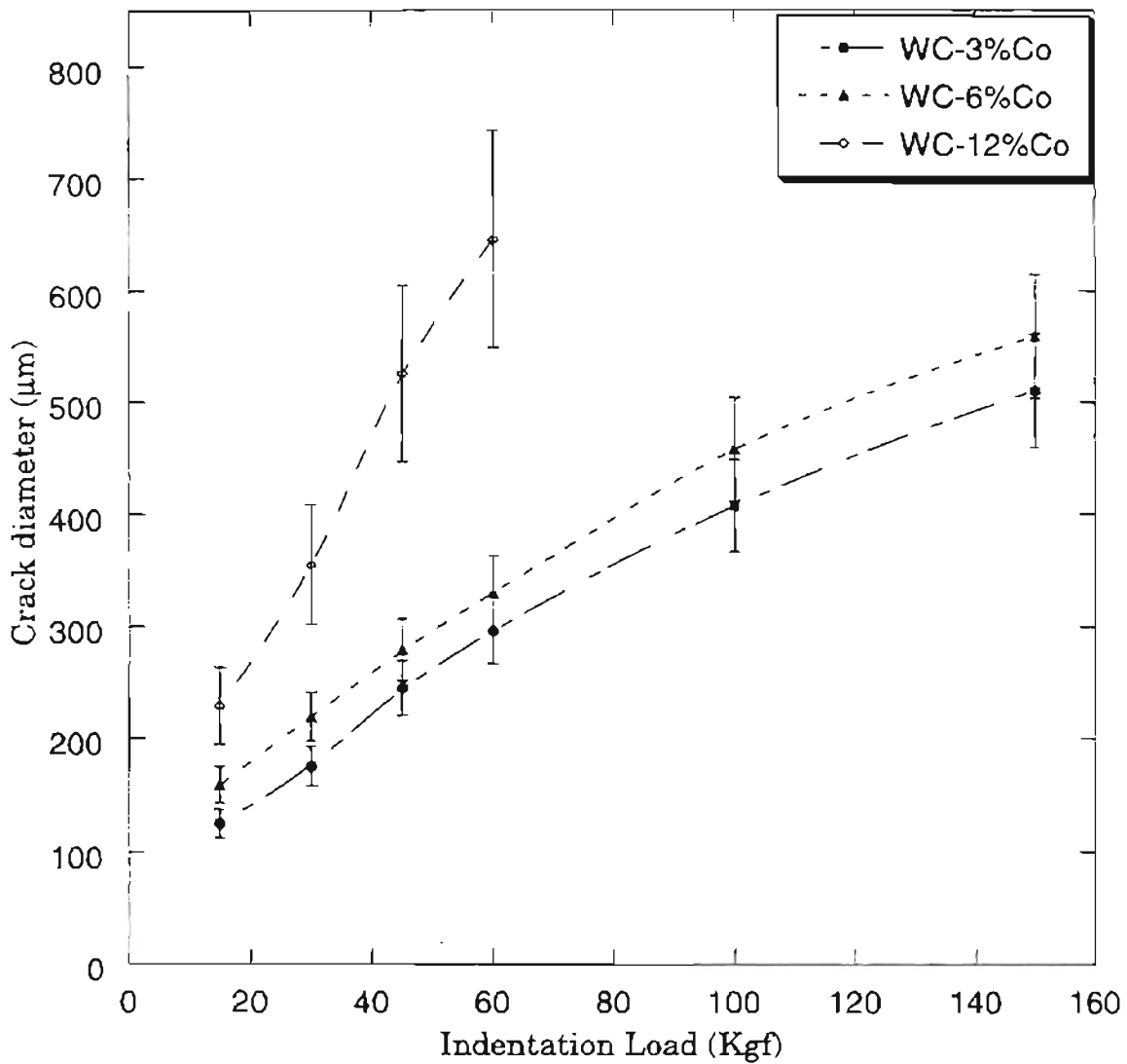
Figure   7.7.1   Crack Diameter Vs Indentation Load Plot for
Rockwell Indentation of the Diamond Coating,
Deposited on WC-3, 6, and 12 % Co with only
Diamond Powder Scratching

It can be seen that higher is the cobalt content poorer is the adhesion. The

effect of substrate treatment prior to the deposition on adhesion can be seen

in Figure 7.7.2. The three curves in the figures correspond to WC-12%Co

with diamond powder scratching, WC1221, and WC1222. The substrates

treated with Murakami show a much better adhesion compared to the

untreated substrate. Figures 7.7.3a, b, c and d show the indentation imprints on the WC-12%Co and WC1222.
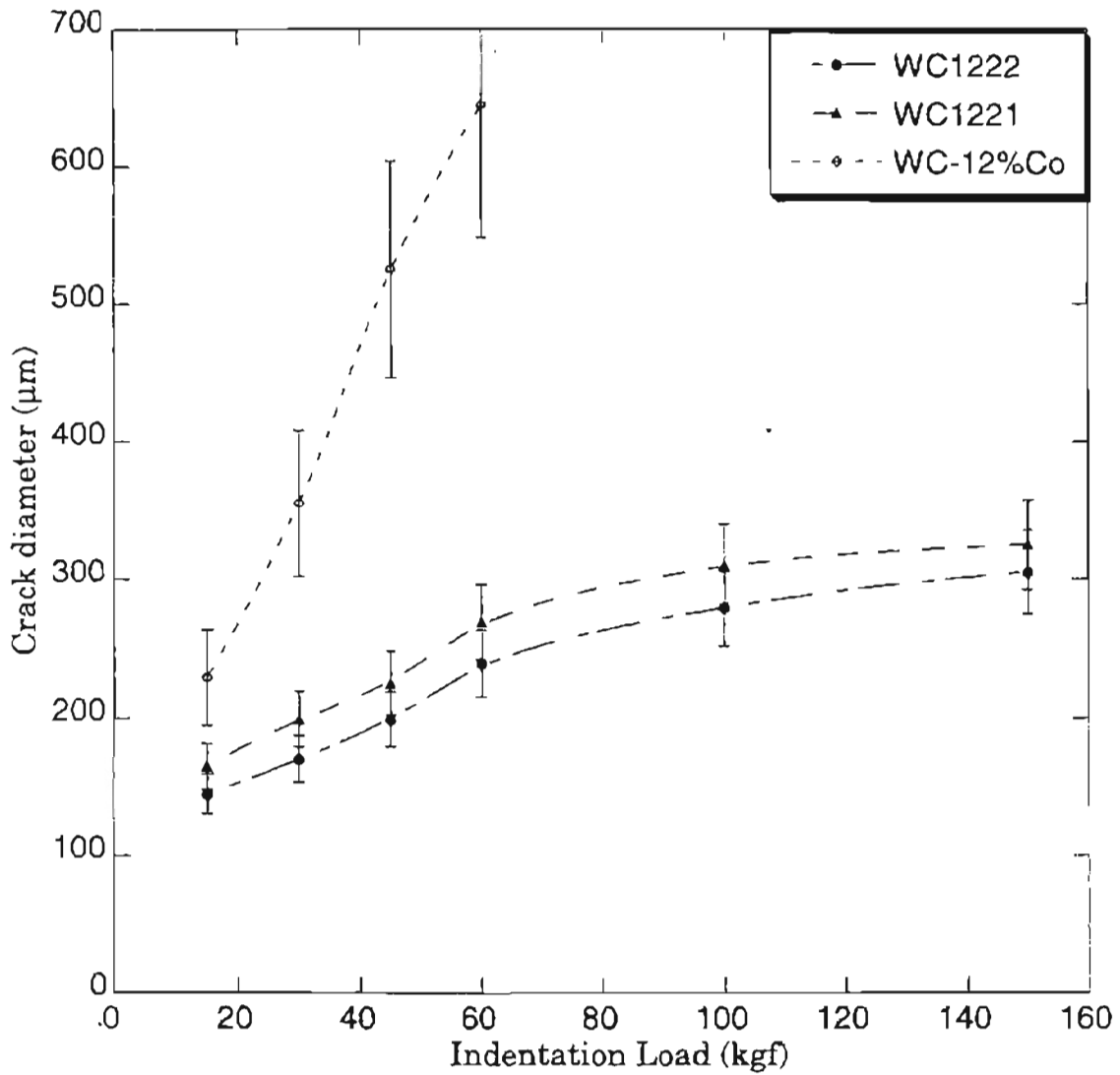
Figure   7.7.2   Crack Diameter Vs Indentation Load Plot for Rockwell
                 Indentation of the Diamond Coating, Deposited on
                 WC-12 % Co Substrates With Different Pretreatments
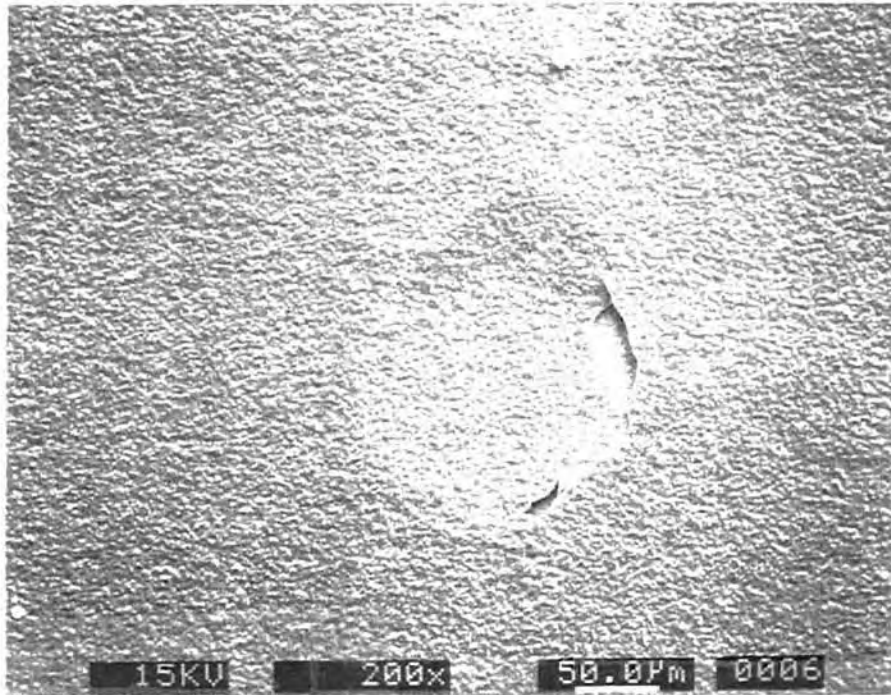
Figure 7.7.3 a) SEM Micrograph of the Indentation Imprint in Diamond Coating on WC-6 % Co with only Diamond Powder Treatment at 45 kgf Load
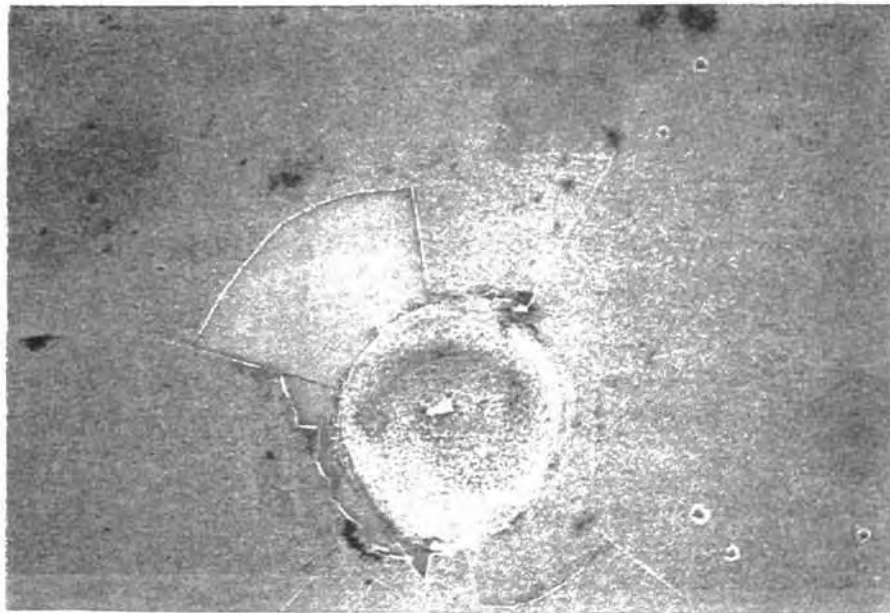
Figure 7.7.3 b) SEM Micrograph of the Indentation Imprint in Diamond Coating on WC-12% Co with only Diamond Powder Treatment at 60 kgf Load Showing the Flaking of Diamond Coating
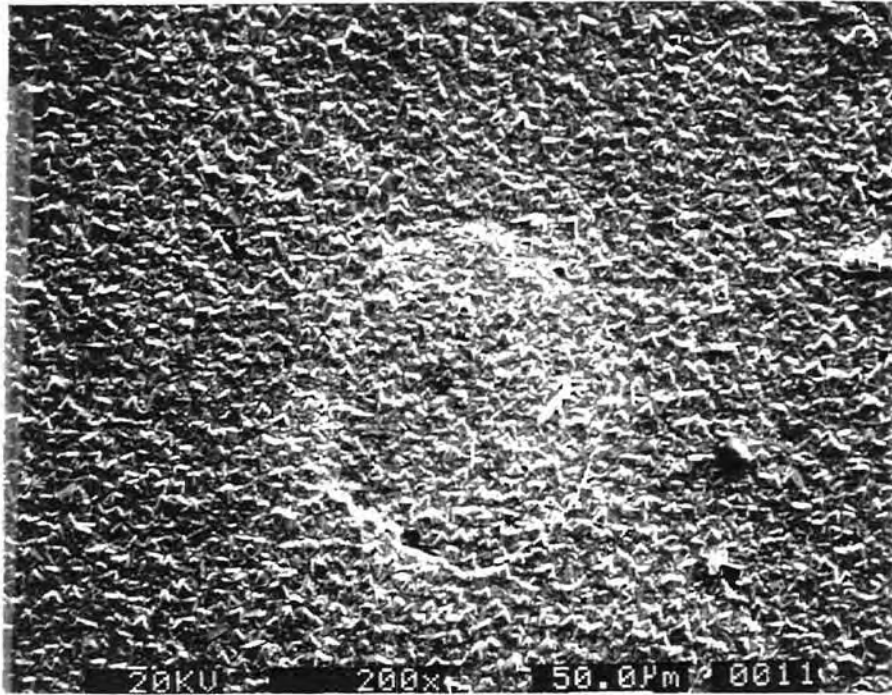
Figure   7.7.3 c)   SEM Micrograph of the Indentation Imprint in
Diamond Coating on WC1221 at 60 kgf Load
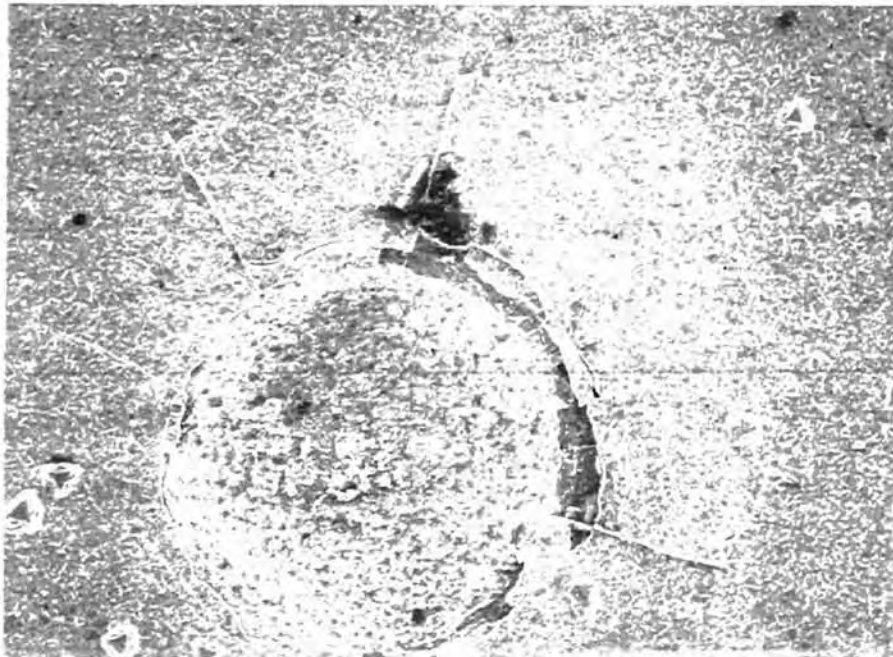
Figure   7.7.3 d)   SEM Micrograph of the Indentation Imprint in
Diamond Coating on WC1221 at 150 kgf Load

The diamond coating on an untreated WC-12%Co sample flaked over a large area for a load of 60 Kgf. However, the coating deposited on the WC1221 sample survived the load of 150 kgf (Figure 7.7.3d). The calculated crack resistance (or adhesion strength) of the diamond coatings are ~ 350, 336, and 106 Kgf μm^{-1} for WC-3, 6, and 12% Co respectively. The values of crack resistance or the adhesion strength of the diamond coatings on Murakami treated tools are ~ 834, and 844 Kgf mm^{-1} for WC1222 and WC1221 respectively. It can be noticed that there is a significant improvement in the adhesion strength of the diamond coating on cemented tungsten carbide following Murakami treatment. Huang et al., (1993) obtained a crack resistance value of ~ 570 kgf mm^{-1} for diamond coatings on WC-6% Co after removal of surface cobalt. Nesladek et al., (1995) also found that the interface toughness of the diamond coatings on cemented carbides improves with surface pretreatment.

Etching with Murakami followed by ultrasonic seeding with diamond particles led to an improvement in adhesion. The isotropic surface roughness created by Murakami facilitates a strong mechanical anchoring of the diamond coating. The etched grain boundary network and the 0.1 μm diamond particles from the ultrasonic treatment improved the adhesion. Absence of cobalt at the interface as indicated by the XRD, is another strong factor contributing to the improvement in adhesion. Figure 7.7.4 shows the crosssection of the WC1213 sample.
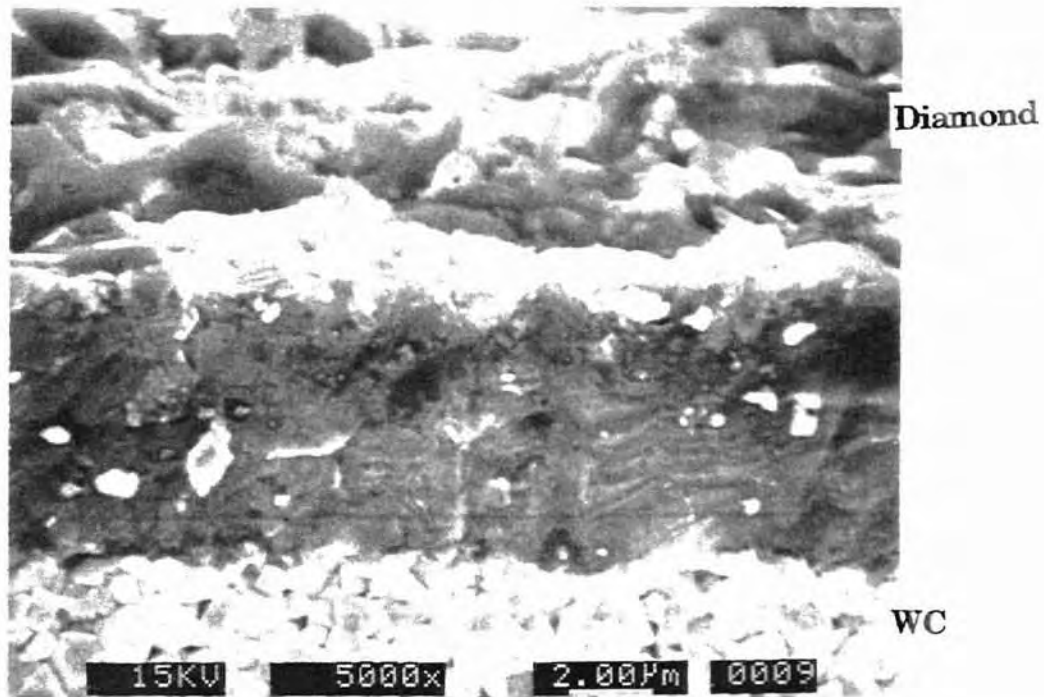
Figure   7.7.4   SEM Micrograph of the Cross Section of the WC1213 Sample
Showing the Mechanical Interlock between WC Grains
and Diamond

The mechanical interlocking between the WC grains and the diamond can
be seen from the micrograph. No cobalt was detected by EDXA analysis. μ-
Raman analysis of the crossection indicated that no amorphous carbon
phases are present at the interface. The Combination of all these factors led
to a significant improvement in adhesion on WC-3,6 and 12%Co samples.

CHAPTER 8

.

ON THE GROWTH OF POLYCRYSTALLINE
DIAMOND ON TRANSITION METALS

8.1 Introduction

Diamond films have been deposited on a variety of substrates using various CVD deposition techniques (Angus & Hayman 1988; Lux & Haubner 1991, 1996; Narayan, Nelson, Oktyabrsky & Jagannadham 1993). On a non-diamond substrate, diamond formation involves heteronucleation and usually results in the formation of polycrystalline diamond films.

Saito et al. (1991) carried out diamond synthesis on several substrate materials, including the metals, such as Ni, Co, W, Mo, Cu and ceramics, such as SiC, SiO_2, Al_2O_3, ZrO_2, AlN. They reported diamond formation on all substrates, except Co and Ni. They reported that the highest nucleation density was obtained on amorphous SiO_2 followed by W, Mo, and SiC. Lux et al. (1991) reported that diamond nucleation on refractory metals is directly related to the carbon diffusion rate. Since refractory metals use most of the available carbon to form carbides, they suggested that a minimum carbon concentration is essential at the substrate surface, which was not reached during the initial stages. They attributed the differences in the nucleation behavior on various substrate materials to the differences in the carbon diffusivities in carbides. However, Park et al. (1991) studied the deposition of diamond on a Ti substrate and reported that the nucleation behavior depends entirely on the initial surface condition and the initial

surface treatment. The TiC layer formed was not found to influence the nucleation behavior.

Lu et al. (1992) reported diamond growth on some of the metal substrates namely, Mo, W, Ta, Cu, and Ni, and argued that under thermal plasma conditions, formation of a carbide layer may not be crucial for diamond deposition. Demazeau et al. (1993) selected W, Mo, and Cu as the substrate materials, based on their tendency to form carbides. They found diamond formation on W and Mo but not on Cu. They identified the diffusion rate of carbon in the substrate, degree of chemical bonding, and the uniformity and thickness of carbon on the surface as the major factors influencing nucleation.

Lux et al. (1993) reported diamond growth on Cr, Co, and Ni. Diamond nucleation was observed only after a relatively long incubation time on these substrates. They observed that Cr substrates formed an intermediate chromium carbide layer prior to diamond nucleation, while on Ni, diamond nucleation occurred only after the substrate and surface became saturated with carbon. Diamond deposition without the formation of amorphous carbon was possible on Co only at low CH_4 concentrations.

Perry et al. (1994) investigated the reaction layers formed at the interface during the growth of diamond films on substrates such as Ti, W, Mo, and Cu by X-ray photoelectron spectroscopy (XPS) and scanning Auger microscopy (SAM). They observed that the reaction layers of Ti, W, and Mo were composed of carbides and oxides, while only traces of C and O_2 were detected in the case of Copper.

Liu et al. (1995) deposited <111> oriented diamond particles on Co substrates by a multi-step process which involved seeding, annealing, nucleation and growth. They proposed the existence of Co-C intermediate metastable phase formation and suggested that a molten Co-C-H surface layer might be responsible for the suppression of graphite co-deposition and oriented diamond nucleation. Ece et al. (1996) studied the nucleation and growth of diamond films on Mo and Cu substrates and reported that under identical conditions diamond grew easily on Mo, while on Cu the nucleation density was relatively low and a continuous film never formed.

Lux et al. (1996) reviewed the possible interactions at the diamond - substrate interface. They pointed out that refractory metals (Ti, Zr, Hf, V, Nb, Ta, Mo, Cr, W) form stable carbides in the presence of hydrocarbons and diamond nucleation starts after the surface is carburized. They also pointed out that for substrates which do not form stable carbides but can dissolve carbon (Fe, Co, Ni, Pt), carbon diffusion occurs only after the entire substrate is saturated.

Liu and Dandy (1996) developed a kinetic model to investigate the diamond nucleation on carbide forming substrates. Even though formation of carbides is a step in the nucleation process on carbide-forming substrates, they found that the diffusion of the surface carbon atoms into a substrate is not a critical factor in determining the incubation period. They observed that the length of the incubation period was closely related to the mean residence time and surface diffusion. In particular, the diffusion of carbon atoms on the substrate surface seems to play a critical role in the nucleation kinetics. They suggest that nucleation can start even at a low surface carbon concentration if the surface diffusivity is large enough for

the atoms to migrate and form critical nuclei during the mean residence period.

Peng and Clyne (1997) investigated the kinetics of the carbide formation on Ti and Ti alloy substrates at different substrate temperatures using hot filament CVD. Formation of TiC was detected after 5 minutes of deposition on both the substrates. They observed that the growth kinetics of the TiC layer obey a quadratic relationship during the initial stages. Diffusion of carbon through the growing layer was found to be the rate determining step and the growth rate of TiC decreased with the formation of the diamond layer. However, they noticed that the subsequent growth of diamond depends on the availability of carbon, since the formation of a TiC layer competes with the formation of diamond. Diamond growth rates were found to be very slow at 850 °C, due to the higher diffusion rates of carbon into the Ti substrate at that temperature. They suggest that surface pretreatment with carbon ion bombardment might be favorable in improving the bonding of the diamond film with the substrate.

Terranova et al., (1996) reported the complete sequence and growth of the various components formed at the diamond/Ti interface during the CVD process using reflection high-energy electron diffraction (RHEED) technique. They noticed that the structure of the interfacial layer evolved via a gradual transition from the titanium-hydride/-carbide/graphite mixed phase at lower temperatures (~ 650 °C) and TiC/graphite mixed phase at higher temperatures (~ 730 °C) to a continuous carbide layer and successively, to a diamond film.

It can thus be seen from the review of literature that nucleation and growth of diamond depends not only on the gas-phase chemistry and process parameters but also on the chemical nature of the substrate. The formation of non-diamond and graphitic carbon varies with the substrate material. The growth rate is faster on Ti, W and Mo. Nucleation is observed on Cr and Co only after a long incubation time (Lux et al., 1991, 1993). This appears to be related to the tendency of these elements to form carbides.

Goldschmidt (1948) studied the relation between the carbide structure and the position of the metal in the periodic table. He found that the stability of the carbides decreases as the structure changes from cubic to hexagonal to orthorhombic. It might be noted that the 3d shell gradually fills up across the period while the stability of the carbides decreases. Thus, it appears that the 3d electrons play an important role in the formation of carbides as well as the diamond formation mechanism.

It can be seen from the review of literature that nucleation and growth of diamond depends not only on the gas-phase chemistry and process parameters but also on the chemical nature of the substrate. The formation of non-diamond and graphitic carbon varies with the substrate material. The growth rate is faster on Ti, W and Mo. Nucleation is observed on Cr and Co only after a long incubation time (Lux et al., 1991, 1993). This appears to be related to the tendency of these elements to form carbides. Even on the carbide forming substrates the nucleation kinetics of diamond depends on the availability of carbon and the diffusion of the carbon into or on the substrate (Peng et al., 1997; Liu et al., 1996). It has been pointed out by Peng and Clyne (1997) that there is a competition between the rates of carbide and diamond growth. Increasing thickness of the growing carbide

layer was found to cause debonding between the diamond film and the substrate (Chandra et al., 1996; Peng et al., 1997).

Narayan et al. (1996) reported that by a alloying Ni substrate with Al, it is possible to reduce the graphite catalyzing effect and form diamond directly on Ni-Al alloys. They found that Ni promoted graphitization and a crystalline layer of graphite was formed initially. Nucleation of diamond was observed on top the graphite layer. By high-resolution TEM and electron diffraction studies, they established that the growth of diamond was not epitaxial. The diamond crystallites were found to be textured with <111> diamond being parallel to [0001] graphite. To minimize the catalytic effects of graphite formation they proposed alloying Ni with Al. They observed diamond deposition directly on the Ni-Al alloy without the interposing graphite layer. They proposed that in Ni-Al alloys, Al donates electrons to fill the 3d shell of Ni which has ($3d^8 4s^2$) configuration and further stabilizes sp^3 bonding.

The present work was carried out to investigate the effect of the chemical nature, in particular, the electronic structure of the substrate materials, on diamond nucleation and growth. Selection of the transition metals was based on their tendency to form carbides. Diamond deposition was carried out on transition metals, namely, Ti, V, Nb, Ta, Cr, Mo, W, Fe, Co, and Ni as substrate materials using the microwave assisted plasma CVD technique. Mn was not used because of its availability only in the form of small chips. Table 8.1 shows the elements used in the present investigation along with their electronic structure. Experiments were conducted on all the elements belonging to the first series as well as those belonging to the two groups (VB and VIB). Raman characterization results are correlated

with the trends in the chemical properties of these elements. It has been found that the chemical nature of the substrate plays an important role in the stabilization of sp^2 (graphite) or sp^3 (diamond) bonded phases. Section 8.2 gives the details of the experimental setup and the test procedure. Experimental results are given in section 8.3. To formulate a mechanism for diamond growth on various transition metals an understanding of the nature of bonding of transition metals carbides and their properties would be helpful. The interaction of transition metals with carbon and the nature of bonding in transition metal carbides are discussed in Section 8.4. Based on the experimental results, a mechanism is proposed for the diamond growth on transition metals.

8.2. Experimental Setup and Test Procedure

All the samples (purity > 99%) except Cr were obtained in the rod form from Alridch Chemicals. Cr was obtained in the form of small pieces. The substrates were polished with Al$_2$O$_3$ (400 grit) and were ultrasonically cleaned in acetone and distilled water separately for 30 minutes each. No diamond scratching/ abrading was applied to any of these substrates. Details of the experimental procedure were given in Chapter 4. Table 8.2.1 gives typical diamond deposition conditions employed for all transition elements which were kept constant throughout the experiments. The diamond films grown were characterized by μ- Raman spectroscopy, scanning electron microscopy and small angle X-ray diffraction apparatus. Details of the various characterization techniques and procedure were given in Chapter 4.

205

Table 8.1   Transition Metals along with their Outer Electronic Configuration and their Crystal Structure (Earnshaw, 1973)

Row Period	IV B	V B	VI B	VII B	-------->	VIII	<----------	I B
4	22Ti $3d^2 4s^2$ hcp < 1173 K bcc < 1933 K MP : 1933 K	23V $3d^3 4s^2$ bcc MP : 2163 K	24Cr $3d^5 4s^1$ bcc MP : 2130 K	25Mn $3d^54s^2$ cubic < 1368K fcc < 1408K MP: 1517 K	26Fe $3d^6 4s^2$ bcc < 1183 K fcc < 1663 K bcc < 1808 K MP : 1808 K	27Co $3d^7 4s^2$ hcp < 661 fcc < MP MP : 1768 K	28Ni $3d^8 4s^2$ fcc MP : 1728 K	29Cu $3d^{10} 4s^1$ fcc MP: 1336.6 K
5	40Zr $4d^25s^2$ hcp < 1138 K bcc <2125 K	41Nb $4d^4 5s^1$ bcc MP : 2741 K	42Mo $4d^5 5s^1$ bcc MP : 2883 K	43Tc $4d^65s^2$ hcp MP : 2445 K	44Ru $4d^75s^2$ hcp MP : 2583 K	45Rh $4d^85s^1$ fcc MP : 2239 K	46Pd $4d^{10}$ fcc MP : 1827 K	47Ag $4d^{10}5s^1$ fcc MP : 1253.8 K
6	72Hf $4f^{14}5d^2$ $6s^2$ hcp < 2268 K bcc <2500 K	73Ta $4f^{14} 5d^2 6s^2$ bcc MP : 3269 K	74W $4f^{14} 5d^4 6s^2$ bcc MP : 3683 K	75Re $4f^{14} 5d^56s^2$ hcp MP : 3453 K	76Os $4f^{14}5d^6$ $6s^2$ hcp MP : 3318 K	77Ir $4f^{14}5d^7$ $6s^2$ fcc MP : 2683 K	77Pt $4f^{14}5d^9$ $6s^1$ fcc MP : 2045 K	79Au $4f^{14}5d^{10}$ $6s^2$ fcc MP: 1337.6K

Note : The elements used in this investigation are denoted in **bold**

TABLE 8.2.1   Deposition Conditions

Chamber pressure	20 ± 0.4 Torr
Substrate heater temperature	850 ± 9.5 °C
Substrate surface temperature measured by an optical pyrometer	900 ± 10 °C
Microwave power	1000 ± 1 W
Total gas flow rate CH_4 (vol. %)	100 sccm 0.5 -1% -(± 0.005 sccm)
Duration	10-15 hrs

8.3. Results

The diamond deposition on each of the substrates was carried out individually as a function of time under the same conditions, and the results of these comparative studies are discussed in this section. Figures 8.3.1 (a)- (g) show the micrographs of the diamond coating on Ti, V, Nb, Ta, Cr, Mo, and W. As can be seen from the micrographs Group VB transition metals (V, Nb, Ta) produced dense films of polycrystalline diamond with crystallographic orientation ranging from cubic form to well developed cubo-octahedral crystals along the edge. The average grain size of diamond crystals on V was ~ 8 µm, on Nb ~ 8 µm and on Ta ~ 6µm. W and Mo produced dense films with uniform microstructure of well developed cubic crystals (~2 µm). Thus, from the SEM characterization a similarity in morphological features of diamond films grown on substrates belonging to the same transition group was observed. Experiments were repeated 2-3 times for each element to ensure the reproducibility of the results.

However, the morphology of diamond differed across the period. Ti and V produced well defined continuous diamond films with cubic morphology. Cr produced a very sparse diamond growth after a long incubation period. After 6 hrs only a few diamond crystals were observed. No diamond growth was observed on Fe. Figure 8.3.1 h shows the micrograph of Fe substrate. A black layer was observed and the μ-Raman observation of this layer indicated the presence of graphite and amorphous carbon [Figure 8.3.2 (a)]. Co and Ni took a long time (~ 7 hrs) for incubation and a complete diamond growth was observed only after a long duration (~ 48 hours). Even after prolonged run (~ 30 hrs) no nucleation of diamond was observed on Cu [Figure 8.3.1(i)]. Figure 8.3.2 (b) shows the Raman spectrum of Cu after deposition. The flat nature of the spectrum indicates the absence of any diamond/non-diamond peaks. Cu, thus seemed to be an inert substrate material.

10μm
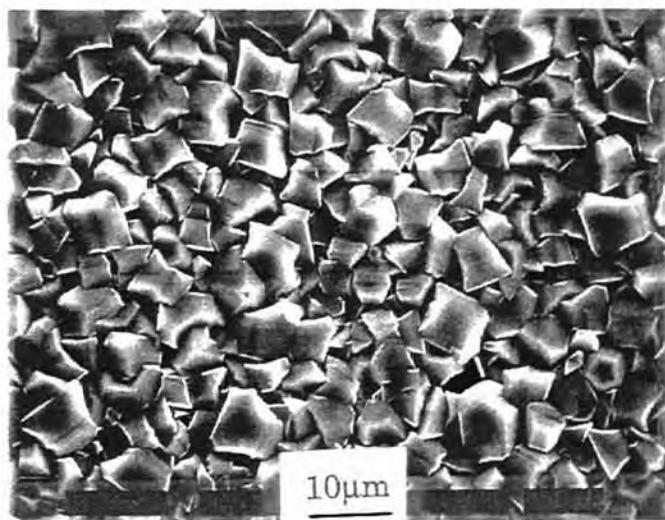
(a) Titanium

(b) Vanadium

(c) Niobium

(d) Tantalum

209
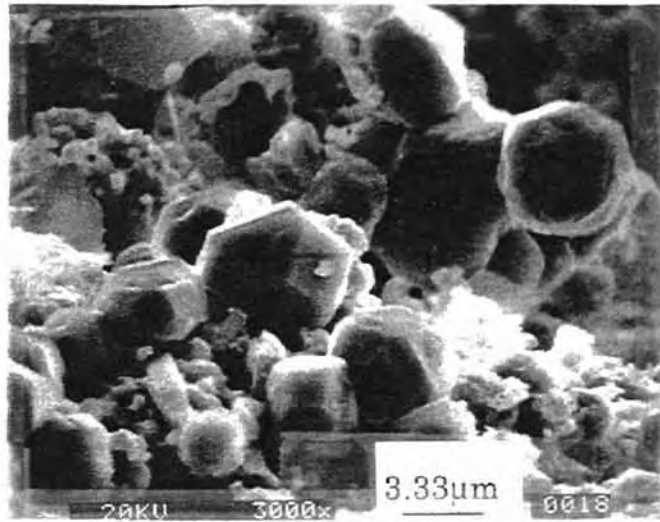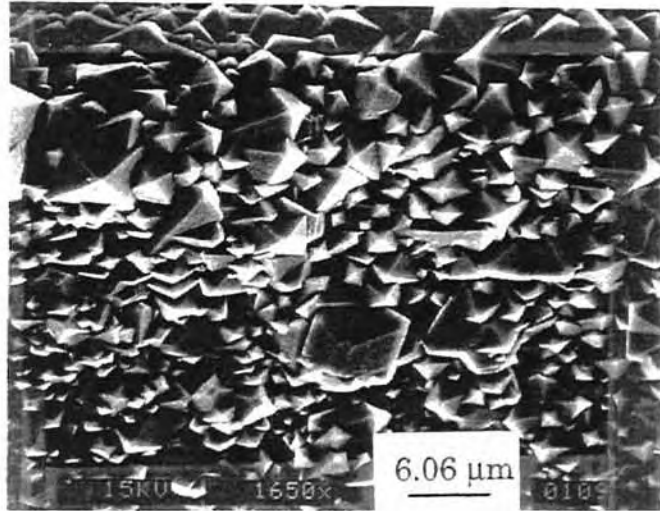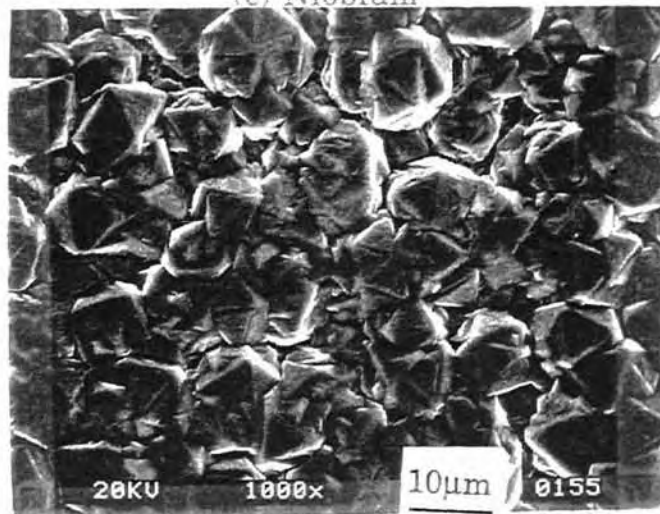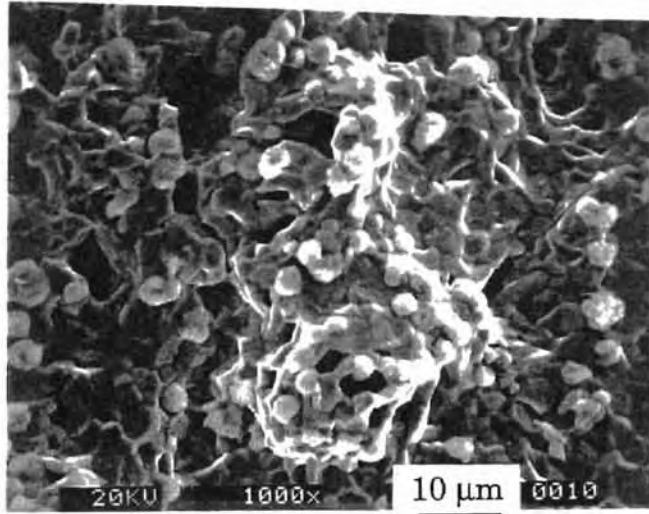
(e) Chromium
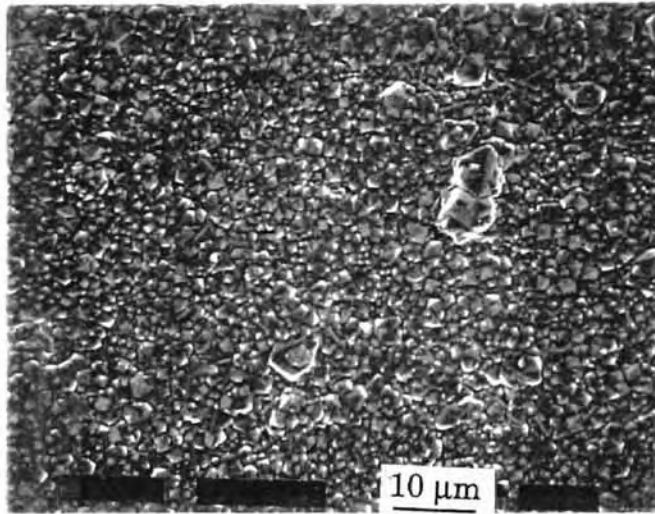
(f) Molybdenum
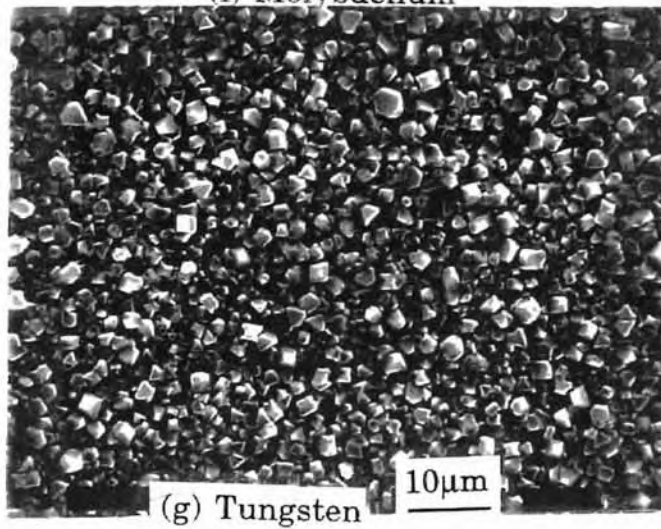
(g) Tungsten
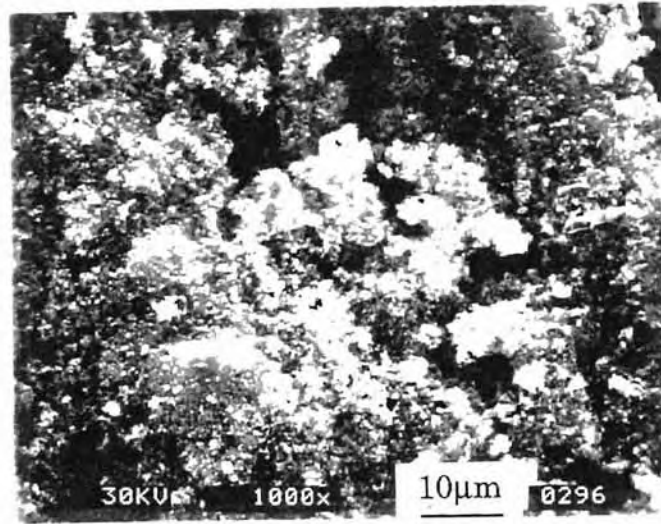
(h) Iron
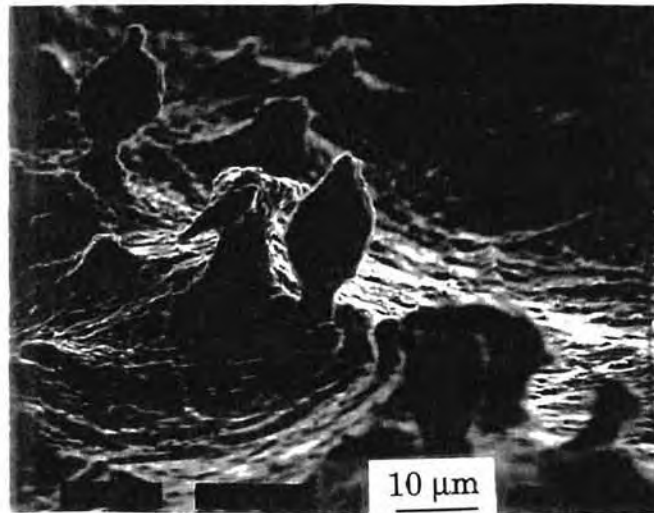
(i) Copper

Figures 8.3.1 a) -i) SEM Micrographs of the Substrates, Ti, V, Nb, Ta, Cr,
Mo, W, Fe, and Cu, Respectively after 8 Hours of Deposition

211
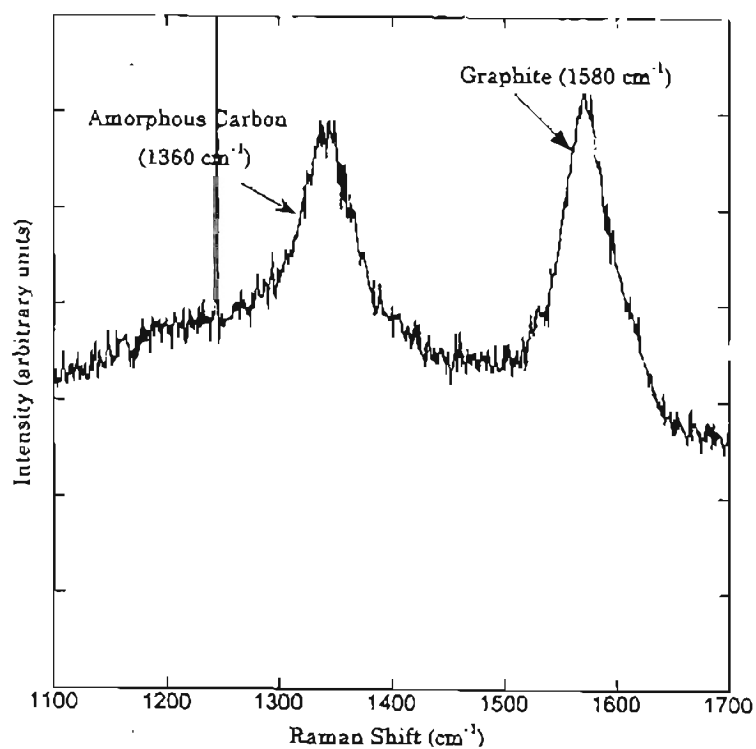
Figure 8.3.2 a) μ-Raman Spectrum of Fe Substrate after 8 Hours of Deposition Showing Peaks Corresponding to Amorphous Carbon
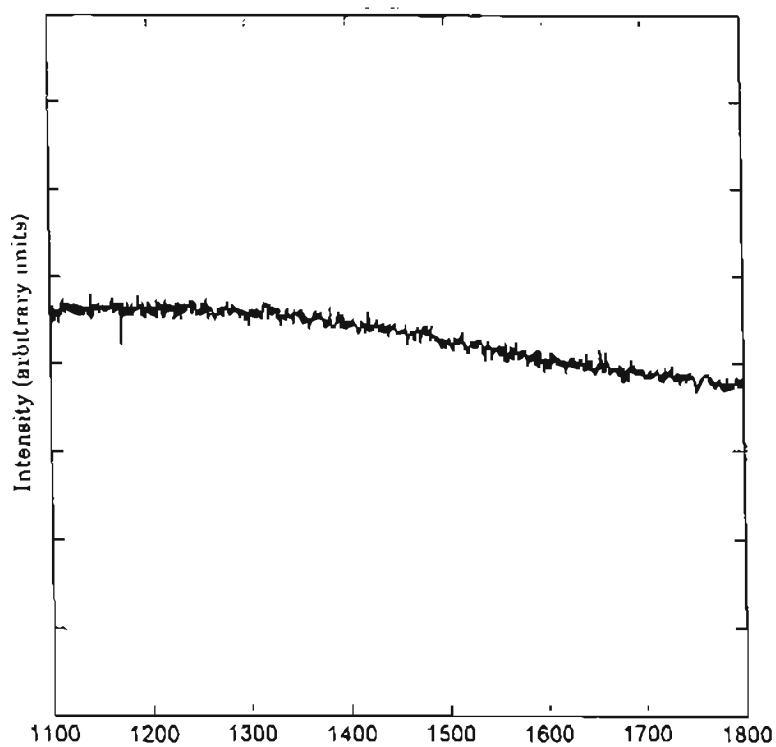
Figure   8.3.2 b)   μ-Raman Spectrum of Cu Substrate after 8 hours of Deposition Showing no Peaks of Graphite or Diamond

Rapid growth of crystalline graphite was also seen in case of Co as evidenced by the sharp peak ~1580 cm^{-1} in the Raman Spectra [Figure 8.3.3 (a)]. Similar deposition after one hour showed no diamond or graphite peaks in the Raman spectra on all other transition metals investigated, indicating that some incubation time is required before diamond is nucleated on the various substrates. However, the Raman spectra of the diamond film on these substrates after 4 hrs of deposition showed a sharp peak ~ 1332 cm^{-1} corresponding to diamond along with a broad peak ~ 1560 cm^{-1} corresponding to diamond-like carbon. Figure 8.3.3 (b) shows the micrograph of the Co substrate after 60 minutes. A black layer was observed and examination of this layer by μ-Raman spectroscopy showed the presence of graphite [Figure 8.3.3 (a)]. After 5 hrs of diamond deposition on Co, some sparse nucleation of diamond was observed. Figures 8.3.3 (c) shows the micrograph of the Co substrate after 5 hrs. It can be observed from the micrograph that the diamond nucleated on the graphite layer. Figure 8.3.3 (d) is the micrograph of the diamond film, deposited on Co after 48 hours, which peeled off immediately. Raman spectrum of the diamond on Cobalt substrate is shown in Figure 8.3.3 (e). Figure 8.3.3 (f) is a micrograph of the Co substrate after the diamond film has been peeled off showing flaky graphite.
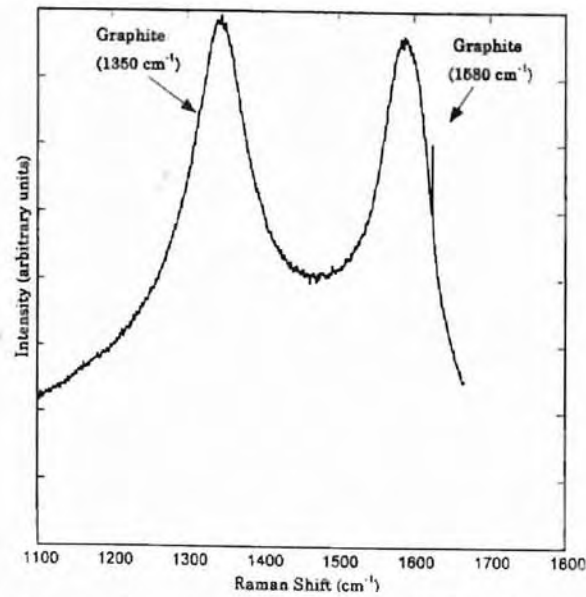
Figure 8.3.3 a) µ- Raman Spectrum of Co after one Hour of Deposition Showing Evidence of Crystalline Graphite Formation
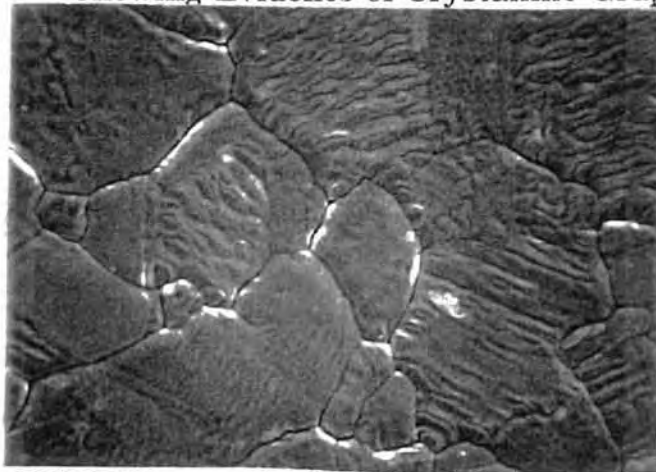
Figure 8.3.3 b) SEM Micrograph of the Co Substrate after one Hour Showing a Black Layer which by µ-Raman Spectroscopy to be Graphite
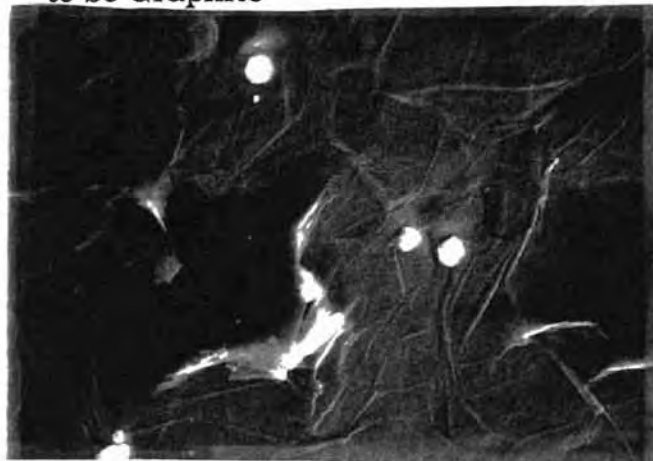
Figure 8.3.3 c) SEM Micrograph of the Co Substrate after 5 hrs Showing Nucleation of Diamond on the Graphite Layer

214
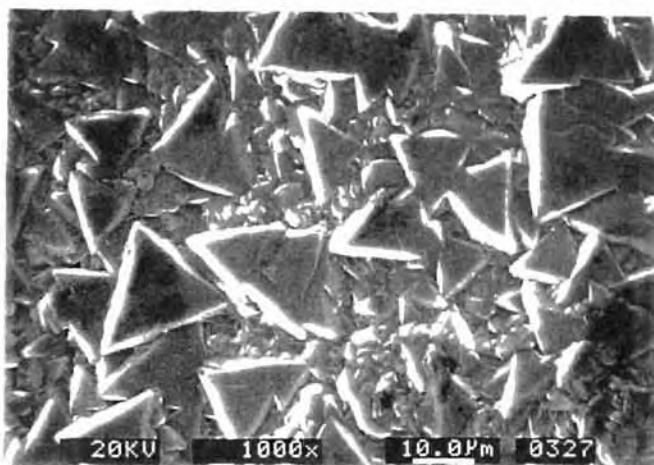
Figure   8.3.3 d)   SEM Micrograph of the Diamond Film Deposited on Co
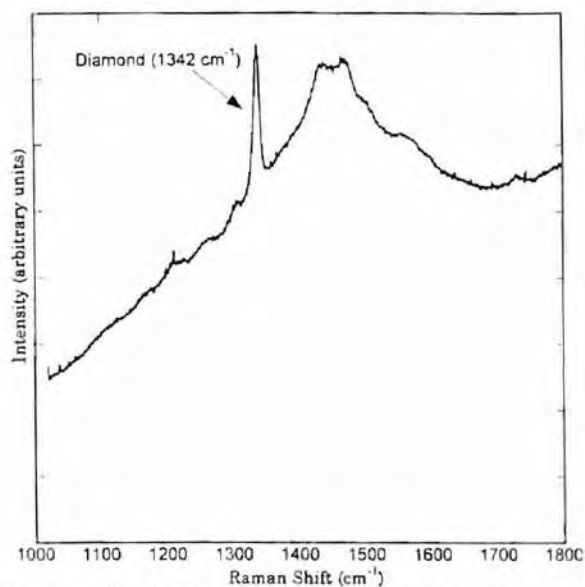
Figure   8.3.3 e)   μ- Raman Spectrum of Diamond on Co after 48 Hours of
Deposition

Figure   8.3.3 f)   SEM Micrograph of the Co Substrate after Removing the
Diamond Film that has been Peeled off Showing Flaky
Graphite

A different observation was made in the case of Ni. Figure 8.3.4 (a) shows the micrograph of Ni after 5 hours showing that Ni has melted in the presence of microwave plasma. Formation of isolated crystals from the molten state can be observed from this figure. Figure 8.3.4 (b) is the SEM micrograph of Ni after a prolonged run (~25-30 hrs). It can be noticed that well defined crystals surrounded by a thin layer of molten layer have emerged from the melt. μ-Raman of the melt in this region showed a peak ~ 1332 cm^{-1} indicating that they are diamond crystallites [Figure 8.3.4 (c)]
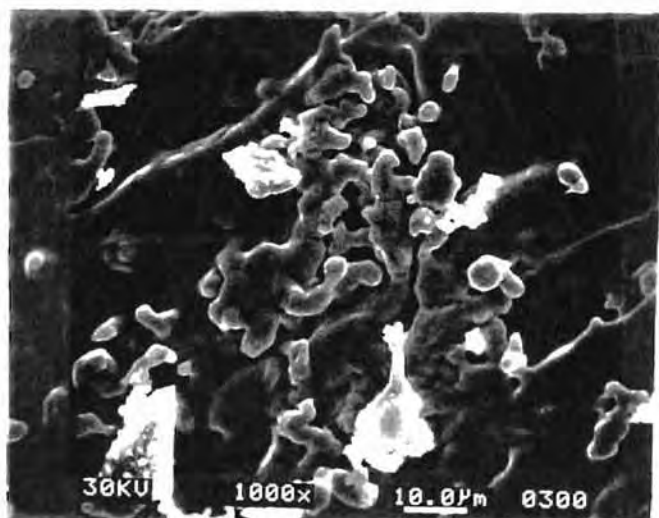
Figure   8.3.4 a)   SEM Micrograph of Ni after 5 Hours of Deposition
Showing Melting of Ni due to High Temperature
Microwave Plasma
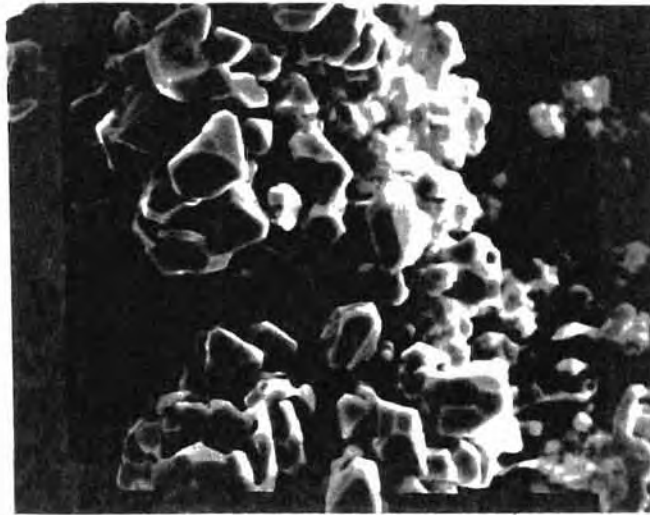
Figure 8.3.4 b) SEM Micrograph of Molten Ni after a Prolonged Run
(~ 30 hrs) Showing Well Defined Crystallites Surrounded
by a Thin Layer of Molten Material. μ-Raman and
XRD Confirmed that they are Diamond Crystallites

(c) Nickel
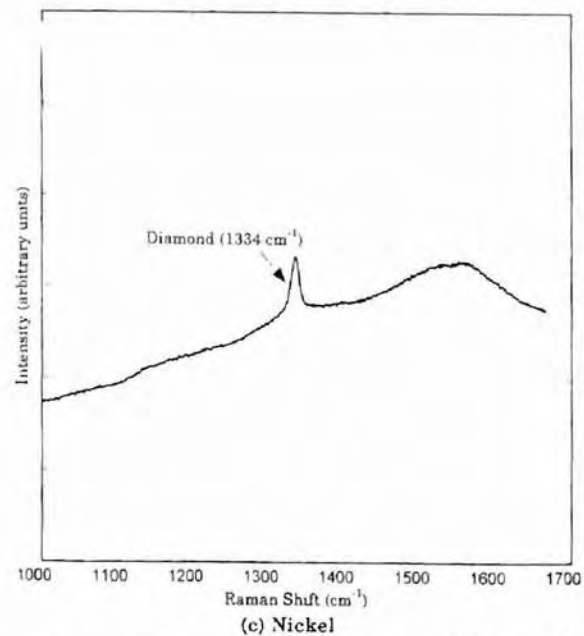
Figure 8.3.4 c) μ- Raman Spectrum of Diamond on Ni after 30 Hours
of Deposition Showing a Peak ~ 1334 cm^{-1} Corresponding
to Diamond

Figures 8.3.5 (a) - (f) are the μ-Raman spectra of the diamond films on different substrate materials. For crystalline diamond, a sharp Raman peak is observed at 1332 cm^{-1}, while for crystalline graphite, it is at 1580 cm^{-1}. The peaks for micro-crystalline graphite are 1350 cm^{-1} (D peak) and 1580 cm^{-1} (G peak), and a single broad peak around 1560 cm^{-1} corresponds to disordered diamond-like carbon.

From the results of the peakfit analysis, it was observed that the intensity ratio of the peaks indicative of sp^3 and sp^2 bonding, respectively increased from the top to bottom in a given group. Also, the Full Width at Half Maximum (FWHM) of the diamond peak decreased similarly from the top to the bottom in a group. However, across the period the results differed between the first and the second half of the transition series. The amount of sp^2 bonded carbon, as indicated by a broad band centered around 1550 cm^{-1} was found to increase across the period for the first half of the transition series elements i. e. for elements belonging to Groups IV - VI (Ti, V, Cr). The amount of sp^2 bonded carbon decreased for the elements belonging to the second half of the transition series, i.e. for Group VIII (Fe, Co and Ni). Also, from the intensity ratios and the FWHM values, it can be observed that good quality diamond films were obtained on Ti, Ta, Mo, and W.
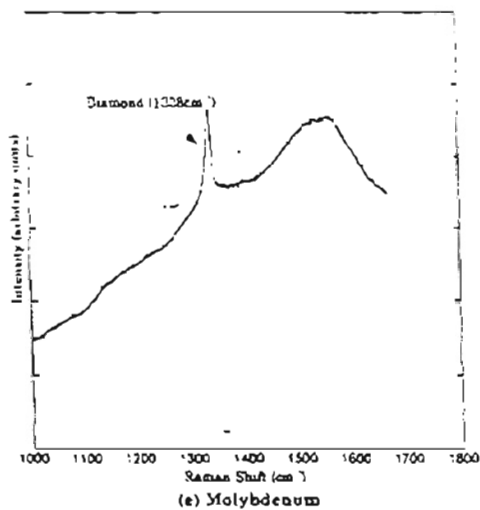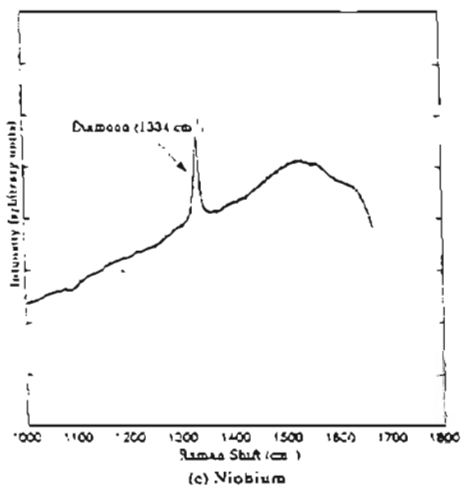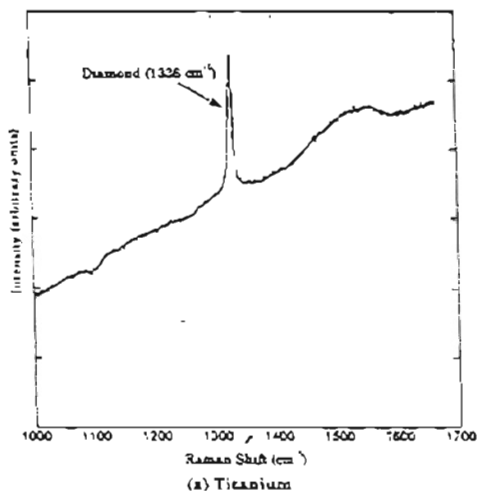
Figures 8.3.5 a) - c) μ-Raman Spectra of the Diamond Films on Different Substrate Materials, namely, Ti, Nb,Mo, Respectively, Showing Peaks Corresponding to Diamond and Diamond-like carbon
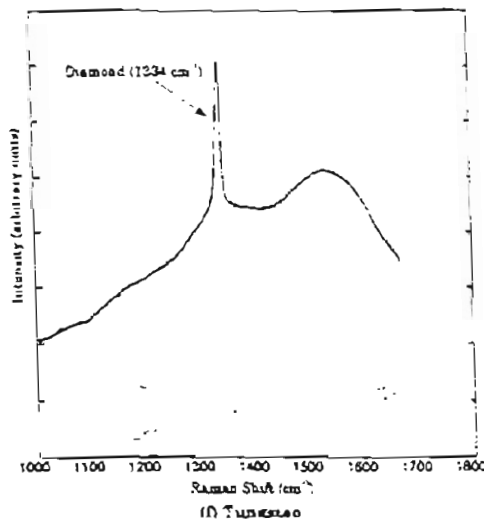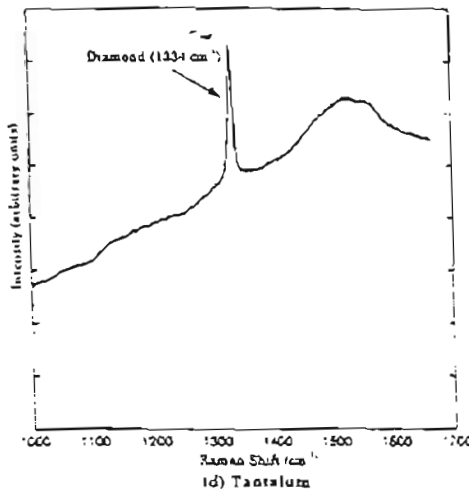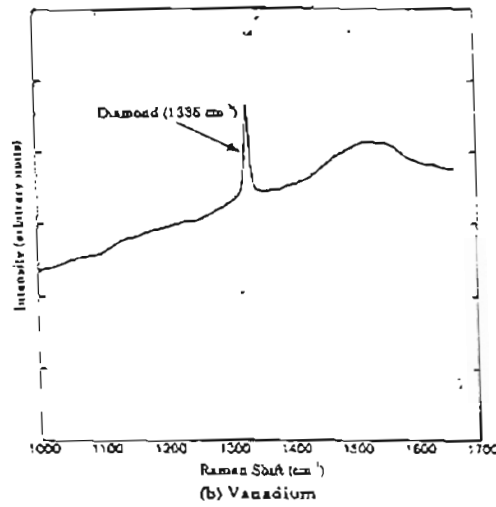
Figures 8.3.5 d) - f)   μ-Raman Spectra of the Diamond Films on Different Substrate Materials, namely, V, Ta, W, Respectively, Showing Peaks Corresponding to Diamond and Diamond-like carbon

The results from the Raman measurements after the background subtraction and peak fitting are presented in Table 8.3.1. It can be noted from the table that the intensity of diamond peaks decreases in passing from left to right in any transition metal series. Coincidentally, the degree of covalency also decreases in a similar manner. The intensity of the diamond peak increases from top to bottom in a given group of transition metals. The ionic radius and melting point increase while electronegativity decreases from top to bottom. Melting point, covalency, and electronegativity depend on the electronic structure of the material. Since the deposition of diamond on these transition metals shows a similar trend, it is plausible that the electronic structure and the availability of the free electrons, can play a key role in the diamond growth.

In all cases, the 1332 cm^{-1} Raman line was found to be shifted to higher wave numbers. A shift between ~ 2 -3 cm^{-1} was observed in the case of Nb, Ta, W, while Ti and V showed a shift of ~ 4 cm^{-1}. A maximum shift of ~ 10 cm^{-1} was observed in the case of Co. These shifts, however, are much smaller and of opposite sign than the shifts that are expected from the differences in the lattice constants between the film and the substrates or the carbides of the same substrates. Thus, a lattice misfit appears to have relatively little influence on the residual strain in the film. Due to a large difference in the thermal expansivities of diamond and transition metal substrates the compressive stresses generated in the diamond film after cooling to room temperature are very large. Chandra et al., (1996) found that the residual stress of diamond films deposited on W substrates were about ~ 1.9 GPa (compressive). The contribution from the thermal stress was calculated to be about ~ 2.0 GPa (compressive). The intrinsic stress

arising during the film deposition was found to be very small ~ 0.1 GPa (tensile).

Thermal Stresses can be calculated from the equation

$$\sigma_{th} = [E/(1-v)] \int_{T_1}^{T_2} (\alpha_s - \alpha_f)\, dT$$

where, α_s and α_f are the thermal expansion coefficients of the substrate and diamond respectively, E is the Young's modulus of diamond = 1050 GPa and v is the Poisson ratio of the diamond film = 0.07. T_1 is the deposition temperature (~ 850 °C) and T_2 is the room temperature (~ 20 °C).

The diamond Raman peak at 1332 cm-1 corresponds to stress free diamond, but it shifts due to the stress in the film (Robins et al., 1990). The peak shifts measured for thin films can be converted to stress using hydrostatic, uniaxial or biaxial models (Chen et al., 1995). The measured stress values from peak shifts, along with the thermal stresses for different substrate materials are given in Table 8.3.2. It can be seen from the table that the measured stresses from the peak shifts correlate reasonably well with the thermal stresses of the transition metals and/or transition metal carbides. Ager et al., (1993) obtained a very large value of stress (~ 6.8 Gpa) in the diamond film obtained on Ti alloy and found it to be consistent with the thermal-expansion mismatch of the diamond film and substrate. Thus it seems plausible to correlate the peak shifts qualitatively with the differences in the thermal expansion coefficients of diamond and the various substrates or the observed carbides on these various substrates. Therefore, the Raman line shifts might be attributed to the thermal strain generated during cooling after growth. Fabisiak et al. (1992) characterized diamond films on Ta, Mo, Si, SiO_2, and Al_2O_3 and observed that as the

Table 8.3.1 Some Properties Of Transition Elements along with μ-Raman Measurements

Substrate	MP * (K)	EN **	IR *** (+4) (pm)	Position of Diamond Peak (cm⁻¹)	Peak Shift (cm⁻¹)	Diamond Peak Intensity (cps)	FWHM of the diamond peak (cm⁻¹)	Position of Non-diamond Peak (cm⁻¹)	Intensity of Non-diamond peak (cps)	FWHM of the Non-diamond (cm⁻¹)	Relative Intensity $I_d/(I_{nd}+I_d)$
Ti	1933	1.5	60.5	1336	4	15000	12.8	1531	2000	105	0.882
V	2163	1.6	58	1336	4	7500	15	1550	2400	95	0.758
Nb	2741	1.6	64	1334	2	8600	14.2	1528	1600	95	0.843
Ta	3269	1.5	64	1334	2	11000	11.2	1546	1500	105.2	0.88
Mo	2883	1.8	61	1338	6	7500	15	1545	3100	126.2	0.707
W	3683	1.7	60	1334	2	9000	14	1520	3000	115.8	0.75
Co	1768	1.9	53	1342	10	7000	52.6	1586.4	4800	84.2	0.59

*MP = Melting Point ** EN = Electro Negativity   *** IR = Ionic Radius

223

thermal expansion coefficient of the material increases, the position of the diamond peak shifted to higher wave numbers. They observed that a minimum FWHM of diamond peak occurred when the thermal expansion coefficient of the substrate is close to that of diamond (i. e. for Si).

Table 8.3.2 Stress Measurements of Diamond Films on
Various Transition Metal Substrates

Substrate	$\alpha \times 10^{-6}$ K^{-1} *			σthermal GPa	σmeasured GPa **
	293K	1200 K	$\alpha_{Ave.}$		
Ti	8.6	11.3	10	-6.51	-4.45
TiC	6.4	8.6	7.5	-4.22	
V	8.4	12.5	10.5	-7.03	-4.83
V C	6.2	7.3	6.8	-3.56	
Nb	7.3	8.8	8.1	-4.78	-3.73
NbC	5.7	7.6	6.7	-3.47	
Ta	6.3	7.4	6.9	-3.66	-3.63
TaC	5.6	7.1	6.4	-3.19	
Mo	4.8	6.7	5.8	-2.62	-6.59
Mo_2C	5.1	6.5	5.8	-2.62	
W	4.5	5.3	4.9	-1.78	-2.16
WC	3.7	5.3	4.5	-1.41	
Co	2.3	17.6	14.8	-11.05	-10.8

*α = Linear thermal expansion coefficient (TPRC data series "Themophysical Properties of Matter", vol: 12,13)
** Δv from Raman measurements $\pm$ 1cm^{-1} corresponding to $\pm$0.46 Gpa

Figures 8.3.6 (a) - (i) show the XRD spectra of diamond coatings on Ti, V, Nb, Ta, Mo, W, Fe, Co and Ni. X-ray diffraction peaks corresponding to graphite was detected in the case of Co. A phase transformation from hexagonal to FCC occurs at temperatures above 417 °C for Co. However

there is a very little change in the peak position of hexagonal versus FCC single crystal Co [(0002)$_{hex}$ at a 2θ of 44.76° and (111)$_{FCC}$ at a 2θ of 44.22°]. It was difficult from the XRD pattern to estimate whether the transition has occurred. Both hexagonal and FCC components of Co were present before and after the diamond deposition. The temperatures utilized in these experiments should result in the phase transformation from the hexagonal to the cubic phase. However, due to the lack of the increased FCC reflection intensities after diamond growth, it can be assumed that upon cooling the substrate to room temperature, the substrate transforms back to the hexagonal structure. In the case of Ti, both hexagonal (α phase) and BCC (β phase) were observed in addition to the FCC phases of TiC. In the case of group V elements V, Nb, and Ta phases corresponding to V_2C, Nb_2C and Ta_2C were observed in addition to monocarbides. In the case of W and Mo, the peaks due to WC and W_2C, and α-Mo_2C were observed in addition to the diamond and substrate peaks. No carbide peaks were detected for Ni and Co. The peaks corresponding to the diamond and the substrate were detected in the case of Co and Ni. The intensities of the carbide peaks were high in the case of Ti [TiC (cubic)], Mo [Mo_2C (hexagonal)], and W [WC (hexagonal) and W_2C (hexagonal)] followed by Ta [Ta_2C (hexagonal)], V [V_2C (hexagonal)] and Nb [Nb_2C(hexagonal)]. This observation is in agreement with the work by Goldschmidt (1948), who suggested that the stability of the carbides decreases as the structure changes from cubic to hexagonal to orthorhombic. The intensities of the diamond peaks were high in the case of Ti, Ta, Mo and W. This is consistent with the μ-Raman observation that good quality diamond films were obtained on Ti, Ta, Mo, and W substrates.
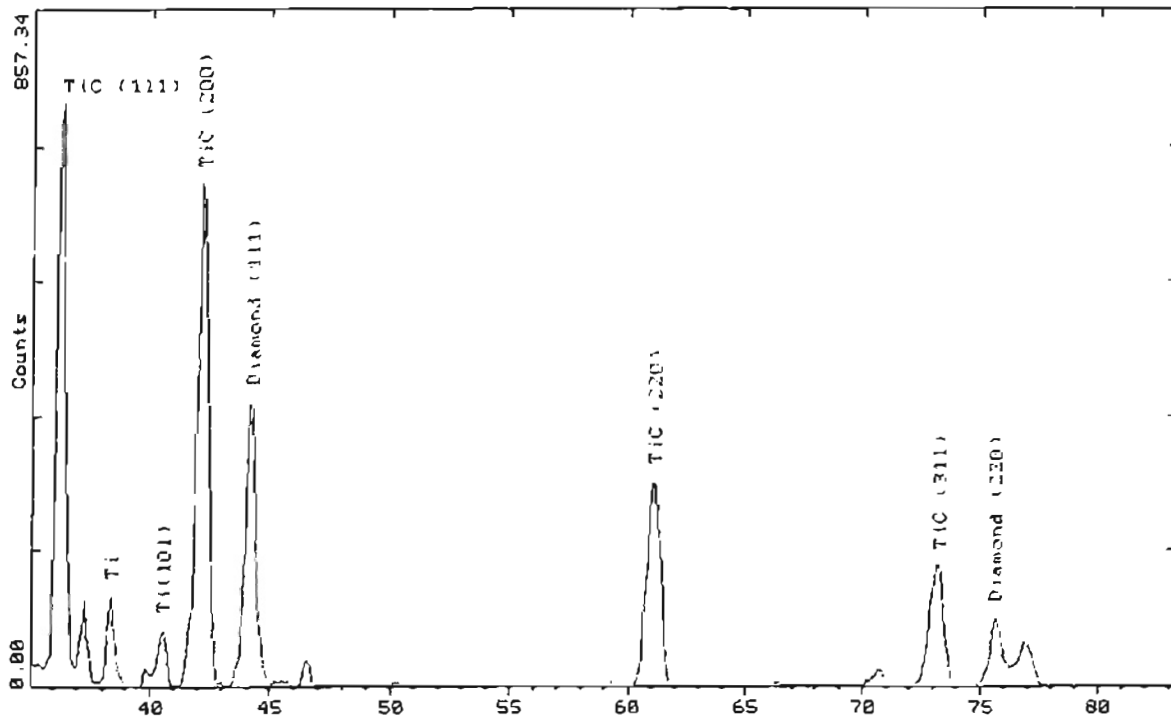
(a) Titanium
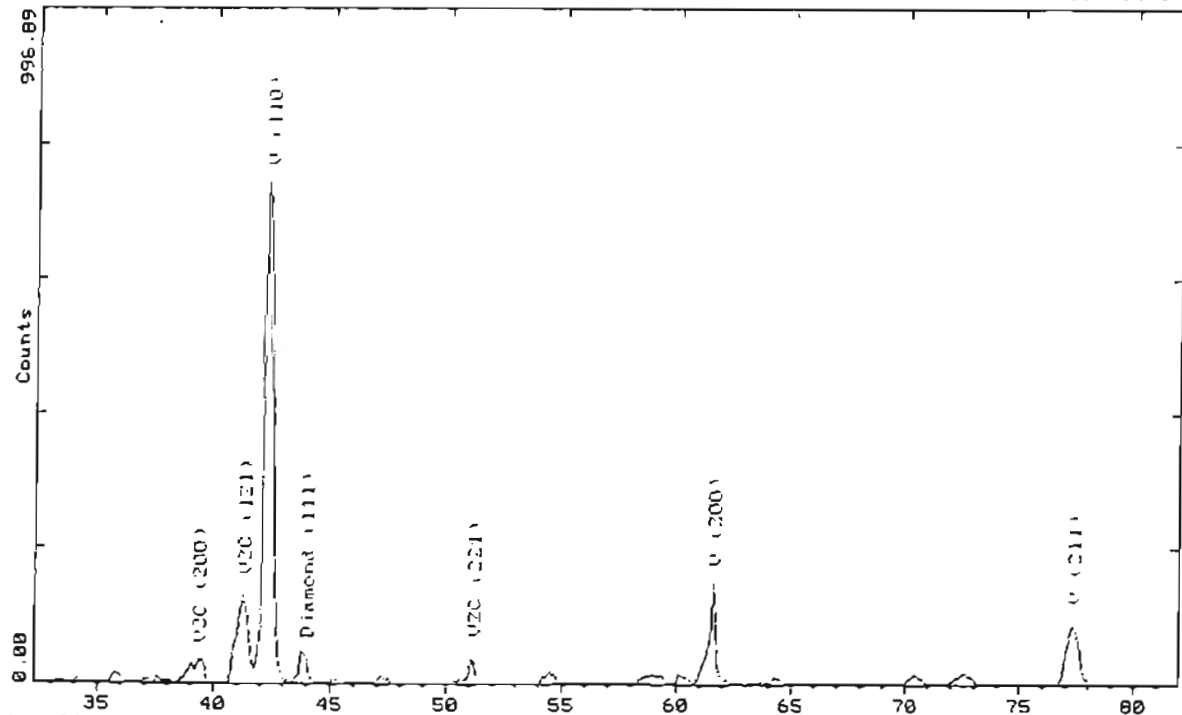
C:\USERS\MALLIKA-TRANSMET\012BMERG.RAW transition metals (CT ......, SS 0.100dg, HL 1.5406Ao)
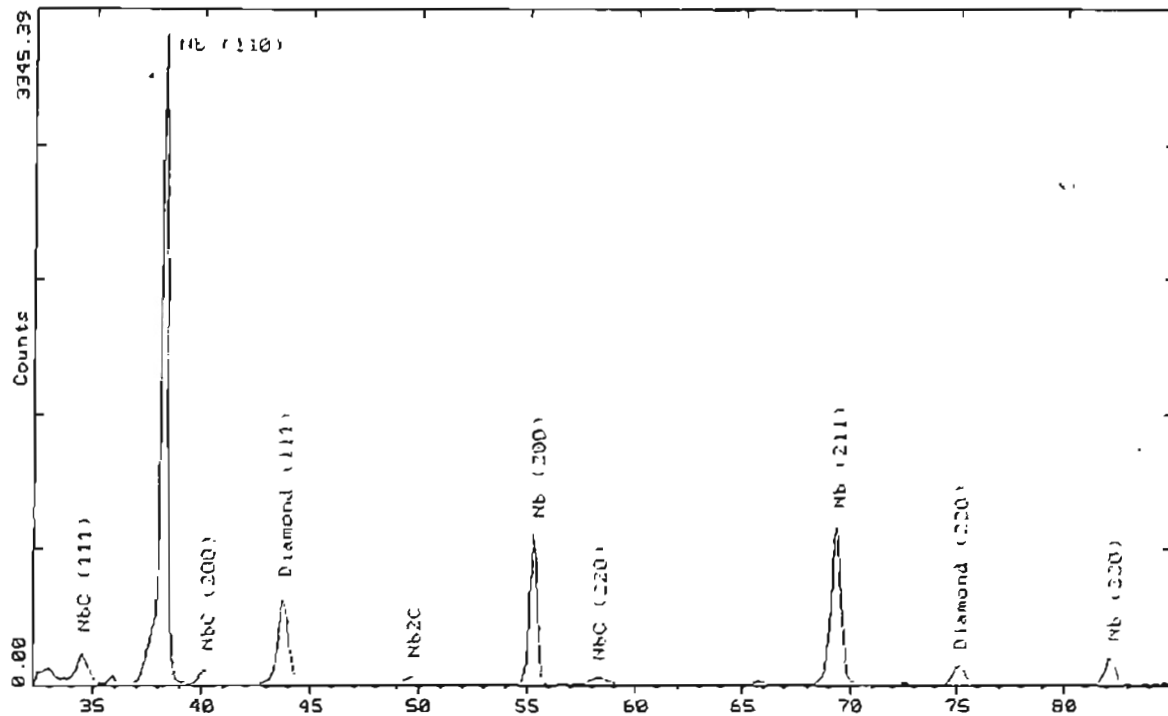
(b) Vanadium

(c) Niobium

(d) Tantalum

(e) Molybdenum

(f) Tungsten

(g) Iron

(h) Cobalt

(i) Nickel
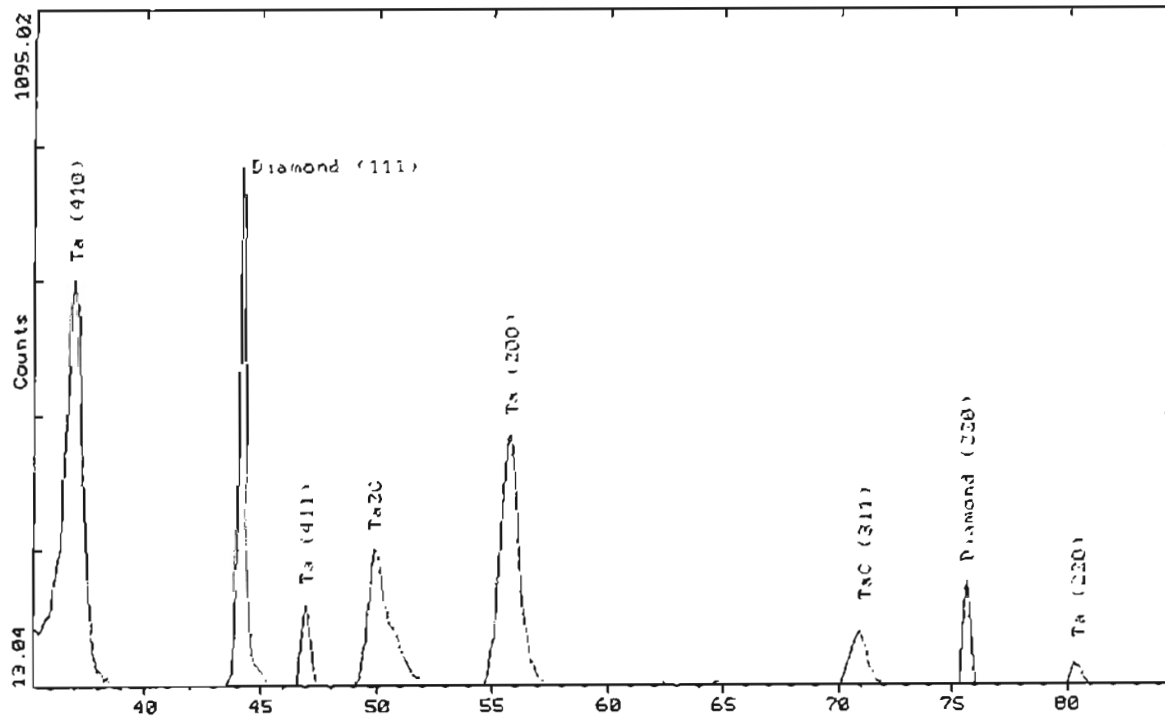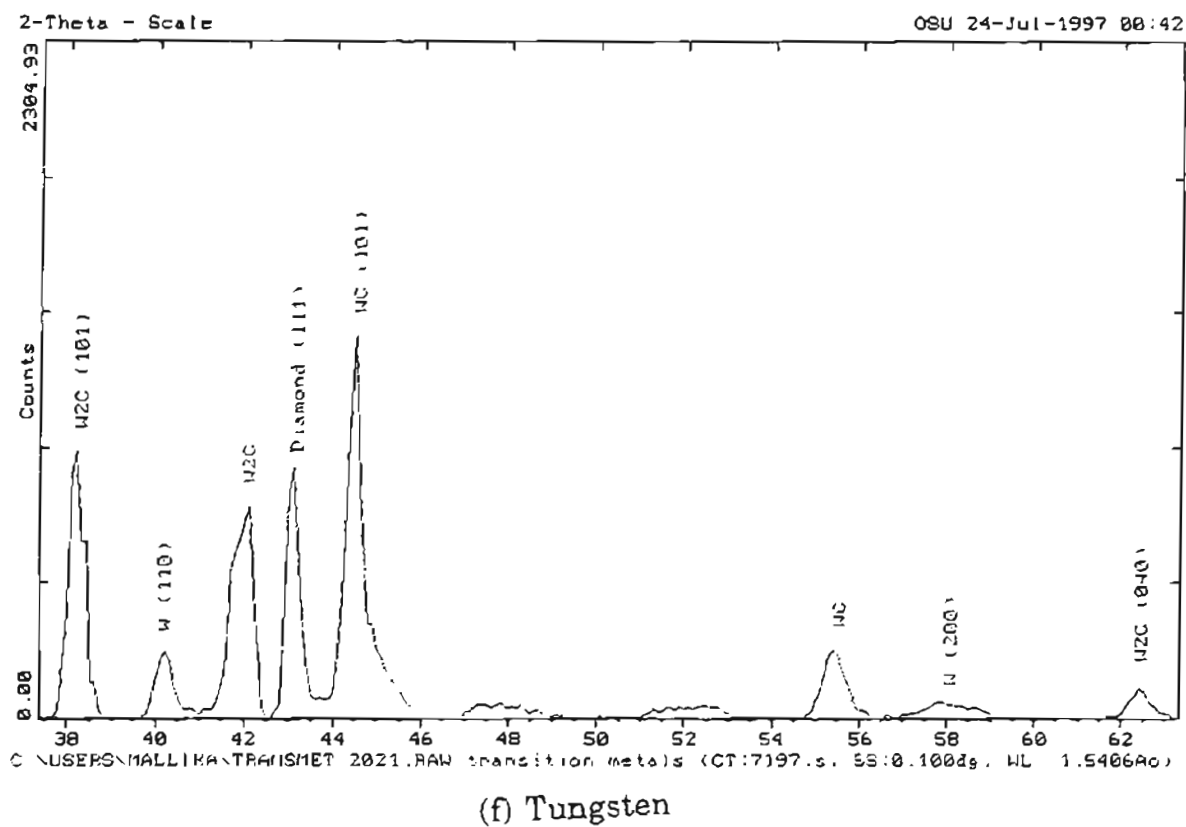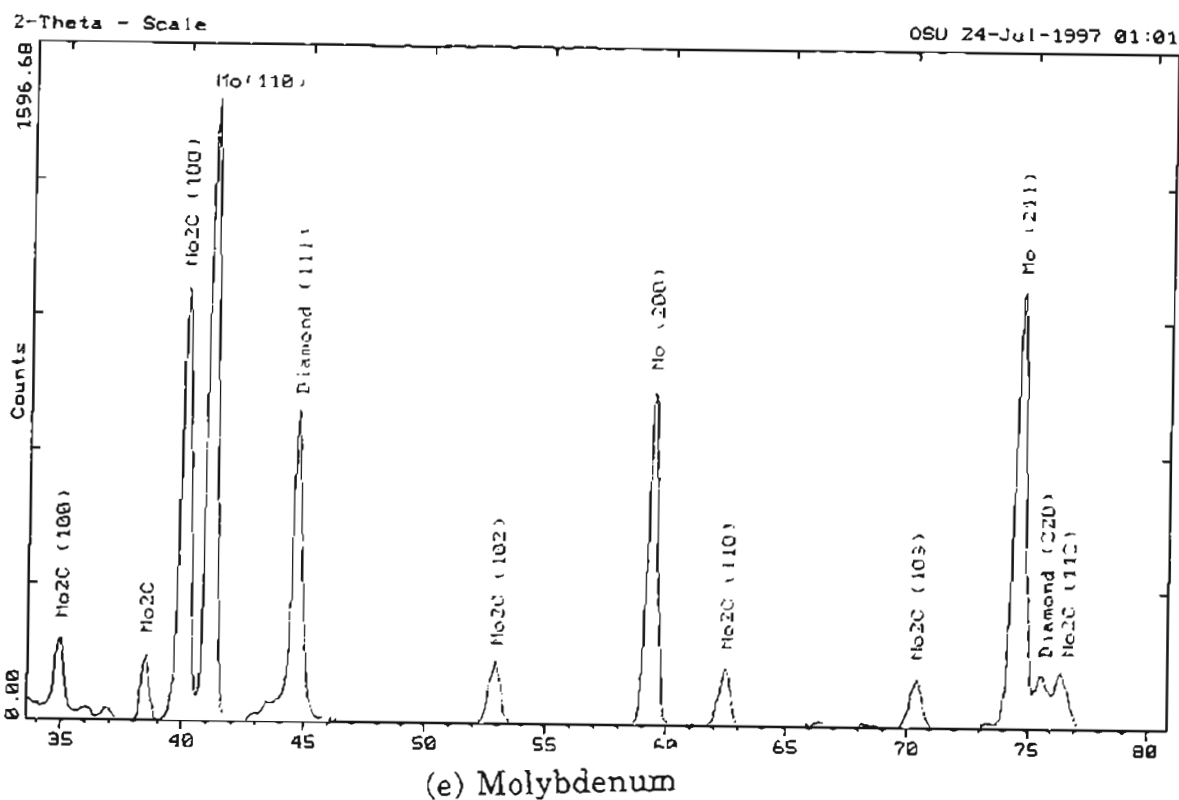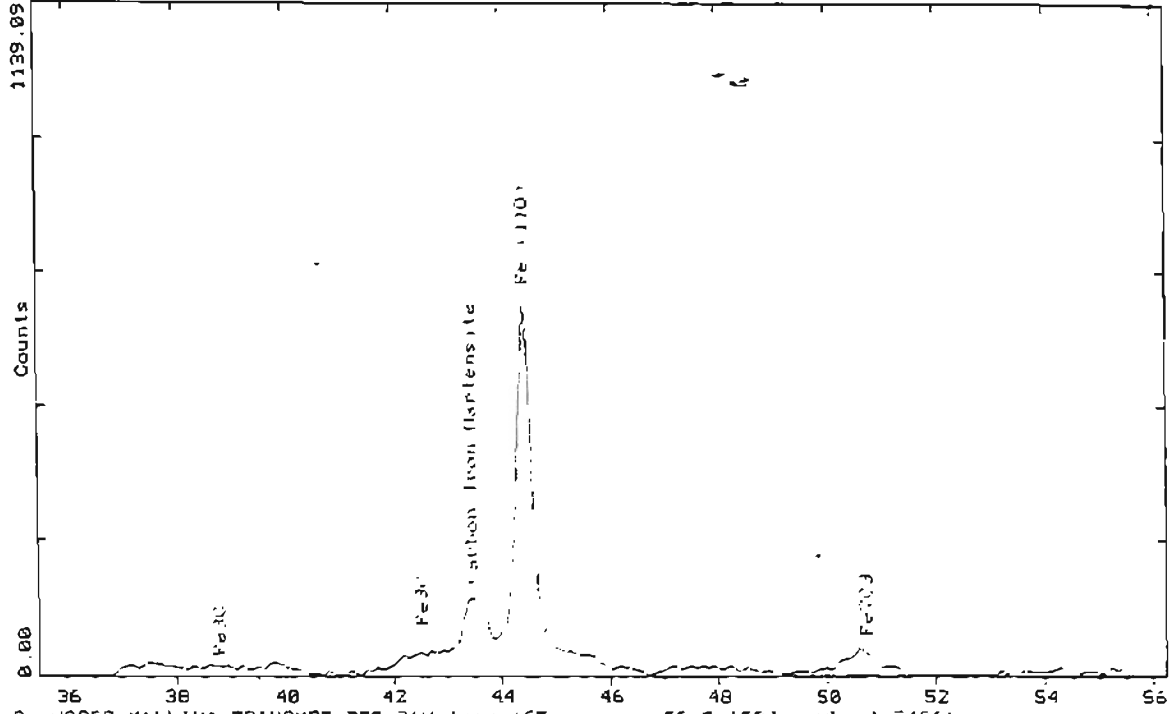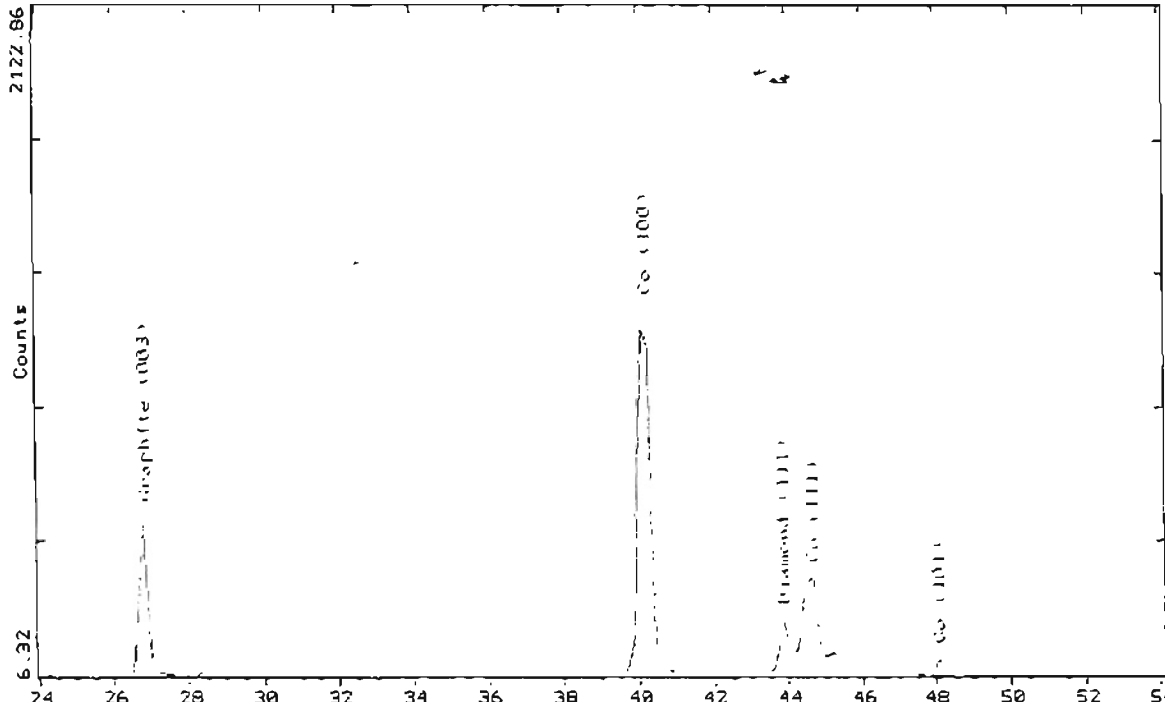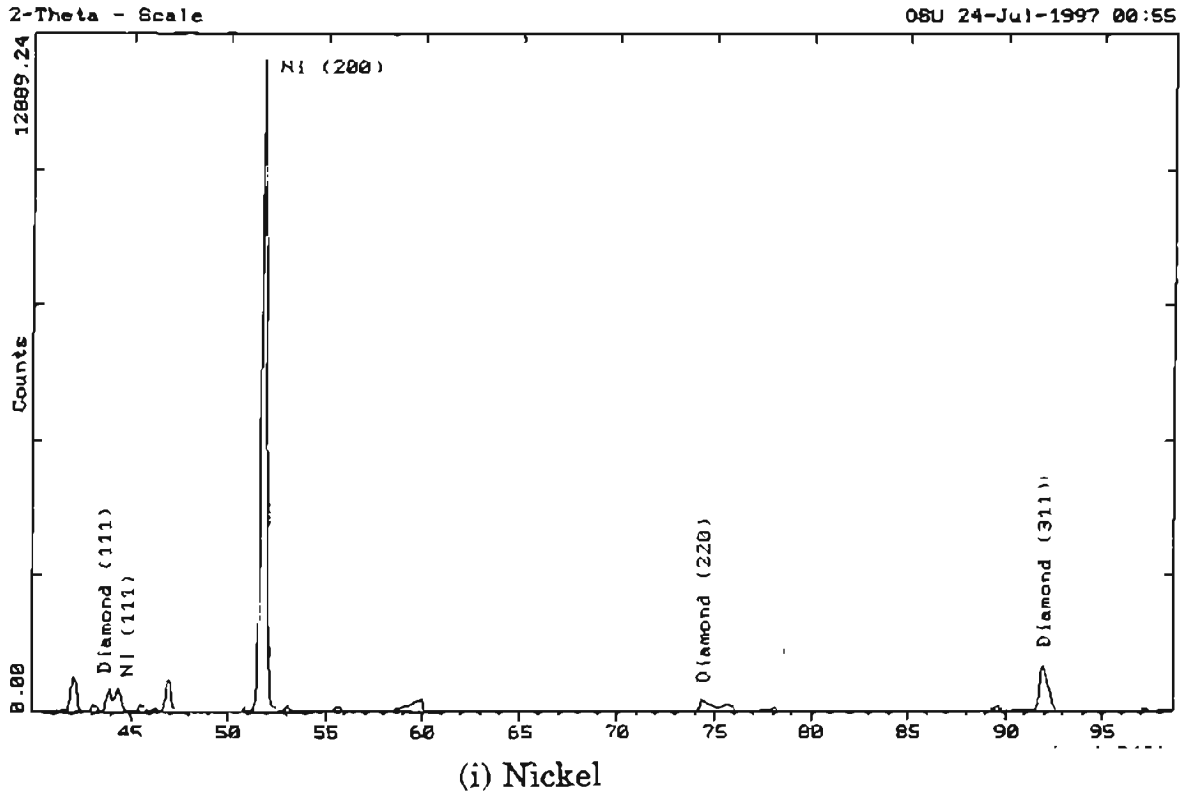
Figures 8.3.6 a) - i)   XRD Spectra on the Surface of Different Substrate Materials, Namely, Ti, V, Nb, Ta, Mo, W, Fe, Co, and Ni, Respectively after Deposition for 8 hours

8.4   Discussion

The experimental results indicate that the mechanism of diamond nucleation and growth varies across a period. Good quality diamond films were obtained on elements such as Ti, Ta, Mo and W. These elements form stable carbides. Diamond nucleation seems to proceed in a different manner in the case of Co and Ni, which do not form stable carbides. Diamond nucleation was very sparse on Cr which forms several complex carbides and no nucleation was observed on Cu which does not form any

carbide. Also the amount of sp^2 bonded carbon varied across the period. All these results seem to relate to the 3d shell structure and the availability of the 3d electrons. The stability of the carbides decreases as the 3d shell gets filled up gradually across the period. Section 8.4.1 discusses the properties of transition metal carbides. The nature of bonding of transition metal carbides differs across the period. Bonding in carbides of the first half of the transition series and the mechanism of diamond formation for these elements is discussed in section 8.4.2. Sections 8.4.3 and 8.4.4 discuss the carbides of group VIII elements and the mechanism of diamond formation for these elements.

8.4.1 Properties of Carbides

Table 8.4.1.1 gives some of the properties of the carbides of the transition metals (Kosolapova 1971). The transition elements are intermediate between the Group I and II elements (Alkali and Alkaline earth metals) and the inner transition elements (f block elements). At the beginning of each series, the ns and (n-1) d orbitals are of similar energy. Sc, Yt and La have $(n-1)d^1$ and ns^2 configuration. All the three electrons are easily lost and hence a group valency of 3 is observed. However, in proceeding across each series, the (n-1) d orbitals fall in energy compared to the ns orbitals. Thus for Zn, Cd, and Hg the (n-1) electrons are embedded in the inert electron core and hence do not contribute to the chemistry of these elements. For the remaining transition elements, both ns and (n-1) d electrons may be involved to varying extents in the bond formation. The participation of the d electrons leads to the transitional characteristics and produces both vertical and horizontal similarities with respect to the

periodic table. A similar trend was noticed in the present experiments. The morphological features and μ-Raman characterization of the elements in the same group showed similar pattern. The morphology of the diamond deposited on the elements belonging to the same group ranged from well defined cubic to cubo-octahedral. The intensity of the diamond peak increased, while the FWHM of the diamond peak decreased from top to bottom in a group.

Table 8.4.1.1   Properties of some Transition Metal Carbides
(Kosolapova, 1971)

Carbide	M.P °C	Density g/cc	Crystal structure	Lattice constant Å	Δf* kJ/(deg . mole)	α** 10⁻⁶/°C	K*** W/m °C	Temp stability °C
Cr_3C_2	895	6.7	Ortho-rhombic	a : 2.82 b : 5.53 c : 11.47	88.83	9.95	------	1895
Mo_2C	2687	8.9	HCP·	a : 2.994 c : 4.722	11.73	7.8	6.7	------
NbC	3760	7.85	FCC (NaCl)	a : 4.461	136.66	6.5	14.2	3760
TaC	3877	14.53	FCC (NaCl)	4.42	159.52	8.29	22.2	3400
TiC	3257	4.938	FCC (NaCl)	4.3316	236.8	8.31	11	3140
V C	2827	5.81	FCC (NaCl)	4.165	-----	7.2	24.7	2650 ± 35
WC	2870	15.8	HCP Cubic	a : 2.897 c : 2.27 a : 2.90	37.60	5.2	29	2600
W_2C	2857	17.3	HCP	a : 2.98 c : 4.71 c/a : 1.38	48.98	1.2	29	2750

*Δf = Change in free energy of formation from elements
**α = Coeffecient of thermal expansion
***K = Thermal Conductivity

232

Also the amount of sp² bonding as indicated by the broad band centered around 1550 cm⁻¹ decreases across the period for the elements belonging to Groups IV-VI.

8.4.2. Nature of Bonding in Carbides of Group IV-VI

The transition metals have incomplete d orbitals and as such have a tendency to receive electrons with relative ease (Goldschmidt, 1967). Small energy differences between the s, p, and d orbitals in transition metals make hybridization possible with relative ease. Basically, the electron supply from (and possibly, exchange with) the carbon atom can enhance this hybridization and facilitate the metal-carbon bond. However, this process does not advance to the ionization of carbon atom; consequently the essence of metallic bonding is maintained, i.e. the interstitial atoms remain substantially in the atomic state. Thus, the molecular volume (12.94 Å³) of WC can be divided into two individual atomic volumes of W(9.53 Å³) and carbon in diamond(3.37Å³).

Ramaswamy (1964) investigated the nature of bonding in carbides and demonstrated that Group IV elements form carbides of the form MeC with a FCC cubic NaCl type lattice. The interstitial phases are formed in accordance with Hägg's rule (rm/rx < 0.59, where rm and rx are the atomic radii of the metal and carbon respectively). In the case of carbides of the form M₂X (where M = Mo, W) for the structure is a hexagonal, densely packed arrangement of cores of the metallic atoms. Thus, in all these compounds there is a linear coordination of the metallic atoms around the carbon and of carbon around the metallic atoms. As pointed out above, one can isolate in the crystals, the compounds M₂X or MX₂ with six direct

bonds M-X having σ nature. The M-X bonding is assumed to be predominately through sp orbitals which may have hybrid nature while the M-M bonding consists of electrons in the sp^3d^2 or the sd^5 state.

Thus, it appears reasonable to assume a two-step basic process in the formation of transition metal carbides. The M-M bond attempts to stabilize the d^5 configuration, while the M-C bond attempts to stabilize the sp^3 configuration of carbon atom. In the case of carbides of Groups III and IV, due to the low localization potentials at the cores of the valence electrons, metals transfer a larger portion of their valence electrons to the non localized state. This leads to the stabilization of the sp^3 configuration of the carbon atoms and a strong electron-electron interaction. Thus, a direct σ bond is formed and pyramidal symmetry of the sp^3 bonding in diamond is preserved. The stabilization of sp^3 bonded carbon on Ni-Al alloy as demonstrated by Narayan et al. (1996) lends support to this hypothesis.

The average values of the chemisorption energies of various hydrocarbon gases on transition metals follow a common pattern (Hayward et al., 1964). The chemisorption energy values were found to decrease from left to right across the periodic table. Ti, V, Nb, Ta, W, and Mo are found to be active metals for chemisorption of CH_4 and C_2H_4 while Fe, Co, and Ni are inactive. Chemisorption involves covalent bonding with the partly filled d-band or with unpaired electrons in atomic d-orbitals (Hayward et al. 1964). Thus Group IV-VI transition metals (Ti, V, Nb, Ta, Mo, W) of the second and third series, have the required amount of covalency together with the ease of removal of d electrons for forming bonds with carbon and hydrogen. These are therefore more suited as substrates for diamond coatings by gas - solid reactions. The presence of carbides as detected by

XRD, in the case of Ti, Ta, W, Nb, V and Mo validates the assumption [Figure 8.3.6 (a)-(f)]. Also the Raman spectra of these elements [Figure 8.3.5 (d)-(i)] indicates the presence of both diamond and diamond-like carbon on the substrate. The tendency for sp^2 bonding as indicated by the amount of non-diamond carbon increases across a period for these elements in Groups IV-VI. This is because the 3d shell is gradually filled as we go across the period. Though the amount of diamond-like carbon deposited on transition-metal substrates depends on deposition conditions, the basic mechanism does not change (Chen et al. 1993). Therefore, chemisorption of carbon from the C_xH_y appears to be a main reason for the deposition of diamond. Etching of non-diamond graphite and replacement of the chain hydrogen atoms by nascent carbon are the other processes which have to simultaneously take place for the successful growth of the diamond film. The formation of diamond films due to solid-gas interactions can be summarized as follows:

- Reaction of nascent hydrogen leading to oxygen removal from the surface of the substrate.

- Approach of the C_xH_y radicals, and its reorientation with hydrogen atom of the chain towards the hot substrate. This is most likely the case for hydrogen reacts with metal surface more readily than carbon.

- Chemisorption of the hydrogen from the C_xH_y chain.

- Reaction of nascent hydrogen with non-diamond carbon/chain hydrogen and their removal. At this stage carbon atoms progressively replace hydrogen atoms from the chain leading to the formation of diamond lattice.

8.4.3 Nature of Bonding in Carbides of Group VIII

The SEM micrographs [Figures 8.3.3(c) and 8.3.4(b)] showing the nucleation of diamond in Co and Ni indicated fine, isolated diamond crystallites after prolonged incubation. The nucleation is patchy and isolated suggesting precipitation from the molten liquid. That diamond nucleation takes place after prolonged melting of the substrate lends credence to this hypothesis. With increase in deposition time, the diamonds are grown as isolated crystals, with a continuous film in some regions. However, they are still impure as indicated by the intensity of the peaks. Another factor is that both Co and Ni do not form stable carbides. The 3d orbitals of substrate surface atoms cannot be deactivated and the substrate surface partially remains fresh and continues to be an effective catalyst for the formation of graphite. However, as pointed earlier, the graphite catalyzing effect reduces as the 3d shell is gradually filled up. $Fe(3d^6)$ was found to promote the formation of graphite rapidly and no diamond growth was observed on Fe. Though Co $(3d^7)$ also promoted the formation of graphite, growth of diamond was observed on Co. It should be noted that this diamond was formed on the graphite layer. Walter et al. (1993), proposed a model for the nucleation of diamond on graphite, according to which diamond nuclei can form through a graphitic precursor, by the initial condensation of graphite and subsequent hydrogenation of the $\{1\bar{1}00\}$ prismatic planes along the edges of the graphite particles.

Angus et al. (1993) proposed a mechanism of nucleation of diamond from the gas phase through a graphitic intermediate. Since the corrugated hexagonal rings in the diamond (111) plane have the same spatial

orientation as the flat hexagonal rings in the graphite (0001) plane, by energy minimization calculations they determined that a low-energy interface was formed when three (111) diamond planes are joined to two (0001) graphitic planes. The model reactions proposed here involve the sequential conversion of monatomic gas-phase carbon species to aromatic sp^2 bonded species , to saturated sp^3 bonded species by reaction with atomic hydrogen. Also, by the application of empirical rules, it was shown the system remains trapped as graphite in the absence of hydrogen. In the presence of hydrogen, the system can further reduce its energy by further condensing from sp^2, trigonally coordinated nuclei to the sp^3, tetrahedrally coordinated nuclei.

Ni ($3d^8$) was found to be less reactive and the graphite catalyzing effect was weaker. The mechanism of diamond nucleation on Ni appears to be different. Cu ($3d^{10}$) with the d-shell completely filled was inert to both graphite catalyzation as well as diamond nucleation. However, Chen et al. (1993) reported deposition of diamond on Cu without the formation of graphite. The lattice constants of FCC Co (3.554 Å), Ni (3.517 Å), and Cu (3.61 Å) are very close to that diamond (3.567Å). The different behavior of these elements during CVD diamond deposition as seen in the present experiments may be presumably related to the activity of the 3d electrons.

The transition metals reach their maximum stability in the d^5 configuration (i.e. for group V elements (Cr, Mo and W) after which the successive groups of elements have excess electrons than required for bonding. According to Pauling, about half the d orbitals are involved in bond formation (2.56 of the total of 5), through hybridization with the 4s and 4p orbitals (Pauling, 1949). The number of covalent bonds resonating

among the available interatomic positions increases from one to nearly six in the sequence K, Ca, Sc, Ti, V, Cr. The number remains nearly constant from Cr to Ni, and begins to decrease with Cu. The remaining 2.44 (5-2.56 = 2.44) orbitals, with very small interatomic overlapping, are occupied by non-bonding electrons which are mainly responsible for the ferromagnetic and paramagnetic properties of the metals. Pauling assumed that Cr utilized 5.78 hybrid (spd) electrons in bonding. Six electrons can be obtained from the 3d and 4s orbitals, leaving a remainder of 0.22 electrons (6.00-5.78). These add to the 3d non-bonding orbitals. Conversely, there are 4.88 (2 x 2.44) electron holes in d shell, or 4.66 (4.88-0.22) net electron holes for Cr. Similarly Pauling considered that the number of spd bonding electrons for Ni, Co, Fe, and Mn to be 5.78. This would cause an increase in non-bonding electrons to 1.22 for Mn, 2.22 for Fe, 3.22 for Co, and 4.22 for Ni. The corresponding values for net holes are 3.66, 2.66, 1.66, and 0.66, respectively. However, for Ni and Co, the electron holes are matched by the available unpaired electrons decreasing their effective number. For Cr, Mn, and Fe all the non-bonding electrons are unpaired.

The melting and boiling points, cohesive strength, and magnetic moments at absolute zero can therefore be related to the unpaired (unmatched) non-bonding electrons and hence would be larger for Fe, followed by Co and least for Ni, which is observed in practice. An interesting aspect is that the decreased number of non-bonding electrons seems to affect the stability of the interstitial compounds of these metals.

Solubility of carbon is maximum for Mn and progressively decreases in the series Mn, Fe, Co, Ni, Cu, and Zn. The stability of the carbide formed also decreases in the same order, i.e. Mn_3C, Fe_3C, Co_3C, and Ni_3C. If it

can be assumed that the unpaired non-bonding electrons are in some way contributing to the M-C bonds in interstitial carbides, then the observed stabilities of carbides can be explained. The C-C bond strength, on the other hand, progressively increases, making graphite more stable than carbide. A theoretical study (Yang et al. 1992) on the effects of CH_3 absorption on Ni (111) also concluded that interstitial H assists in bonding strongly tetrahedral CH_3, while interstitial carbon may facilitate a planar graphite structure.

Carbides of the transition metals mainly form interstitial phases or phases similar to them with isolated carbon atoms and with a structural chain of carbon atoms. Interstitial phases are formed when the radius ratio of carbon to that of metal does not exceed 0.59 (Hagg's rule). The covalent radius of carbon is 0.77 Å and the atomic radius is 0.91 Å, while the C^{4+} ionic radius is 0.15 Å and the C^{4-} ionic radius is 2.6 Å. While applying Hagg's rule, the covalent radius of carbon and the metallic radius of the metal have usually been employed for determining the radius ratio (Earnshaw, 1973). There is an apparent inconsistency for the choice of covalent radius for carbon. Choice of a covalent radius implies the formation of covalent WC with 85% covalency on the surface. The strong covalent bonding would prevent further diffusion. On the other hand, the choice of an ionic radius for carbon can make its incorporation into interstitial voids much easier, but it violates the electronegativity concept (Samansov, 1964).

Therefore, the mechanism of incorporation of carbon in the latter half of the transition series is not clear. The difficulty arises mainly because of the

size of interstitial voids which are smaller than the atomic or covalent radius of carbon(Goldschmidt, 1967).

8.4.4 Interaction of Carbon and Group VIII Metals

Assuming that Pauling's hypothesis regarding the electronic structure of transition metals holds, the following model is proposed to account for diamond growth in the case of Ni. Consider the case of Group VIII transition metals, Fe, Co and Ni. When atoms form metallic crystals, the net number of non-bonding electrons left in the atomic 'd' orbitals are 2.66, 1.66, and 0.66 respectively. The remaining non-bonding electrons will be paired because of opposite spins and are not expected to be available for the formation of new bonds. Since carbon is found to occupy octahedral voids in transition metal carbides, the net non-bonding electrons in the six neighboring metal atoms are assumed to participate in the metal - carbon bonding.

Carbon has s^2p^2 outer shell in its ground state and for achieving stability in the condensed state, it requires four more electrons. They can be obtained by sharing of electrons with other atoms and forming covalent bonds in the process. Ni and Co form metastable carbides with a structure similar to that of Fe_3C where each carbon is surrounded by six iron atoms. The six metal atoms can contribute half of their net non-bonding electrons towards the bond formation with carbon. Thus the interstitial carbon can form bonds with 7.98 net non-bonding electrons in Fe_3C, 4.98 electrons in Co_3C, and only 1.98 electrons in Ni_3C. This suggests a weaker bond between Ni and carbon.

The outer electronic configuration for Ni is $3d^8 4s^2$, as compared to $5d^4$ $6s^2$ for W. Thus, the d shell of Ni has less tendency to attract electrons from a carbon atom than W. Therefore, the scope for strengthening the C-C bond and a corresponding weakening of the M-C bond increases in Group VIII metallic elements, in general, and Ni in particular. The metal-carbon system can no longer be classified under interstitial carbides. Rather, it is in reality a border between interstitial carbides and carbon solid solutions. The solubility of carbon in Ni increases with increase in temperature and at 1318 °C, Ni forms an eutectic with 9 atomic % C (the corresponding parameters for Co-C are 12 atomic % C, 1320 °C and for Fe-C are 17.3 atomic % C, 1130 °C). Even in the melt, the solubility of carbon increases with increase in temperature and in the case of Fe-C system it is 25 atomic % C in the melt as Fe_3C and reaches a maximum of 33 atomic % at 2200 °C as Fe_2C. The melt thus contains solid iron carbide groups which move freely. A similar situation is expected in Co-C and Ni-C systems (Singleton et al., 1989). As already mentioned, the metal-carbon bonds in these systems are progressively weaker and hence there is scope for equilibrium of liquid metal with either Co_3C, Ni_3C, or graphite itself.

Roy et al. (1993) reported a new process for the synthesis of diamond termed as low-pressure solid-state source process (LPSSS). By this process, they reported conversion of any solid carbon into diamond. This process uses a di-phasic mixture of any form of carbon (other than diamond) with a selected set of second phases. The semiconductor phases used were isostructural with diamond (diamond, cubic BN, Si, SiC). Cu, Mo, Ni, and Pt were selected among metals. Both the phases were thoroughly mixed by sol-gel and ultrasonic techniques and the resulting gel was shaped into various morphologies. The shaped materials were then placed in a

chamber in a pure H_2 plasma at temperatures of 500-1000 $^{\circ}$C. These diphasic mixtures were found to convert partly or completely to diamond depending on the thickness. Ni was found to give excellent results Later Roy et al. (1995) demonstrated the precipitation of diamond from $Me_xC_yH_z$ (Me = Ni, Cu, Au, Ag) alloys in a hydrogen, microwave-stimulated plasma below 1 atm. In the temperature range of 800-950 $^{\circ}$C, they observed the precipitation of cubo-octahedral diamond crystals from the liquid.

Yang et al. (1994) reported growth of oriented diamond films on single crystal Ni substrates seeded with non-diamond carbon and annealed at high temperature in atomic hydrogen. They proposed a mechanism involving the saturation of the Ni surface with gaseous carbon at 1100 $^{\circ}$C They suggested that in the presence of atomic hydrogen, reactions between Ni, carbon and atomic hydrogen occur, leading to the formation of molten, terenary eutectic compounds of Ni-C-H. During subsequent cooling to a substrate temperature of 900-950 $^{\circ}$C, diamond nucleation occurs on the solidified molten eutectic compounds.

Badzian et al. (1996) proposed that ($CH_4 + H_2$) plasma results in the higher concentration of C in Ni, which subsequently leads to the formation of NiC_x carbides. They proposed the formation of nickel carbide as a non-stoichiometric interstitial solid - solution. They also suggested that nickel carbide has a NaCl type structure, where Ni atoms take the positions of Na atoms and only some of the positions of Cl atoms are occupied by C atoms. Atomic hydrogen again plays an important role in the formation of a terenary solid phase $Ni_xC_yH_z$. They suggested the nucleation of diamond on this ternary phase.

Zhao et al. (1997), reported the nucleation and growth of diamond crystals in a hydrothermal environment from a mixture of carbon, water and metal (usually pure Ni) near 800°C and 1.4 kbar. 95 wt% glassy carbon was mixed with 3 wt% powdered Ni and 2 wt% 0.25 μm diamond seeds and water (50-100 wt% of glassy carbon). They observed large bonded aggregates of individual particles of different morphologies after ~ 100 hrs. Formation of hydrothermal diamond was confirmed by XRD and Raman analysis. They proposed diamond precipitation from a $Me_xC_yH_z$ metallic liquid as a possible mechanism for the hydrothermal growth.

Thus, from the above theoretical considerations along with the relevant literature review (Angus et al., 1993; Narayan et al. 1996; Roy et al. 1993, 1995), the mechanism of formation of diamond in Nickel may be postulated as follows:

• An increase in temperature increases the carbon solubility in Ni both in the solid and in the liquid state. Solid solutions of carbon in Ni expand the Ni lattice by amounts which are related to the atomic fraction of the dissolved carbon.

• Ni has an FCC structure in which each Ni atom is surrounded by 12 nearest neighbors, six in plane and three atoms each above and below the plane. Removing the outer two electrons for the 's-p' hybridization as in pure metallic bond formation, there can be only 8 nearest neighbors around each Ni atom without violating Pauli's exclusion principle. Therefore, the 12 nearest neighbors in the Ni structure signify the involvement of 'd' orbitals in the bonding. Thus, the structures of Ni and other transition metals can be considered as a partly symmetric metallic bonding and partly directional covalent bonding as follows (Pauling, 1948).

NiA   ↑↓ ↑ ↑ • •   •   • • •   6 covalent and
                                      2 non-bonding
       3d   4s   4p   orbitals

NiB   ↑↓ ↑↓ • • •   •   • • ○   6 covalent and
                                      1 metallic
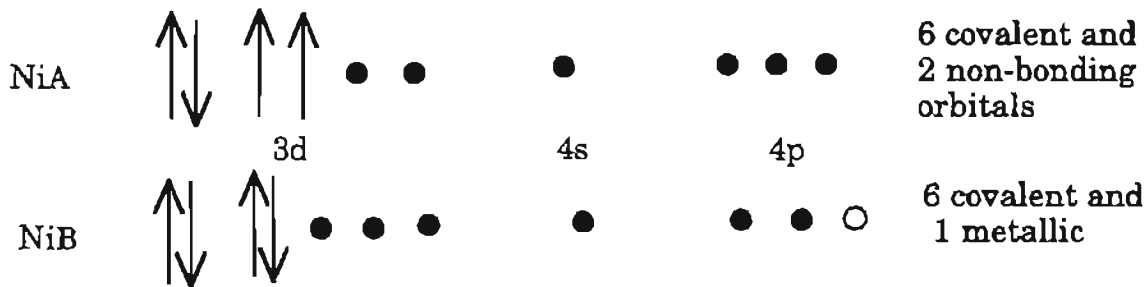
where, atomic electrons are indicated by spin vectors, bonding electrons by dots, and the metallic orbitals by open circles. Thus, the Ni_A is a covalent Ni, paramagnetic because of its two non-bonding orbitals, and Ni_B is a diamagnetic metal. The actual Ni structure represents a combination of these configurations.

• Group VIII metals in general and Ni in particular have fewer unpaired electrons as demonstrated by the magnetic moments. Hence the interstitial carbides exhibit weak M-C bonds. The systems Ni-C and Co-C resemble the Fe-C system in that the stable equilibrium involves the metal and graphite. However orthorhombic metastable carbides Ni_3C and Co_3C are also known to exist having the same crystal structure as cementite, Fe_3C. In this structure, each carbon atom has 6 metal neighbors located at the corners of a trigonal prism but may be distorted resulting in the variation of the Fe-C distances from 1.85 to 2.15 Å. The iron atoms are divided into two structural types, namely, those with 11 and 12 close neighbors, respectively, at distances varying between 2.49 and 2.68 Å, so that the coordination number is approximately the same as in the FCC structure. As per the model proposed here, since Ni has fewer unpaired non-bonding electrons, the Ni-C bonds will become much weaker and the interstitial C-C bonds would become stronger.

• An increase in the temperature progressively weakens the Ni-C bonds and is likely to increase the strength of the C-C bonds. Eventually at the melting point, Ni atoms farther from the interstitial carbon, typically at the corners of the square base of the trigonal prism are likely to form the Ni melt containing isolated Ni_xC_y groups, isolated carbon atoms, and carbon clusters. Supersaturation of the melt with carbon (approximately 11 atomic % C) would most likely occur in the Ni_xC_y region which can lead to the precipitation of diamond on the (100) FCC cubic face of the carbon-rich Ni. This is likely to set up a concentration gradient in the Ni_xC_y region, and carbon atoms diffuse to the growing diamond surface thereby providing continuous growth.

• It might be even possible that the carbon freed from Ni can form colloidal clusters which slowly rearrange into a diamond lattice and under the influence of surface forces, the phase transformation to graphite would be hindered as long as the crystallite size is below a critical value. Hydrogen or oxygen in the surrounding atmosphere may also hinder the formation of graphite as they remove the non-diamond carbon.

• Thus, the growth of diamond by this process is now similar to the growth of diamond by low-pressure CVD process (Angus et al., 1988). In fact both the processes may be visualized as condensation polymerization processes as follows:

$$M \qquad C \qquad \qquad C\ M$$
$$M\text{-}C^* + C\text{-}C^* \;=\; C\text{-}C\text{-}C^* \;+\; M$$
$$M \qquad C \qquad \qquad C\ M$$

$$M \qquad C\ M \qquad \quad C\ M\ M$$
$$M\text{-}C^* + C\text{-}C\text{-}C^* \;=\; C\text{-}C\text{-}C\text{-}C^* \;+\; M \quad \text{and so on.}$$
$$M \qquad C\ M \qquad \quad C\ M\ M$$
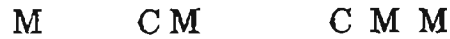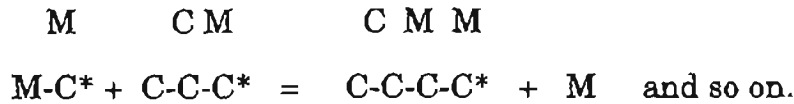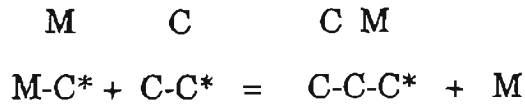
Since the M-C bonds are weaker, the metal atom can be removed and in its place another M_3C group can be added for the growth to proceed. This is similar to the growth of diamond by low-pressure CVD using methane as a carbon source, as advanced by Angus et al. (1993).

$$H \qquad C \qquad \qquad C\ H$$
$$H\text{-}C^* + C\text{-}C^* \;=\; C\text{-}C\text{-}C^* \;+\; H$$
$$H \qquad C \qquad \qquad C\ H$$

$$H \qquad C\ H \qquad \quad C\ H\ H$$
$$H\text{-}C^* + C\text{-}C\text{-}C^* \;=\; C\text{-}C\text{-}C\text{-}C^* \;+\; H \quad \text{and so on.}$$
$$H \qquad C\ H \qquad \quad C\ H\ H$$
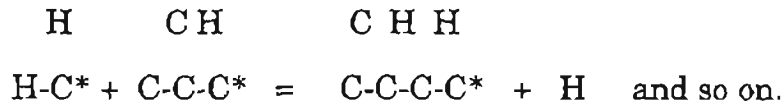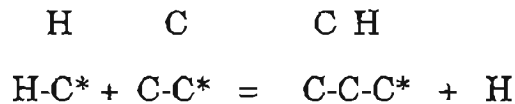
When a metal-carbon system is cooled in the solid state, carbon is likely to precipitate as metastable M_3C, which in turn decomposes to graphite. Diamond cannot be formed under these conditions as there is no mobility for the carbon carrier to cause bond bending.

The mechanism of diamond growth now seems to depend both on the precipitation from the liquid, transport of carbon and hydrogen from the

liquid and surrounding gas to the growth of diamond and for etching of non- diamond carbon, and metallic film surrounding diamond.

8.5   Evaluation of Adhesion

The diamond films deposited using various substrate treatments were tested for adhesion using a Rockwell hardness tester with a Brale indentor. Discrete loads of 15, 30, 45, 60, 100 and 150 Kgf were used. Atleast 3 indentations were made at each load level. Figures 8.5.1 (a) - (f) show the micrographs of the indentation imprints on various transition metal substrates. Figure 8.5.2 shows the plot of the lateral crack diameter Vs the indent load. The relative error in the measurement of the lateral crack diameter is ~ 10 %. To facilitate the measurement of the lateral crack diameters, the specimens were ultrasonically vibrated in acetone to remove the delaminated film. From the micrographs it can be observed that there is severe delamination and spalling of the diamond films on Ti, V, Mo. Diamond films on Nb, Ta and W appear to have adhered reasonably well.
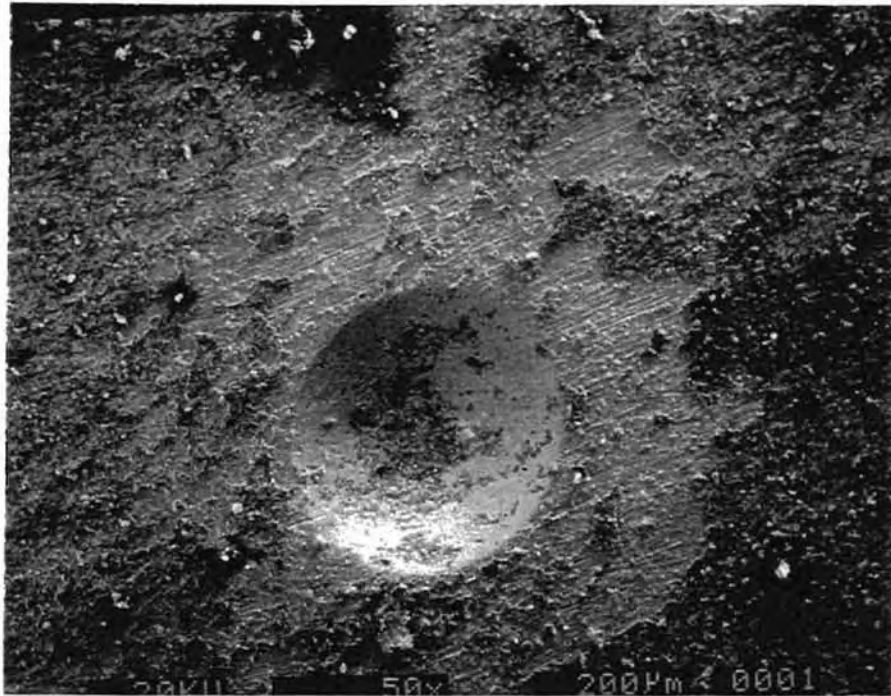
Figure   8.5.1 (a)   SEM Micrograph Showing Delamination of Diamond
Film on Ti Substrate (Load = 60 kgf)
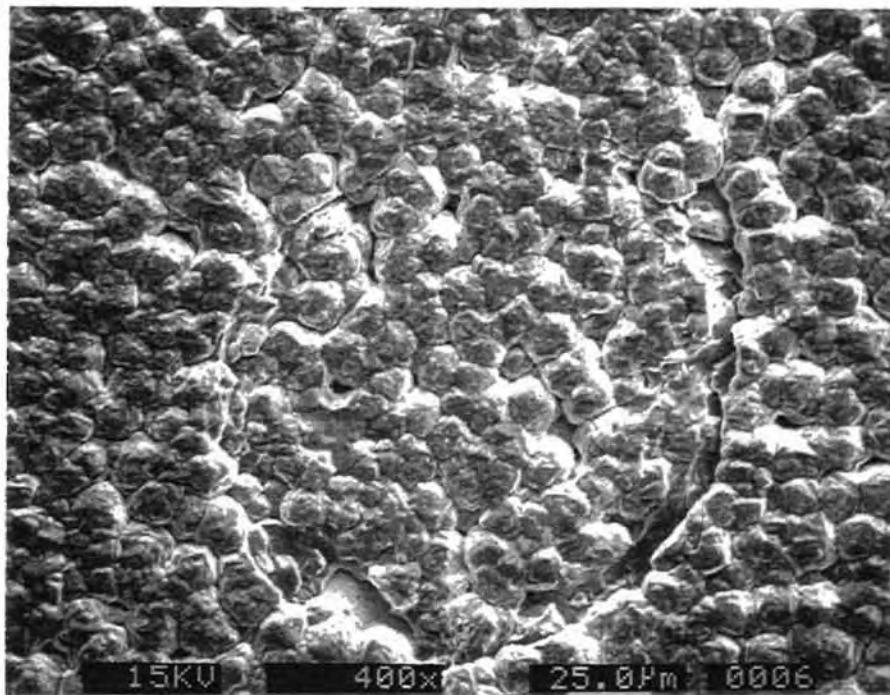
Figure   8.5.1 (b)   SEM Micrograph of Diamond Film on Ta Substrate
Showing an Indentation Imprint (Load = 60 kgf)

248
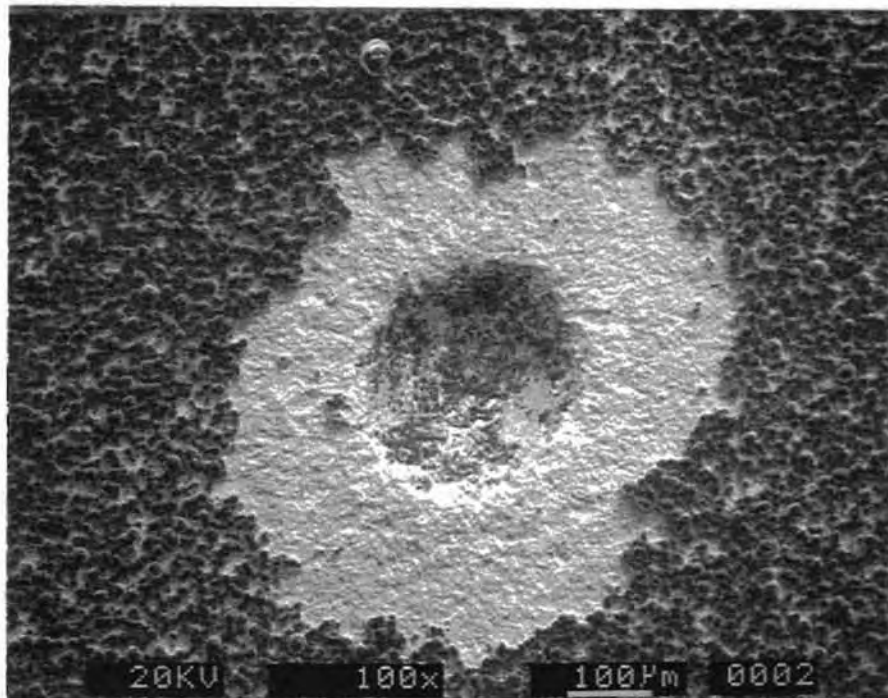
Figure 8.5.1 (c) SEM Micrograph Showing Delamination of Diamond Film on V substrate (Load = 45 kgf)
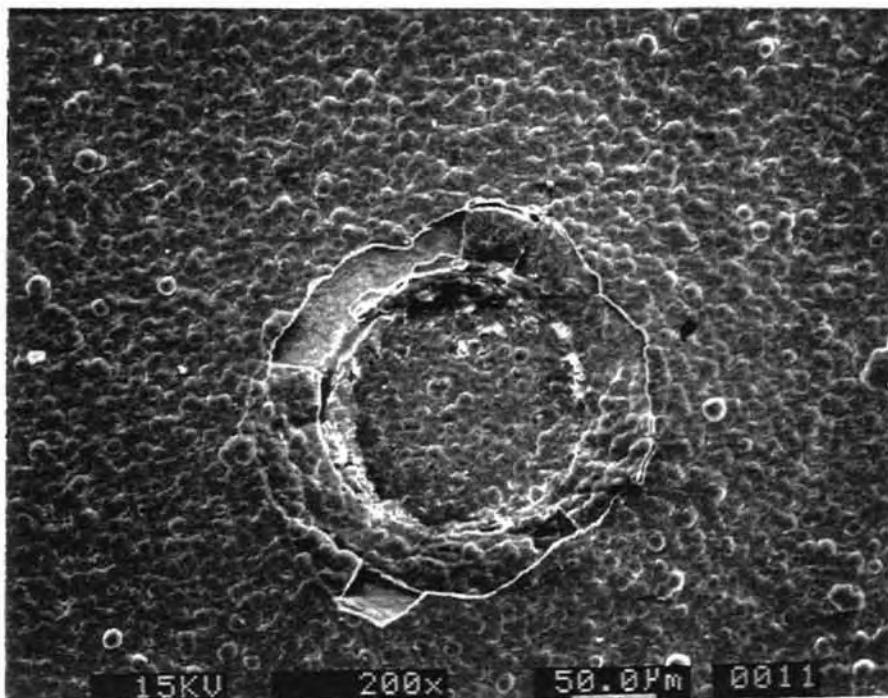
Figure 8.5.1 (d) SEM Micrograph of Diamond film on Nb substrate Showing an Indentation Imprint (Load -= 60 kgf)
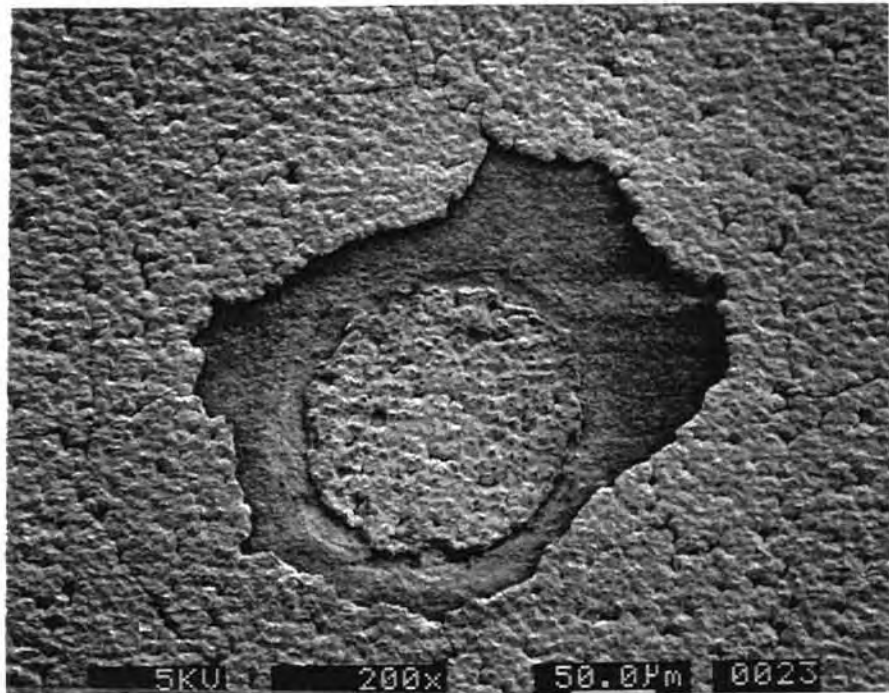
Figure   8.5.1 (e)   SEM Micrograph Showing the Delamination of the
Diamond Coating on Mo Substrate (Load = 45 kgf)
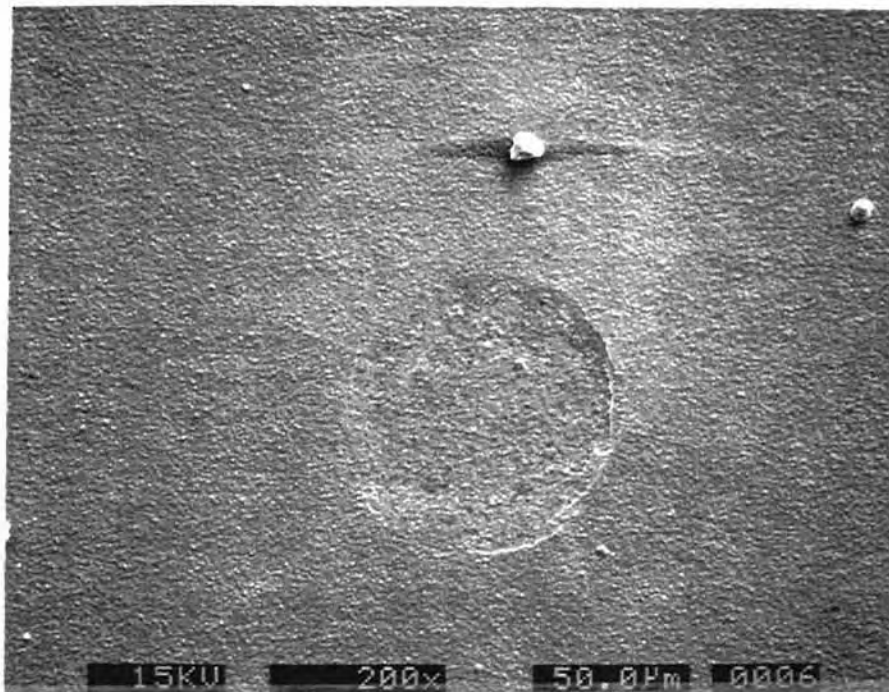
Figure   8.5.1 (f)   SEM Micrograph of Diamond Film on W substrate
Showing the Indentation Imprint (Load = 60 kgf)
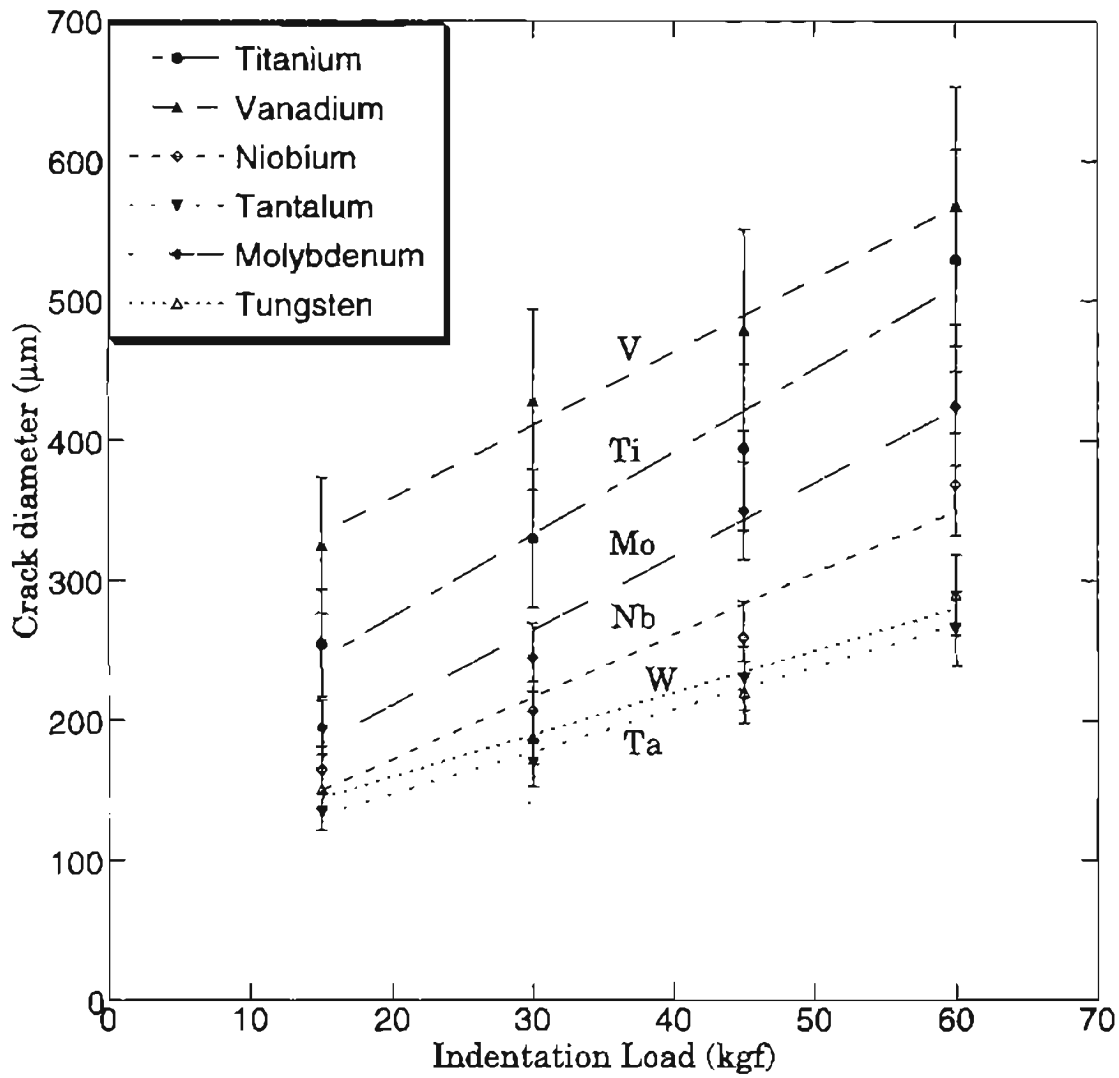
Figure   8.5.2   Crack Diameter Vs Indentation Load Plot for Diamond
Films, Deposited on Various Transition Metals

In contrast to the indentation imprints on cemented carbides and Si_3N_4 tools, no radial cracks were observed in the case of transition elements. Also, the lateral crack diameter values are higher in case of transition metal elements. The thickness of the diamond coatings on these transition metals was ~ 8-12 μm, while those on cemented WC and Si_3N_4 tools are ~18-22 μm. Thus it can be seen that the diameter of the lateral crack is smaller for the thicker diamond coating. This is apparently contrary to the "spring model", where increased elastic energy stored in the thicker layer would cause earlier delamination (Drory, et al., 1996). On the other hand this observation is in agreement with Perry's analysis (1985) of the indentation imprints. It reflects the fact that the diamond film hardness is significantly higher than the substrate hardness. An increase of the diamond film thickness would reduce the plastic deformation volume in the cemented WC.

From the slopes of the lateral crack diameter Vs indent plot, it can be seen that Ti exhibits poorest adhesion, followed by V, Nb, and Mo. Among the transition metals W, Nb and Ta seem to show reasonably good adhesion. It has been already pointed out that the residual stresses play a major role in determining the adhesion of the coatings. The residual stress is the sum of thermal stress and the intrinsic stress. In the case of Si_3N_4, because of the compatibility of the thermal expansion coefficients between Si_3N_4 and diamond, thermal stresses were found to be minimal. It has been shown that by proper choice of the deposition conditions intrinsic stresses can be minimized and adhesion of the diamond coatings can be improved. However one of the problems experienced with Si_3N_4 is the lack of toughness. In the case of cemented WC tools, Co was found to have a

detrimental effect and it was possible to obtain good adhesion of diamond coatings on cemented carbides by proper surface pretreatment. Table 8.3.2 shows the stress measurements of diamond films on various substrates. It can be seen from that there is a large mismatch in the thermal expansion coefficients between most of the transition metals and diamond. Residual stresses obtained from the Raman measurements could be correlated to the thermal stresses. Diamond coatings on W was found to have minimum residual stress followed by Ta and Nb. The crack resistance values of the diamond films on the transition metals are ~ 169 (Ti), 192 (V), 188 (Mo), 225 (Nb), 332 (Ta) and 334 (W), kgf mm^{-1} respectively. Thus the diamond films on elements with minimum residual stresses were found to show better crack resistance (or adhesion strength)..

CHAPTER 9

CONCLUSIONS

A systematic study was conducted to assess the effect of various process variables and substrate materials on the quality and adhesion of diamond coatings on Si_3N_4 and cemented tungsten carbide tools. Indentation tests with Brale indentors were used to evaluate the adhesion of the coatings to the various substrate materials. Adhesion strength of the diamond coatings was also evaluated by wear tests. μ-Raman spectroscopy, SEM, and XRD were employed to characterize the diamond coatings deposited on various tool materials. Fractional factorial experimental design has enabled an assessment of the influences of process variables, on film quality and adhesion. It has provided an insight into the relationship between various controlling factors, such as non-diamond inclusions during the deposition, phase purity of the deposited diamond coatings, residual stresses, and substrate treatments and adhesion of resultant diamond coatings. It also provided a better understanding on the optimization of the process parameters in producing diamond coatings on cutting tools with good quality and adherence. Diamond growth studies on transition metals have shown the importance of the chemical nature of the substrate in influencing diamond formation. Specific conclusions that may be drawn from this research are as follows:

1. Effect of process parameters

• Fractional factorial design experiments on Si_3N_4 substrates enabled identification of temperature and methane concentration as the two important process variables affecting the diamond nucleation

• Grain size and morphology of the diamond coatings were found to be influenced primarily by the methane concentration in the hydrogen/methane gas mixture. Within deposition temperature range used in this research, temperature did not appear to have a significant influence on the grain size and morphology. However, it had notable effects on the quality of diamond coatings

• The phase purity of the diamond coatings was found to decrease with the increase in methane content at all deposition temperatures. However, the phase purity was found to increase with deposition temperatures

2. Diamond coatings on Si_3N_4 substrates

• Stresses in the diamond coatings deposited on Si_3N_4 were found to be sensitive to the deposition conditions. A change in the stress state from tensile to compressive was observed at ~ 1.5% CH_4. Methane concentration in the range of 0.5-1% is found to yield minimum residual stresses

• A pressure of 20 Torr, microwave power of 1000 W, CH_4 concentration of 0.5-1% and substrate temperature in the range of 850-900 °C were identified as deposition conditions for producing good quality diamond coatings on Si_3N_4 substrates

255

- The adhesion strength of the diamond coatings on Si_3N_4 substrates as measured by the Rockwell indentation method was found to yield satisfactory results. The diamond coatings on the substrates investigated did not delaminate upto a load of ~ 60 kgf

- Adhesion of the diamond coatings deposited under optimal conditions was also determined by polishing the diamond film against the diamond paste. Removal of diamond film after several hours of polishing and smooth wear surface indicated good adhesion. In the case of adherent diamond coatings, the removal of the diamond coating was due to erosion and abrasion by the polishing process

- Diamond coatings deposited at higher methane concentrations (~ 1.5 - 2 %) showed poor adhesion. Wear tests with diamond paste showed the removal of diamond from several regions even after a short duration of polishing (< 30 minutes). In the case of poor adhesion between the diamond coatings and the substrate the removal process was found to be due to the cleavage of diamond

3. Role of cobalt on the adhesion of diamond coatings on cemented WC substrates

    - Presence of the surface cobalt has been confirmed by XRD

    - At low deposition temperatures, cobalt is found to cover the surface and prolong the incubation period for diamond nucleation

- At high deposition temperatures, cobalt was found to diffuse from the grain boundaries to the surface. Consequently the quality and adhesion of the diamond coatings was found to deteriorate

4. Diamond coatings on cemented WC substrates

- Treatment by Murakami agent was found to prevent the diffusion of cobalt to the bulk. This was established by the XRD spectra of the diamond coatings on WC-Co substrates treated with Murakami agent at glancing angle which did not indicate the presence of cobalt at the interface

- Murakami treatment was found to be the most effective pretreatment in terms of improving both quality and adhesion of diamond coatings on WC-Co substrates

- A combination of chemical and mechanical treatment have been shown to improve the adhesion strength of the diamond coatings deposited on WC-Co substrates significantly. The isotropic surface roughness created by the Murakami treatment, together with the improved nucleation density by ultrasonic microscratching facilitated a strong mechanical anchoring of the diamond coating thereby improving adhesion

5. Growth of diamond on transition metals

- The chemical nature of the transition metals was found to play an important role in the formation of diamond on transition elements

- Similar morphologies were observed for diamond coatings grown on the substrates belonging to the same group. Based on the μ-Raman measurements, it was found that good quality diamond coatings were grown on Ti, Ta, Nb and W

- Cr with a half-filled d shell produced a very sparse diamond nucleation while Cu with the completely filled 3d shell did not nucleate any diamond

- The stability of the carbides decreased as the 3d shell progressively gets filled across a period. Diamond nucleation was rapid on elements such as Ti, Ta, Mo, and W which form stable carbides

- Nucleation was very sparse on Cr which forms several complex carbides. Elements such as Fe and Co which do not form stable carbides seem to promote graphite formation. No nucleation of diamond/graphite was observed on Cu which does not form any carbide

- The mechanism of diamond growth varies along the period. Ti, V, Nb, Ta , Mo and W with the ease of removal of d electrons tend to favor diamond deposition by gas-solid phase reactions. Ni, belonging to the second half, tends to form diamond by precipitation from the molten liquid

- Residual stresses calculated from Raman spectroscopy correlated reasonably well with the calculated thermal stresses of the transition metals or transition metal carbides.

CHAPTER 10

FUTURE WORK

- While, evaluation of adhesion by indentation tests were convenient, practical and semi-quantitative a model for the mechanics of the test should be established. In particular, the understanding of the mechanical relationship between the lateral crack length and the film adhesion should be developed similar to fracture toughness studies.

- On a laboratory research scale, the diamond coatings on Si_3N_4 and cemented WC showed good adhesion. Machining tests need be conducted to evaluate the performance of these diamond coated tools in metal cutting applications

- Treatment by Murakami agent has prevented the diffusion of the cobalt from the bulk as suggested by the XRD. Formation of a layer of stable cobalt compound in the plasma atmosphere has been suggested as one of the reasons. XPS or SIMS analysis need to be performed to confirm the formation of such compounds

- Surface modification using a laser as a means of activating the surface and improving adhesion needs to be investigated

- Use of multi layers to reduce the thermal mismatch between diamond and various substrate materials should be explored

• Morphology of the diamond coatings on the cutting tools has thus far been studied on a microscopic scale. However, this has not been investigated macroscopically for metal cutting applications. This would be another area of interest for further investigation.

REFERENCES

Ager, J. W., and M. D. Drory, (1993), "Quantitative Measurement of Residual Biaxial Stress by Raman Spectroscopy in Diamond grown on a Ti Alloy by Chemical Vapor Deposition," Physical Review B, 48 (4), 2601-2606.

Alam, M., Peebles, D. E., and D. R. Tallant, (1997), "Diamond Deposition onto WC-6% Co Cutting Tool Material : Coating Structure and Interfacial Bond Strength," Thin Solid Films, 300, 164-170.

Angus, J. C., and C. C Hayman, (1988), "Low-Pressure, Metastable Growth of Diamond and "Diamond like" Phases," Science, 241, 913-920.

Angus, J. C., Argoitia, A., Roy, G, Li, Z., Sunkara, M., Wang, L., and Y.Wang, (1993), "Chemical Vapor Deposition of Diamond," Phil. Trans. R. Soc. London A, 342, 195-208.

Angus, J. C., Hoffman, R. W., and P. H. Schmidt, (1988), "Studies of Amorphous Hydrogenated Diamond-like Hydrocarbons and Crystalline Diamond," Science and Technology of New Diamond, 9-16.

Angus, J. C., Li, Z., Sunkara, M., Gat, R., Anderson, A. B., Mehandru, S. P., and M. W. Geis, (1991), "Nucleation and Growth Processes in Chemical Vapor Deposition of Diamonds," Proceedings Electrochem. Soc. Symp. Series, 91 (8), Pennington, New Jersey, 125-141.

Angus, J. C., Li, Z., Sunkara, M., Wang, Y., Lee, M., Segall, L., and B. Segall, (1993), "Nucleation and Growth in the Chemical Vapor Deposition of Diamond," Proceedings of the Second International Conference on the Applications of Diamond Films and Related Materials, Omiya, Saitama, Japan, 159-168.

Angus, J. C., Sunkara, M., Sahaida, S. R., and J. T. Glass, (1992), "Twinning and Faceting in the Early Stages of Diamond Growth by Chemical Vapor Deposition," J. Mater. Research, 7, 3001-3009.

Angus, J. C., Will, H. A., W.S. Stanko, (1968), "Growth of Diamond Seed Crystals by Vapor Deposition," Journal of Applied Physics, 39, 2915-2922.

Anthony, T. R., (1990), "Metastable Synthesis of Diamond," R. Freer (ed.), The Physics and Chemistry of Carbides; Nitrides and Borides, 133-158.

Anthony, T. R., (1991), "Methods of Diamond Making," Diamond and Diamond-Like Films and Coatings, NATO - ASI Ser B: Physics, 266, Plenum Press, New York, 555-577.

Ascarelli, P., Cappeli, E., Mattei, G., Pinzari, F., Fares, V., Veroli, C., and S. Martelli, (1996), "Relation among Growth Rate, Microstructure and the Physical Properties of Diamond Films," Diamond and Related Materials, 5, 308-311.

Ashfold, M. N. R., May, P. W., Rego, C. A., and N. M. Everitt, (1994), "Thin Film Diamond by Chemical Vapor Deposition Methods," Chemical Society Reviews, 23, 21-30.

Bachmann, P. K., and D. U. Wiechert, (1992), "Optical Characterization of Diamond," Diamond and Related Materials, 1, 422-433.

Bachmann, P. K., and H. Lydtin, (1991), "High Rate Versus Low Rate Diamond CVD Methods," Diamond and Diamond-Like Films and Coatings, NATO-ASI Ser B: Physics, 266, Plenum, New York, 829-853.

Bachmann, P. K., Bausen, H. D., Lade, H., Leers, D., Wiechert, D. U., Herres, N., Kohl, R., and P. Koidl, (1994), "Raman and X-ray Studies of Polycrystalline CVD Diamond Films," Diamond and Related Materials, 3, 1308-1314.

Bachmann, P. K., Leers, D., and H. Lydtin, (1991), "Towards a General Concept of Diamond Chemical Vapor Deposition," Diamond and Related Materials, 1, 1-12.

Badzain, A. R., (1988), "Defect Structure of Synthetic Diamond and Related Phases," Advances in X-Ray Analysis, 31, Plenum, New York, 113-128.

Badziag, P., Verwoerd, W. S., Ellis, W. P., and N. R. Greiner, (1990), "Nanometer-sized Diamonds are more Stable than Graphite," Nature, 343, 244-245.

Badzian, A. R., Badzian, T., Roy, R., Messier, R., and K. E. Spear, (1988), "Crystallization of Diamond Crystals and Films by Microwave Assisted CVD (Part II)," Mat. Research Bulletin., 23, 531-548.

Badzian, A., and T. Badzian, (1996), "Growth of Diamond and Nickel Carbide Crystals in the Ni-C-H System," Diamond and Related Materials, 5 93-101.

Bang, K, (1994a), "Experimental and Computational Investigation of the Thermal Effects on CVD Diamond Films by Oxy-Acetylene Combustion Method," Ph.D. Thesis, Oklahoma State University, Oklahoma.

Bang, K., Ghajar, A. J., and R. Komanduri, (1994b), "The Effect of Substrate Temperature on the Morphology and Quality of Diamond Films Produced by the Oxyacetylene Combustion Method," Thin Solid Films, 238, 172-183.

Barrat, S., Michel, H., and E. Bauer-Grosse, (1993), "A Microstructural and Morphological Study of Diamond Crytals and Films Elaborated by Microwave Plasma Assisted Chemical Vapor Deposition," Surface and Coatings Technology, 59, 330-337.

Beckmann, R., Sobisch, B., and W. Kulisch, (1995), "On the Gas-Phase Mechanisms in MWCVD and HFCVD Diamond Deposition," Diamond and Related Materials, 4, 256-260.

Belton, D. N., and S. J. Schmieg, (1990),"States of Surface of Carbon during Diamond Growth on Pt," Surf. Science, 233, 131-140.

Bent, H. A, (1965), "Second Law of thermodynamics," Oxford University Press, New York.

Bichler, R., Haubner, R., and B. Lux, (1987), "Low Pressure Diamond Deposition from a Methane-Hydrogen Gas Mixture," Proceedings of the 6th European CVD Conference, Jerusalem, Israel, 413-422.

Blackey, G. G., (1977), "The Diamond," BAS Printers Limited, London.

Bovenkerk, H. P., Bundy, F. P., Hall, H. T., Strong, H. M., and R. H. Wentorf, (1959), "Preparation of Diamond," Nature, 184, 1094.

Bragg, W. H., and W. L. Bragg, (1913), Proc. R. Soc., A89, 277-280.

Bridgman, P. W., (1947) J. Chem. Physics, 15, 92-95.

Bridgman, P.W., (1955), "Synthetic Diamond," Scientific American, 193, 42-46.

Buckel, W., (1969), "Internal Stresses," The Journal of Vacuum Science and Technology," 6 (4), 606-610

Buckel, W., (1969), "Internal Stresses," The Journal of Vacuum Science and Technology, 6 (4), 606-610.

Bulkin, B. J., (1991), " The Raman Effect : An Introduction," in Analytical Raman Spectroscopy, John Wiley and Sons., New York, 1.

Bundy, F. P., Hall, H. T., Strong, H. M., and R. J. Wentorf Jr., (1955), "Man made Diamond," Nature, 176, 51-54.

Bundy, F. P., Strong, H. M., R. H. Wentorf, (1973), "Chemistry and Physics of Carbon," Marcel Drekker, New York

Butler, J. E., and R. L. Woodin, (1993), "Thin Film Diamond Growth Mechanisms," Phil. Trans. R. Soc. London A, 342, 209-224.

Cappelli, E., Pinzari, F., Ascarelli, P., and G. Righini, (1996), "Diamond Nucleation and Growth on Different Cutting Tool Materials: Influence of Substrate Pre-Treatments," Diamond and Related Materials, 5, 292-298.

Celii, F. G., Pehrsson, P. E., Wang, H. T., and J. E. Butler, (1988), "Infrared Detection of Gaseous Species during the Filament-Assisted Growth of Diamond," Applied Physics Letters, 52 [24], 2043-2045.

Cerdeira, F., Buchenauer, C. J., Pollak, F. H., and M. Cardona, (1972), "Stress-Induced Shifts of First-Order Raman Frequencies of Diamond- and Zinc-Blende- Type Semiconductors," Physical Review B, 5 (2), 580-593.

Chandra, L., Chhowalla, M., Amaratunga, G. A. J., and T. W. Clyne, (1996), "Residual Stress and Debonding of Diamond Films on Titanium Alloy Substrates," Diamond and Related Materials, 5, 674-681.

Chang, C. P., Flamm, D. L., Ibbotson, D. E., and J. A. Mucha, (1988), "Diamond Crystal Growth by Plasma Vapor Deposition," Journal of Applied Physics, 63 [5], 1744-1748.

Chang, Y. X., Perry, M., Peploski, J., Thompson, D. L., and L. M. Raff, (1993), "Theoretical Studies of Hydrogen-Abstraction Reactions From Diamond and Diamond-like Surfaces," J. Chemical Physics, 99 (6), 4748-4758.

Chang, Y. X., Thompson, D. L., and L. M. Raff, (1993), "Minimum Energy Paths for Elementary Reactions in Low-Pressure Diamond-Film Formation," J. Physical Chemistry, 97 (39), 10112-10118.

Chapman, B. N., (1974), "Thin-Film Adhesion," J. Vac. Sci. Technology, 11 (1), 106-113.

Chauhan, S. P., Angus, J. C., N. C. Gardner, (1976), "Kinetics of Carbon Deposition on Diamond Powder," Journal of Applied Physics, 47 [11], 4746-4754.

Chen X., and J. Narayan, (1993), "Effect of the Chemical Nature of Transition-Metal Substrates on Chemical-Vapor Deposition of Diamond," J. Appl. Phys., 74(6), 4168-4173.

Chen, K. H., Lai, Y. L., Lin, J. C., Song, K. J., Chen, L. C., and C. Y. Huang, (1995), "Micro-Raman for Diamond Film Stress Analysis," Diamond and Related Materials, 4, 460-463.

Clark, M. M., Raff, L. M., and H. L. Scott, (1996), "Hybrid Monte Carlo Method for Off-Lattice Simulation of Processes Involving Steps with Widely Varying Rates," Computers in Physics, 10 (6) 584-590.

Clark, M. M., Raff, L. M., and H. L. Scott, (1996), "Kinetic Monte Carlo Studies of Early Surface Morphology in Diamond Film Growth by Chemical Vapor Deposition of Methyl Radical," Physical Rev. B, 54 (8), 5914-5919.

Clausing, R. E., Horton, L. H., Angus, J. C., and K. Peter, (1990), "Diamond and Diamond-like Films and Coatings," Plenum Press, New York.

Conner, L. C, (1994), "Diamond - Coated Tools Cut Automotive and Aerospace Materials Efficiently," American Machinist, 52-53.

Davies, G, (1984), "Diamond," Adam Hilger Ltd., Bristol.

Demazeau, G., Michau, D., and B. Tanguy, (1993), "Role of the Substrate in the Nucleation and Crystal Growth of Diamond Thin Films Using CVD Techniques," Le Vide, les Couches Minces, 267 , 6-15.

Deryagin, B. V., and D. V. Fedoseev, (1977), "Growth of Diamond and Graphite from Gas Phase," Ch. 4, Izd. Nauka, Moscow.

Deryagin, B.V. and D. B. Fedoseev, (1975), "The Synthesis of Diamond at Low pressure," Scientific American, 233, 102-109.

Deuerler, F., Van den Berg, H., Tabersky, R., Freundlieb, A., Pies, M., and V. Buck, (1996), "Pretreatment of Substrate Surface for Improved Adhesion of Diamond Films on Hard Metal Cutting Tools," Diamond and Related Materials, 5, 1478-1489.

Deutchman, A. H., and R. J. Partyka, (1989)," Diamond Deposition- A Gem of a Process", Advanced Materials and Processes, 6, 29-33.

Devries, R. C, (1987), "Synthesis of Diamond under Metastable Conditions," Ann Rev Mater Science, 17, 161-187.

Dieter, G., and A. Krauss, (1997), "The Buckyball Precursors Produce Ultra-Smooth Diamond Films," R&D Magazine, 39 (5), 57-60.

Drory, D. M., Bogy, D. B., Donley, M. S., and J. E. Field, (1995), "Mechanical Behavior of Diamond and Other Forms of Carbon," Materials Research Society, Pittsburgh, PA.

Drory, M. D., (1997), "Performance of Diamond-Coated Silicon Nitride Bearings," J. Spacecraft, 34, (5), 683-684.

Drory, M. D., and J. W. Hutchison, (1996), "Measurement of Adhesion of a Brittle Film on a Ductile Substrate by Indentation," Proc. R. Soc. London, A, 452, 2319-2341.

Earnshaw A., and T. J. Harrington, (1973), "The Chemistry of the Transition Elements," Clarendon Press Oxford, UK.

Ece, M., Oral, B., and J. Patscheider, (1996), "Nucleation and Growth of Diamond Films on Mo and Cu Substrates," Diamond and Related Materials, 5 .211-216.

Endler, I., Leonhardt, A., Scheibe, H. J., and R. Born, (1996), "Interlayers for Diamond Deposition on Tool Materials," Diamond and Related Materials, 5, 299-303.

Everitt, N. M., Silva, R. F., Vieira, J., Rego, C. A., Henderson, C. R., and P. W. May, (1995), "Friction Measurements on Hot Filament CVD Diamond Films Deposited on Etched Tungsten Carbide Substrates," Diamond and Related Materials, 4, 730-734.

Eversole, W. G, (1962), "Synthesis of Diamond," U. S. Patent Nos. 3,030,187 and 3,030,188.

Fabisiak, K., Philippoz, J. M., and H. Vanden Bergh, (1992), "The Raman Spectroscopy of Diamond Films Deposited on Metal and Insulator

Substrates with Varying Thermal Expansion Coefficient," Diamond and Related Materials, 1 77-82.

Fan, W. D., Jagannadham, K., and B. C. Goral, (1996), "Multilayer Diamond Coatings on Silicon Carbide," Surface and Coatings Technology, 81, 172-182.

Fayette, L., Mermoux, M., Marcus, B., Brunet, F., Germi, P., Pernet, M., Abello, L., Lucazeau, G., and J. Garden, (1995), "Analysis of the Fine Structure of the Raman Line and the X-Ray Reflection Profiles for Textured CVD Diamond Films," Diamond and Related Materials, 4, 1243-1250.

Fedoseev, D. V., Deryagin, B. V., Varshavskaja, and A. C. Semienova-Tjan-Shanskaja, (1984), "Crystallization of Diamond," (in Russian), Izd. Nauka, Moscow.

Fedoseev, D. V., Varnin, V. P., and B. V. Deryagin, (1984), "Synthesis of Diamond in its Thermodynamic Metastability Region," Russian Chem. Rev. (in English), 53 [5], 435-444.

Field, J. E., (1979), "The properties of Diamond," Academic Press, New York.

Frenklach, M., and K. E. Spear, (1988), "Growth Mechanism of Vapor-Deposited Diamond," Journal of Materials Research, 3 [1], 133-140.

Frenklach, M., Clary, D. W., Gardiner, W. C., and S. E. Stein, (1985), "Detailed Kinetic Modeling of Soot Formation in Shock-tube Pyrolysis of Acetylene," Proc. 20th Int. Symp. on Combustion, Pittsburgh, 887-901.

Glass, J. T., Williams, B. E., and R. F. Davis, (1988), "Chemical Vapor Deposition and Characterization of Diamond Films Grown via Microwave Plasma Enhanced CVD," SPIE, 877, Micro-Optoelectronic Materials, 56-63.

Goldschmidt, H. J, (1948), "The Structure of Carbides in Alloy Steels," J. Iron Steel Institute., 160, 350.

Goldschmidt, H. J, (1967), "Interstitial Alloys," Butterworth & Co., London.

Grannen, K. J., and R. P. H. Chang, (1994), "Diamond Growth on Carbide Surfaces Using a Selective Etching Technique," *J. Mater. Res.*, 9(8), 2154-2163

Grimsditch, M. H., Anastassakis, E., and M. Cardona, (1978), "Effect of Uniaxial Stress on the Zone-Center Optical Phonon of Diamond," Physical Review B, 18 (2), 901-904.

Guan, Z. F., Deng, F., Liu, Q. Z., Lau, S. S., and C. A. Hewett, (1996), "Ni-Diamond Interactions," Materials Chemistry and Physics., 46, 230-232.

Guseva, M. B., Babaev, V. G., Khvostov, V. V., Ludena, G. M., Bregadze, A. Yu., Konyashin, I. Y., and A. E. Alexenko, (1997), "High Quality Diamond Films on WC-Co Surfaces," Diamond and Related Materials, 6, 89-94.

Hanssen, L. M., Carrington, W. A., Butler, J. E., and K. A. Snail, (1988), "Diamond Synthesis Using an Oxygen-Acetylene Torch," Mater. Letters, 7, 289-296.

Harris, S. J., Weiner, A. M., and T. A. Perry, (1988), "Measurement of Stable Species Present during Filament-Assisted Growth of Diamond," Applied Physics Letters, 53, 1605-1608.

Hartnett, T. M., (1988), "Characterization of Diamond Deposition in a Microwave Plasma," M. S. in Solid State Science Thesis. The Pennsylvania State University, University Park, PA.

Haubner, R., and B. Lux, (1987), 'Influence of Inhomogeneous Microwave Plasma on Diamond Morphology," Int. Journal of Refract. Hard Met., 6, 30-35.

Haubner, R., and B. Lux, (1989), "Influence of the Cobalt Content in Hot Pressed Cemented Carbides on the Deposition of Low Pressure Diamond Layers, "Journal De Physique, C5, 169-176.

Haubner, R., and B. Lux, (1993), "Diamond Grown by Hot-Filament Chemical Vapor Deposition: State of the Art," Diamond and Related Materials, 2, 1277-1294.

Haubner, R., Lindlbauer, A., and B. Lux, (1993), "Diamond Deposition on Chromium, Cobalt and Nickel Substrates by Microwave Plasma Chemical Vapor Deposition," Diamond and Related Materials., 2, .1505-1515.

Hay, R. A., and C.D. Dean, (1991), "Cutting Tool Performance of CVD Thick Film Diamond," Applications of Diamond Films and Related Materials, Elsevier Science Publishers, B. V., 53-60.

Hayward, D. O., and B. M. W. Trapnell, (1964), "Chemisorption," Butterworth Inc., Washington.

Heggie, M. I., Jungnickel, G., and C. D. Latham, (1996), "The Theory of CVD Diamond Growth," Diamond and Related Materials, 5, 236-241.

Hintermann, H. E., (1996), "Advances and Development in CVD Technology," Materials Science and Engineering, A209, 366-371.

Hisako, H., and O.Fukunaga, (1991), "Effect of Microwave Power on Hydrogen Content in Chemically Vapor Deposited Diamond Films," Journal of the American Ceramic Society, 74 [7], 1715-1718.

Hisako, H., Fukunaga, O., and O. Odawara, (1991), "Effect of Microwave Power on the Hydrogen Content in Chemically Vapor Deposited Diamond Films," J. American Ceramic Society, 74 (7), 1715-1718.

Huang, T. H., Cheng, T. K., Chang, C. S., Kao, C. T., and H. Y. Wen, (1992), "Tribological Behaviors of the Diamond-Coated Cemented Carbide Tools with Various Cobalt Contents," Diamond and Related Materials, 1, 594-599.

Huang, T. H., Kuo, C. T., and T. S. Lin, (1992), "The Role of Cemented WC Substrate Morphology on the Diamond Film Growth and Cracking Resistance," Scripta Metallurgica, 26, 1481-1486.

Isozaki, T., Saito, Y., Masuda, K., Fukumoto, M., Chosa, M., Ito, T., Oles, E. J., Inspector, A., and C. E. Bauer, (1993), "Improvement on Adhesion

Strength of Diamond Film on Cemented Carbide by Heated Intermediate Layer," Diamond and Related Materials, 2, 1156-1159.

Itoh, H., Osaki, T., Iwahara, H., and H. Sakamoto, (1991), "Diamond Coated Cutting Tools Synthesized from CO," Applications of Diamond Films and Related Materials, Elsevier Science Publishers, B. V., 77-83.

Itoh, H., Shimura, S., Sugiyama, K., Iwahara, H., and H. Sakamoto, (1996), "Adherent Diamond Coating on Silicon Nitride Substrate," Journal of the Ceramic Society of Japan, 14, 12, 1137-1142.

Itoh, H., Shimura, S., Sugiyama, K., Iwahara, H., and H. Sakamoto, (1997), "Improvement of Cutting Performance of Silicon Nitride Tool by Adherent Coating of Thick Diamond Film," Journal of the American Ceramic Society, 80, 1, 189-196.

Iyengar, S, (1995), "Diamond Coatings on Cutting Tools by Hot Filament CVD," M. S. Thesis, Oklahoma State University, Oklahoma.

Jagannadham, K., Fan, N. D., Komanduri, R., and J. Narayan, (1997), "Comparison of Microstructural Features of Diamond Composite Coatings with Polycrystalline Diamond or Boron Nitride Brazed on Tungsten Carbide Tools," J. Vac. Sci. Technology, A, 15 (4), 2262-2275.

Jindal, P. C., Dennis, T., Quinto, T., and G. J. Wolfe, (1987), "Adhesion Measurements of Chemically Vapor Deposited Hard Coatings on WC-Co substrates," Thin Solid Films, 154, 361-375.

Jungnickel, G., Porezag, D., Frauenheim, Th., Heggie, M. I., Lambrecht, W. R., Segall, B., and J. C. Angus, (1996), "Graphitization Effects on Diamond Surfaces and the Diamond/Graphite Interface," Phys. Stat. Sol. (a), 154, 109-125.

Kamo, M., Sato, Y., Matsumoto, S., and N. Setaka, (1983), "Diamond Synthesis from Gas Phase in Microwave Plasma," J. Crystal Growth, 62, 642-644.

Karner, J., Pedrazzini, M., Reineck, I., Sjostrand, M. E., and E. Bergmann, (1996), "CVD Diamond Coated Cemented Carbide Cutting Tools," Materials Science and Engineering, A209, 405-413.

Kawato, T., and K. Kondo, (1987), "Effects of Oxygen on CVD Diamond Synthesis," Japanese Journal of Applied Physics, 26 [9], 1429-1432.

Kikuchi, N., Eto, H., Okamura, T., and H. Yoshimura, (1991), "Diamond Coated Inserts: Characteristics and Performance," Applications of Diamond Films and Related Materials, Elsevier Science Publishers, B. V., 61-68.

Kikuchi, N., Komatsu, T., and H. Yoshimura, (1988), "Characteristics of Thin Film Growth in the Synthesis of Diamond by Chemical Vapor Deposition and Application of the Thin Film Synthesis Technology for Tools," Materials Science and Engineering, A105/106, 525-534.

Klages, C. P., (1993), "Chemical Vapor Deposition of Diamond," Appl. Phys., A, 56, 513-526.

Knight, D. S., and W. B. White., (1989), "Characterization of Diamond Films by Raman Spectroscopy," J. Materials Research, 4 [2], 385-393.

Kobashi, K., Nishimura, K., Kawate, Y., and T. Horiuchi, (1988) "Synthesis of Diamonds by the Use of Microwave Plasma Chemical-Vapor Deposition: Morphology and Growth of Diamond Films," Physical Review B, 38, 4067-4083.

Kobashi, K., Nishimura, K, Miyata, K., Kawate, Y., Glass, J., and B. Williams, (1988), "Surface Morphology and Defect Structures in Microwave CVD Diamond Films,' SPIE Proceedings, 969, Diamond Optics, SPIE -International Society for Optical Engineering, Bellingham, WA.

Koepfer, C, (1996) "Diamond-Coated Carbide Inserts-Ready, Set, Go! ," Modern Machine Shop, 15-20.

Komanduri, R, (1993), "Low Pressure Diamond Synthesis for Manufacturing Applications," Keynote paper presented at IMCC, Hongkong.

Komanduri, R., and S. Nandyal, (1993), "Low Pressure Synthesis of Polycrystalline Diamond Abrasive," Int. J. of Mech. Tools Manufact., 33, 2, 285-296.

Konyashin, I. Yu., and M. B. Guseva, (1996), "Thin Films Comparable with WC-Co Cemented Carbides as Under layers for Hard and Superhard Coatings: The State of the Art," Diamond and Related Materials, 5, 575-579.

Kosolapova. T. IA, (1971), "Carbides- Properties, Production, and Applications," Plenum Press, New York - London

Kubelka, S., Haubner, R., Lux, B., Steiner, R., Stingeder, G., and M. Grasserbauer, (1994), "Influences of WC-Co Hard Metal Substrate Pre-Treatments with Boron and Silicon on Low Pressure Diamond Deposition," Diamond and Related Materials, 3, 1360-1369.

Kuezmarski, M. A., (1992), "Modeling of Chemical Vapor Deposition Reactors for Silicon Carbide and Diamond Growth," Ph.D. Thesis, Case Western Reserve University, Cleveland, Ohio.

Kuo, C. T., Lin, C. R., and H. M. Lien, (1996), "Origins of Residual Stresses in CVD Diamond Films," Thin Solid Films, 290-291, 254-259.

Lander, J. J., and J. Morrison, (1966), "Low-Energy Electron Diffraction Study of the (111) Diamond Surface," Surf. Sci., 4, 241-246.

Lavoisier, A. L., (1772), Memoire Academie des Sciences, 564-591.

Leipunski, O. I., (1939), "Synthetic Diamonds," Usp. Khim. 8, 1519-1534.

Leyendecker, T., Lemmer, O., Jurgens, A., Esser, S., and J. Ebberink, (1991), "Industrial Application and Quality Control of Crystalline Diamond Coated Tools," Applications of Diamond Films and Related Materials, Elsevier Science Publishers, B. V., 105-110.

Li, Z., Wang, L., Suzuki, T., Argoitia, A., Pirouz, P., and J. C. Angus, (1993), "Orientation Relationship between Chemical Vapor Deposited Diamond and Graphite Substrates," J. Applied Physics, 73, 711-718.

Liu, H., and D. D. Dandy, (1995), "Studies on Nucleation Process in Diamond CVD: An Overview of Recent Developments," Diamond and Related Materials, 4, 1173-1188.

Liu, W., Tucker, D. A., Yang, P., and J. T. Glass, (1995), "Nucleation of Oriented Diamond particles on Cobalt Substrates,", J. App. Physics, 78 (2), . 1291-1296.

Lu, Z. P., Heberlein, J., and E. Pfender, (1992), "Process Study of Thermal Plasma Chemical Vapor Deposition of Diamond, Part I : Substrate Material, Temperature, and Methane Concentration," Plasma Chemistry and Plasma Processing, 12 (1), 35-52.

Lux, B., and R. Haubner, (1991), "Nucleation and Growth of Low-Pressure Diamond," Diamond and Diamond-Like Films and Coatings, Plenum Press, New York

Lux, B., and R. Haubner, (1996), "Diamond Deposition on Cutting Tools," Ceramics International, 22, 347-351.

Mason, F, (1990), "Diamond : The Material of the Future," American Machinist, 43-46.

Matsui, Y., Matsumoto, S., and N. Setaka, (1983), "TEM-Electron Energy Loss Spectroscope Study of the Diamond Particles Prepared by Chemical Vapor Deposition from Methane," J. Mater. Science Letters, 2, 532-534.

Matsumoto, O., and T. Katagiri, (1987), "Effect of Dilution Gases in Methane on the Deposition of Diamond-Like Carbon in a Microwave Plasma, II: Effect of Hydrogen," Thin Solid Films, 146, 283-289.

Matsumoto, O., Toshima, H., and Y. Kanzaki, (1985), 'Effect of Dilution Gases in Methane on the Deposition of Diamond-Like Carbon in a Microwave Plasma," Thin Solid Films, 146, 283-289.

Matsumoto, S., (1985), "Chemical Vapor Deposition of Diamond in RF Glow Discharge," J. Mater. Science letters, 4, 600-602.

Matsumoto, S., and Y. Matsui, (1983), "Electron Microscopic Observation of Diamond Particles Grown from the Vapor Phase," J. Materials Science, 18, 1785-1793.

Matsumoto, S., Sato, Y., Kamo, M., and N. Setaka, (1982), "Vapor Deposition of Diamond Particles from Methane," Japanese Journal of Applied Physics, 21 [4], L183-L185.

Mccune, R. C., Chase, R. E., and E. L. Cartwright, (1992), "Methodology for Adhesion Characterization of Microwave PECVD Diamond Films on SiALON Tool Inserts," Surface and Coatings Technology, 53, 189-197.

Mehandru, S. P., Anderson, A. B., and J. C. Angus, (1992a), "Hydrogenation of the {10$\bar{1}$0} Graphite Edge. Structural Considerations from Band Calculations," Journal of Physical Chemistry, 96 (26) 10978-10982.

Mehandru, S. P., Anderson, A. B., and J. C. Angus, (1992b), "Hydrogen Binding and Diffusion in Diamond," J. Mater. Research, 7, 689-695.

Mehlmann, A. K., Berger, S., Fayer, A., Dirnfeld, S. F., Bamberger, M., Avigal, Y., Hoffman, A., and R. Porath, (1994), "Investigation of Cobalt Behavior During Diamond Deposition on Cemented Carbides," Diamond and Related Materials, 3, 804-809.

Mehlmann, A. K., Dirnfeld, S. F., and Y. Avigal, (1992), "Investigation of Low Pressure Diamond Deposition on Cemented Carbides," Diamond and Related Materials, 1, 600-604.

Messier, R., Glass, J. T., Butler, J. E., and R. Roy, (1991) "New Diamond Science and Technology," Materials Research Society, Pittsburgh, PA.

Mitsuda, Y., Kojima, J., Yoshida, T., and K. Akashi, (1987), "The Growth of Diamond in Microwave Plasma under Low Pressure," Journal of Materials Science, 22, 1557-1562.

Mittal, K. L., (1976), "Adhesion Measurement of Thin Films, Thick Films, and Bulk Coatings," ASTM Special Technical Publication 640, ASTM, Philadelphia, Pa.

Mohrbacher, H., Van Acker, K., Blanpain, B., Van Houtte, P., and J. P. Celis, (1996), "Comparative Measurement of Residual Stress in Diamond Coatings by Low-Incident-Beam-Angle-Diffraction and Micro-Raman Spectroscopy," Journal of Materials Research, 11 (7), 1776-1782.

Murakawa, S., Takeuchi, H., Miyazawa, H., and Y. Hirose, (1988), "Chemical Vapor Deposition of a Diamond Coating onto a Tungsten Carbide Tool using Ethanol," Surface and Coatings Technology, 36, 303-310.

Nandyal, S., (1991), "Combustion Synthesis of Diamond Films," M. S. Thesis, Oklahoma State University, Oklahoma.

Narayan, J., Nelson, M., Oktyabrsky, S., and K. Jagannadham, (1996), "Diamond Deposition on 3d Transition Metals and their Alloys," Materials Science and Engineering B., 38, 45-52.

Nemanich, R. J., (1991), "Growth and Characterization of Diamond Thin Films," Ann. Rev. Mater. Sci., 21, 535-558.

Nemanich, R. J., and S. A. Solin, (1979), "First- and Second-Order Raman Scattering from Finite-Size Crystals of Graphite," Physical Review B, 20 (2), 392-400.

Nemanich, R. J., Bergman, L., LeGrice, Y. M., and R. E. Shroder, (1991), "Raman Characterization of Diamond Film Growth," Proceedings of the Second International Conference on New Diamond Science and Technology, Eds. Messier, R., Glass, J. T., Butler, J. E., and R. Roy, MRS Pittsbugh, Pennsylvania, 741-764.

Nesladek, M., Spinnewyn, J., Asinari, C., Lebout, R., and R. Lorent, (1993), "Improved Adhesion of CVD Diamond Films to Steel and WC-Co Substrates," Diamond and Related Materials, 3, 98-104.

Nesladek, M., Vandierendonck, K., Quaeyhaegens, Kerkhofs, M., and L. M. Stals, (1995), "Adhesion of Diamond Coatings on Cemented Carbides," Thin Solid Films, 270, 184-188.

Newton, Isaac., (1704), "optiks", London.

Nishimura, K., Kobashi, K., Kawate, Y., and T. Horiuchi, (1987), "Growth of Diamonds using Plasma Chemical Vapor Deposition," KOBELCO Technol. Rev., 2, 49-52.

Oakes, J., Pan, X. X., Haubner, R., and B.Lux, (1991), "Chemical Vapor Deposition Diamond Coatings on Cemented Carbide Tools," Surface and Coatings Technology, 47, 600-607.

Oda S., Ishihara, S., Shibata, N., Shirai, H., Miyauchi, A., Fukuda, K., Tanabe, A., Ohtoshi, H., Hanna, J., and I. Shimizu, (1986), "The Role of Hydrogen Radicals in the Growth of a-Si and Related Alloys," Japanese Journal of Applied Physics, 25 [3], L188-L190.

Oles, E. J., Inspektor, A., and C. E. Bauer, (1996), "The New Diamond-Coated Carbide Cutting Tools," Diamond and Related Materials, 5, 617-624.

Oslon, J. M., and M. J. Dawes, (1996), "Examination of the Material Properties and Performance of Thin-Diamond Film Cutting Tool Inserts Produced by Arc-jet and Hot Filament Chemical Vapor Deposition," J. Mater. Research, 11, 7, 1765-1775.

Pandy, K. C., (1982), "New Dimerized-Chain Model for the Reconstruction of the Diamond (111) - (2 X 1) Surface,' Phys. Rev. B, 25 [6], 4338-4341.

Park, B. S., Baik, Y. J., Lee, K. R., Eun, K. Y., and D. H. Kim, (1993), "Behavior of Co Binder Phase during Diamond Deposition on WC-Co Substrate," Diamond and Related Materials, 2, 910-917.

Park, S. S., and J. Y. Lee, "Synthesis of Diamond Films on Titanium Substrates by Hot-Filament Chemical Vapor Deposition," (1991), J. Appl. Phys., 69(4), 2618-2622.

Pate, B. B., (1986), "The Diamond Surface: Atomic and Electronic Structure," Surf. Sci., 165, 83-142.

Pauling, L, (1938), "The Nature of Interatomic Forces in Metals," Phys. Rev., 54, 899-904.

Pauling, L, (1949), "A Resonating-valence-bond Theory of Metals and Intermetallic Compounds," Proc. Roy. Soc., [A] 196, 343-362.

Peng, X. L., and T. W. Clyne, (1997), "Formation and Adhesion of Hot Filament CVD Diamond Films on Titanium Substrates," Thin Solid Films, 293, 261-269.

Peng, X. L., Liu, H. F., Gan, Z. P., Li, H. Q., and H. D. Li, (1995), "Characterization and Adhesion Strength of Diamond Films Deposited on Silicon Nitride Inserts by d. c. Plasma Jet Chemical Vapor Deposition," Diamond and Related Materials, 4, 1260-1266.

Peploski, J., Thompson, D. L., and L. M. Raff, (1992), "Molecular Dynamics Studies of Elementary Surface Reactions of C_2H_2 and C_2H in Low-Pressure Diamond-Film Formation," Journal of Physical Chemistry, 96 (21), 8538-8544.

Perry, A. G., (1983), "Scratch Adhesion Testing of Hard Materials," Thin Solid Films, 107, 181-189.

Perry, M. D., and L. M. Raff, (1994), "Theoretical Studies of Elementary Chemisorption Reactions on an Activated Diamond (111) Terrace," Journal of Physical Chemistry, 98 (33), 8128-8133.

Perry, S. S., and G. A. Somorjai, (1994), "Reaction Layer Formation and Fracture at Chemically Vapor Deposited Diamond/Metal Interfaces," J. Vac. Sci. Technology, A 12 (4), 1513-1518.

Peters, M.G., and R. H. Cummings, (1993), "Methods for Coating Adherent Diamond Films on Cemented Tungsten Carbide Substrates," U.S. Patent No. 5,236,740.

Phillip, J., Milne, D. K., Jubber, M. G., and J. I. B. Wilson, (1997), "Is Interfacial Silicon Carbide Necessary for the Epitaxy of Diamond on (100) Silicon," Chemical Vapor Deposition, 3 (1), 30-32.

Poferl, D. J., Gardner, N. C., and J. C. Angus, (1973), "Growth of Boron-Doped Diamond Seed Crystals by Vapor Deposition," Journal of Applied Physics, 44 [4], 1428-1434.

Quinto, D. T, (May, 1996), "Cutting Tools," Tooling and Production, 10-14.

Rats, D., Vandenbulcke, L., Herbin, R., Bou, P, and C. Beny, (1995), "Pressure Influence on the Diamond Deposition Domain from Various C-H-O (-Ar)- Containing Gaseous Mixtures," Diamond and Related Materials, 4, 207-215.

Ridgen, J. S., Newport, R. J., and G. Bushnell-Wye, (1997), "The Structural Characterization of Amorphous Thin Films and Coatings in their As-Deposited State using X-Rays at Shallow Angles of Incidence," J. Materials Research, 12 (1), 264-276.

Robins, L. H., Farabaugh, E. N., A. Feldman, (1990), "Line Shape Analysis of the Raman Spectrum of Diamond Films Grown by Hot-Filament and Microwave -Plasma Chemical Vapor Deposition," J. Materials Research, 5 (11).

Rossini F. D., and R. S. Jessup, (1938), "Heat and Free Energy of Formation of Carbon Dioxide, and the Transition between Graphite and Diamond," J. Res. Nat. Bur. Standards, 21, 491.

Roy, R., Dewan, H. S., and P. Ravindranathan, (1993a), "Crystallization of Diamond below 1 atm from Carbon-Metal Mixtures," J. Materials Chemistry, 3 (6), 685-686

Roy, R., Dewan, H. S., and P. Ravindranathan, (1993b), "Diamond Synthesis via a Low-Pressure Solid-State-Source Process," Materials Research Bulletin, 28, 861-866

Roy, R., Dewan, H. S., Cherian, K. A., Cheng, J. P., Badzian, A., Drawl, W., and C. Langlade, (1995), "Precipitation of Diamond from Metallic Liquids below 1 atm," Materials Letters, 25, 191-193

Saijo, K., Uno, K., Yagi, M., Shibuki, K., and S. Takatsu, (1991), "The Tool life of Diamond Coatings in Milling an Al-Si Alloy," Applications of Diamond Films and Related Materials, Elsevier Science Publishers, B. V., 69-76.

Saito, Y., Isozaki, T., Masuda, A., Fukumoto, K., Chosa, M., Ito, T., Bauer, C. E., Inspektor, A., and E. J. Oles, (1993), "Adhesion Strength of Diamond Film on Cemented Carbide Insert," Diamond and Related Materials, 2, 1391-1395.

Saito, Y., Matsuda, S., and S. Nogita, (1986), "Synthesis of Diamond by Decomposition of Methane in Microwave Plasma," Journal of Materials Science Letters, 5 [5] 565-568.

Saito, Y., Sato, K., Matuda, S., and H. Koinuma, (1991), "Effects of Substrate Material on Diamond Growth from CO-H$_2$ Plasma," Journal of Materials Science, 26, 2441-2444.

Saito, Y., Sato, K., Tanaka, H., Fujita, K., and S. Matsuda, (1988), "Diamond Synthesis from Methane-Hydrogen-Water Mixed Gas using a Microwave Plasma," Journal of Materials Science, 23 [3], 842-846.

Samsonov. G, (1964), "Refractory Transition Metal Compounds; High Temperature Cermets," Academic Press, New York.

Sato, Y., Kamo, M., and N. Setaka, (1987), "Growth of Diamond from Various Hydrocarbon-Hydrogen Mixtures," Proceedings of the 8th International Symposium on Plasma Chemistry, 1, International Union of Pure and Applied Chemistry, Oxford, England, 2446-2451.

Scardi, P., Veneri, S., Leoni, M., Polini, R., and E. Traversa, (1996), "Lattice Disorder and Texture in Diamond Coatings Deposited by HFCVD on Co-Cemented Tungsten Carbide," Thin Solid Films, 290-291, 136-142.

Schwarzbach, D., Haubner, R., and B. Lux, (1994), "Internal Stresses in CVD Diamond Layers," Diamond and Related Materials, 3, 757-764.

Setaka, N., (1987), "Vapor Deposition of Diamond," Proceedings of the Tenth International Conference on Chemical Vapor Deposition, Electrochemical Society, Pennington, New Jersey, 1156-1163.

Sharda, T., and D. S. Misra, (1996), "Dissociation Kinetics of Molecular Hydrogen in a Microwave Plasma and its Influence on the Hydrogen Content in Diamond Films," Solid State Communications, 98 (10), 879-883.

Sharma, S. K., Mao, H. K., Bell, P. M., and J. A. Xu, (1985), "Measurement of Stress in Diamond Anvils with Micro-Raman Spectroscopy," Journal of Raman Spectroscopy, 16 (5), 350-352.

Shen, C. H., (1996), "The Importance of Diamond Coated Tools for Agile Manufacturing and Dry Machining," Surface and Coatings Technology, 86-87, 672-677.

Shuji, Y., and T. Nakai, (1991), "Tool Applications of Diamond and cBN," Applications of Diamond Films and Related Materials, Elsevier Science Publishers, B. V., 37-41.

Silveira, M., Becucci, M., Castellucci, E., Polla Mattiot, F., Barbarossa, V., Tomaciello, R., and F. Galluzzi, (1993), "Non-Diamond Carbon Phases in Plasma - Assisted Deposition of Crystalline Diamond Films: A Raman Study," Diamond and Related Materials, 2, 1257-1262.

Singh, R. K., Gilbert, D. R., Gerald, J. F., Harkness, S., and D. G. Lee, (1996), "Engineered Interfaces for Adherent Coatings on Large Thermal-Expansion Coefficient Mismatched Substrates," Science, 272, 396-398.

Singleton, M., and P. Nash, (1989), "Variable Composition Compounds and Their Solid Solutions," Bulletin of Alloy Phase Diagrams, 10, 121-129.

Soderberg, S., Westergren, K., Reineck, I., Ekholm, P. E., and H. Shahani, (1991), "Properties and Performance of Diamond Coated Ceramic Cutting Tools," Applications of Diamond and Related Materials, Elsevier Science Publishers B. V., 43-51.

Solin, S. A., and A. K. Ramdas, (1970), "Raman Spectrum of Diamond," Physical Review B, 1(4), 1687-1698.

Sommer, M., Mui, K., and F. W. Smith., (1988), "Thermodynamic Analysis of the Chemical Vapor Deposited Diamond Films," Presented at the Strategic Defense Initiative Office/Innovative Science and Technology-Office of Naval Research Diamond Technology Initiative Symposium, Crystal City, VA, July 12-14.

Spear, K. E., (1987), "Growth of Crystalline Diamond from Low Pressure Gases,' Earth Miner. Sci., 56 [4], 53-59.

Spear, K. E., (1989), "Diamond-Ceramic Coating of the Future," Journal of American Ceramic Society, 72 [2], 171-191.

Spear, K. E., Frenklach, M., Badzian, A., Badzian, T., and R. Messier, (1988), "Vapor Deposition of Crystalline Diamond," Ceram. Eng. Sci. Proc., 9 [9-10], 1095-1102.

Spear., K. E., and J. P. Dismukes, (1994), "Synthetic Diamond : Emerging CVD Science and Technology," John Wiley and Sons, New York.

Spistyn, B. V., Bouilov, L. L., and B. V. Deryagin, (1981), "Vapor Growth of Diamond on Diamond and other Surfaces," J. Crystal Growth, 52, 219-226.

Sprow, E. E., (Feb., 1995), "Diamond Coatings: Ready to Rip," Manufacturing Engineering, 41-46.

Stein, S. E., (1990), "Diamond and Graphite Precursors," Nature, 346,517.

Steinmann, P. A., and Hintermann, H. E., (1989), "A Review of the Mechanical Tests for Assessment of Adhesion," J. Vac. Science and Technology, A 7, 2267-2272.

Stephan, P. M., Hay, R. A., and C. D. Dean, (1992), "The New Diamond Technology and its Application in Cutting Tools," Diamond and Related Materials, 1, 710-716.

Stiegler, J., Lang, T., Ferguson, M., Kaenel, Y., and E. Blank, (1996) "Low Temperature Limits of Diamond Film Growth by Microwave Plasma Assisted CVD," Diamond and Related Materials, 5, 226-230.

Sunkara, M, (1992), "Monte Carlo Simulation of Diamond Nucleation and Growth," Ph.D. Thesis, Case Western University, Cleveland, Ohio.

Sunkara, M., Angus, J. C., Hayman, C. C., and F. A. Buck, (1990), "Nucleation of Diamond Crystals," Carbon, 28, 745-746.

Takatsu, T., Saijo, K., Yagi, M., Shibuki, K., and J. Echigoya, (1991), "Microstructure of Diamond Films Near the Interface with WC Substrate," Materials Science and Engineering, A140, 747-752.

Tennant, S., (1797), Phil. Trans. R. Soc., 87, 123.

Terranova, M. L., Rossi, M., and G. Vitali, (1996), "Structural Investigation of the Titanium/Diamond Film Interface," J. Appl. Physics, 80 (6), 3552-3559.

Touloukian, Y. S., Kirby, R. K., Taylor, R. E., and T. Y. Lee, editors, (1975), "Themophysical Properties of Matter, "The TPRC Data Series, 12,13, Plenum, New York.

Tsuda, M., Nakajima, M., S. Oikawa, (1987), "Epitaxial Growth Mechanism of Diamond Crystals in CH4-H2 Plasma," Journal of American Ceramic Society, 108, 5780-5783.

Vasilash, G. S., (December, 1995), "Superhard Coatings: More Than Meets the Eye," Tooling and Production, 18-21.

Walter, R. L. L., Lee, C. H., Segall, B., Angus, J. C., Li, Z., and M. Sunkara, (1993), "Diamond Nucleation by Hydrogenation of the Edges of Graphitic Precursors," Nature, 364, 607-610.

Wang, W. N., Fox, N. A., May, P. W., Knapper, M. P., Meaden, G., Partridge, P. G., Ashfold, M. N. R., Steeds, J. W., Hayward, I. P., and G. D. Pitt, (1996), "Laser Raman Studies of Polycrystalline and Amorphic Diamond Films," Phys. Stat. Solidi (a), 154, 255-268.

Wang, W., Kejun, L., Jinying, G., and L. Aimin, (1992), "Internal Stresses in Diamond Films Formed by d.c Plasma Chemical Vapor Deposition," Thin Solid Films, 215, 174-178.

Wang, Y., and J. C. Angus., (1993), "Microbalance Studies of the Kinetics of Diamond Growth," Electrochemical Society Proceedings, 93 (17), Pennington, New Jersey, 16-21.

Wei, J., and J. T. Yates, Jr., (1995), "Diamond Surface Chemistry I- A Review," Critical Reviews in Surface Chemistry, 5 (1-3), 1-71.

Weihnacht, V., Fan. W. D., Jagannadham, K., Narayan, J., and C. T. Liu, (1996), "A New Design of Tungsten Carbide Tools with Diamond Coatings," J. Materials Research, 11 (9), 2220-2230.

Windischmann, H., G. F. Epps., Cong, Y., and R. W. Collins, (1991), "Intrinsic Stress in Diamond Films Prepared by Microwave Plasma CVD," J. Applied Physics, 69 (4), 2231-2237.

Wolden, C. A., and K. K. Gleason,(1996), "On the Pressure Limits of Diamond Chemical Vapor Deposition," Diamond and Related Materials, 5, 1503-1508.

Xing, J., and H. L. Scott, (1993), "Diamond Film Growth by Chemical Vapor Deposition: A Molecular Simulation," Physical Review B, 48, 7, 4806-4809.

Xing, Z. Z., Roy, R., Cherian, K. A., and A. Badzian, (1997), "Hydrothermal Growth of Diamond in Metal-C-H_2O Systems," Nature, 385, 513-515.

Xu, N., and Z, H. Zheng, (1996), "Growth of Diamond Films on Si_3N_4 Coated Silicon Substrates," Materials Science and Technology, 12, 1-6.

Yang, P. C., Zhu, W., and J. T. Glass, (1994), "Diamond Nucleation on Nickel Substrates Seeded with Non-Diamond Carbon," J. Mater. Res., 9(5), 1063-1066.

Yen, T. Y., Kuo, C. T., and Hsu, S. E., (1990), "Adhesion of Diamond films on Various Substrates," Mat. Res. Soc. Proceedings, 168, 207-212.

Yoshikawa, M., Katagiri, G., Ishida, H., and A. Ishitani, (1988), "Raman Spectra of Diamond-Like Amorphous Carbon Films," J. Appl. Physics, 64 (11), 6464-6468.

Yoshikawa, M., Katagiri, G., Ishida, H., Ishitani, A., Ono, M., K. Matsumura, (1989), "Characterization of Crystalline Quality of Diamond Films by Raman Spectroscopy," Applied Phys. Lett., 55 (25), 2608-2610.

Yoshikawa, M., Mori, Y., Maegawa, M., Katagiri, G., Ishida, H., and A. Ishitani, (1993), "Raman Scattering from Diamond Particles," Applied Physics Letters, 62 (24), 3114-3116.

Young, R. S., (1961), "Cobalt-Its Chemistry, Metallurgy, and Uses," Reinhold Pub. Corp, New York, 64-74.

Zhu, W., Badzian, A. R., and R. Messier, (1990), "Morphological Phenomena of CVD Diamond (Part I)," SPIE, 1325, Diamond Optics III, 187-200.

Zhu, W., Mccune, R. C., Devries, R. C., Tamor, M. A., and K. Y. Simon Ng, (1994), "Characterization of Diamond Films on Binderless W-Mo Composite Carbide," Diamond and Related Materials, 3, 1270-1276.

Zhu, W., Messier, R., and A. R. Badzian, (1989), "Effect of Process Parameters on CVD Diamond Films," Diamond and Diamond-Like Films, The Electrochemical Society, Pennington, New Jersey, 61-79.

APPENDIX A

PROPERTIES OF DIAMOND

The many unique properties of diamond have made it prominent as a gem stone, industrial tool and as a material for solid state research. Synthesis of single and polycrystalline films with desirable properties for tailor made applications have broadened the scope of this explicit material. In this appendix the various properties of diamond which have been exploited for industrial applications are summarized.

A.1 Classification of Diamonds

Based on their optical and electrical properties and their impurity content diamonds are classified into four types of single and two types of polycrystalline material.

Type IA : about 98% of natural diamonds are of this type and contain nitrogen as an impurity in fairly substantial amounts. This nitrogen strongly absorbs UV and IR light since it is not paramagnetic. These diamonds are optically transparent at wavelengths greater than 320 nm and the thermal conductivity at room temperature is 1000 watts/m-Kelvin.

Type IB : All synthetic(HP-HT) are of this type and contain paramagnetic nitrogen on isolated substitutional lattice sites up to 0.2%. Optical, thermal and electrical properties are similar to type IA. These are

transparent to UV above 225 nm. Thermal conductivity at room temperature is 2000 W/m/K.

Type IIB : Occurrence is extremely low in nature and contain very low concentration of nitrogen. Presence of boron makes them a p-type semiconductor and gives them a bluish color.

carbonados and ballas : These are naturally occurring polycrystalline diamonds. Carbonados contain graphite and other impurities and are tougher than single crystal diamond. Ballas are round dense randomly oriented polycrystalline diamond which have very high impact resistance and do not cleave.

A.2   Mechanical Properties

Extreme high hardness, high thermal conductivity coupled with low coefficient of thermal expansion and friction have been effectively exploited in its use as an abrasive and wear resistant applications. Table A.1 lists the mechanical properties of diamond.

The fracture behavior of diamond is dominated by cleavage on the {111} plane, although cleavage has also been observed on the {110} plane. this behavior is not clear as the energy differences for the different planes are small. The most likely answer may be due to defects on the {111} plane giving preferential weakening. Cleavage cracks in diamond can propagate at very high velocities ($\sim$ 7200 ms^{-1}). comparison of the strengths of good quality diamonds indicate the best value of the tensile strength to be roughly 300 kg mm^{-2}.

The adhesion and friction of diamond depend both on the bulk and the surface properties of diamond. In air the friction of diamond on diamond is relatively low, μ =0.1. The friction depends on the crystal face and orientation. On the octahedral face the friction is low and there is no anisotropicity. The lowest friction is along the <011> direction and the highest along the <100> direction. In vacuum, the friction can reach high values ($\mu = 1$).

Table A.1   Mechanical properties of diamond

(Field, 1979)

Properties	Values
Hardness (kg/mm^2)	10000
Pressure Coefficient (dC/dP) C_{11} C_{12} C_{44}	6.0 3.1 3.0
Young's Modulus, E (N/m^2)	10.5 X 10^{11}
Poisson's ratio	0.104
Bulk Modulus (N/m^2)	4.42 X 10^{11}
Elastic Modulii (X 10^{11} N/m^2) C_{11} C_{12} C_{44}	10.8 1.25 5.7
Coefficient of Friction	~0.1 in Air ~1 in Vacuum

At room temperature, diamond behaves as an elastic brittle solid. By contrast at 1800 °C, in vacuum, dislocations become relatively mobile and it is possible to produce appreciable plastic deformation. However it is still not clear whether plastic deformation can occur around an indenter at room temperature.

A.2 Thermal properties

At room temperatures the thermal conductivity of type II a diamond is 4-5 times better than that of copper. The maximum thermal conductivity occurs at 80K. However, the thermal conductivity drops significantly even if small amounts of nitrogen is present as an impurity. The presence of C^{13} isotope also affects the thermal conductivity of diamond. The thermal properties of diamond are listed in Table A.2 The coefficient of linear expansion of diamond at room temperature is only 8×10^{-7} k^{-1}. In contrast copper has an expansion coefficient of 170×10^{-7} K^{-1}, at room temperature. The special low expansion alloy Invar (nickel-steel alloy) has an expansion coefficient similar to that of diamond at 9×10^{-7} K^{-1}.

A.3 Optical and Electrical Properties

The transparency of diamond is one important reason why it makes an prominent gem. Diamonds with low nitrogen content are transparent down to 220 nm. If they have nitrogen impurities they absorb at

wavelengths lower than 320 nm. Diamond also has an high refractive index. ~2.4.

Table A.2   Thermal properties of diamond

(Field, 1979)

Properties	Values
Thermal Conductivity (W/m-K) Typical values at 293 K	
Type Ia	600-1000
Type IIa	2000-2100
Thermal Expansion (X 10^{-6} K^{-1})	
193 K	0.4
293 K	0.8
400-1200 K	1.5-4.8
Debye Temperature, at T> 600 K	1880
Bulk Modulus, B (Pa)	4.2 X10^{-4}
C_p-C_v at T > 1100 K(J/mol. K)	
C_p at 1800 K	24.7
C_p at 3000 K	26.3

A pure perfect diamond is an insulator with resistivities greater than 10^{14} ohm-meters being frequently observed. However, diamond can be made semiconducting by properly doping with phosphorus (n-type) or with boron (p-type). The mobility of these positively and negatively charged carriers are equal and high in diamond. Table A.3 lists the electrical and optical properties of diamond.

Table A.3   Electrical and optical properties

of diamond (Field , 1979)

Properties	Values
Lattice Constant ($^\circ$Å)	3.567
Density (gm./cm^3)	3.515
Band Gap (eV)	5,45
Saturated Electron Velocity (x 10^7 cm/s)	2.7
Carrier Mobility (cm^2/V-s) Electron Hole	2200 1600
Breakdown (x 10^5 V/cm)	100
Dielectric Constant	5.5
Resistivity (Ohm-m)	10^{13}
Refractive Index	2.42

A.4   Chemical Properties

Diamond is an extremely inert chemically and is not affected by any acids or chemicals. Substances such as sodium nitrate are known to affect diamond in the molten state at temperatures as low as ~ 450 $^\circ$C. O_2, CO, CO_2, H_2, H_2O, and Cl_2 at high temperatures have been to etch diamonds. In oxygen itself, diamond starts to be oxidized at ~ 7000 $^\circ$C.

Two groups of metals have been found to chemically attack diamonds. The first group consists of carbide formers and include

tungsten, tantalum, titanium, and zirconium. At high temperatures, these metals form carbides. The second group includes iron, cobalt, manganese, nickel, chromium, and also the platinum group of metals. In the molten state these metals are true solvents for carbon.

When diamond is heated to high temperatures it transforms to graphite. Results of experiments on the heating of diamond in vacuum, show that the onset of graphitization is detectable around 1500 °C and the rate of graphitization increases rapidly until around 2000 °C diamond completely transforms into graphite in a short time.

APPENDIX B

INSTRUMENT SPECIFICATIONS

1. Mass Flow Meters

Model : MKS type 247C

Feature : 4 channel read out

Input signal range : 0 to +5VDC (5.5V Maximum)

Output range : 0 to +5VDC

Zero correction : ± 3% of full scale

set point adjust : 0.1% to 100 % of full scale (flow)

: 0.1% to 100 % of input level (ratio)

Display accuracy : ± 0.1 % ± 1 digit

2. Mass Flow Controller

Model : MKS type 1159B

Feature : Closed loop PID controller

Full scale Ranges : 100 SCCM (H_2) and 50 SCCM (CH_4)

Control Range : 1.0 to 100 % of full scale

Accuracy : ± 1.0 % of full scale (Linearized error)

Repeatability : ± 0.2 % of full scale

Resolution : 0.1 % of full scale

Settling time : < 2 seconds to within 2% of the set point

Maximum inlet pressure : 150 psig

3. Pressure Controller

Model : MKS type 250C

Feature: Closed loop PID controller

Input signal : 0 to 10VDC, or 0 to 1VDC, or 0 to 0.1 VDC

Valve outputs : Current - 0 to 120 mA

: Voltage - 0 to 110VDC

Voltage outputs : Input signal - 0 to 10 volts (5K minimum resistance)

: Controller output- 0 to 10 volts (5K minimum resistance)

Accuracy : ± 0.25 % of full scale

4. Pressure Transducer

Model : MKS type 127A

Full scale range : 100 Torr

Accuracy : 0.15% of reading (± temperature coefficients)

Temperature coefficients : Zero: 0.005% full scale/^{o}C

: Span : 0.02% reading/^{o}C

Operating temperature range : 15 ^{o}C to 40 ^{o}C; temperature controlled at 45 ^{o}C

Time constant : < 16 msec

Input : ± 15VDC @ 250mA, regulated ±5%

Output : 0 to +10VDC into ≥ 10kW load

Additional features : Heated sensor for improved accuracy

Lowest recommended pressure reading : 2 X 10 $^{-3}$ Torr

Lowest pressure control : 5 X 10 $^{-2}$ Torr

5. Substrate Temperature Controller

Model : Eurotherm type 847 digital temperature controller

Feature : Closed loop PID controller (ON/OFF) with ramp-to-setpoint feature

Calibration accuracy : 0.5 ^{o}C ± 1/2 l.s.d

Sampling frequency : 8 Hz

Maximum sensor break reaction time : 30s

Number of thermocouple types : 7 (J, K, L, R, S, PL2, T)

6. Dual Wavelength Infrared Pyrometer

Model : Williamson Tempmatic 8000 Series

Accuracy : ± 1 % of span

Repeatability : 0.25 % of full scale

Working distance : 15 to 91 cm

Response time : adjustable. 0.2 to 5 seconds

Emissivity adjustment : automatic emissivity compensation : 0.1 to 1.0

Temperature Range : 500 - 1200 ºC

Field of View :Minimum 0.64 cm of diameter at the working distance of 46 cm

7. Microwave Power Generator

Model : S-1500i power supply and control unit with HS-1500 power head

Power output : 0.125 to 1.5 KW CW

Frequency : 2455 MHz, ± 15 MHz

Frequency stability : < 1 MHz long term drift after initial warm up. Less than 2 MHz pulling from 300 W to 150 W output

Ripple : < 1% of output power

Regulation : 0.5% of output power

Additional Features : Automatic control of the magnetron filament power for optimum operation at every power level. Digital metering of forward and reflected power, and availability of all status signals to a remote system.

8. Substrate Heating system

Model : Advanced Energy IPX-3750 induction heating power supply

Features : Operates with Pulse Width Modulated Resonant Mode conversion technique. Delivers required power in conjunction with a load match box as programmed and holds power at that level during input variations.

Output power : 3750 W

Output frequency : 30 KHz-75 KHz

Efficiency : 90 % from line to load

VITA

Mallika Kamarajugadda

Candidate for the Degree of

Doctor of Philosophy

Thesis: ANALYTICAL AND EXPERIMENTAL STUDIES ON MICROWAVE ASSISTED CVD DIAMOND COATINGS ON SI_3N_4 AND CEMENTED WC TOOLS AND GROWTH OF POLYCRYSTALLINE DIAMOND ON SEVERAL TRANSITION METALS

Major Field: Mechanical Engineering

Biographical:

   Education: Received Bachelor of Science degree from Osmania University, Hyderabad, India in 1988. Received Master of Science degree in Physics from Osmania University, Hyderabad, India in 1990. Completed the requirements for the Doctor of Philosophy degree with a major in Mechanical Engineering at Oklahoma State University in May, 1998.

   Experience: Graduate resarch assistant in the Department of Physics at the Indian Institute of Technology, Bombay, India, from 1991-1993. Graduate research assistant at Oklahoma State University, Department of Mechanical and Aerospace Engineering, 1993 to present.